AN ABSTRACT OF THE THESIS OF

Muthanna H. Al Dahhan for the degree of Master of Science in Chemical Engineering, presented on June 10, 1988

Title: Design of Liquid-Liquid Contactor for the Experimental Studies of Mass Transfer - The Evaluation of Interface Mass Transfer Coefficients on the Binary System Water-n-butanol

Abstract approved: Redacted for Privacy
Charles L. Wicks

A contactor has been designed and constructed for experimental studies of mass transfer with or without chemical reaction between two fluid phases. The contactor is flexible enough to investigate a wide range of variables affecting mass transfer coefficients. It is easy to operate; it could be operated either as a batch process or continuous process. The testing of the contactor verified the uniform mixing within a phase and the stability of the interface within the desired range of agitation.

Water-n-butanol system was used to verify the contactor and to evaluate the mass transfer coefficient. A new concept was deduced to explain the turbulent mass transfer across liquid-liquid interface. It was found that when both phases were agitated at the same speed, there was no effect of the Reynolds number of one phase on the other phase mass transfer coefficient. These mass transfer

coefficient values versus the agitated rates (or Reynolds number in each phase) were callsed asymtotic values or asymtotic line. If the agitation rate (rps) of a given phase is lower than the agitation in the other phase, its mass transfer coefficient is influenced by the mixing within the other phase below a critical Reynolds number, while the influence diminishes above it and its mass transfer coefficient approaches its asymtotic values.

New simple correlations were developed for the water and organic liquid mass transfer coefficients. These correlations verified a diffusivity dependency of 0.5 for low diffusivity values and a diffusivity dependency of 0.67 for larger diffusivity values. This was in agreement with the King model for explaining mass transfer coefficients based upon interfacial turbulence.

Since the asymtotic line conditions for both water and organic phases seems to represent the desired range of many industrial process conditions, the asymtotic mass transfer coefficient values with their corresponding agitation rate or Reynolds number were used to develop the correlations.

The contactor, the new concepts about the transport phenomena in turbulent mass transfer across the liquid-liquid interface, and the new correlations will be useful in future studies toward design of industrial equipment.

Design of Liquid-Liquid Contactor for the Experimental Studies of Mass Transfer - The Evaluation of Interface Mass Transfer Coefficients on the Binary System Water-n-butanol

by

Muthana H. Al Dahhan

A Thesis

Submitted to

Oregon State University

in partial fulfillment of
the requirements for the
degree of

Master of Science

Date Completed: June 10, 1988

Commencement: June 1989

APPROVED:

Redacted for Privacy

Professor of Chemical Engineering in charge of major

Redacted for Privacy

Head of Chemical Engineering Department

Redacted for Privacy

Dean of Graduate School

Date thesis is presented: June 10, 1988

ACKNOWLEDGMENTS

I wish to express my thanks and gratitude to Dr. Charles E. Wicks, my major professor, for his help, advice, guidance and continued encouragement during this academic experience.

I am very grateful to the members of my committee, Dr. Octave Levenspiel, Dr. Andrew D. Klein and Dr. Michael W. Schuyler.

I am very thankful to Mr. Nick for his help and advice during the equipment construction and set-up.

Appreciation is due to all the Chemical Engineering Department faculty, staff and Nuclear Engineering Department faculty for this educational opportunity.

I would like to express my thanks and gratitude to the people and government of my country, Iraq, who awarded me a scholarship to pursue my advanced education.

I am very grateful and appreciative to my wife, Dr. Etihad, for her patience, understanding and continued encouragement, and to all my family members who remained at my home eagerly awaiting my return.

وَقَضَىٰ رَبُّكَ أَلَّا تَعْبُدُوٓا۟ إِلَّآ إِيَّاهُ وَبِٱلْوَٰلِدَيْنِ إِحْسَٰنًا ۚ إِمَّا يَبْلُغَنَّ
عِندَكَ ٱلْكِبَرَ أَحَدُهُمَآ أَوْ كِلَاهُمَا فَلَا تَقُل لَّهُمَآ أُفٍّ وَلَا تَنْهَرْهُمَا
وَقُل لَّهُمَا قَوْلًا كَرِيمًا ﴿٢٣﴾ وَٱخْفِضْ لَهُمَا جَنَاحَ ٱلذُّلِّ
مِنَ ٱلرَّحْمَةِ وَقُل رَّبِّ ٱرْحَمْهُمَا كَمَا رَبَّيَانِى صَغِيرًا ﴿٢٤﴾

In the name of God, Most Gracious, Most Merciful.[2]

23. Thy Lord hath decreed
That ye worship none but Him,
And that ye be kind
To parents. Whether one
Or both of them attain
Old age in thy life,[2304]
Say not to them a word
Of contempt, nor repel them,
But address them
In terms of honour.

24. And, out of kindness,
Lower to them the wing [2305]
Of humility, and say:
"My Lord! bestow on them
Thy Mercy even as they
Cherished me in childhood." [2306]

DEDICATION

TO

MY MOTHER AND MY FATHER

WITH GRATITUDE

TABLE OF CONTENTS

LIST OF FIGURES

LIST OF TABLES

NOMENCLATURE

a	proportionality constant in eddy diffusivity expression, L^{2-n}/T
A	interfacial area, L^2
b	constant in the eddy diffusivity equation at the interface, L^2/T
c	concentration, M/L^3
c^*	equilibrium concentration, M/L^3
c^i	concentration at the interface, M/L^3
d	cell diameter, L
D	molecular diffusivity, L^2/T
e,el,...	exponent value
ew,eo	exponent of Reynolds number in the developed correlations
E	eddy diffusivity, L^2/T
f	function
F	flow rate, L^3/T
g	acceleration due to gravity, L/T^2
H	depth of phase in transfer cell, L
$J_{A,y}$	flux of species in y direction, M/L^2T
k, k_c	convective mass transfer coefficient, L/T
k_L	liquid side convective mass transfer coefficient, L/T
k_w	aqueous side convective mass transfer coefficient, L/T
k_o	organic side convective mass transfer coefficient, L/T
K_w	overall aqueous phase mass transfer coefficient, L/T
K_o	overall organic phase mass transfer coefficient, L/T
l	characteristic eddy dimension or length, L
L	impeller diameter, L

m	equilibrium constant
n	exponent on distance in the eddy diffusivity expression
N	number of impeller revolutions per time, rps or rpm
$\bar{N}_A$	flux at species A, M/L^2T
$\bar{N}_i$	flux of species i, M/L^2T
$(\bar{N}_A)_I$	instantaneous flux of species A, M/L^2T
$(\bar{N}_A)_{ave.}$	average flux of species A, M/L^2T
P,P1...	constant
P_w, P_o	constants in the developed correlation
r	exponent value
R_A	Chemical production rate of species A, $M/L^3.T$
s	fractional rate of surface renewal, T^{-1}
t	time, T
$\bar{t}$	age of an element of surface, T
$t_{exp.}$	time of exposure, T
u	macroflow velocity, L/T
V	volume, L^3
$\bar{V}_A$	average velocity of species A, L/T
y	normal distance to the interface, L
y_A	mole or mass fraction

Greek Symbols:

ϵ	rate of energy dissipation per unit mass of liquid, L^2/T^3
θ	time scale of turbulence, T
$\bar{\theta}$	average age of the surface element, T
λ_o	scale of turbulence in the viscous subrange, L
μ	viscosity, FT/L^2

ν	kinematic viscosity, L^2/T
ρ	density, M/L^3
$\Delta\rho$	density difference, M/L^3
$\lvert\Delta\rho\rvert$	absolute value of density difference, M/L^3
σ	interfacial tension, F/L
τ	dimensionless surface age
$\overline{\tau}$	tangential stress, M/LT^2
v_o	turbulence fluctuation velocity near interface but outside zone of damped turbulence, L/T
v'	turbulence fluctuation velocity, L/T
$\overline{v}'$	mean square fluctuation velocity, L/T
v_A	velocity of species A relative to fixed coordinate in space, L/T
ϕ (t)	Danckwerts function of time
Φ	correction factor
ψ	dimensionless mass transfer coefficient
φ	interaction factor
∇ , $\nabla\cdot$	differential vector operations

Subscripts:

A	species A
Ab	species A in bulk phase
Ai	initial species A
A_1, A_2	species A at point 1 and 2
Ao	species A in organic phase
Aoi	initial species A in organic phase
Aot	species A in organic phase at time t
Aw	species A in aqueous phase
Awi	initial species A in aqueous phase

Awt	species in A in aqueous phase at time t
i	species i
L	liquid phase
o	organic phase or organic species
ob	organic species in bulk phase
oi	initial organic species
ot	organic species at time t
w	water phase or water species
wb	water species in bulk phase
wi	initial water species
wt	water species at time t
in	inlet stream
out	outlet stream

Superscripts:

*	equilibrium
i	interface

Dimensionless Numbers:

Ar	Archimedes Number	$L^3 \rho g \lvert \Delta \rho \rvert / \mu^2$
Ca	Capillary Number	$gL^2 \rho / \sigma$
Fr	Froude Number	LN^2/g
Mo	Morton Number	$g \mu^4 \lvert \Delta \rho \rvert / \rho^2 \sigma^3$
Re	Reynolds Number	$NL^2 \rho / \mu$
Sc	Schmidt Number	$\mu / \rho D$
Sh	Sherwood Number	kL/D
We	Weber Number	$L^3N^2 \rho / \sigma$
We'	modified Weber Number	$NL(\rho L / \sigma_{equiv.})^{0.5}$

Design of a Liquid-Liquid Contractor for the Experimental Studies of Mass Transfer - The Evaluation of Interface Mass Transfer Coefficient on the Binary System Water-nbutanol

Chapter 1

Introduction

Many industrial processes such as absorption, extraction, distillation, etc. involve mass transfer between two phases. They have wide applications in chemical processes, petrochemical processes, nuclear chemical processes, biochemical processes, etc. In recent years considerable attention has been given to mass transfer studies with and without chemical reaction in order to improve the design of the mass transfer process equipments.

Many theories have been proposed to explain the convective mass transfer coefficient, including the film model (Whitman, 1927), the penetration and surface renewal models (Higbie, 1935; Danckwerts, 1951) and the boundary layer model [70, 71]. The mechanism of mass transfer across the free surface between two fluid phases is not fully understood, particularly when there is turbulent motion. Because of the complexity of the convective mass transfer mechanism no fundamental theoretical approach has been developed. Accordingly, different complex empirical correlations for the mass transfer coefficient have been proposed. These correlations have predicted the influence of the molecular diffusivity, (which has ranged from no dependency to a dependence of $D^{0.5}$-$D^{0.67}$), the other physical properties and the hydrodynamic conditions.

Many types of experimental equipment have been used to obtain

the data used in developing these correlations. However, there is still a need to design and develop an equipment that will be flexible enough to enable easier investigations of all the variables which affect mass transfer between two fluid phases.

The objective of this study consists of the following two parts: (I) To develop and verify an equipment and system having the following features:

1 - A system which closely approaches the operating conditions within industrial equipment.

2 - A system which can be operated as a batch process or a continuous process with independent control of transferred component in each phase.

3 - Sufficient mixing of each phase so that the concentration in each phase is uniform.

4 - Independent control of the mixing in each phase.

5 - The ability to obtain a stable interface and to easily vary the size of the interface area.

6 - The ability to change the configuration of the baffles and the cylindrical wiremesh in each compartment to stabilize the interface.

7 - The ability to use different types of impellers, located at different positions away from the interface.

8 - A temperature controlling bath or jacket and a pressure control particularly for gas-liquid systems.

A stirrer cell was designed and constructed so that its operation would best meet the desired objectives.

(II) To evaluate mass transfer coefficient in the binary system water-n-butanol, obtaining data which would permit:

1 - Studying the effect of mixing rate in one phase on the mass transfer rate in the other phase.

2 - Developing a new simple correlation or model, particularly for the mass transfer coefficient in a liquid-liquid system without chemical reaction; this model will cover the influence of diffusivity. Most of the previous correlations are very complex with a relatively high percentage of error, up to 40%. None of the current models give an accurate description, particularly for liquid-liquid mass transfer under process conditions.

Chapter 2

Theory

2.1 General Theoretical Review

The mechanism of mass transfer in a single fluid phase has been studied extensively in recent years. This has attempted to explain the roles of molecular and eddy diffusion, both for streamline and turbulent flow, and in interrelating the processes of heat transfer, mass transfer and momentum transfer.

Fick in 1855 [70, 71] provided the first mathematical explanation for molecular mass transfer when he postulated that the molecular transport of mass was proportional to a concentration difference at two different positions:

$$J_{Ay} = - D \frac{dC_A}{dy} \tag{2.1}$$

When both the concentration gradient contribution and the bulk motion contribution are important, the general mathematical explanation for molecular transport is:

$$\bar{N}_A = - CD \nabla y_A + y_A \Sigma \bar{N}_i \tag{2.2}$$

where $- CD \nabla y_A$ is the flux of A resulting from the concentration gradient of species A, as defined by Fick, and $y_A \Sigma N_i$ (or its equivalent, $C_A (\upsilon_A - \bar{V}_A)$) is the flux of A relative to the molar average velocity.

When the transfer is aided by fluid mixing so that the mass is transferred by packets or eddies, the transfer relative to a fixed,

stationary point is by convective mass transfer; for this case the flux is defined by

$$\bar{N}_A = k_c \, (C_{A_1} - C_{A_2}) \tag{2.3}$$

where k_c is the convective mass transfer coefficient.

The general differential equation of mass transfer can be written for any particular set of axis by:

$$\nabla \cdot \bar{N}_A + \frac{\partial C_A}{\partial t} - R_A = 0 \tag{2.4}$$

Several different mechanisms have been proposed to explain how mass is transferred from the bulk of a flowing medium to the interface or to a surface. Whitman [71] first proposed the two film theory in 1923; this theory does not depend on the existence of stagnant films, but on the validity of four assumptions:

1 - If there are turbulent conditions in the core of flowing fluid, the eddy effects essentially die out near the interface.

2 - The entire resistance to transfer is contained in a fictitious film equivalent to the resistance which would be encountered if the entire transfer is by molecular diffusion.

3 - The phases are at equilibrium at the phase boundary.

4 - The concentration gradient in the film is established in a relatively short time compared to the total time of contact. Accordingly, steady-state diffusion is assumed.

The Whitman film theory predicts the mass transfer convective coefficient $k_c \propto D$. In 1924 Lewis and Whitman proposed the additivity of

film resistances in terms of the reciprocals of the film coefficients [39].

Higbie in 1935 [71] postulated the penetration model in which turbulent eddies traveled from the bulk of the flowing medium to the interface where they remained a short but constant time before being displaced back into the bulk of the fluid. The mass transfer was explained by the following steps:

1 - Mass brought by the eddy comes into contact with the interface for the same exposure time.

2 - Exchange of mass occurs by transient mass transfer as:

$$\frac{\partial C_A}{\partial t} = D \frac{\partial^2 C_A}{\partial^2 y} \qquad (2.5)$$

with the boundary conditions:

at $t = 0$ and $0 \leq y \leq \infty$ $\qquad C_A = C_{Ab}$

at $t > 0$ and $y = 0$ $\qquad C_A = C_{Ai}$

at $t > 0$ and $y = \infty$ $\qquad C_A = C_{Ab}$

3 - After a time of exposure, t_{exp}, the eddy is displaced by a new eddy and is swept back into the bulk of the fluid.

When this partial differential equation is solved, the mass transfer coefficient is related to the time of exposure, t_{exp}, by

$$k_c = 2 \sqrt{\frac{D}{\pi t_{exp}}} \qquad (2.6)$$

in which $k_c \propto D^{0.5}$.

Danckwerts in 1951 [71] introduced the concept that the eddies which reach a surface or an interface could have an infinite range of ages or exposure time; this inferred that there is a probability that the eddy would be replaced by a fresh eddy from the core of the fluid which would be independent of the age of the eddy. He introduced a surface age distribution function, $\phi(t)$, which presents the probability that any element of the surface area would be exposed for a time, t, before that element is replaced by a fresh eddy from the bulk of the fluid; the average mass transfer then becomes,

$$(\bar{N}_A)_{ave} = \int_0^\infty (\bar{N}_A)_I \quad \phi(t)\, dt \tag{2.7}$$

Danckwerts theory predicts:

$$k_c = \sqrt{Ds} \tag{2.8}$$

in which s is the fractional rate of surface renewal; this term is an unpredictable quantity and must be experimentally measured for a given system. Danckwerts theory stipulates that convective transfer coefficient is proportional to $D^{0.5}$.

When mass is transferred through the laminar boundary layer, the convective mass transfer coefficient, k_c, is proportional to $D^{0.67}$ [70, 71].

2.2 The Interfacial Turbulence Model of King (1966)

King in 1966 [33, 34, 68] developed an interfacial turbulence model for the analysis of liquid phase mass transfer processes to and from a free gas-liquid interface which involved the concepts of surface renewal and of a damped eddy diffusion. The model is able

to explain the change in dependence of the mass transfer coefficient on diffusivity. It describes the mass transfer by a combination of unsteady diffusion and eddy diffusion. An eddy diffusivity is given by

$$E = ay^n + b \tag{2.9}$$

where y is distance normal to the interface. It allows E to retain a significant value up to and at the interface [30, 31]. It seems that surface tension would dampen the eddy diffusivity near an interface; therefore b expects to be equal to zero or very small, which allows E to equal 0 at $y = 0$; this was proposed by Levich [37].

The mass transfer behavior is described as follows:

$$\frac{\partial C_A}{\partial \bar{t}} = \frac{\partial}{\partial y}\left[(D + ay^n) \frac{\partial C_A}{\partial y} \right] \tag{2.10}$$

a and n are independent of t. The boundary conditions are:

at $\bar{t} = 0$ and $y > 0$ $\quad C = C_{Ab}$

at $\bar{t} = 0$ and $y = \infty$ $\quad C = C_{Ab}$

at $\bar{t} > 0$ and $y = 0$ $\quad C = C_{Ai}$

There is no general analytical solution for equation (2.10) for all n values in any simple fashion. King partly solved equation (2.10) with dimensional analysis and the introduction of the following dimensionless parameters:

1 - The dimensionless mass transfer coefficient,

$$\psi = \frac{k_L}{a^{1/n} - D^{1/n}} \tag{2.11}$$

2 - The dimensionless surface age,

$$\tau = \frac{a^{2/n}\,\bar{t}}{D^{2/n}\,\bar{l}} \qquad (2.12)$$

He assumed ψ was a function of τ and n.

The general model for free surface mass transfer is shown in Figure (2.1) below.

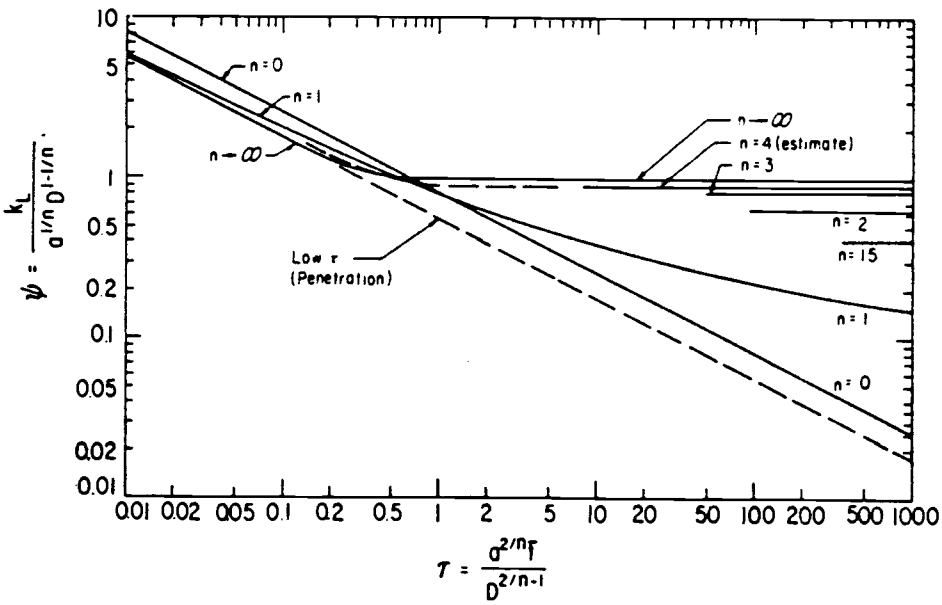

Figure (2.1). King's general model for free surface mass transfer.

The figure shows that the transition of the curves occurs near $\tau = 1.0$. For $\tau << 1$ the eddy diffusivity, ay^n, then becomes negligible compared to the diffusivity, D, and the penetration model is approached, i.e., $k \propto D^{0.5}$. Conversely for $\tau >> 1$, the species has penetrated to a depth where the eddy diffusivity is large. In this case steady state is approached and k is independent of the surface age, τ, where ψ is constant and equal to [68]

$$\psi = \frac{n}{\pi} \sin\left(\frac{\pi}{n}\right) \qquad (2.13)$$

This means that $k \propto D^{1-1/n}$. Therefore for $n \geq 2$ the present model is similar to that of the film-penetration theory which describes the mass transfer with a gradual change from the penetration, $k \propto D^{0.5}$, to the film model, $k \propto D^{1.0}$. In the region between these limits, there is a transition where the dependence changes from proportional to $D^{0.5}$ (low τ) up to $D^{1-1/n}$ (high τ). This model is able to explain the transition in dependency of the mass transfer coefficient on diffusivity from $D^{0.5}$ to $D^{1-1/n}$.

King's model requires the evaluation of the parameters n, a and $\bar{t}$. The parameter, n, can be evaluated from measurements of the influence of D upon k at high τ. The parameters a and $\bar{t}$ reflect the hydrodynamic behavior of the system. Despite the limitation in the evaluation of these parameters, the model gives a basis for qualitative interpretation of the mechanism of mass transfer under various conditions and provides a help toward quantitative analysis and correlation.

2.3 Mass Transfer Coefficient Evaluation When the Stirred Cell is Operated as a Batch Process

For the batch operation of a stirred cell, the mass transfer coefficient can be calculated using unsteady-state changes in the solute concentration within each phase. The basic assumption for this process are [4, 45]:

1 - Each phase is well mixed; thus the concentration of the species will not depend on the distance away from the interface.

2 - An equilibrium exists at the interface.

3 - The rate of transfer in each phase is the rate of transfer of the species away from the interface into the bulk of that phase.

4 - No chemical reaction takes place.

Simplifying the general equation (2.4) results in

$$\frac{d\bar{N}_A}{dy} = 0 \qquad (2.14)$$

In general the mass transfer flux $\bar{N}_A$ is:

$$\bar{N}_A = k_A (C_A^* - C_{Ab}) = - \frac{V}{A} \frac{dC_A}{dt} \qquad (2.15)$$

These equations can be solved for particular systems.

2.3.1 Binary System; involving two partially miscible liquid phases

In this system each species can be transferred into the other as shown in Figure (2.2) below:

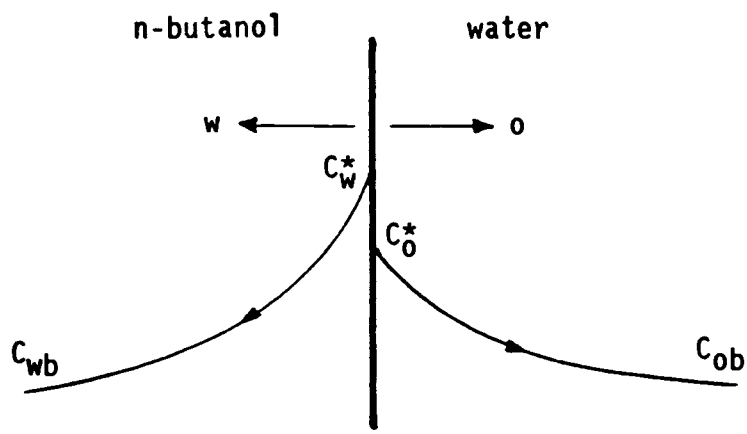

Figure (2.2). Binary system mass transfer during batch process.

The flux of the water species into the organic phase is,

$$\bar{N}_w = k_o (C_w^* - C_w) = \frac{V_o}{A} \frac{dC_w}{dt} \tag{2.16}$$

By integrating equation (2.16) between the limit,

$$\text{at } t = 0 \qquad C_w = C_{wi}$$

$$\text{at } t = t \qquad C_w = C_{wt}$$

$$\text{i.e., } \int_{C_{wi}}^{C_{wt}} \frac{dC_w}{C_w^* - C_w} = \int_0^t \frac{k_o A}{V_o} \, dt$$

one obtains the following relations:

$$\ln \frac{C_w^* - C_{wi}}{C_w^* - C_{wt}} = \frac{k_o A}{V_o} t \tag{2.17a}$$

$$k_o = \frac{V_o}{A_t} \ln \frac{C_w^* - C_{wi}}{C_w^* - C_{wt}} \tag{2.17b}$$

With a similar derivation, the mass transfer coefficient in the water phase is

$$\ln \frac{C_o^* - C_{oi}}{C_o^* - C_{ot}} = \frac{k_w A}{V_w} t \tag{2.18a}$$

$$k_w = \frac{V_w}{At} \ln \frac{C_o^* - C_{oi}}{C_o^* - C_{ot}} \tag{2.18b}$$

Measuring C_{wt} and C_{ot} in each phase with time and plotting $\ln (C_w^* - C_{wi})/(C_w^* - C_{wt})$ and $\ln (C_o^* - C_{oi})/(C_o^* - C_{ot})$ vs. t permits the evaluation of k_o and k_w from the slopes as follows:

$$k = \frac{\text{Slope} \cdot V}{A} \qquad (2.19)$$

2.3.2 Ternary system ; involving two immiscible solvents.

In this system, species A is transferred either from the organic phase to the water phase or vice versa. The transfer from the water phase is shown in Figure (2.3) below.

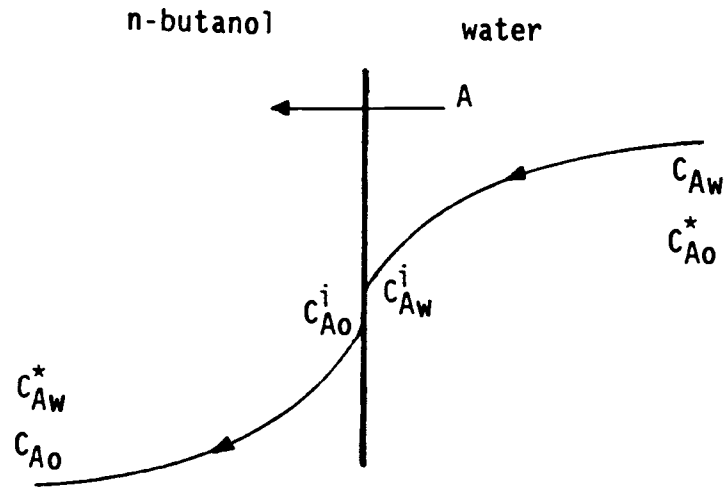

Figure (2.3). Transfer of species A in a ternary system during batch process.

In this case an overall mass transfer coefficient will be calculated where C_{Ao} is in equilibrium with C^*_{Aw} and C_{Aw} is in equilibrium with C^*_{Ao}, thus [17]:

$$C^i_{Ao} = m\, C^i_{Aw} \qquad (2.20a)$$

$$C^*_{Ao} = m\, C_{Aw} \tag{2.20b}$$

$$C_{Ao} = m\, C^*_{Aw} \tag{2.20c}$$

The reciprocal of the overall mass transfer coefficient is equal to the additivity of the films resistances, which may be written in terms of the reciprocals of the film coefficients as [15, 42]:

$$\frac{1}{K_w} = \frac{1}{k_w} + \frac{1}{mk_o} \tag{2.21}$$

$$\frac{1}{K_o} = \frac{m}{k_w} + \frac{1}{k_o} \tag{2.22}$$

Therefore the overall mass transfer flux of species A from the water phase is:

$$\bar{N}_A = K_w\,(C_{Aw} - C^*_{Aw}) = -\frac{V_w}{A}\frac{dC_{Aw}}{dt} \tag{2.23}$$

Substituting equation (2.20c) into equation (2.23) gives

$$K_w\,(C_{Aw} - \frac{C_{Ao}}{m}) = -\frac{V_w}{A}\frac{dC_{Aw}}{dt} \tag{2.24}$$

By integrating equation (2.24) between the limits:

at $t = 0$ $\quad C_{Aw} = C_{Awi}$

at $t = t$ $\quad C_{Aw} = C_{Awt}$ and $C_{Ao} = C_{Aot}$

$$\int_{C_{Awi}}^{C_{Awt}} \frac{dC_{Aw}}{(C_{Aw} - \frac{C_{Ao}}{m})} = \frac{K_w A}{V_w}\, t \tag{2.25}$$

$$\ln \frac{C_{Awt} - \frac{C_{Aot}}{m}}{C_{Awi} - \frac{C_{Aot}}{m}} = \frac{K_w A}{V_w} t \tag{2.26}$$

With a similar derivation, the overall organic phase mass transfer coefficient is

$$K_o(mC_{Aw} - C_{Ao}) = + \frac{V_o}{A} \frac{dC_{Ao}}{dt} \tag{2.27}$$

$$\ln \frac{mC_{Awt} - C_{Aoi}}{mC_{Awt} - C_{Aot}} = \frac{K_o A}{V_o} t \tag{2.28}$$

By measuring the slope of equation (2.26) and (2.28), which is $\frac{K_w A}{V_w}$ and $\frac{K_o A}{V_o}$, respectively, K_w and K_o can be calculated. By solving equations (2.21) and (2.22), the individual mass transfer coefficients, k_w and k_o can be calculated.

2.4 Mass Transfer Coefficient Evaluation When the Stirred Cell is Operated as a Continuous Process

For the continuous operation of the stirred cell, each phase flows into its section of the cell, where the mass transfer occurs between the two phases. The mass transfer coefficient can be evaluated by a simple material balance on the cell. The basic assumptions are the same as for the batch process operation. The convective mass transfer coefficient can be evaluated in a binary or ternary system, as follows:

2.4.1 Binary system; involving two partially miscible liquid phases.

The mass transfer flux of the water to the organic phase is shown in Figure (2.4) below:

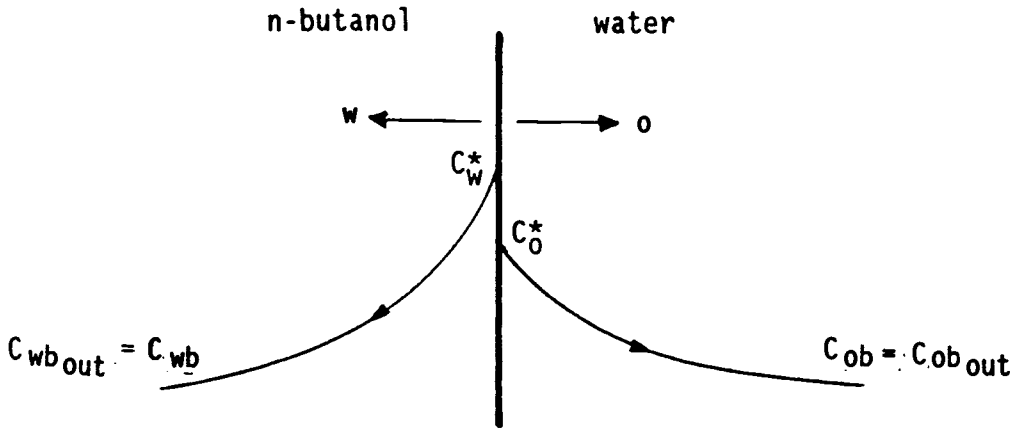

Figure (2.4). Binary system mass fransfer during continuous process.

For the water species, which is transferred into the organic phase,

$$\bar{N}_w \cdot A = k_o \cdot A \, (C_w^* - C_{w_{out}}) \qquad (2.29)$$

By the material balance on the inlet and outlet streams of the organic phase, $N_w \cdot A$ is:

$$N_w \cdot A = F_o \, (C_{w_{out}} - C_{w_{in}}) \qquad (2.30)$$

where F_o is the volumetric flow rate of the organic phase.

Thus:

$$F_o(C_{w_{out}} - C_{w_{in}}) = k_o \cdot A\ (C_w^* - C_{w_{out}}) \tag{2.31}$$

$$k_o = \frac{F_o}{A} \frac{C_{w_{out}} - C_{w_{in}}}{C_w^* - C_{w_{out}}} \tag{2.32}$$

A similar derivation proves k_w is

$$k_w = \frac{F_w}{A} \frac{C_{o_{out}} - C_{o_{in}}}{C_o^* - C_{o_{out}}} \tag{2.33}$$

2.4.2 Ternary system, involving two immiscible solvents.

Species A is transferred from one phase to the other phase, as shown in Figure (2.5) below:

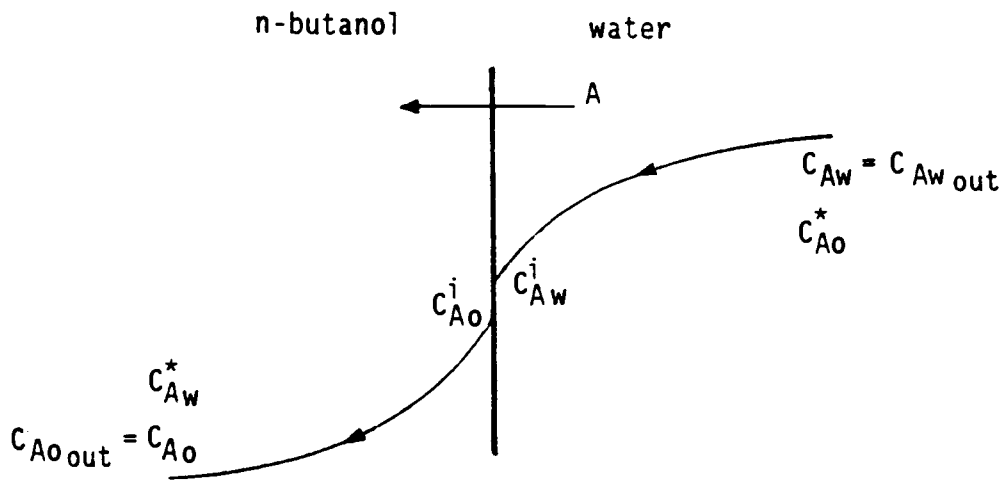

Figure (2.5). Transfer of species A in a ternary system during continuous process.

For this system, the overall mass transfer coefficient can be calculated as:

$$\bar{N}_A \cdot A = K_w \cdot A \, (C_{Aw_{out}} - C^*_{Aw}) \tag{2.34}$$

$$\bar{N}_A \cdot A = F_w \, (C_{Aw_{out}} - C_{Aw_{in}}) \tag{2.35}$$

$$K_w = \frac{1}{A} \frac{F_w \, (C_{Aw_{out}} - C_{Aw_{in}})}{(C_{Aw_{out}} - C^*_{Aw})} \tag{2.36}$$

With a similar derivation, K_o is

$$K_o = \frac{1}{A} \frac{F_o \, (C_{Ao_{out}} - C_{Ao_{in}})}{(C^*_{Ao} - C_{Ao_{out}})} \tag{2.37}$$

By solving equations (2.18), (2.19) and (2.20), the individual mass transfer coefficients can be evaluated.

The coefficients have been found to be dependent on the cell geometry; accordingly it is advantageous to make the geometry symmetrical for each phase.

2.5 Advantage of the Continuous Process over the Batch Operation of the Stirred Cell.

Most of the past investigations were done using the batch operation of the stirred cell. The batch operation technique for measuring mass transfer coefficient presents five following main

drawbacks, particularly when contacting either liquid-liquid or gas-liquid phases [34]:

1 - Under the condition of high agitation certain liquid phases tend to approach saturation quickly, thus reducing the time available for concentration measurement.

2 There is a possibility of significant error due to small temperature changes especially for the substances in which their solubilities are significantly temperature dependent.

3 - Particularly for the gas-liquid contacting, gas leakage (i.e. from cell, etc.) gives significant error.

4 - The analysis of the data in a batch system is based on the assumption that the bulk liquid within the cell is completely mixed at all times.

5 - Sample drawing causes a reduction in the phase volume during unsteady-state operation.

In the continuous system operation the measurements involve analyzing the inlet and the outlet streams of the stirred cell. Accordingly, the previously mentioned problems in 1, 2, 3, and 5 will be circumvented. In addition an overall mass balance will be available as an experimental check. Uncertainties associated with the assumption of complete mixing could also be overcome if the degree of species concentration decreasing in one phase and accumulating in the other phase are kept low.

The disadvantage of the continuous process operation comes from its operating cost, which is more than the operating cost of batch operation since it involves larger quantities of both contacting fluid phases than that involved in the batch operation.

2.6 Correlations of Mass Transfer Coefficient

The mechanism of mass transfer across the free surface between two fluid phases is not fully understood. Understanding this phenomenon particularly becomes complex if one or both of the phases are in turbulent motion. Due to the complexity of the problem, no fundamental theoretical approach has been developed. Various empirical correlations for the mass transfer coefficient have been proposed by several investigators. These correlations differ in the interpretation of the factors that influence mass transfer coefficient, such as the influence of molecular diffusivity (which has ranged from a definite no dependency [38] to a dependency of $D^{0.5}$ - $D^{0.67}$) [2, 45, 46], the physical properties, the hydrodynamic conditions, etc.

The most common correlations for the mass transfer coefficient that have been proposed are:

2.6.1 Lewis Correlation

Lewis in 1954 [38] came up with a correlation for the data obtained in his batch cell. He assumed that k_w was a function of the following dimensionless group.

$$\frac{k_w}{\nu} = f\left[\frac{\mu_o}{\mu_w}, \frac{\nabla\rho}{\rho_w}, Re_w, Re_o, we_w, Fr_w, Sc_w\right]$$

Lewis assumed that all groups could be neglected except Re_w and $Re_o \frac{\mu_o}{\mu_w}$; accordingly the correlation is

$$60 \frac{k_w}{\nu} = 6.76\text{x}10^{-6} \left(Re_w + Re_o \frac{\mu_o}{\mu_w}\right)^{1.65} + 1 \qquad (2.38)$$

The coefficient k_w was apparently independent of D. Sherwood in 1955 claimed that Lewis experimental data were consistent with k_w, varying as $D^{0.5}$ [12].

2.6.2 McManamey Correlation

McManamey in 1961 [44] proposed a correlation for mass transfer coefficient which involves the effect of molecular diffusion on the mass transfer. The correlation which was obtained by dimensionless analysis, is

$$\frac{60k_w}{\nu} = P\,(Sc_w)^{-0.37}\,(Re_w)^{0.9}\,\left(1 + \frac{\mu_o}{\mu_w}\,\frac{Re_o}{Re_w}\right) \qquad (2.39)$$

where $P = 0.102\ cm^{-1}$ for brass stirrer

$P = 0.0861\ cm^{-1}$ for glass stirrer.

This correlation stipulates k_w is proportional to $D^{0.37}$.

2.6.3 - Mayer Correlation

Mayer in 1961 [39] developed the following correlation based upon the Lewis data.

$$\frac{k_w L}{D_w} = 0.00316\,(Re_w Re_o)^{1/2}\left(\frac{\mu_o}{\mu_w}\right)^{1.9}\left(0.6 + \frac{\mu_o}{\mu_w}\right)^{-2.4}(Sc_w)^{5/6} \qquad (2.40)$$

k_w is proportional to $D^{1/6}$. This is less than 0.5, which holds when the transfer takes place only by unsteady-state diffusion into stagnant surface element; it is nearer to exponent of zero which would be expected if the transfer takes place by a completely turbulent mixing process. This correlation has a maximum deviation of 40% [44].

2.6.4 Orland and Benedict Correlation

These authors obtained their correlation in 1962 [49] by assuming that neither the interfacial tension nor the transport properties of solute phase appreciably affect the mass transfer rates in their investigation on the mechanism of water extraction into tributyl phosphate-n-hexane solvent. They correlated their data as follows:

$$\frac{k_w}{\nu_w} = 0.046 \left(\frac{N_w}{\nu_w}\right)^{0.67} (Sc_w)^{0.44} \qquad (2.41)$$

where k_w is proportional to $D^{0.44}$. The average deviation of the points from their correlation was $\pm$ 10%.

2.6.5 McManamey-Davis et al Correlation Involving Turbulent Model

McManamey, Davis, Woollen and Coe in 1973 [46] came up with a correlation based on the approach of an eddy to a free surface. They extended the Levich model [12] for the approach of an eddy to a free surface in gas-liquid mass transfer to liquid-liquid mass transfer, since there is apparently no great difference in the basic mechanism of mass transfer at the gas-liquid and liquid-liquid interface [12, p. 225]. The derivation of this model [12] was based on the concept that the total fluctuation velocity in the x-direction within the phase of the surface (i.e. interface plane) will be increased at those moments when the turbulent fluctuations in both phases happen to be synchronized, thus leading to faster mass transfer. Indeed, most of the mass transfer will occur then. The radius of curvature (deformation) at certain region of the interface will likewise be reduced when the eddies from each phase are suitably

phased, again strongly promoting mass transfer at such times. A full derivation of this model is given in Ref. [12, Chap. 5]. The expression obtained

$$k_w = 0.32 \frac{D_w^{0.5} \rho_w v_{ow}^{1.5}}{\sigma_{equiv}^{0.5}} \left(1 + \frac{\rho_o}{\rho_w} \frac{v_{oo}^2}{v_{ow}^2}\right)^{0.5} \left(1 + \frac{v_{oo}}{v_{ow}}\right)^{0.5} \tag{2.42}$$

They proposed that this relation should be valid for various methods of agitation [12, 46]. The term involving v_{oo} shows quantitatively how the momentum of an eddy in upper phase is transmitted across the interface into the adjacent region of the heavy phase, thereby increasing k_w. $\sigma_{equiv.}$ represents the interfacial tension and gravitational forces opposing the movement of an eddy to the interface; it is defined by.

$$\sigma_{equiv.} = \sigma + \frac{l^2 \rho g}{16} \tag{2.43}$$

where σ is interfacial tension and l is the eddy length. By rearranging equation (2.42), obtains:

$$k_w = 0.32 \left[\frac{D_w(v_{ow} + v_{oo})(\rho_w v_{ow}^2 + \rho_o v_{oo}^2)}{\sigma_{equiv.}}\right]^{0.5} \tag{2.44}$$

This equation predicts:

$$\frac{k_w}{k_o} = \left(\frac{D_w}{D_o}\right)^{0.5} \tag{2.45}$$

For the special case of geometrically similar stirred cell, v_{ow} and v_{oo} can be related to the phase agitation rate (rpm), N_w, N_o, as follow [12, eq. 1.114]:

$$v_o \propto NL \tag{2.46a}$$

$$v_o = p_1 NL \tag{2.46b}$$

which N is either N_o or N_w.

equiv. becomes approximately equal to $l^2 |\nabla \rho| g/16$ when the eddies are relatively large and the interfacial tension is relatively low; in general:

$$\sigma_{equiv.} = \sigma + l^2 |\nabla \rho| g/16 \tag{2.47}$$

The eddy length, l, is related to the scale of turbulence, which for eddies produced by an impeller is equal to some fraction of the impeller length, L, and does not depend on its speed [12, 46]. Values of l were found to be between 0.1L -1L. The surface tension and hydrostatic pressure of the deformation in the surface are equal when $\sigma = l^2 \rho g/16$ [12, p. 182]. For smaller eddies ($l < \sqrt{\frac{16\sigma}{\rho g}}$) the surface tension term is dominant at horizontal surface, while for large eddies, the hydrostatic head of the deformation in the surface is dominant. The magnitude of l (above 1 cm) suggests that mass transfer is mainly produced by the largest eddies [46]. When l=0.3L, equation (2.47) becomes:

$$\sigma_{equiv.} = \sigma + 0.00562\ L^2 |\nabla \rho| / g \tag{2.48}$$

The gravity term will be completely negligible compared with σ for eddies smaller than about 3 mm at a horizontal water surface or smaller than 2 mm for organic phase. Near the impeller blades the turbulence velocity fluctuation v', can be as high as NL [12, p. 68]. Accordingly, the experimental value of P_1 in equation (2.46b) can be compared with the typical values for the turbulence velocity

fluctuation produced by the impeller [46]. The turbulence velocity fluctuation, $\vec{v}$, obtained from the power input per unit volume is [12, p. 65]:

$$\bar{v}' = 1^{1/3} (6.4\ N^3 L^5 / d^2 H)^{1/3} \tag{2.49}$$

Accordingly, the correlation of McManamey, Davies, Woollen and Coe is:

$$Sh_w = P_2 (Sc_w)^{0.5} (we'_w)[Re_w + (\frac{\nu_o}{\nu_w}) Re_o]^{0.5} [1 + (\frac{\rho_o}{\rho_w} \frac{\nu_o^2}{\nu_w^2})(\frac{Re_o}{Re_w})^2]^{0.5} \tag{2.50}$$

where P_2 is equal to:

1 - 0.023 for Woollen's data

2 - 0.035 for Coe's data

3 - 0.04 for McManamey, Multani and Davis [42], which gave P_1 = 0.25 in equation (2.46b).

The correlation gave k_w is proportional to $D^{0.5}$.

2.6.6 McManamey, et al Correlation Involving Laminar Boundary Layer Model.

McManamey, Multani and Davis [45] in 1975 noticed that the mass transfer coefficient for the helium-butanol-water system depended on the exponent of the diffusivity greater than 0.5. They suggested that the turbulent model as mentioned in (2.6.5) is not strictly valid for this system. Accordingly, they considered representing the system in a transition regime between boundary layers and surface renewal at the interface by applying the Levich three-zone model [12, 37]. The fluctuation velocities in the laminar sublayer

are assumed to have the same form as for a liquid-solid interface [12]. In this case the fluctuation velocities, both in the direction parallel to the interface and perpendicular to it, were functions of the distance from the interface and were zero at the interface. This differs from the case when surface renewal exist, where the fluctuation velocity in the plane of the interface is not zero [12, p. 227]. Thus the authors assumed that the velocity gradients in liquid-liquid surface are similar to those at a solid surface; accordingly the following equation [12] could be applied:

$$k = 0.075 \ \nu_0 \ (S_c)^{-2/3} \tag{2.51}$$

By substituting $\upsilon_0 = 0.25$ NL and rearranging equation (2.51) in terms of dimensionless groups yields

$$Sh = 0.0187 \ Re \ Sc^{1/3} \tag{2.52}$$

in which k_w is proportional to $D^{0.67}$.

This correlation was tested on the water-butanol system. This test confirms the previous observations that suggested this system represents the transition regime. The previous investigation showed that the diffusivity dependency was between 0.59-0.64; this is between the value predicted by correlation (2.50) involving turbulent model and correlation (2.52) involving boundary layer model [45].

2.6.7 Bulicka and Prochazka Correlation Involving Homogeneous Isotropic Turbulence Theory

Bulicka and Prochazka in 1971 and 1976 [4, 54] proposed a correlation based on the theory of homogeneous isotropic turbulence.

Their derivation started from the concept of surface renewal by turbulence disturbances and unsteady mass transfer into the elementary vortices by molecular diffusion. Their basic assumption were as follows:

1 - The surface is renewed by the whole spectrum of vortices present in the turbulent core of the phase. The thickness of the diffusional boundary layer is proportional to the scale of turbulence in the viscous subrange λ_0.

2 - The vortices of the above dimensions obey Kolomogorov's assumption of local isotropic turbulence [4].

3 - The turbulence in the core of the phases is approximately homogeneous.

4 - The rate of renewal of the boundary layers is proportional to the characteristic frequency $\bar{v}_0'/\lambda_0$. The mass transfer within the boundary layer takes place by unsteady diffusion into a semi-infinite layer, with an initial concentration equal to that within the core of the given phase.

5 - The boundary layers affect each other in such a way that the total energy dissipation in both boundary layers equals the sum of the dissipation which would occur in each layer separately if there were no mutual interference; the frequency of the renewal in both layers is the same.

From assumptions (1) and (2) it gives λ_0, $\bar{v}_0'$ and θ_0 as follows:

$$\lambda_o = (\nu^3/\epsilon)^{1/2} \tag{2.53}$$

$$\bar{v}_o' = (\epsilon \nu)^{1/4} \tag{2.54}$$

$$\theta = \frac{\lambda_o}{\bar{v}_o'} = (\frac{\nu}{\epsilon})^{1/2} \tag{2.55}$$

According to assumption (3),

$$\epsilon \propto u^3/L \tag{2.56}$$

where u is the macroflow velocity and it is proportional to the agitation rate (rpm), N.

Using assumption (4), k is

$$K = \sqrt{\frac{D}{\theta}} \tag{2.57}$$

By using assumption (5), one has

$$\epsilon_{ib}\, \rho_i\, \lambda_{oi} + \epsilon_{jb}\, \rho_j\, \lambda_{oj} = \epsilon_i\, \rho_i\, \lambda_{oi} + \epsilon_j\, \rho_j\, \lambda_{oj} \tag{2.58}$$

$$\theta_i = \theta_j \tag{2.59}$$

where i,j are the light phase and the heavy phase, respectively.

By combining the above equations and rearranging in terms of dimensionless group, one obtains:

$$Sh_w = P_3\, Sc_w^{1/2}\, Re_w^{3/4}\, \varphi_{wo} \tag{2.60}$$

where φ_{wo} is

$$\varphi_{wo} = \left[\frac{1 + (\frac{N_o}{N_w})^3 (\frac{\nu_o}{\nu_w})^{1/2} \frac{\rho_o}{\rho_w}}{1 + (\frac{\nu_o}{\nu_w})^{3/2} \frac{\rho_o}{\rho_w}} \right]^{0.25}$$

The average value of P_3 is equal to 0.06, which characterizes: the cell geometry [4]. The factor φ_{wo} expresses the effect of the turbulence in the organic phase on the mass transfer in the water phase. In this correlation, k_w is proportional to $D^{0.5}$. In an earlier publication [54], the authors reported $\bar{\tau}_w = \bar{\tau}_o$. Accordingly, they ended up with $k_w/k_o = \sqrt{D_w \mu_o/D_o \mu_w}$ which did not fit their results nor the results of other investigators [46].

2.6.8 Asai et al Correlation

Asai, Hatanaka and Uekawa in 1983 [2] correlated the mass transfer coefficient using data from 30 systems based on the following expression (5).

$$Sh_w^{\bar{m}} = f_w^{\bar{m}} + f_o^{\bar{m}} \tag{2.61}$$

where

$$f_j^{\bar{m}} = p_4 \, Re_j^{e1} \, Mo_w^{e2} \, Sc_w^{e3} \, Ar_w^{e4} \left(\frac{\mu_o}{\mu_w}\right)^{e5} \left(\frac{\rho_o}{\rho_w}\right)^{e6} \left(\frac{|\Delta\rho|}{\rho_w}\right)^{e7} \tag{2.62}$$

with

$$Mo_w = \frac{g \, \mu_w^4 \, |\Delta\rho|}{\rho_w^2 \, \sigma^3} \quad \text{and} \quad Ar_w = \frac{L^3 \, \rho_w \, g \, |\Delta\rho|}{\mu_w^2} \quad , \; j = w \text{ or } o$$

By calculating the constant and exponents and arranging equation (2.61) and (2.62), the following correlation was obtained

$$Sh_w = 0.0119 \, Sc_w^{1/3} \, Ca_w^{6/13} \left[\Phi^4 \, Re_w^3 + \left(Re_o \frac{\nu_o}{\nu_w}\right)^{8/3} \right]^{1/4} \tag{2.64}$$

where $\Phi = 1.0$ for $\frac{\mu_o}{\mu_w} \leq 7.0$

$$\Phi = \left(\frac{\mu_o}{7\mu_w}\right)^{1/5} \quad \text{for} \quad \frac{\mu_o}{\mu_w} > 7.0$$

The range of dimensionless groups covered in this experiment are as follows:

$$690 < Re_w < 6300 \ , \ 0 < Re_o \frac{\nu_o}{\nu_w} < 7600$$

$$190 < Sc_w < 1.1 \times 10^5 \ , \ 200 < Ca_w < 5100$$

$$0.029 < \mu_o/\mu_w < 36$$

The coefficient, k, in this correlation is proportional to $D^{0.67}$. The correlation represents all their data with an average deviation of $\pm$ 12.7%, and a maximum deviation of $\pm$ 30%.

2.6.9 Versteeg et al Correlation

Versteeg, Blauwhof and Van Swaau in 1987 [68] studied mass transfer in gas-liquid phases. The liquid phase mass transfer coefficient was correlated according to the interfacial turbulence model of King. Their correlations were able to explain the change in the dependence of the mass transfer coefficient on diffusivity, D. The authors found that for large Sc numbers, the dependence of k tends to a value proportional to $D^{0.5}$, which represents a penetration model. For small Sc numbers, the k dependency tends to be a value proportional to $D^{0.67}$, which represents a laminar boundary layer model. The following Figure (2.6) shows the result of their numerical solution [8, 68] of King's model for some values of n.

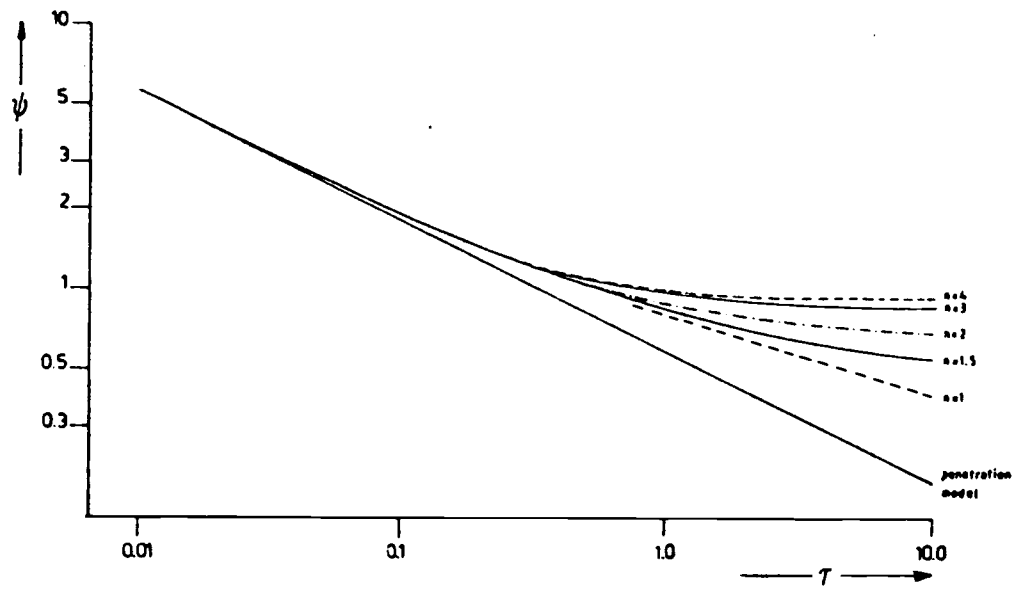

Figure (2.6). Versteeg et al numerical solution of the King model for some values of n.

In their solution they used time-averaged values instead of instantaneous values of k_L and $\bar{t}$. Therefore

$$\tau = \frac{a^{2/n}\ \bar{\theta}}{4D^{(2/n)\ -\ 1}} \tag{2.64}$$

with $\bar{\theta}$ equal to the average age of the surface elements. To compare King's model with their results, $\frac{Sh}{Re^{0.72}}$ was plotted vs Sc numbers as shown in Figure (2.7). The parameters, n, a, and $\bar{\theta}$ which depend upon the hydrodynamics and the physical properties of the system were evaluated from Figure (2.7) using its asymptotic dependence of Sh on Sc. The asymptotic dependence of Sh on Sc is 1/3 and therefore the value of n equals 3. $\bar{\theta}$ can be found from the asymptotic of large Sc numbers (small τ), while a can be found from the

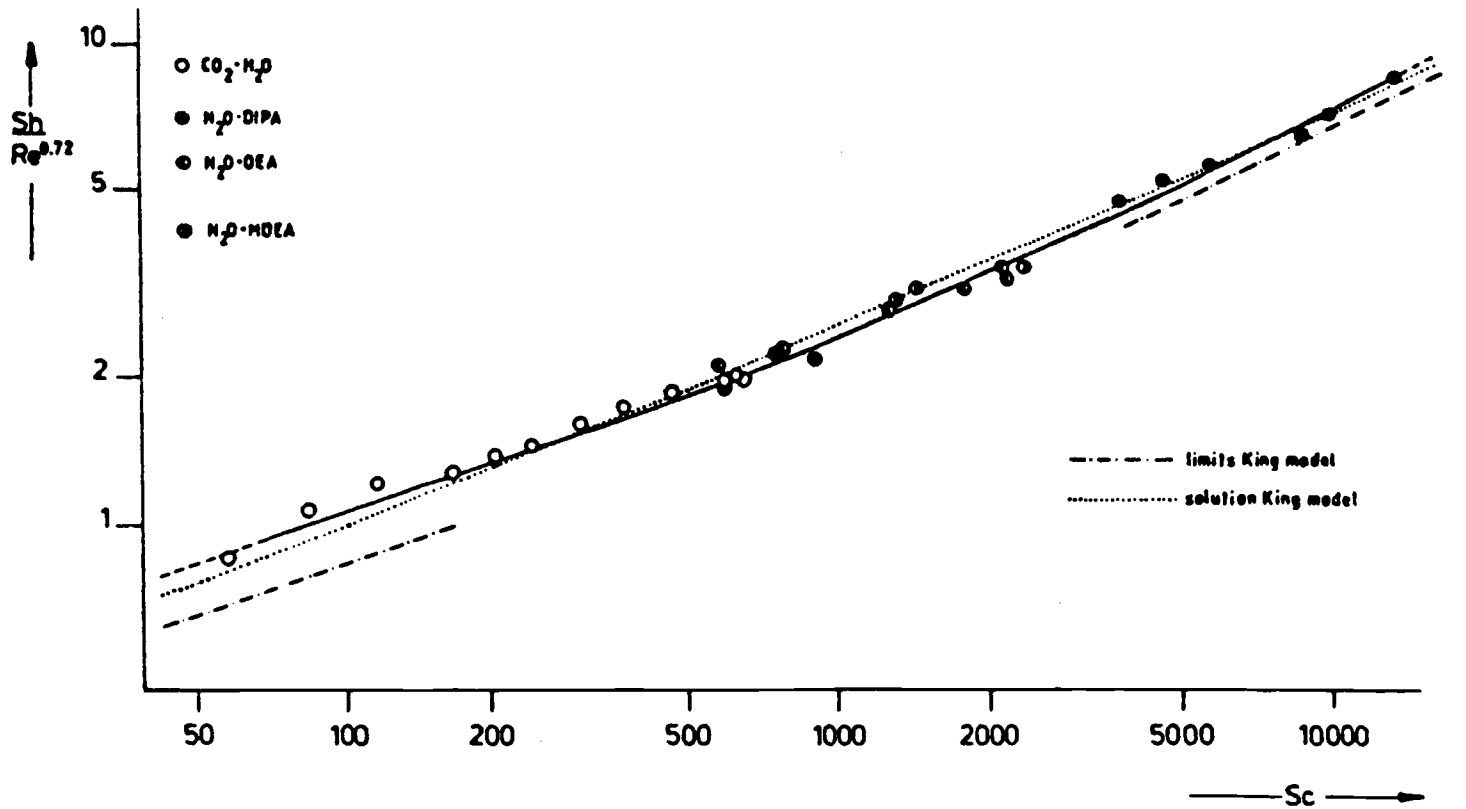

Figure (2.7). Overall Versteeg et al results of the liquid phase experiments compared with the results obtained from King model.

asymptotic of small Sc numbers (large τ). Figure (2.8) shows the comparison between the King model and Versteeg et al. experimental data.

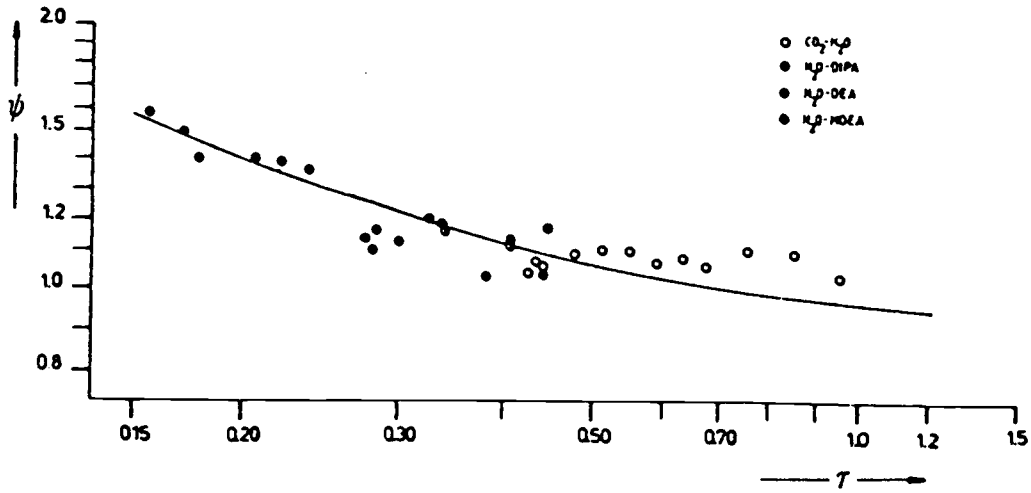

Figure (2.8). Comparison between the King model and the Versteeg et al experimental data.

The authors proposed two correlations as asymptotic cases of King's model as follows:

a - For large Sc numbers (small τ)

$$Sh_L = 0.064\ Re_L^{0.72}\ Sc_L^{0.5} \qquad (2.65)$$

The coefficient, k, is proportional to $D^{0.5}$, which represents penetration model.

b - For small Sc numbers (large τ)

$$Sh_L = 0.181\ Re_L^{0.72}\ Sc_L^{0.33} \qquad (2.66)$$

The coefficient, k, is proportional to $D^{0.67}$, which represents the laminar boundary layer model.

The authors concluded that the King model is able to correlate the dependency of the mass transfer on diffusivity over a wide experimental range.

Chapter 3

Description of Previous Equipments Used in Mass Transfer Studies

The application of mass transfer with and without chemical reaction in both liquid-liquid and gas-liquid systems has had rapid growth in the last three decades. This has resulted in a desire to improve mass transfer equipment design. For better design, it is essential to understand the exact role of convective mass transfer in order to determine systematically the effects of the physical properties on mass transfer rate and thus obtain more reliable correlations as models of the mass transfer coefficient [2, 15].

Many different types of mass transfer equipment have been used in experimental research. For example, equipment has been built to investigate the transfer into both quiescent fluids and into agitated fluids. Agitated fluids equipment more closely represent the behavior of industrial equipment. Let us consider some of the equipment which has been designed for mass transfer investigations.

3.1 Equipment Involving Mass Transfer Into Quiescent Liquids

Many studies have been done in equipment involving quiescent liquids. A brief list of such equipment would include:

1 - An apparatus which consists of passing a film or jet of liquid continuously through a gas for a short contact time. The liquid phase is assumed quiescent while in contact with the gas phase. Figure (3.1) illustrates this apparatus [15].

2 - A wetted-wall column as shown in Figure (3.2) involved a liquid

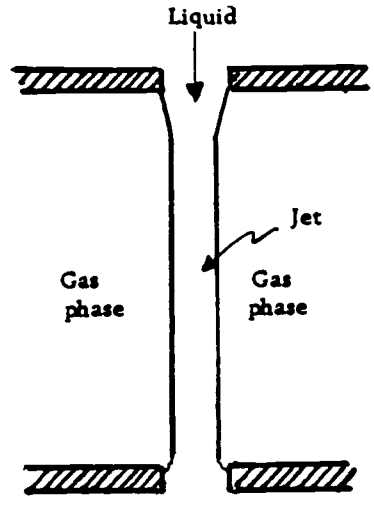

Figure (3.1). Laminar jet apparatus.

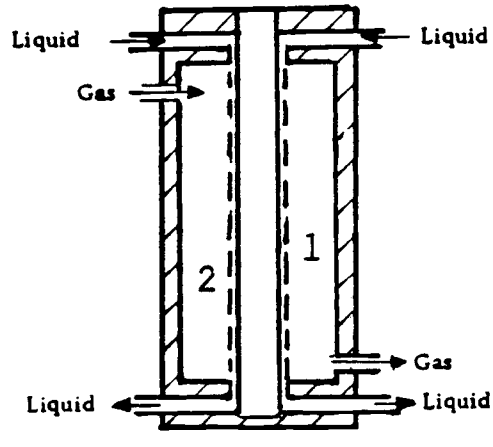

Figure (3.2). Wetted wall column.1. Film, 2. column.

film flowing by gravity down a vertical column surface enclosing the gas phase [15].

3 - A rotating drum apparatus, as illustrated in Figure (3.3) was used by Danckwert and Kennedy [11, 15]. It provided a film of liquid to be carried by the surface of the drum through a gas phase.

4 - A moving band apparatus, which was used by Govindon and Quinn [18], is illustrated in Figure (3.4). It carried a film of liquid on a band of inchrome ribbon through a gas phase.

Although these experimental apparatuses had the advantage of having well defined mass transfer area, they did not provide independent control of all the variables which might effect the transfer rate.

3.2 Equipment Involving Mass Transfer into Agitated Fluids

Most mass transfer with and without chemical reaction studies have been achieved in equipments involving agitated fluids. They could be classified into stirred cell and column equipments as follows:

3.2.1 The Stirred-Cell Equipments

A stirred-transfer cell, in which each phase is independently stirred, has been used in several investigations evaluating mechanism of liquid-liquid and gas-liquid mass transfer. The stirred-cell provides the following advantages: The interface is well defined, the bulk phases are of uniform concentration and the effect of the stirring rate can be easily investigated. The following investigators used the stirred transfer-cells in their investigations:

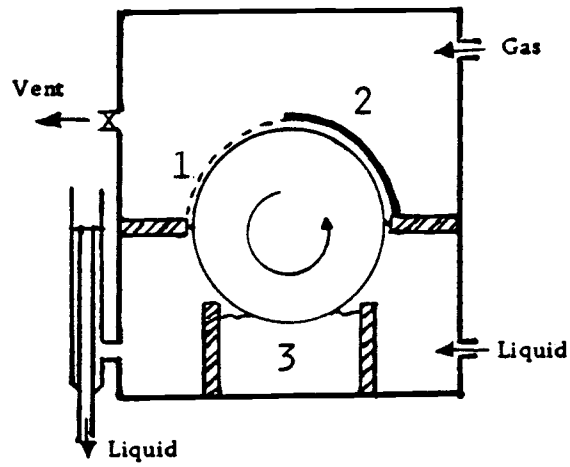

Figure (3.3). Dankwerts and Kennedy rotating drum.
1. Film, 2. Gas tight screen, 3. mercury seal.

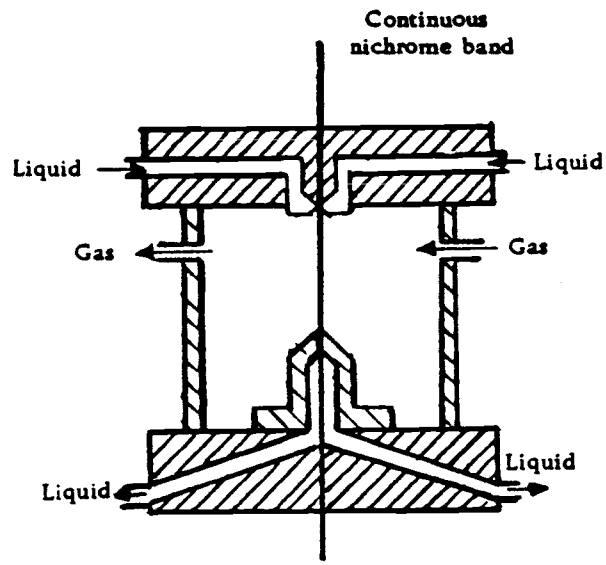

Figure (3.4). Govindon and Quiun moving band absorber.

1 - Gordon and Sherwood Cell

Gordon and Sherwood [17] studied mass transfer to liquid phases in the stirred cell, shown in Figure (3.5). It consisted of a glass cylindrical vessel resting in a 25°C water bath. A single stirrer shaft held separate stirrer arms in each of the two phases. In this apparatus the two phases were dependently mixed with the same speed of rotation. The interface was easily subjected to surface wave motion so it limited the degree of turbulency.

2 - Lewis Cell

Lewis in 1954 [38] designed a stirred cell as shown in Figure (3.6); this became the traditional cell used for determining individual mass transfer coefficients. The cell provided central paddles for independently stirring each phase. Its two halves were made geometrically similar and separated by a circumferential baffle; this together with the central baffle formed the annular interface area, which was approximately 30 cm^2. The cell was suspended in a constant water temperature bath. It was found that the interface in the same cell was subjected to breaking up even at low agitation speeds [4]; accordingly high turbulency could not be achieved [4, 54].

3 - Mayers and McManamey Cell

Mayers [42] and McManamey [44] in 1961 separately studied liquid-liquid mass transfer in the cell illustrated in Figure (3.7). Their cells were compromised between the types of Lewis and of Gordon. Each cell had an independently-control rotating stirrers. The stirrers were similar to those used in the Lewis cell. The cell was situated in a constant temperature water bath. The cell inter-

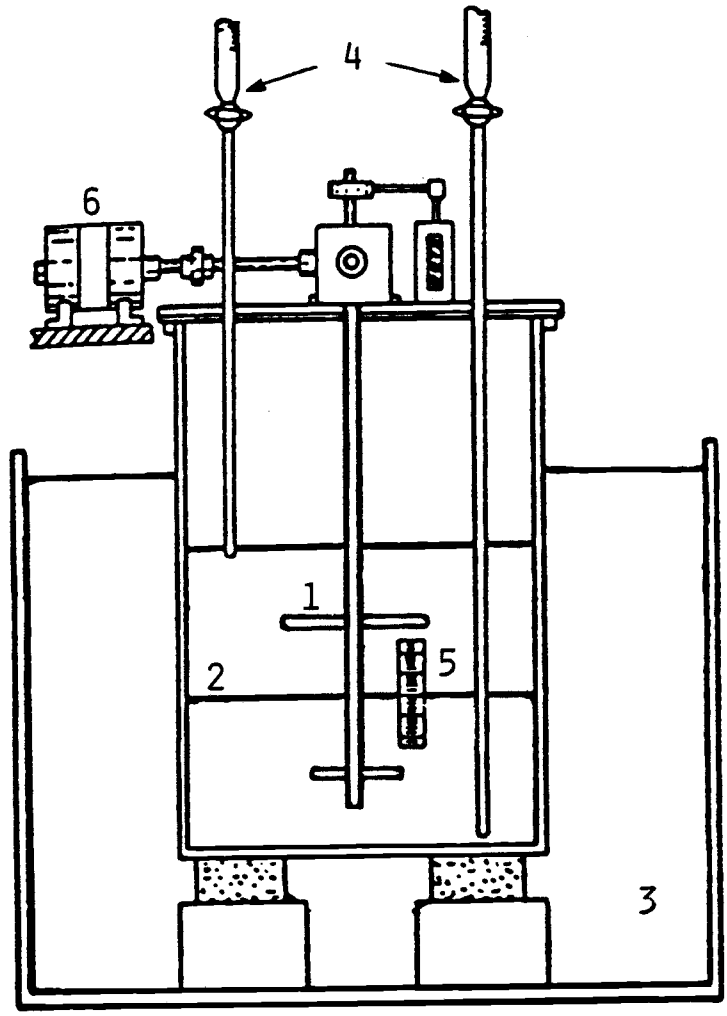

Figure (3.5). Gordon and Sherwood cell. 1. Impeller, 2. Interface, 3. Thermostat bath, 4. Filling buretts, 5. Plastic scale, 6. Stirrer motor.

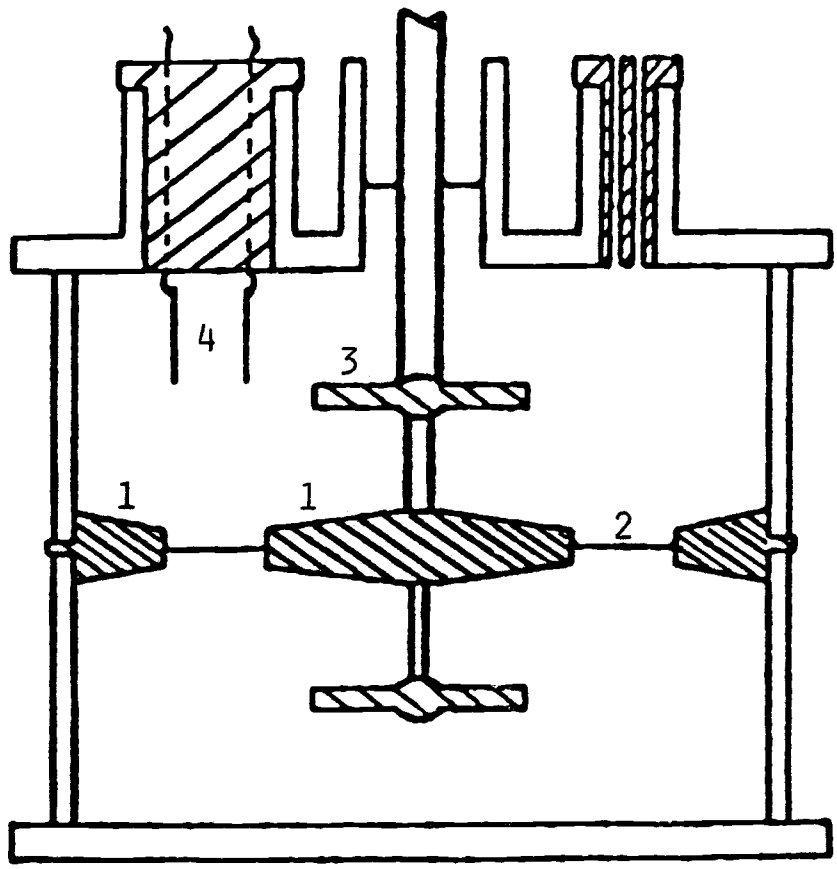

Figure (3.6). Lewis cell. 1. Baffle, 2. Interface, 3. Impeller, 4. Electrode probe.

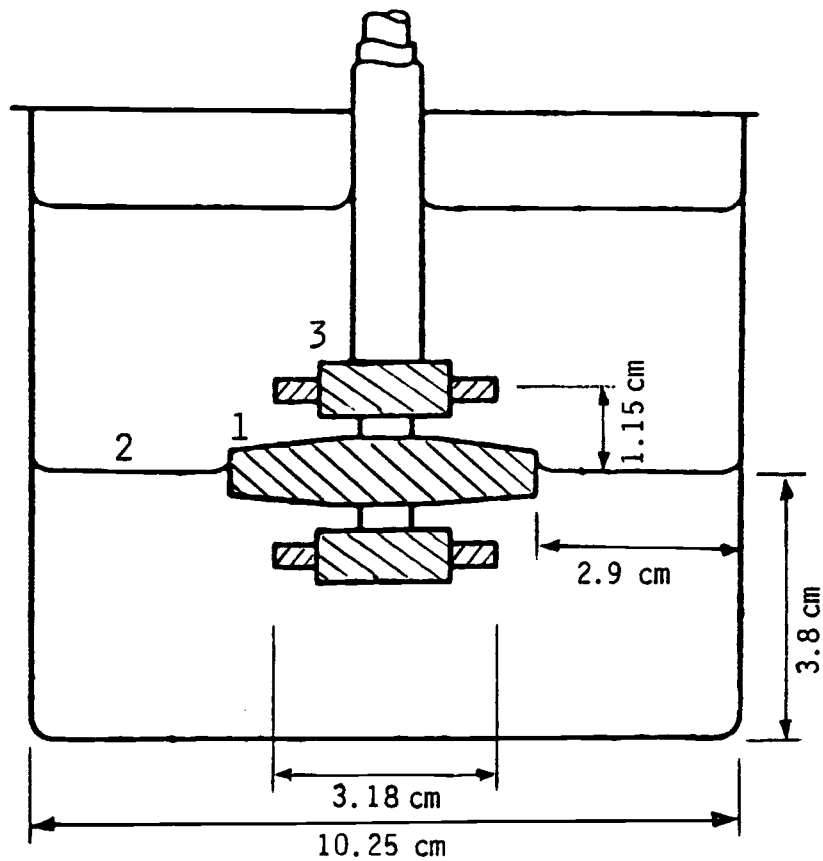

Figure (3.7). McManamey cell. 1. Baffle, 2. Interface, 3. Impeller.

face could be easily subjected to wave motion since a stirrer was located close to the interface.

4 - Danckwerts and Gillham Cell

Danckwerts and Gillham [10] in 1966 used an agitated cell to predict rates of mass transfer with chemical reaction. The cell is shown in Figure (3.8). A turbine-type stirrer was used. Static baffles were attached to the base of the cell to promote bulk mixing. The stirrer was positioned so that its bottom edge cut the plane of the interface. It had high sensitivity interface for rippling.

5 - Prochazka and Bulicka Cell

Prochazka and Bulicka [54] in 1971 used a modified Lewis cell in studying mass transfer coefficients. The cell is shown in Figure (3.9). The annular interface was formed between the horizontal baffle and the cylindrical wall. Unlike the Lewis cell, impellers with 45° inclined blades were used. The stirrers were surrounded by two cylindrical grids, which allowed a considerable increase in the rate of stirring with no rippling of the interface. In 1975 Bulicka and Prochazka [4] developed new mixing cells, as shown in Figure (3.10). The cell differed from their previous one to provide a better stability of the interface. The impellers were surrounded by a stator equipped with 12 vertical baffles mounted on a horizontal plate, so that the tangential velocity component was cancelled and the axial flow leaving the impeller was transformed to a radial direction at the interface. The stator included a cylindrical grids with a circular 3 mm opening to facilitate formation of a uniform turbulent flow structure. Its perforations were omitted over the height of the impeller and over 4 mm wide strip on each side of the

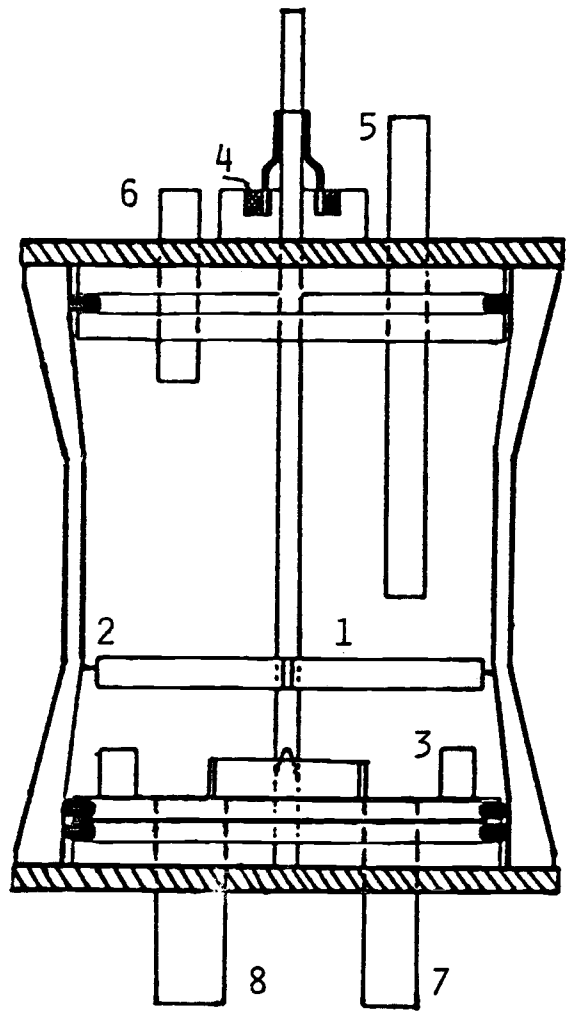

Figure (3.8). Danckwerts and Gillham cell. 1. Impeller, 2. Interface, 3. Static baffles, 4. Mercury seal, 5, 6. Gas inlet and outlet, 7, 8. Liquid inlet and outlet.

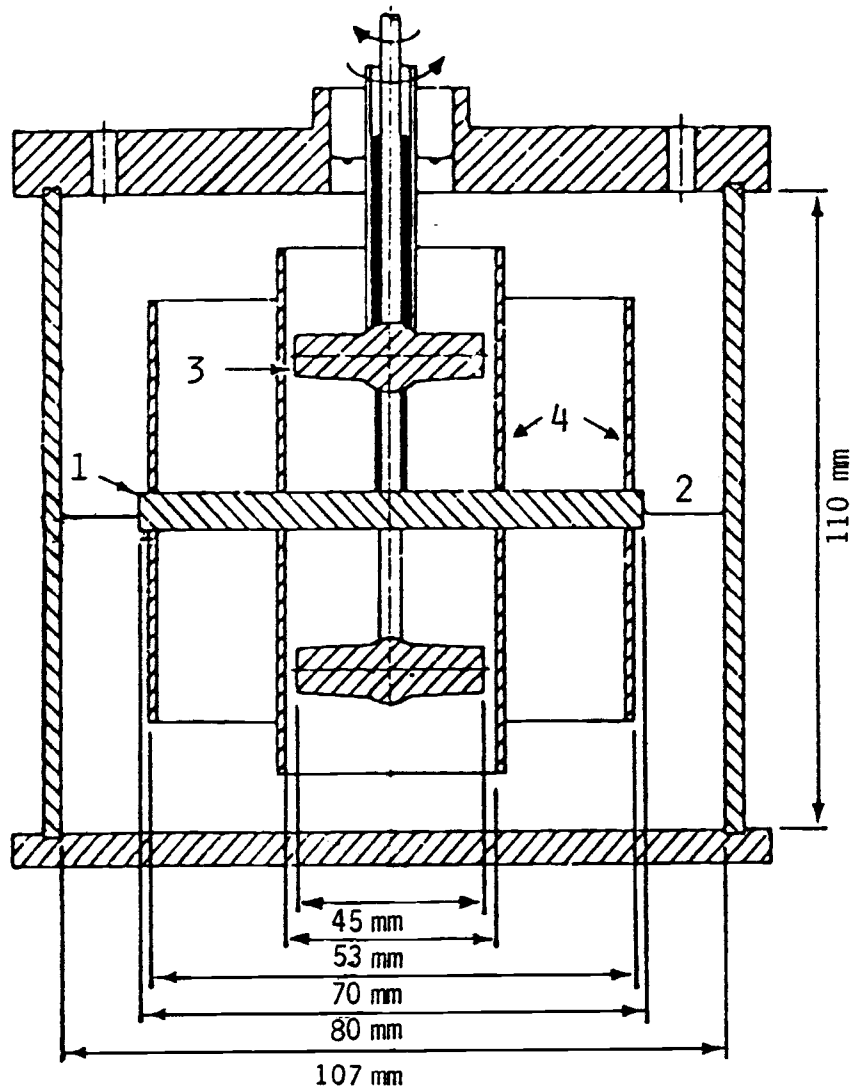

Figure (3.9). Prochazk and Bulicka cell. 1. Horizontal baffle, 2. Interface, 3. Impeller, 4. Cylindrical grids.

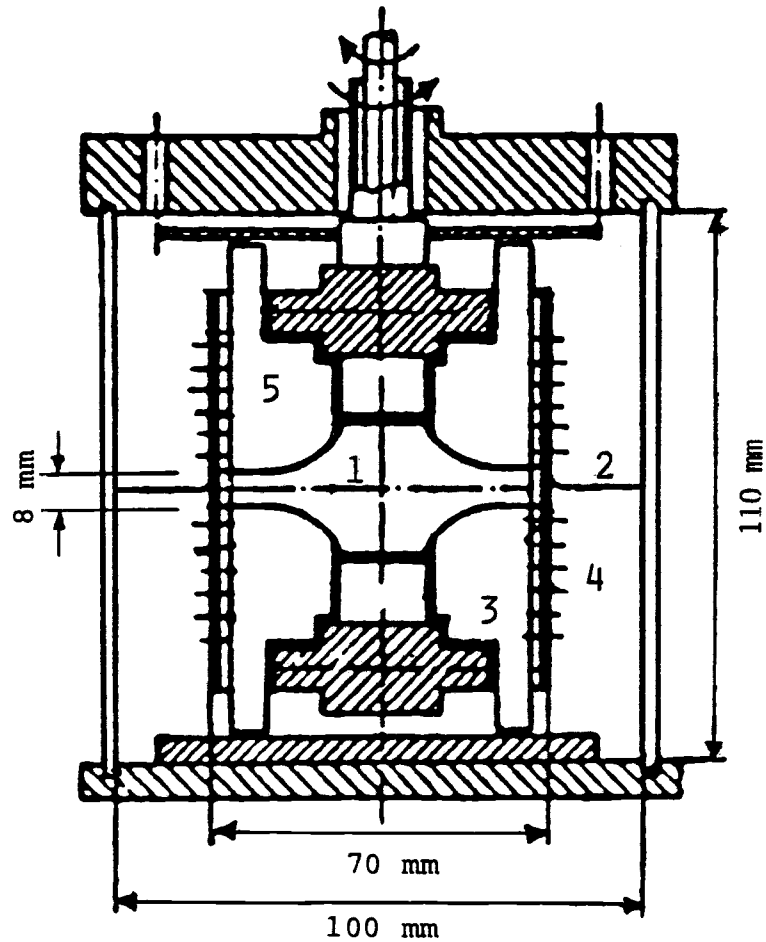

Figure 3.10. Bulicka and Prochazka cell. 1. Inner stator ring, 2. Interface, 3. Impeller, 4. Cylindrical grids, 5. Vertical baffles.

interface. The thickness of the interface plate was 8 mm. The cell was submerged in a constant temperature water bath.

6 - Godfrey Cell

Godfrey [15] in 1973 designed an apparatus to study gas-liquid mass transfer with chemical reaction, as shown in Figure (3.11). It was constructed from two cylindrical sections. Both phases were mixed independently by using three-blade propeller-type agitators for the liquid phase and four-blade turbine agitator or three-blade propeller agitators for the gas phase. Four baffles were equally spaced on the inside of the wall to promote bulk mixing. The interface plate contained drilled holes of 0.25 in. diameter, which were symmetrically distributed. This form of interface plate enabled the investigator to change the interface area by inserting new plates with different number or size of holes.

7 - Landau and Chin Cell

Landau and Chin [36] in 1977 developed an agitated cell, as shown in Figure (3.12). It consisted of a glass cylinder. The two phases were separated by a tapered ring. The annular interface area was between the ring and the glass cylinder. The stirrers were housed in a perforated shell with vertical baffles to maintain a stable interface. The liquid left the shell in a radial direction through circular perforations on its cylindrical part. The overall circulation patterns also are indicated in Figure (3.12) by arrows.

8 - Asai et al Cell

Asai, Hatanaka and Uekawa [2] in 1983 studied liquid-liquid mass transfer in an agitated cell, as shown in Figure (3.13). The cell consisted of an inner and outer glass cylinder. The space between

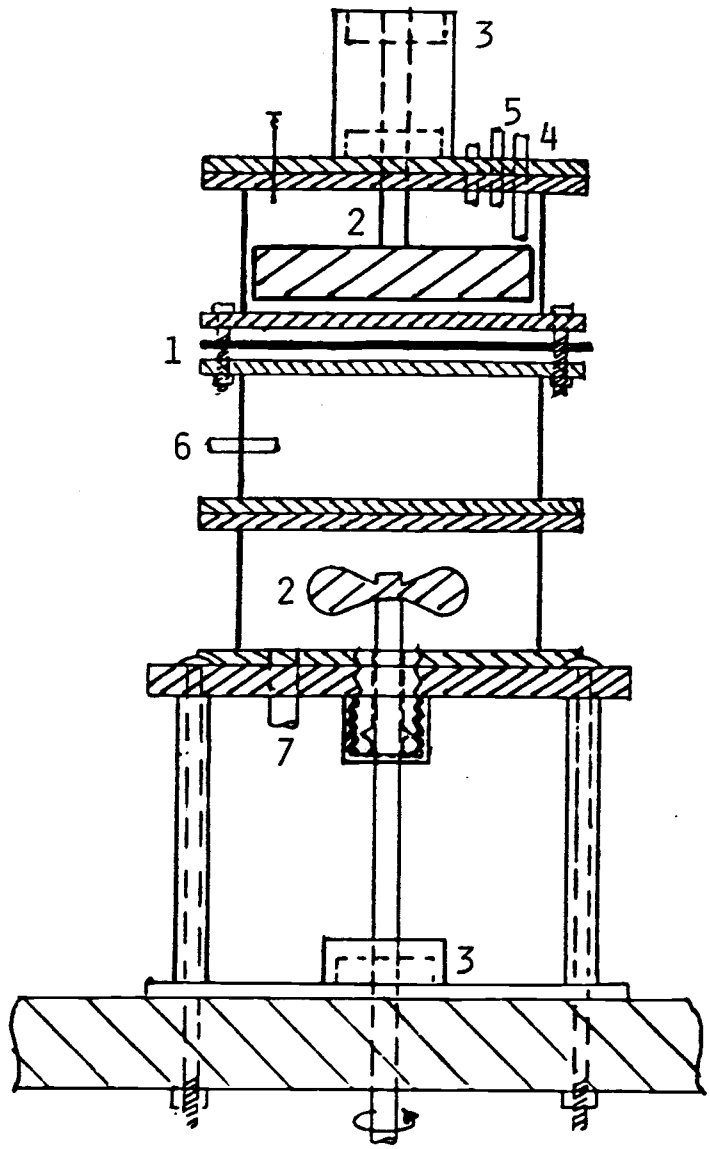

Figure (3.11). Godfrey cell. 1. Interface plate, 2. Impeller, 3. Bearing, 4, 5. Gas inlet and outlet, 6, 7. Liquid inlet and outlet.

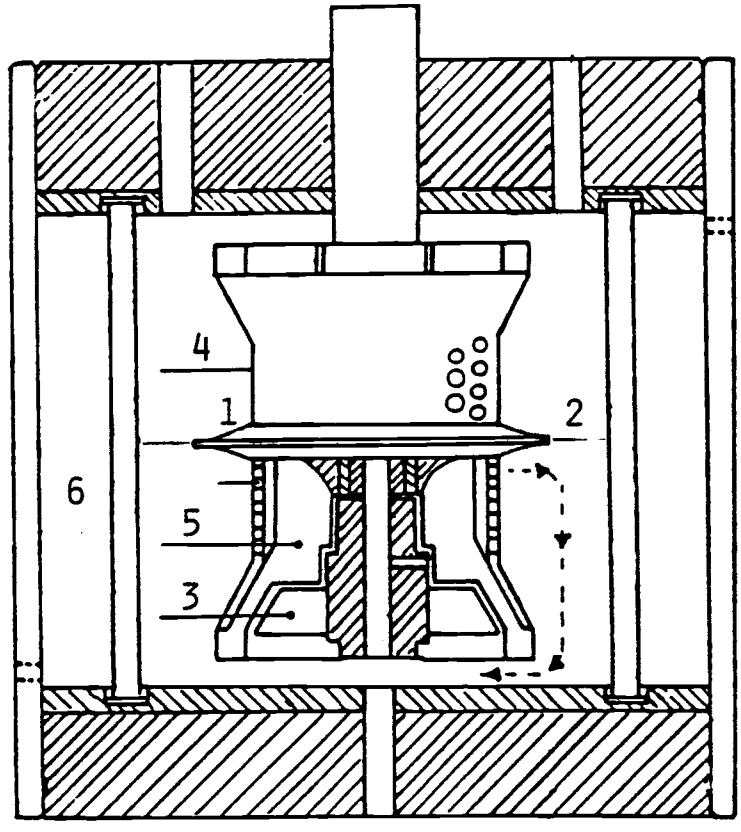

Figure (3.12). Landau and Chin cell. 1. Tapered ring, 2. Interface, 3. Impeller, 4. Perforated shell, 5. Baffles, 6. Jacket.

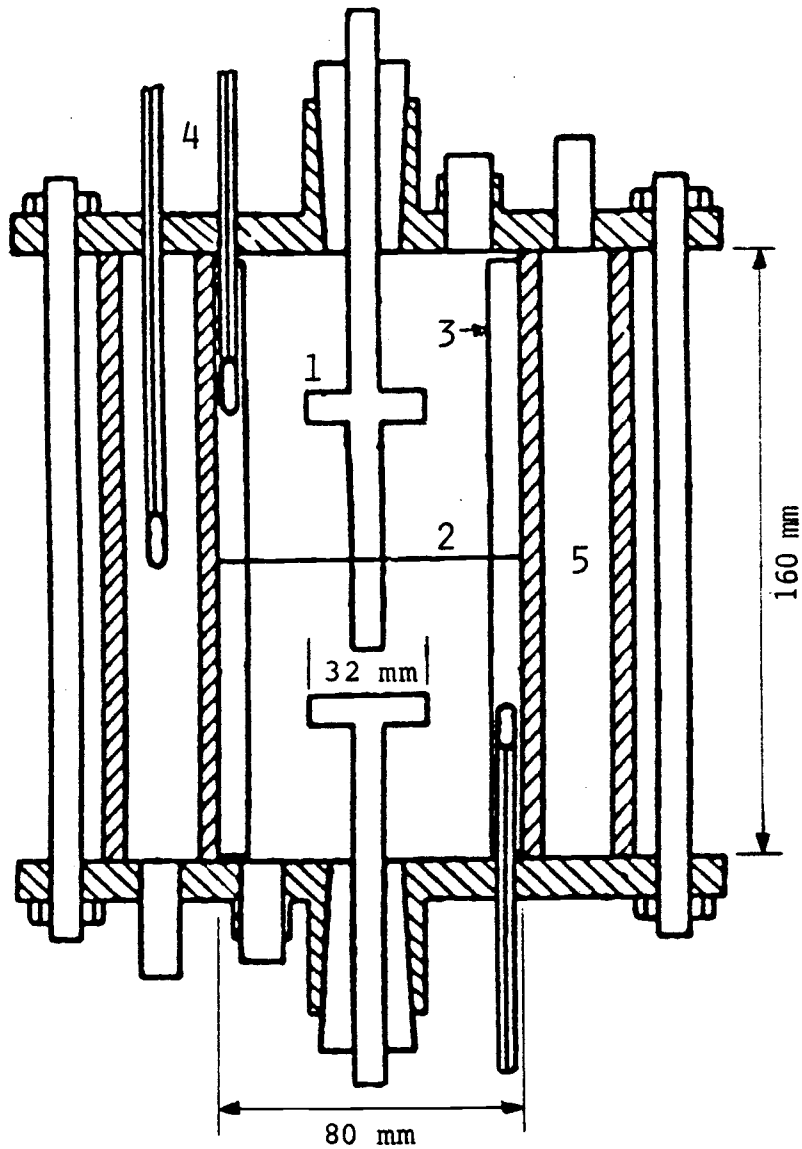

Figure (3.13). Asai et al cell. 1. Impeller, 2. Interface, 3. Baffles, 4. Thermometer, 5. Jacket.

them was used as a water jacket. Four equally spaced vertical glass baffles were attached to the wall. The stirrers were glass paddle agitators with two flat blades. The blades were placed at the middle of each phase. The upper rotating shaft was extended through the interface to near the middle of the liquid depth in the lower part of the cell to prevent vortex formation near the center of the interface. The cell was subjected to a surface wave motion, but the authors assumed that the surface wave affect on the mass transfer rate could be neglected.

9 - Hancil et al Cell

Hancil, Rod and Rettakova [19] in 1977 came up with a new cell to study mass transfer in liquid-liquid system as shown in Figure (3.14). It consisted of a cylindrical jacketed vessel. Each phase was mixed by a vibrating perforated plate. The vibration of the plate developed macroflow in each phase. The flow was directed by the shape of the perforations, which were oriented toward the interface. In this cell, the turbulence in each phase was affected independently by frequency, amplitude and the distance of the plates from the interface. Both phases were dependently mixed, which would cause a limitation of the study. The interface might be easily subjected to wave motion.

10 - Versteeg et al Cell

Versteeg, Blauwhoff and Van Swaau [68] in 1987 studied the effect of mass diffusivity on gas-liquid mass transfer. Figure (3.15) shows the continuously operated cell. The gas phase was stirred with either two turbine impellers of four blades or two propeller impellers of four blades. The liquid phase was stirred

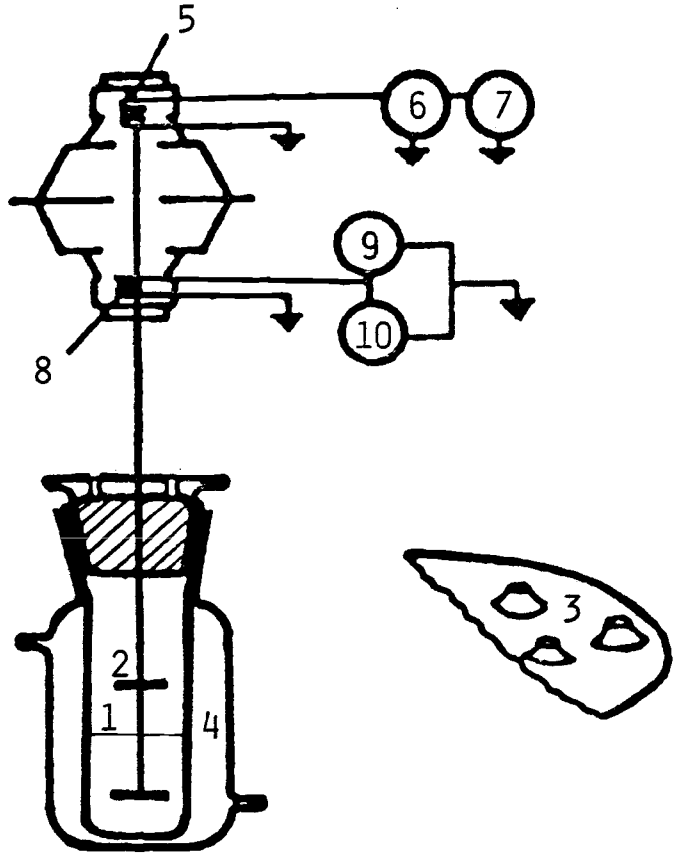

Figure (3.14). Hancil et al cell. 1. Interface, 2. Perforated plates, 3. Detail of plate perforations, 4. Jacket, 5. Moving coil of the driving loudspeaker, 6. Amplifier, 7. Sine-wave generator, 8. Moving coil of the measuring loudspeaker, 9. Electronic voltmeter, 10. Oscilloscope.

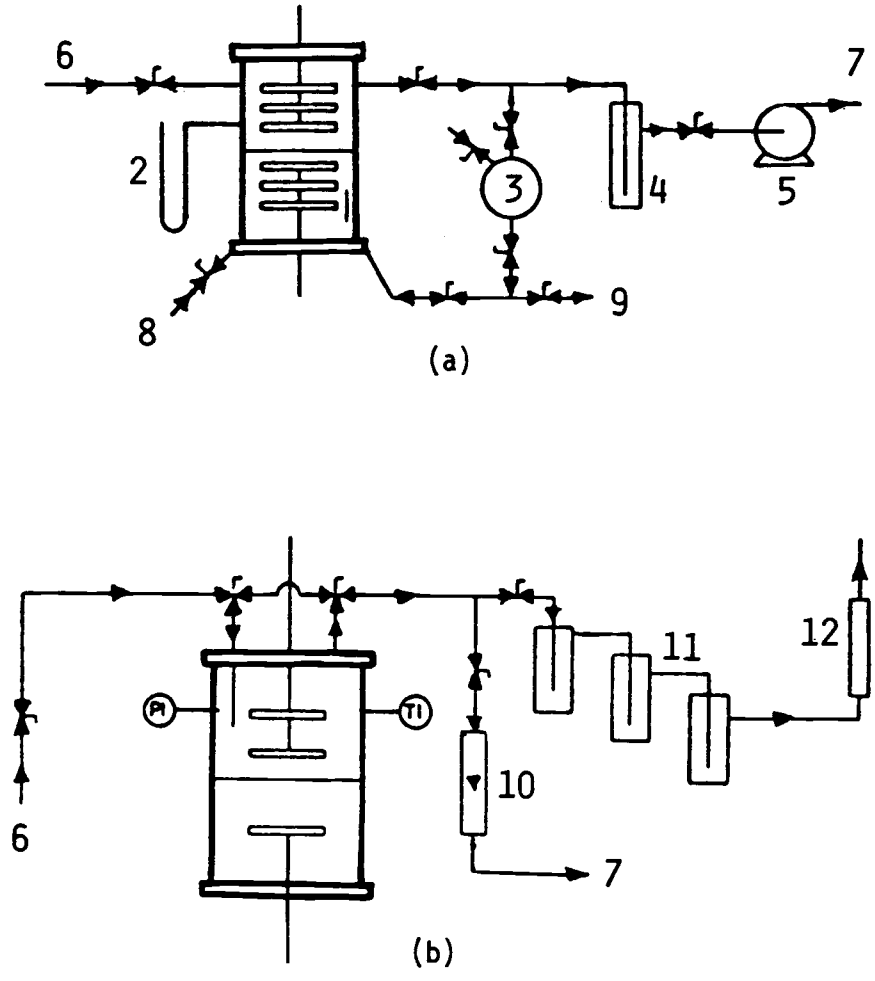

Figure (3.15). Versteeg et al cell. a. Liquid phase system, b. Gas phase system. 1. Impeller, 2. Manometer, 3. Degasing vessel, 4. Cold trap, 5. Vaccum pump, 6, 7. Gas inlet and outlet, 8, 9. Liquid inlet and outlet, 10. Flowmeter, 11. Glass bubblers, 12. Soap film meter.

with one turbine or propeller impeller of four blades for the gas mass transfer coefficient measurements. For liquid mass transfer coefficient measurement, the gas phase and the liquid phase were stirred with three turbine impellers of four blades. The interface was easily subjected to wave motion.

3.2.2 The Column Equipments

There were many types of mass transfer equipment columns which have been used in experimental investigations; these columns had different design and used different techniques than those used in the stirred cell. The common apparatuses were:

1 - Colburn and Welsh Packed Column

Colburn and Welsh [7] in 1941 studied individual mass transfer resistance in counter current liquid-liquid packed column, as shown in Figure (3.16). It consisted of a glass cylinder, which was packed to a height of 21 inches with ceramic Rashing rings. The outlet line of the heavier solution was equipped with a swivel arm which could be easily raised or lowered to control the height of the interface. Both liquid phases were supplied from constant head tanks.

2 - Stephens and Morris Discs Column

Stephens and Morris [60] in 1951 studied liquid film absorption in a column, as shown in Figure (3.17). It consisted of discs enclosed in a glass tube. Lynn, Straatemeier and Kramers [40] used the same technique, but instead of discs, they used spheres, as shown in Figure (3.18). The discs or spheres were supported by a thin wire suspended vertically in a column. The liquid flowed over the discs or spheres from the top countercurrent to the rising gas phase. In

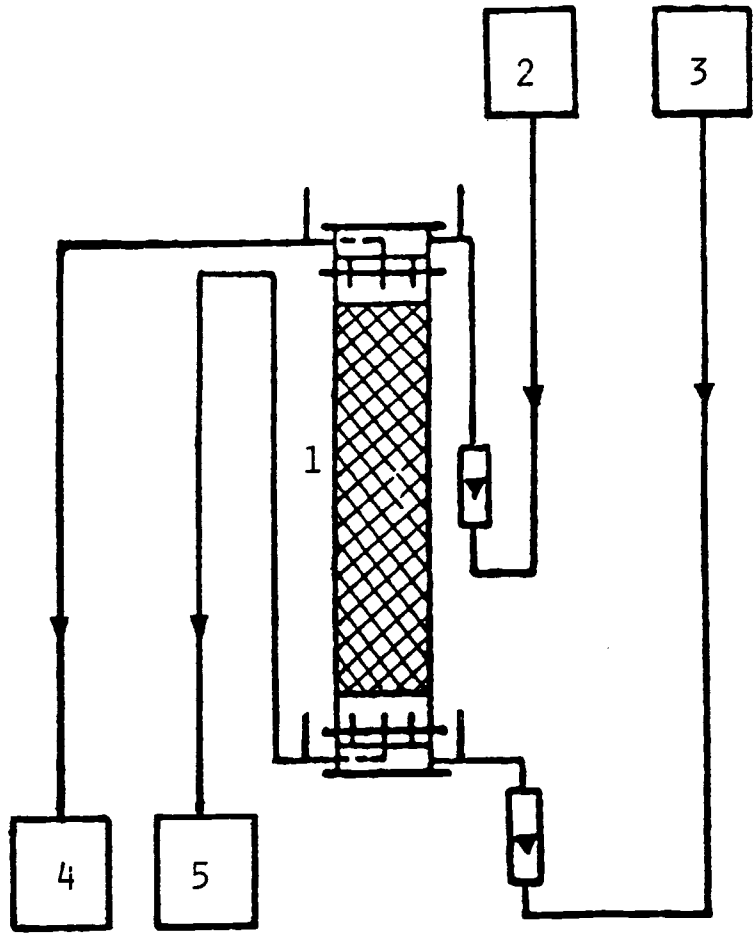

Figure (3.16). Colburn and Welsh packed column. 1. Packed column, 2, 5. Water supply and receiving tank, 3, 4. Organic supply and receiving tank.

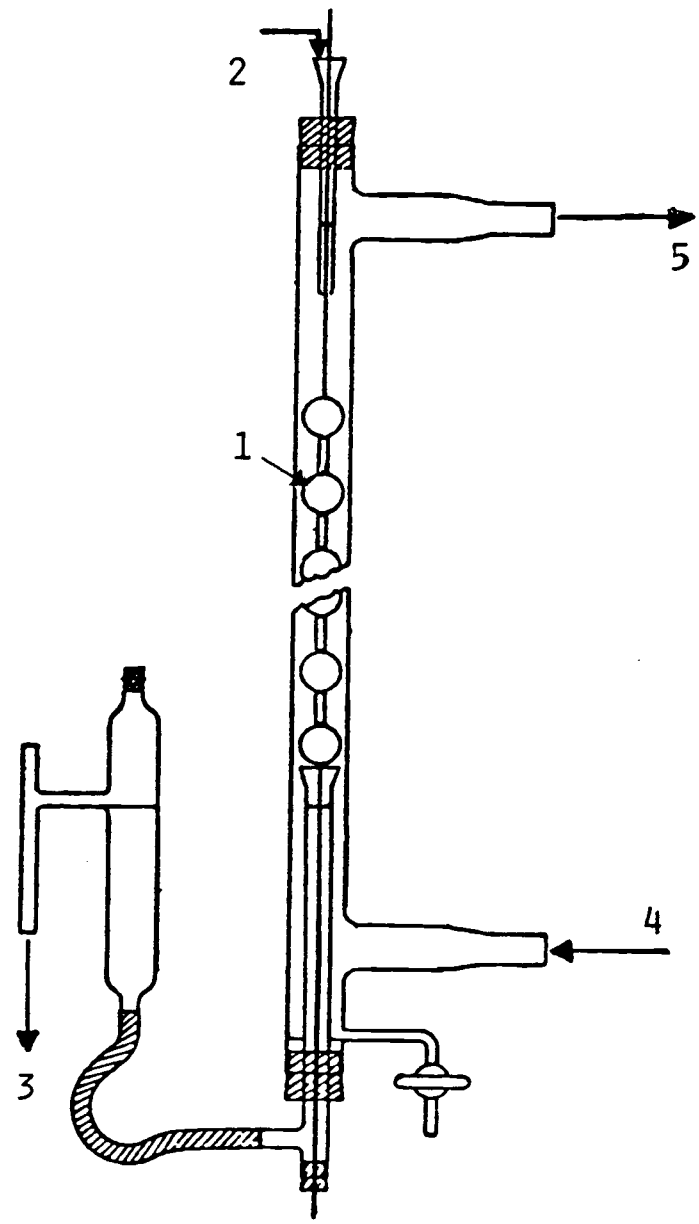

Figure (3.17). Stephens and Morris wetted discs column.
1. Discs, 2, 3. Liquid inlet and outlet,
3, 4. Gas inlet and outlet.

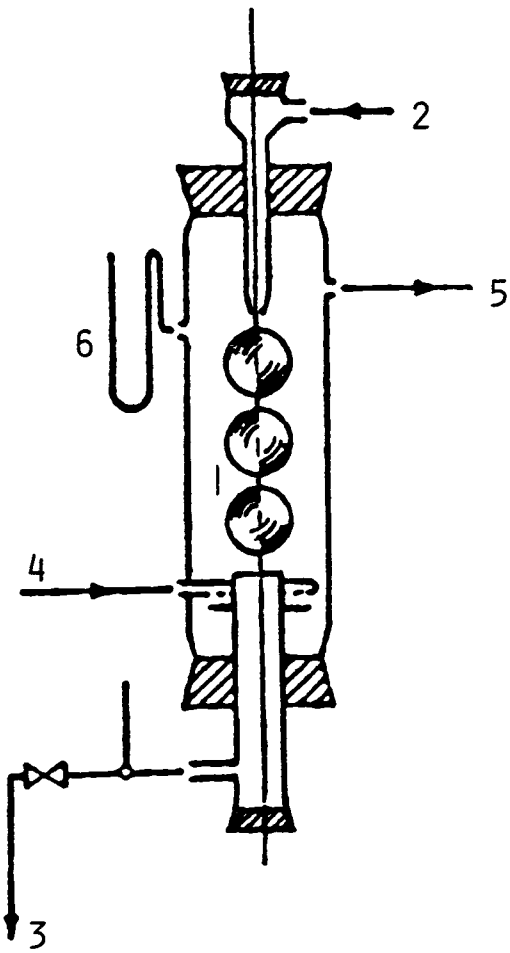

Figure (3.18). Lynn et al wetted spheres column. 1. Spheres, 2, 3. Water inlet and outlet, 4,5. Gas inlet and outlet, 6. Manometer.

this apparatus the amount of mixing that occurred within each phase was not well defined.

3 - Murdoch and Pratt Wetted Wall Column

Murdoch and Pratt [48] in 1953 used a wetted-wall column in their studies of the rate of transfer of uranyl nitrate between water and another solvent. The column is shown in Figure (3.19). Water and organic phases were pumped to the column. Although the hydrodynamics behavior of this type of column is less well understood for liquid-liquid systems gas-liquid systems, it has been used since it is considerably less complex than that of packed column.

4 - Vermijs and Kramers Rotating Disc Column

Vermijs and Kramers [67] in 1954 studied liquid-liquid extraction in a rotating disc contactor (RDC). It is shown in Figure (3.20). It consisted of a vertical cylindrical tube fitted with a number of horizontal flat rings spaced at equal distances. The coaxially mounted rotor was provided with a number of equally spaced flat discs.

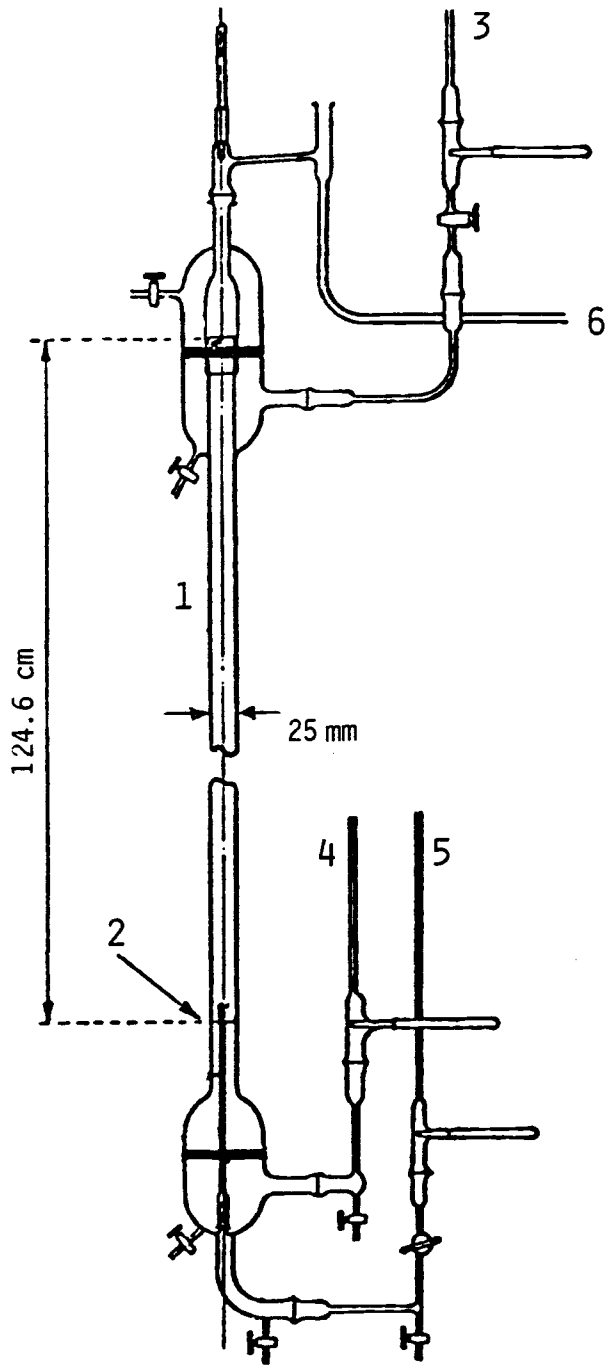

Figure (3.19). Murdoch and Pratt wetted wall column. 1. Column, 2. Interface level, 3, 4. Aqueous inlet and outlet, 5, 6. Organic inlet and outlet.

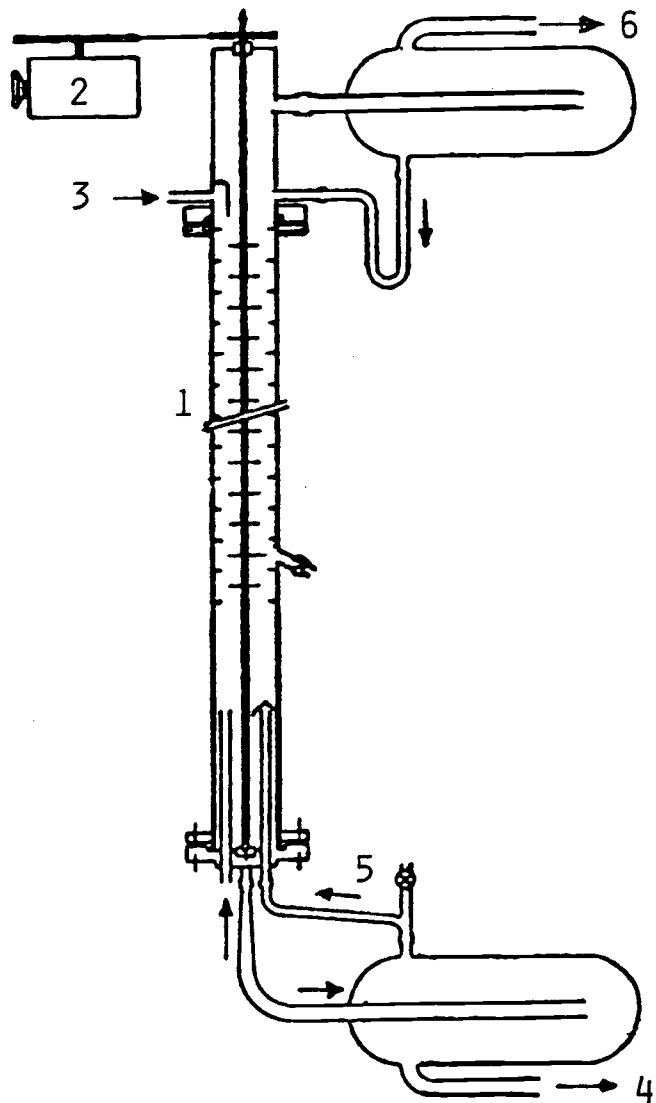

Figure (3.20). Vermijs and Kramers rotating disc contactor. 1. Column, 2. Motor, 3, 4. Water inlet and outlet, 5, 6. Organic inlet and outlet.

Chapter 4

The Equipment Design, Construction and Testing

Mass transfer into agitated fluid phase equipments more closely approaches the operating conditions within industrial equipment in which the agitation of the liquid phase involves turbulent flow over vertical or horizontal surfaces, bubbling of gases through the liquid phase, mechanical agitation of the liquid phase, spraying of the liquid into the gas phase or combination of any of the above. A stirred cell has been chosen for the purpose of the mass transfer studies, since it provides the following:

1 - Well-defined interfacial area

2 - Sufficient mixing of each phase

3 - Easily varied stirred rate, which provides variable Reynold numbers in each phase.

4 - The flexibility to study wide range of variables that affect mass transfer coefficients.

4.1 Description of the Design and Construction

The cell was designed to be flexible enough for studying the variables affecting mass transfer of any two fluid phase systems with and without chemical reaction. Such a design has the following cell features:

1 - It consists of two sections, geometrically identical.

2 - It should be able to be operated as either a batch process or a continuous process.

3 - It should be constructed from transparent plastic, so that the stability of the interface can be observed.

4 - Adequate mixing of both phases should be provided to give a uniform concentration throughout each cell section.

5 - The mixing of each cell should be controlled independently; the impellers should have the ability to rotate at variable speed in both directions.

6 - A stable interface should be obtainable with the use of various interface plates, providing different interfacial area.

7 - The cell should be designed to permit change in the configuration of the baffles and the cylindrical wiremesh around the impeller in each cell section.

8 - The cell should be designed to provide an easy change in the type of the impeller in each cell section.

9 - It should have constant temperature and constant pressure control for the gas-liquid system.

This flexible design was chosen to enable the study of a wide range of variables affecting the mass transfer rate.

The following description of the design and construction is divided into three main headings; the cell, the liquid systems and the support structure.

4.1.1 The Cell

1 - The Body of the Cell

Each of the two sections of the cell, being 100 mm inside-diameter by 50 mm high, as shown in Figure (4.1a, b), was constructed

of transparent acrylic plastic. The volume of each cell section was 392 cm^3. Each cell section had a transparent acrylic plastic cap of 112 mm outside diameter by 18 mm thick. The cap had a 6 mm recess into which the cell shell was glued. Each cap had a 6 mm hole in the center, through which the impeller shaft entered the cell. To accommodate a shaft seal and 12.7 diameter part of the shaft, two recessed steps were machined into the outside center of the cell cap. The shaft recess was 13 mm in diameter and 9 mm deep. The seal recess was 25.4 mm in diameter and 8 mm deep. A sample port was drilled 44.7 mm away from the center of each cap. It was drilled with an 8.7 mm (11/32 in.) steel drill and tapped by a 6.4 mm (1/4 in.) pipe thread tap to make a 13 mm deep hole. The remaining 5 mm was drilled to form a 3.5 mm hole into the cell so that the sampling needle could pass through it. Samples were drawn through a diaphram mounted in a stainless steel fitting which is fitted in the threaded sampling hole in each cap.

Two holes of 8.7 mm (11/32 in.) in diameter were drilled and tapped by 6.4 mm (1/4 in.) pipe thread to 12 mm into each cap. One of them was 23 mm away from the cap center, this was for the inlet stream to the cell. The other was 44.7 mm away from the center, which was for the outlet stream.

The other end of each cell shell section was designed to hold various shapes of interface plates. Each end had an acrylic plastic flange of 152 mm O.D glued to it. Eight holes of 5 mm diameter were drilled equally spaced around the circumference of each flange to fix the interface plate and its gasket. A 113 mm I.D. and 5 mm wide

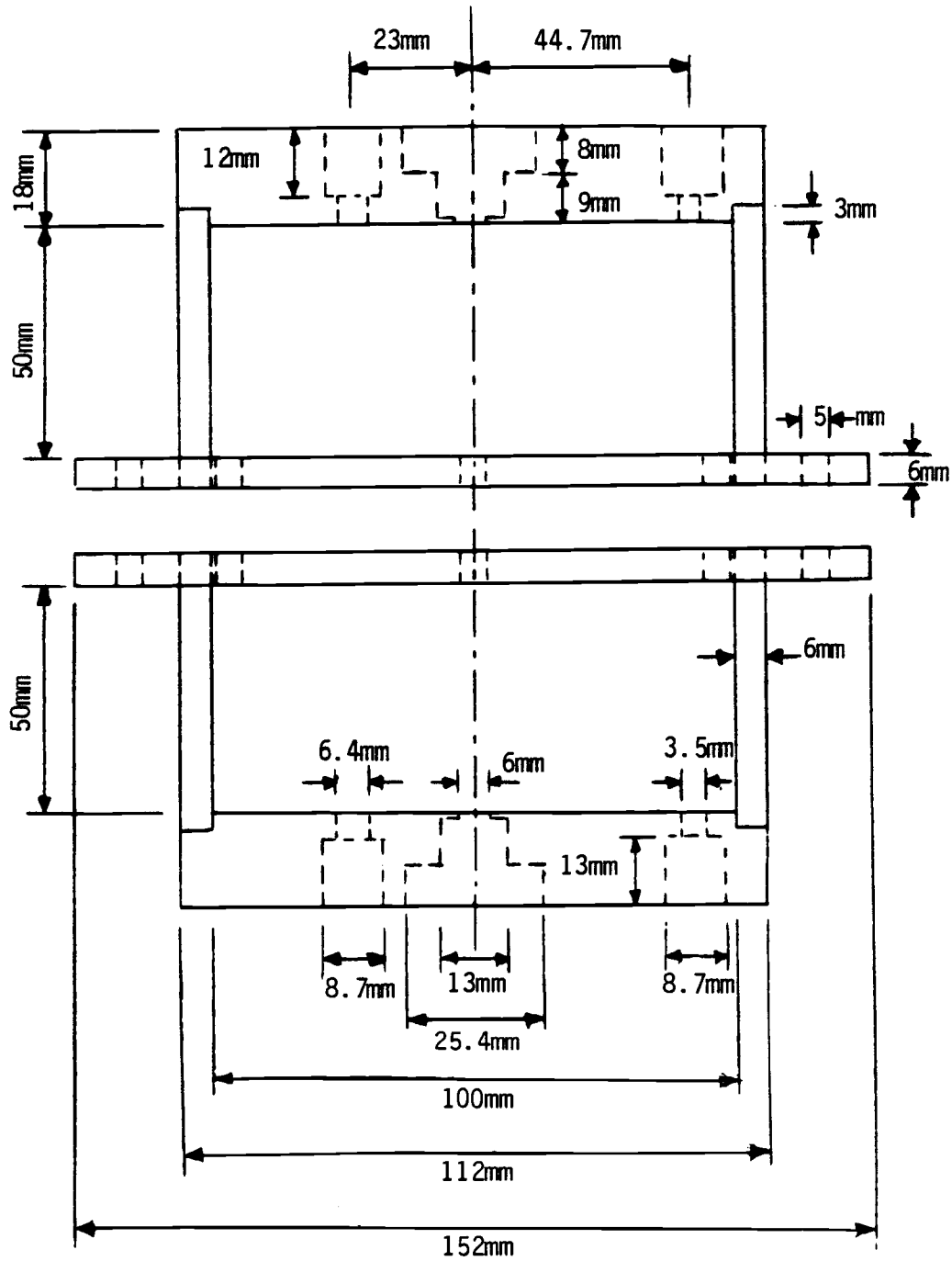

Figure (4.1a). Side view of the experimental cell body.
Scale 1/1.25

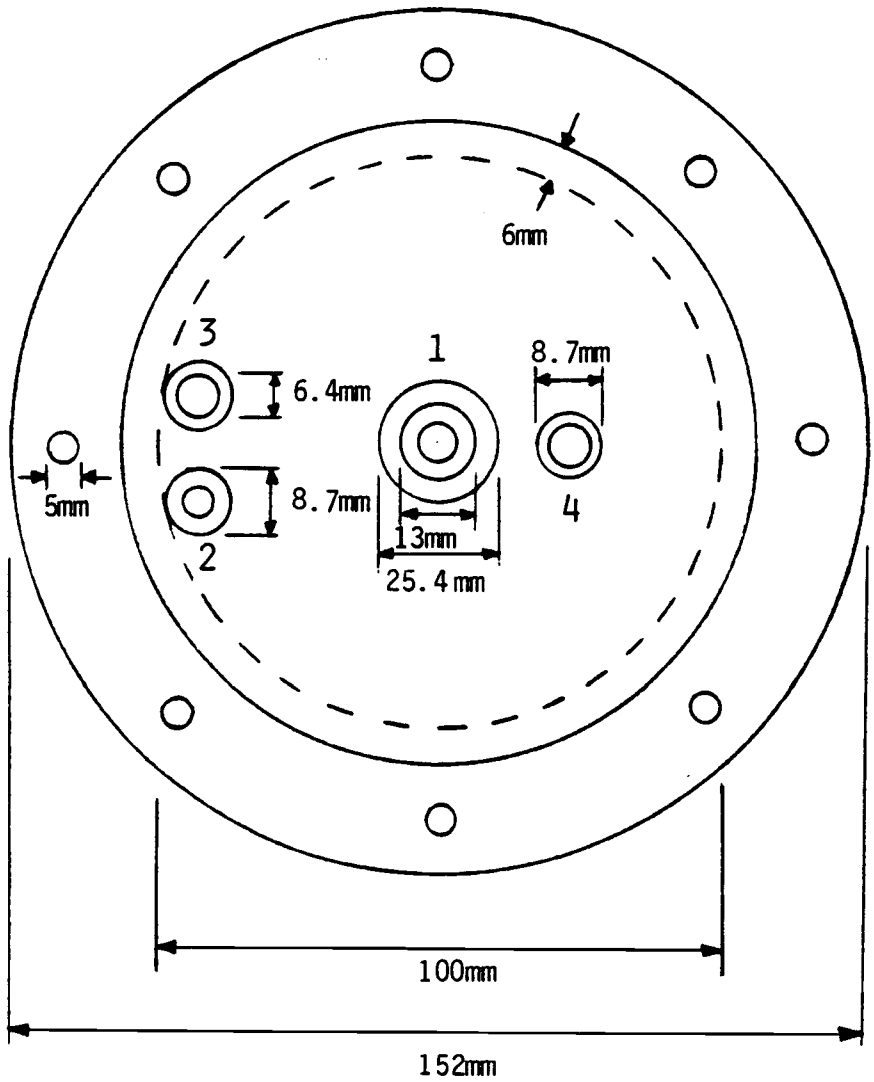

Figure (4.1b). Top view of the experimental cell body.
1. Shaft inlet, 2. Sampling port,
3. Outlet stream, 4. Inlet stream.
Scale 1/1.25

rubber gasket was used between the two cell flanges to prevent leakage. Temperature controlling jacket was not designed and constructed due to the desire to observe the interface stability. Accordingly the cell operation was done at room temperature.

2 - Interface Plate

Although various shapes of interface plates could be used with the cell, the stainless steel interface plate of 0.8 mm thick, shown in Figure (4.2) was designed to be used in this cell. It was chosen to be thin to let the turbulence eddies reach the interface from both contacting phases, and rigid to avoid its vibration, which causes interface rippling. It consisted of three annular open areas. The annular opening was of 12.5 mm in width between the inside cell wall and the central solid part of the interface plate, which was 75 mm in diameter. The total interfacial area formed by the three annular open areas is approximately 31.6 $cm.^2$

3 - Mixing of the Cell Fluid Phases

The mixing in each fluid phase was one of the critical parts of mass transfer studies in this kind of equipment. In liquid mixing there must be: (1) overall bulk or convective flow and (2) a reduction in inhomogeneities. It is convenient to classify the mixing mechanisms into the following [23]:

a - Laminar mixing

Laminar mixing is associated normally with high viscosity liquids. Viscosities required for laminar mixing are greater than about 10 Pa.s. In laminar mixing inertial forces quickly die out under the action of the high viscosity. Therefore, a large impeller

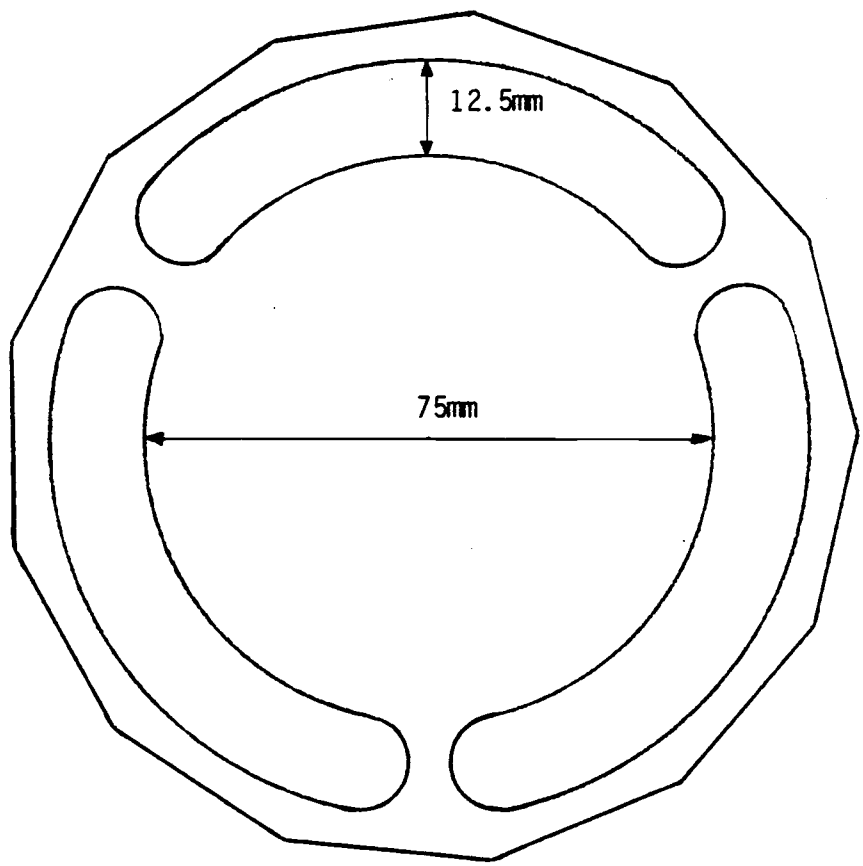

Figure (4.2). Interface plate. Scale 1/1

diameter is required to achieve adequate bulk motion. Large velocity gradient exist close to the rotating surfaces. Molecular diffusion is occurring, which is required to achieve ultimate homogenization of miscible fluids.

b - Turbulent Mixing

For all practical purposes, the fluid mixing is turbulent if the fluid viscosity is less than about 10 mPa.s. The inertia imparted to the fluid by the rotating impeller is sufficient to circulate the fluid throughout the vessel and back to the impeller again. During the fluid's mixing, turbulent eddy diffusion takes place, which is at its maximum in the impeller region. The rate of mixing associated with the turbulent mixing is much more than that associated with the laminar mixing. Molecular diffusion is also required here for the homogenization at the molecular scale; but it is much faster in the low-viscosity fluids than in the high-viscosity liquids. The rate of mixing or homogenization of the miscible fluids is greatest near the impeller since there are a high-shear rate, large Reynolds stresses and a high portion of the energy introduced by the impeller is dissipated.

The hydrodynamic conditions of the mixing in the designed cell were affected mostly by the impeller type, its position away from the interface and the baffles configurations around the impeller.

I - Impeller Mixing

The cell was designed to be mixed by some form of rotating impeller to achieve adequate stirring action in each phase, while maintaining a stable interface.

In impeller mixing [1, 23, 51, 66], there is a turbulent region of high shear near its blades. The essential mixing occurs at the high-velocity liquid streams. Slow-moving liquid is entrained by the current of the liquid velocity streams. Inside this current turbulent eddies exist and the entrained fluid is rapidly incorporated into the stream. The higher the velocity the more intense the turbulence and convection; the mixing action becomes more effective. In all impeller mixers a current of liquid is maintained by the rotating impeller. The velocity of the fluid streams leaving the impeller must be sufficient to carry portions of the fluid from all parts of the mixing vessel to the impeller region. The ratio of inertial forces to viscous forces needs to be high enough to prevent any viscous effects from damping out fluid motion. According to the purpose of the cell, the types of impeller and their position away from the interface must achieve the following:

1 - Adequate circulation so that the fluid can be carried to all parts of the cell section.

2 - Ample turbulence.

3 - Sufficient stability of the interface between the two mixed phases.

II - Types of Impellers

There are many different types of impellers used industrially, according to their application. Table (4.1) shows the range of impellers' application, depending upon the mixed phase viscosity [23]. It turns out that an impeller of propeller, turbine and paddle types should be used in the mixing of low viscosity fluids. Various

Table(4.1). Impeller Applications

Impeller	Range of Viscosities Applied for	Rotating Speed	Application
I - Propeller Turbine Paddle	< 2 kg/ms < 50 kg/ms < 1000 kg/ms	↑ viscosity decrease ↓ decrease	I - low viscosity bending - dispersing gases and liquids of low viscosity - liquid-liquid contacting - Suspending solid in low viscosity liquids
II - Anchor Helical ribbon Helical screw	high high high		II - high viscosity bending
III - Kneaders	very high		III - Blending pastes, rubbers, doughs - Dispersing fine solids in viscous liquids, etc.

types of these kind of impellers [66, 23] are shown in Figure (4.3).

Each one of these types were evaluated in the design of the cell for mass transfer studies.

III - Impellers Flow Pattern

The flow pattern of mixed fluid in the vessel produced by the propeller, turbine and paddle types could be axial, radial or both, as shown in Figure (4.4) [25]. The axial flow is the flow of mixed fluid parallel to the impeller shaft. The radial flow is the flow of the fluid along the impeller radius, or to the vessel wall in horizontal or radial direction. Axial flow impellers normally produce more flow per horsepower than that of radial flow impellers. Radial flow impellers produce strong top to bottom flow patterns from the radial discharge; when the vessel is unbaffled, swirling and vortexing may develop [51]. The flow pattern of mixed fluid depends on the following factors [23, 26, 51]:

1 - Impeller type

2 - The impeller size and its portion of the vessel

3 - The baffles around the impeller

4 - The fluid properties.

According to the impeller type, the propeller gives an axial flow pattern. Turbine and paddle give a radial flow pattern. if the turbine blades are angled to the vertical, a stronger axial flow component will be produced. Therefore, pitched blade turbine, which has a constant blade angle over its entire blade length gives both a stronger axial and a radial flow [23]. The radial component of its flow can predominate if the impeller is located close to the vessel

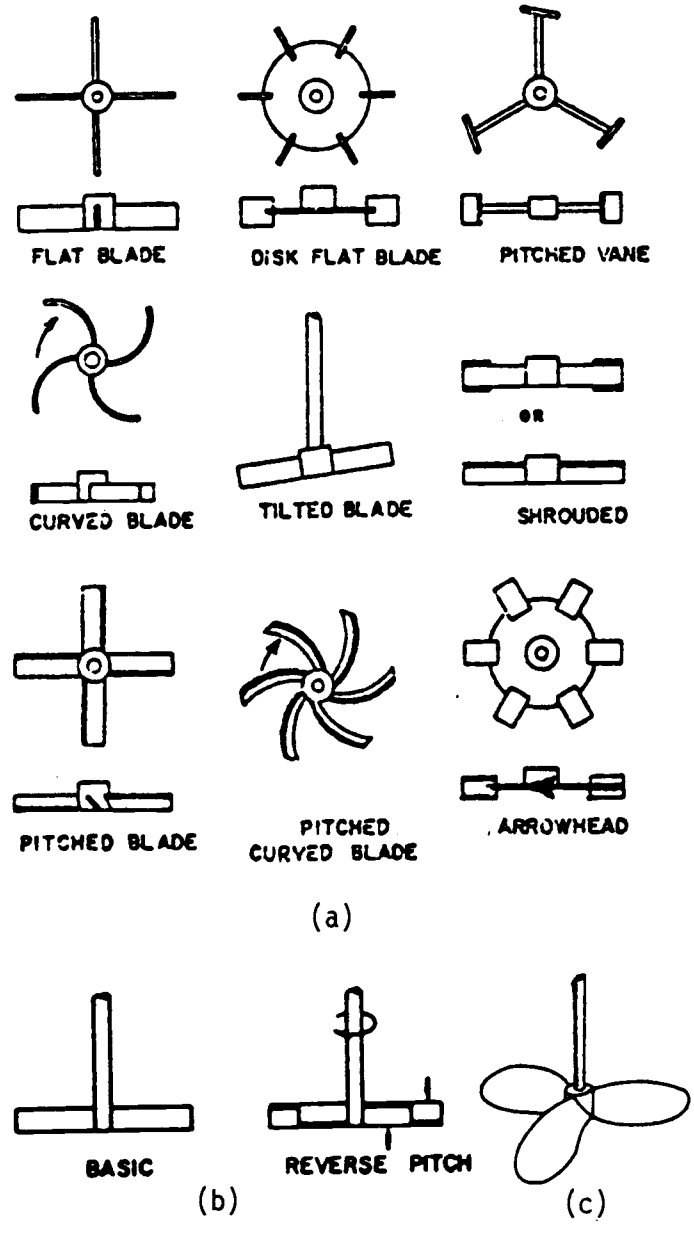

Figure (4.3). Various types of impellers. a - turbine, b - paddle, c - three-bladed propeller.

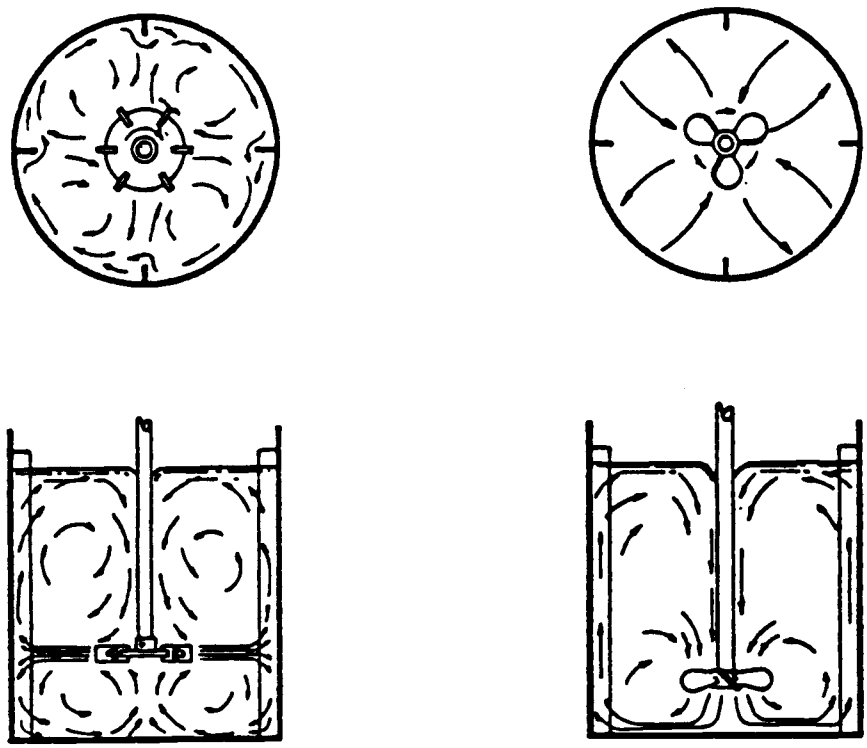

(a) radial flow pattern

(b) axial flow pattern

Figure (4.4). Radial and axial flow patterns.

bottom. The flat paddle produces a radial flow field with large tangential component velocity [23]. Axial and radial flow are useful but the tangential component has disadvantages.

4 - The Mixer Cell Unit Description

The mixer unit consisted of a motor and its controller, shaft and impeller. The motor was a 1/18-hp Dayton permanent magnet DC motor, model 42141. A stainless steel shaft of 12.7 mm (1/2 in.) diameter by 37 mm long was connected. The Dayton SCR motor controller unit contained a speed regulator knob and a direction reversing knob, which enables the impeller to be rotated at various speeds, either forward or backward in direction.

The impeller shaft was designed to be flexible enough to use with different types of impellers and to be mounted in different positions away from the interface by moving it upward or downward throughout its hole in the cell shell cap. As shown in Figure (4.5), it was constructed from a stainless steel rod of 12.7 mm (1/2 in.) in diameter. It consisted of two parts; the main part of 12.7 mm diameter by 50 mm long. It was connected with the motor shaft through a sleeve, 12.7 mm I.D. and 22.2 mm O.D. by 25.6 mm long. The sleeve tied the two shafts together. The other part of the mixer shaft was turned down to 5 mm in diameter by 33 mm long. The end of this section was threaded to No. 10 x 32 T.P.I. for 6.4 mm so that various types of impellers could be screwed in place.

Although various types of impellers could be used in this cell, the pitched-blade turbine was chosen. It provided the desired fluid

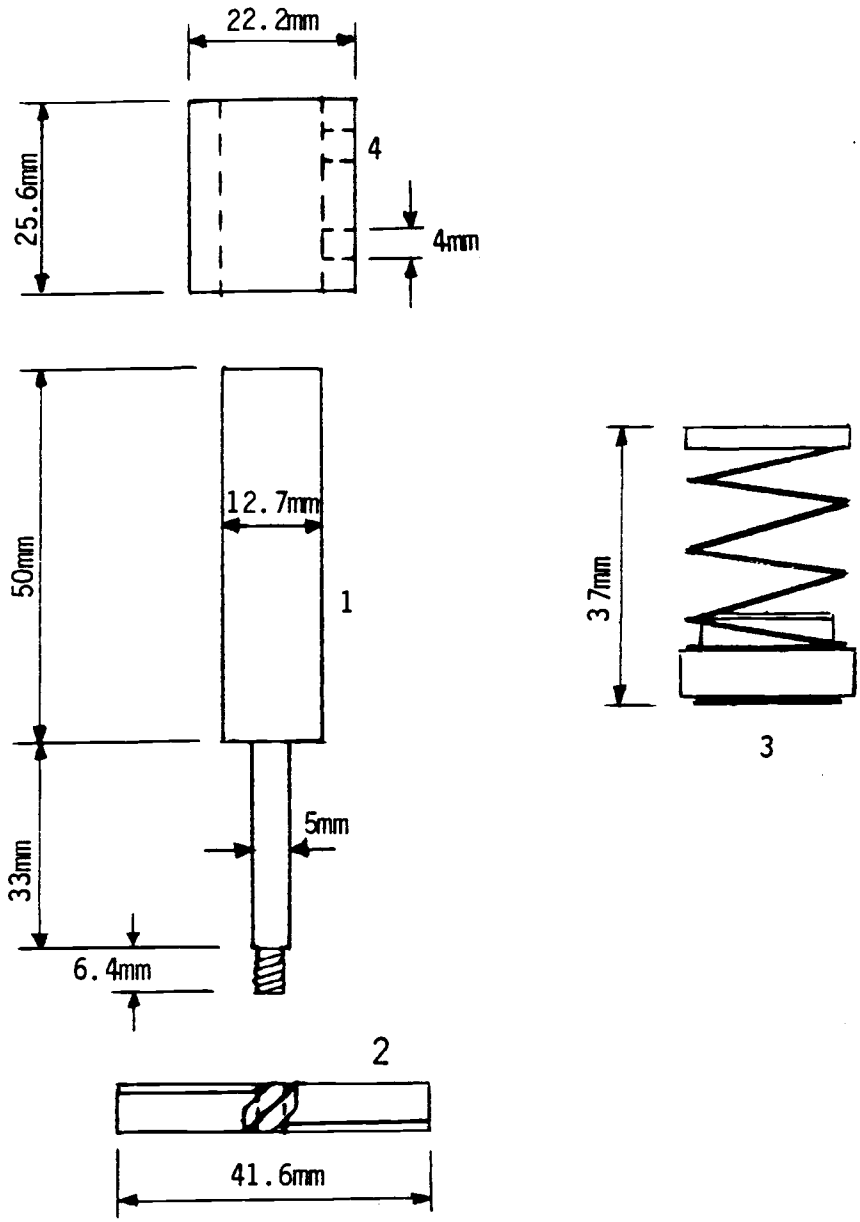

Figure (4.5). Impeller shaft. 1. shaft, 2. Pitched blade turbine, 3. Shaft sealing, 4. Sleeve. Scale 1/1

flow pattern, both axial and radial flow, which were needed to get a well-mixed phase with sufficient interfact stability. The axial flow is pumped toward the interface, while the radial flow is pumped around the cell circumference. By achieving this kind of a flow pattern, the transferred component was quickly carried away from the interface to the mixed bulk. The flow pattern required in the cell was achieved by both the pitched-blade turbine and the baffles' configuration around it, which will transfer the axial flow toward the interface to a radial one near it, as shown in Figure (4.6).

The pitched-blade turbine had four 45° inclined blades, with dimensions as listed in Table (4.2a). It did not represent the optimum dimensions, but it provided an ample mixing with sufficient interface stability over an adequate range of impeller revolutions per minute (rpm) needed for the investigation. Its dimensions were among the following: (1) The standard dimensions of the pitched-blade turbine used in industry, as shown in Table (4.2c), (2) Strake and Karcz dimensions [61] of the pitch-blade turbine, recommended as the optimum dimensions for their heat transfer investigation, as shown in Table (4.2d), (3) Bulicka and Prochazka [4] dimensions of the pitched-blade turbine, used in their cell, as shown in Table (4.2e), which was designed first as shown in Table (4.2b). The pitched-blade turbine was constructed by welding four stainless steel blades at a 45° angle to the stainless steel base of 6.4 mm O.D. and 3.5 mm tapped inside diameter, as shown in Figure (4.7). The blades base was machined from 12.7 mm (1/2 in.) stainless steel rod and tapped by (no. 10 x 32 T.P.I.).

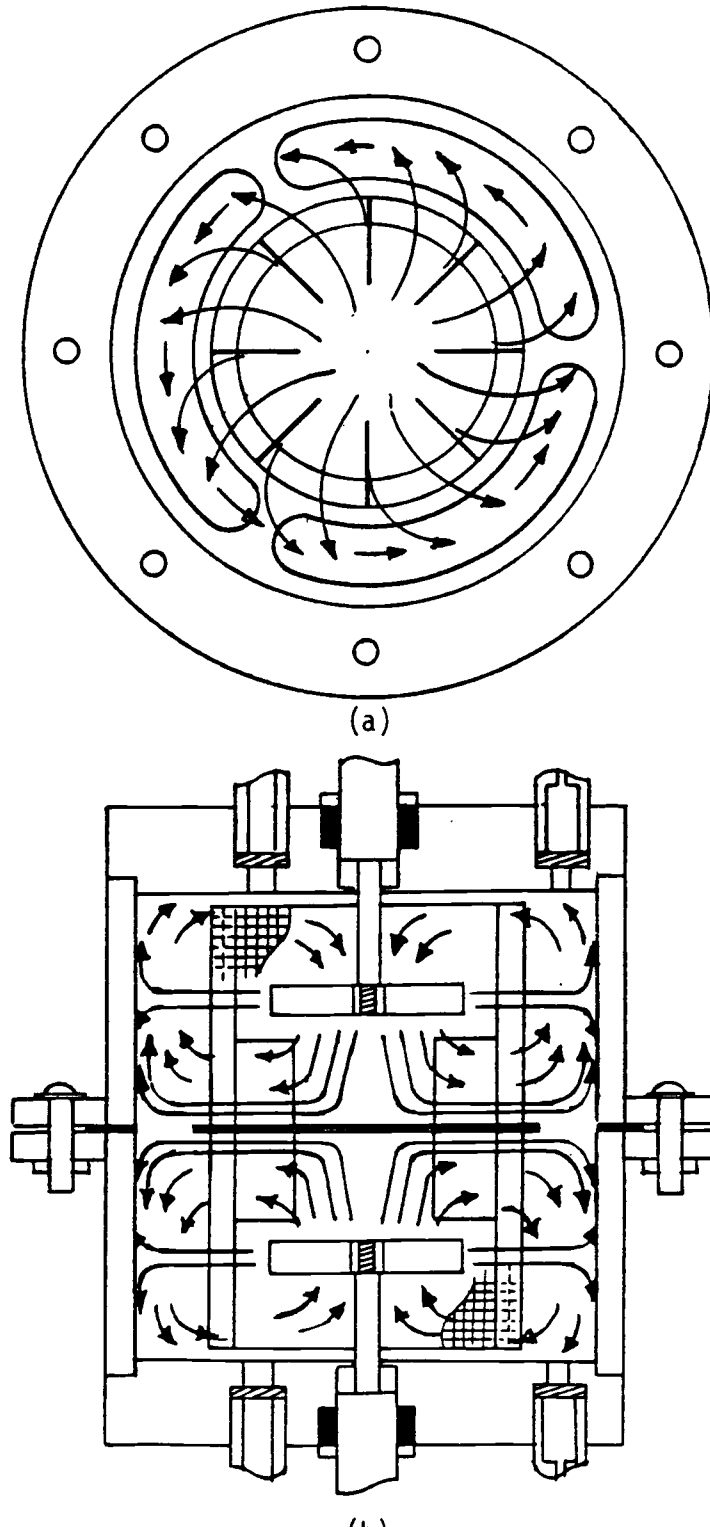

Figure (4.6). Experimental cell flow pattern. a. Flow pattern near the interface, b. Mixed bulk flow pattern

Table (4.2). Pitched Blade Turbine Dimensions

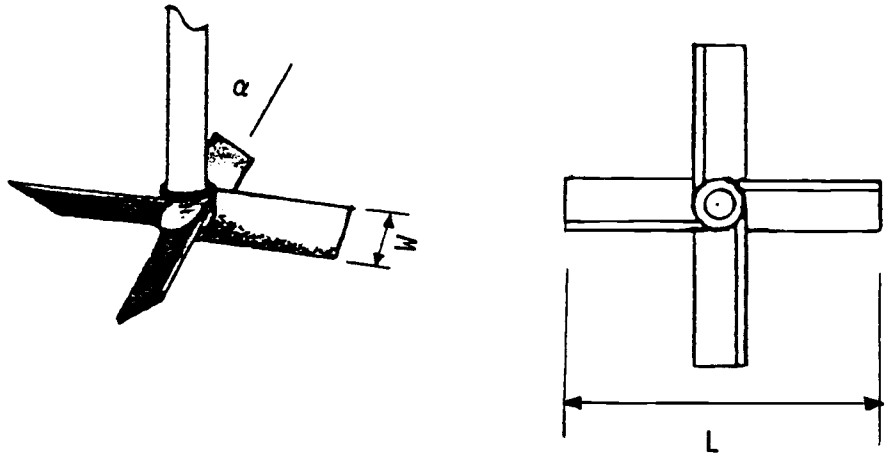

d = vessel diameter

Turbine	α	Blade Number	L	W
a - Used pitched blade	45°	4	0.416d	0.2L
b - Tested pitched blade	45°	4	0.45d	0.2L
c - Standard pitched blade (51, 26)	45°	4	0.33d	0.2L
d - Stake et al. pitched blade (61)	45°	4	0.5d	0.13L
e - Bulicka et al. pitched blade (4)	45°	4	0.45d	-

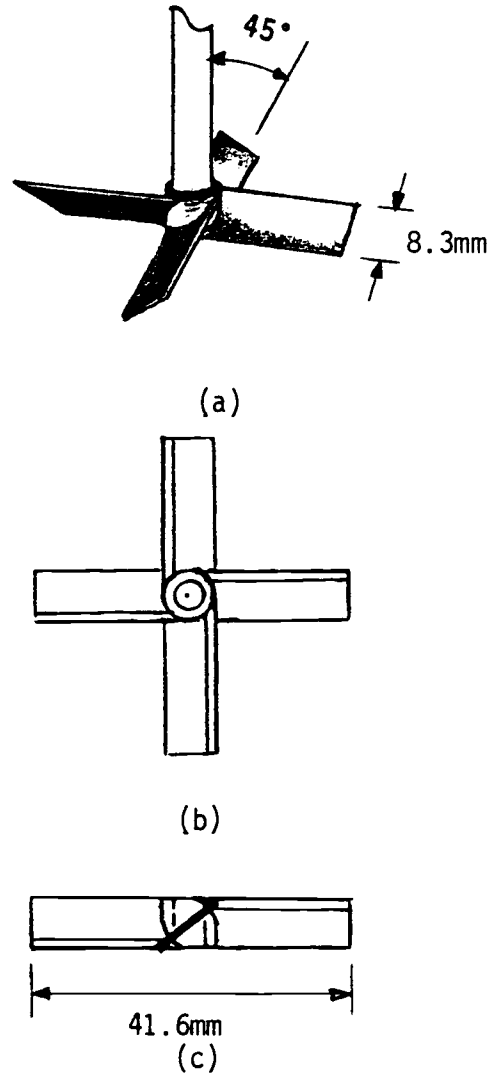

Figure (4.7). Pitched blade turbine . a.Turbine picture, b. Turbine top view, c. Turbine side view.

5 - Baffles and Wiremesh Cylinders

The grids of a wiremesh cylinder surrounding the impeller served to limit the size of eddies; accordingly, it facilitated the formation of a uniform turbulent flow structure. It was also used to eliminate any tangential velocity components of the bulk flow. The baffles were designed to transform the axial flow, leaving the impeller to a radial one near the interface. It also canceled the tangential velocity components.

Different configurations of both baffles and wiremesh cylinders combination were tested for good fluid circulation and interface stability at relatively high rotational speed of the impeller. The best combination that gave an adequate circulation of fluid and a sufficiently stable interface in each section, as is shown in Figure (4.8). It consisted of two stainless steel wiremesh cylinders, having a width of 2 mm square opening. These cylinders were mounted on the central solid part of the interface plate by an adhesive. The inner cylinder was 56 mm diameter by 48 mm high, while the outer cylinder was 68 mm diameter by 48 mm high. Eight stainless steel baffles of 4 mm in width were mounted between these two cylinders and were equally spaced around the impeller. Eight additional baffles, 13 mm width and 20 mm long, were vertically fixed by adhesive inside the inner cylinder. They were spaced equally and in line to the eight baffles in between the two cylinders.

Other forms of baffles and wiremesh cylinder combination in each cell section were tested and did not give the desired stability of the interface. These forms were:

1 - Two wiremesh cylinders placed only around the impeller of

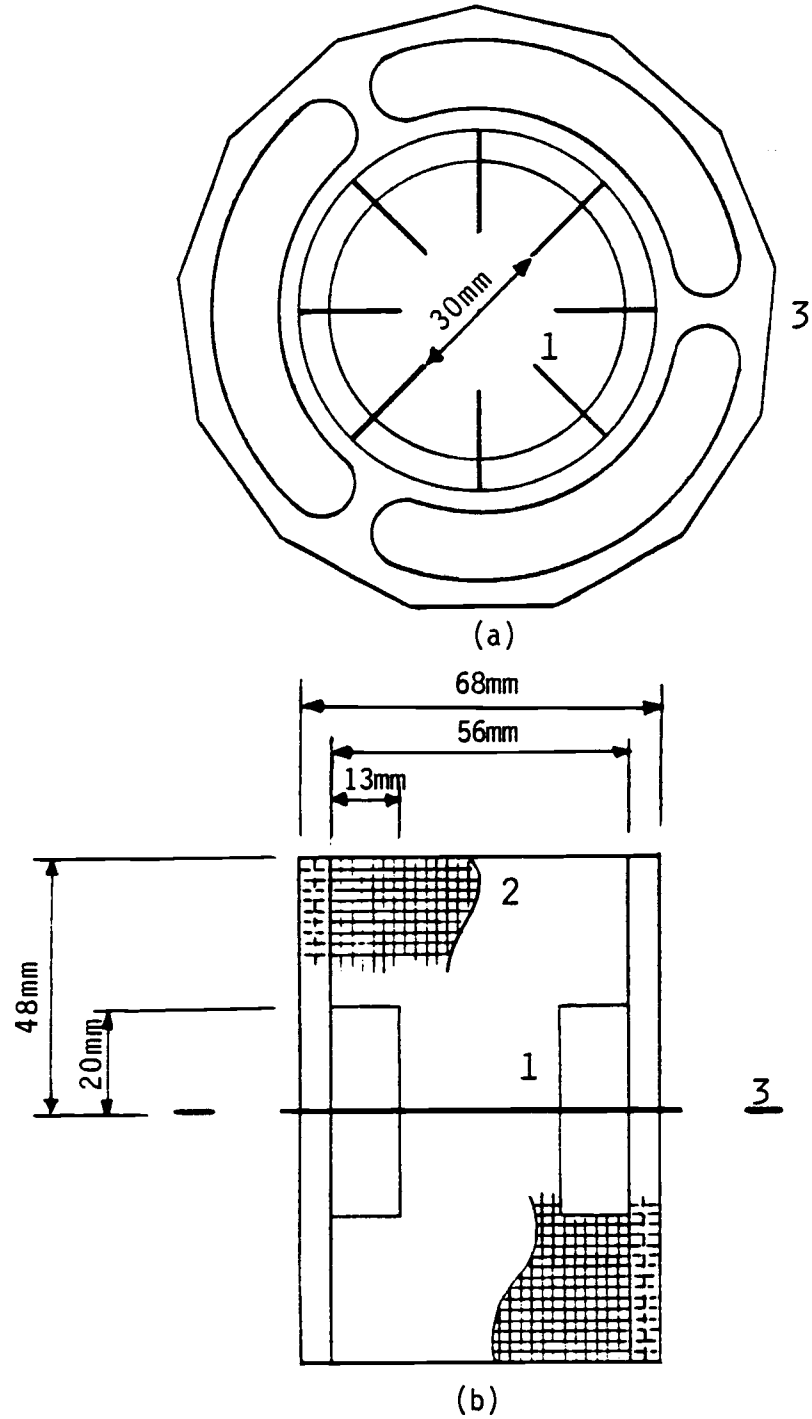

Figure (4.8). The cell baffles and wiremesh cylinders combination. a. Top view, b. Side view.
1. Baffles, 2. Wiremesh of 2mm square opening,
3. Interface plate. Scale 1/1.4

each cell section, as shown in Figure (4.9). The inner cylinder was of 56 mm diameter and 48 mm high; the outer cylinder was of 68 mm diameter and 30 mm high. The absence of vertical baffles produced high axial flow toward the interface, which caused interface rippling.

2 - Two wiremesh cylinders with four baffles between them and in the base of the inner cylinder, as shown in Figure (4.10). The baffles and the wiremesh cylinders of the same dimensions, as mentioned above, were used. This form of combination did not give the interfacial stability as obtained with the eight baffles.

3 - Two wiremesh cylinders with twelve baffles between the wiremesh cylinders and in the base of the inner cylinder, as shown in Figure (4.11). They had the same dimensions as mentioned above, except that inner baffles, 11 mm wide and 20 mm high were used. The narrow space between each baffle produced a high flow of fluid out of it to the interface. It produced interface ripples, even at low impeller speed.

4 - The same form and dimensions mentioned in (3) above, but adding an annular stainless steel disk, 18.6 mm inside diameter and 56 mm outside diameter, around the 12 baffles at a level of 10 mm above the interface plate as shown in Figure (4.12). This combination produced even higher observed flow out of the baffles adjacent to the interface than produced in the (3) combination, causing easily induced rippling.

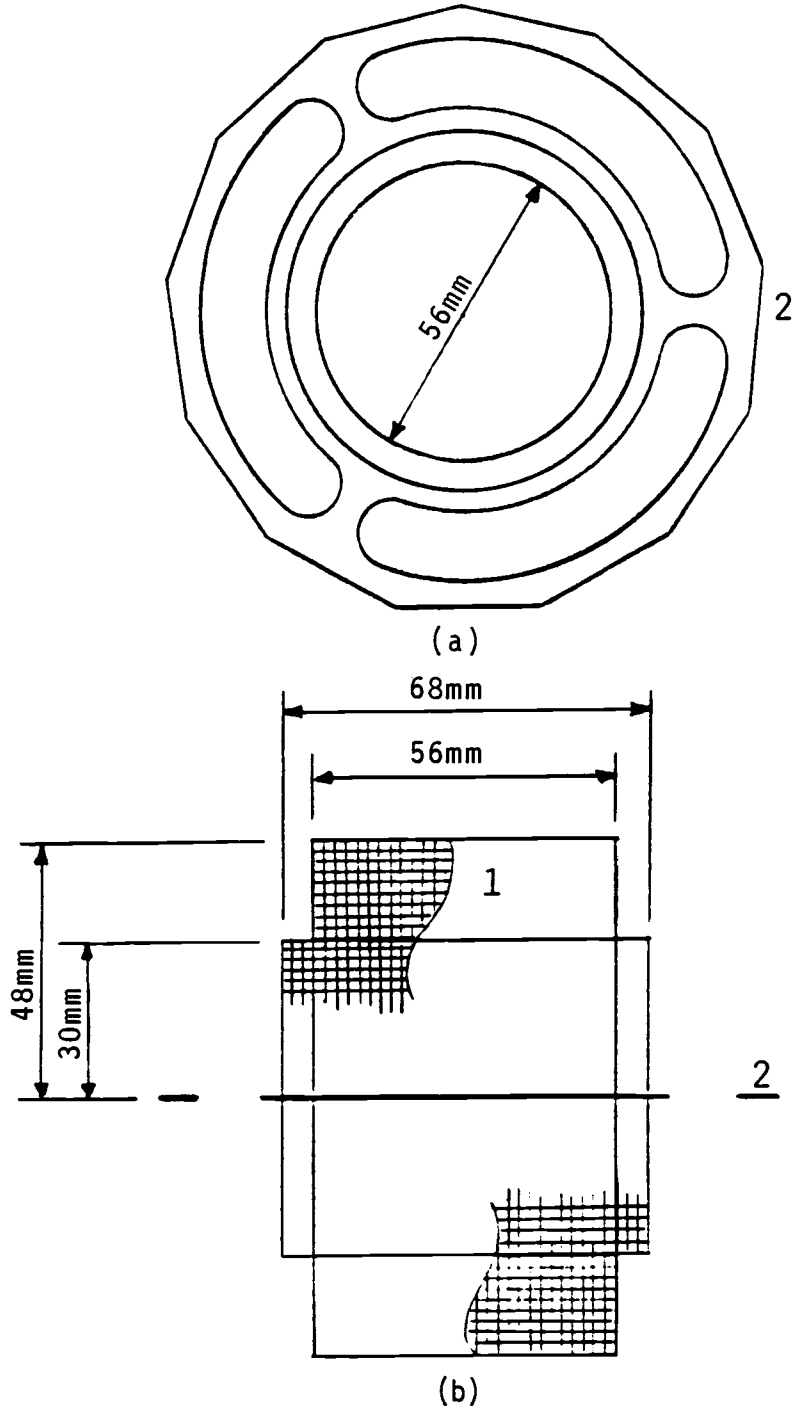

Figure (4.9). Wiremesh cylinders without baffles. a. Top view, b. Side view. 1. Wiremesh of 2mm square opening, 2. Interface plate. Scale 1/1.4

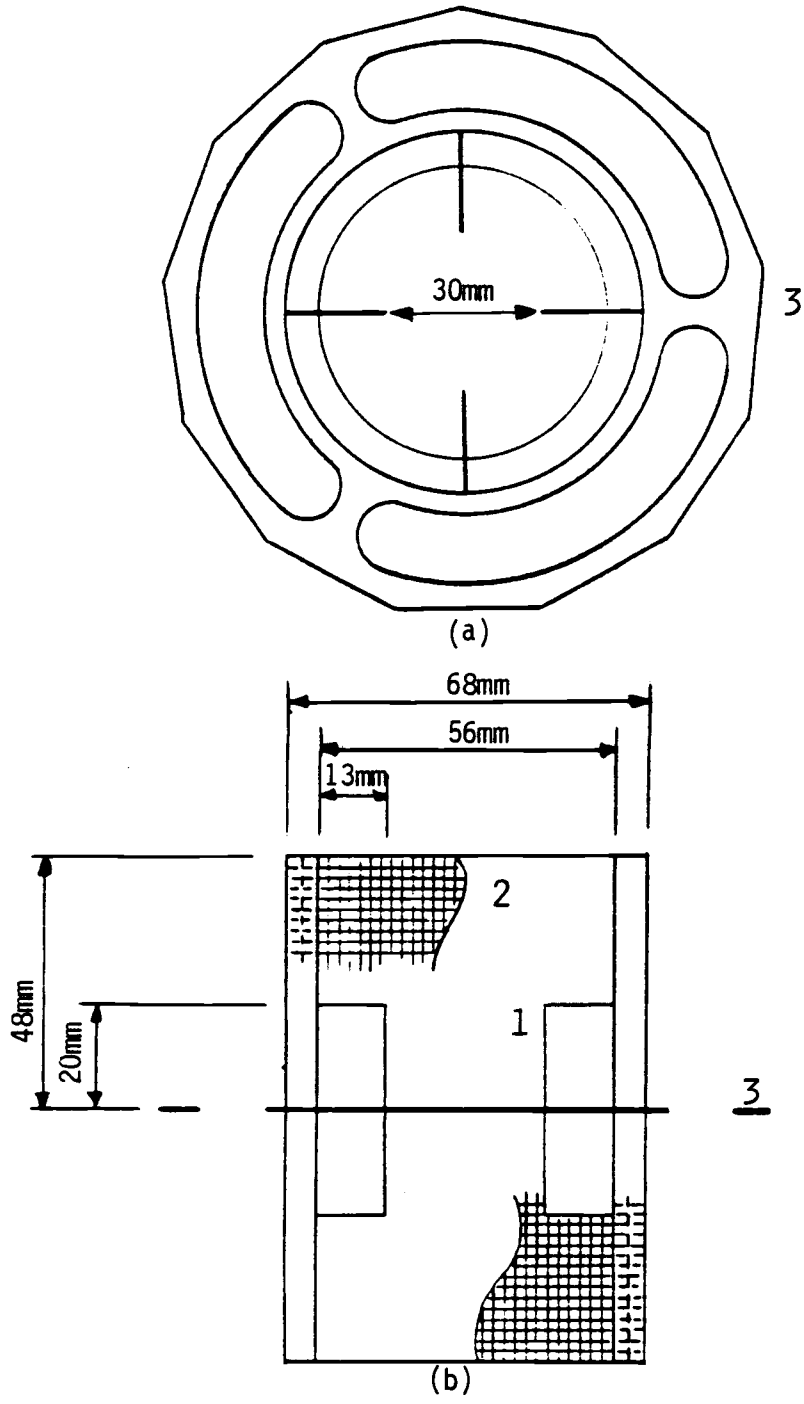

Figure (4.10). Four baffles and two wiremesh cylinders combination. a. Top view, b. Side view. 1. Baffles, 2. Wiremesh of 2mm square opening, 3. Interface plate. Scale 1/1.4

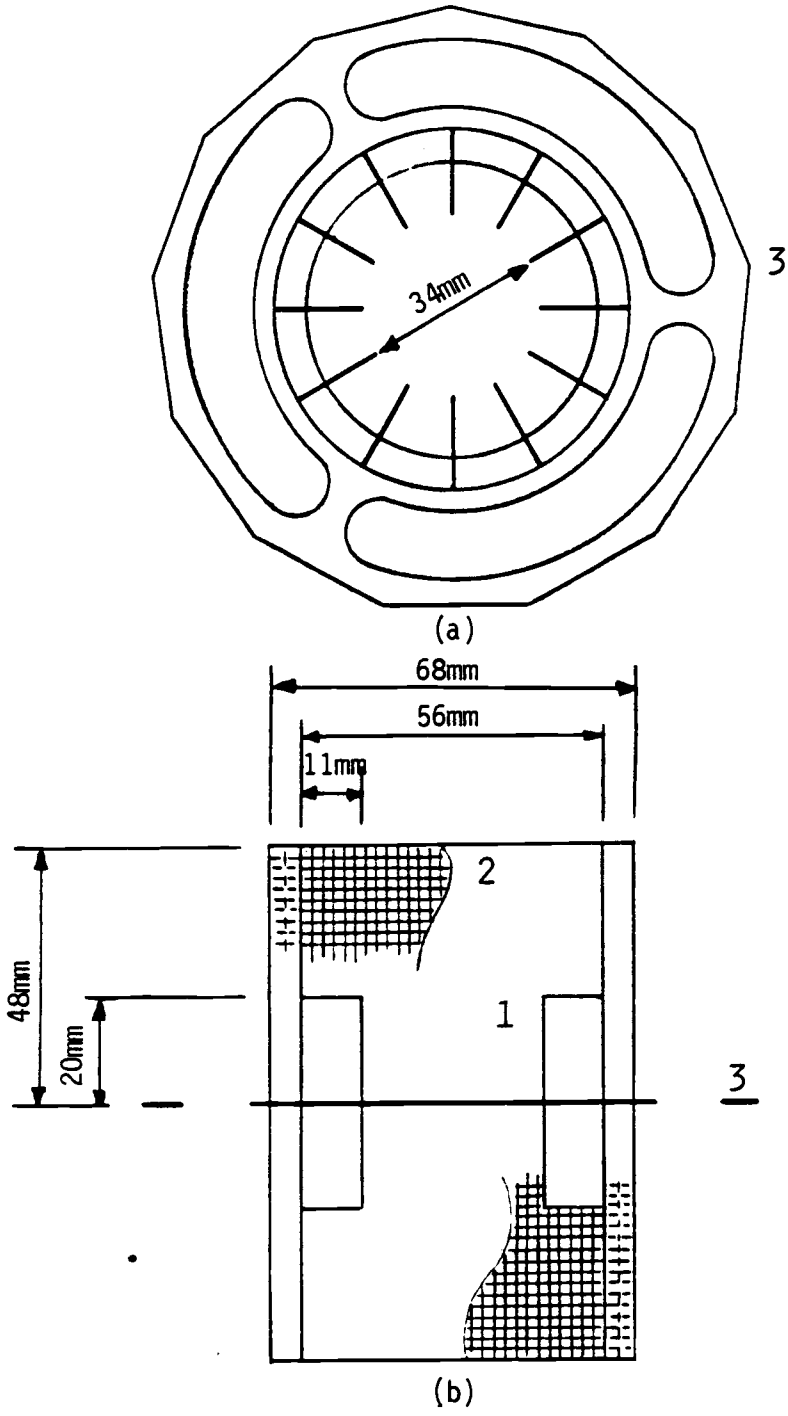

Figure (4.11). Twelve baffles and two wiremesh cylinders combination. a. Top view, b. Side view. 1. Baffles, 2. Wiremesh of 2mm square opening , 3. Interface plate. Scale 1/1.4

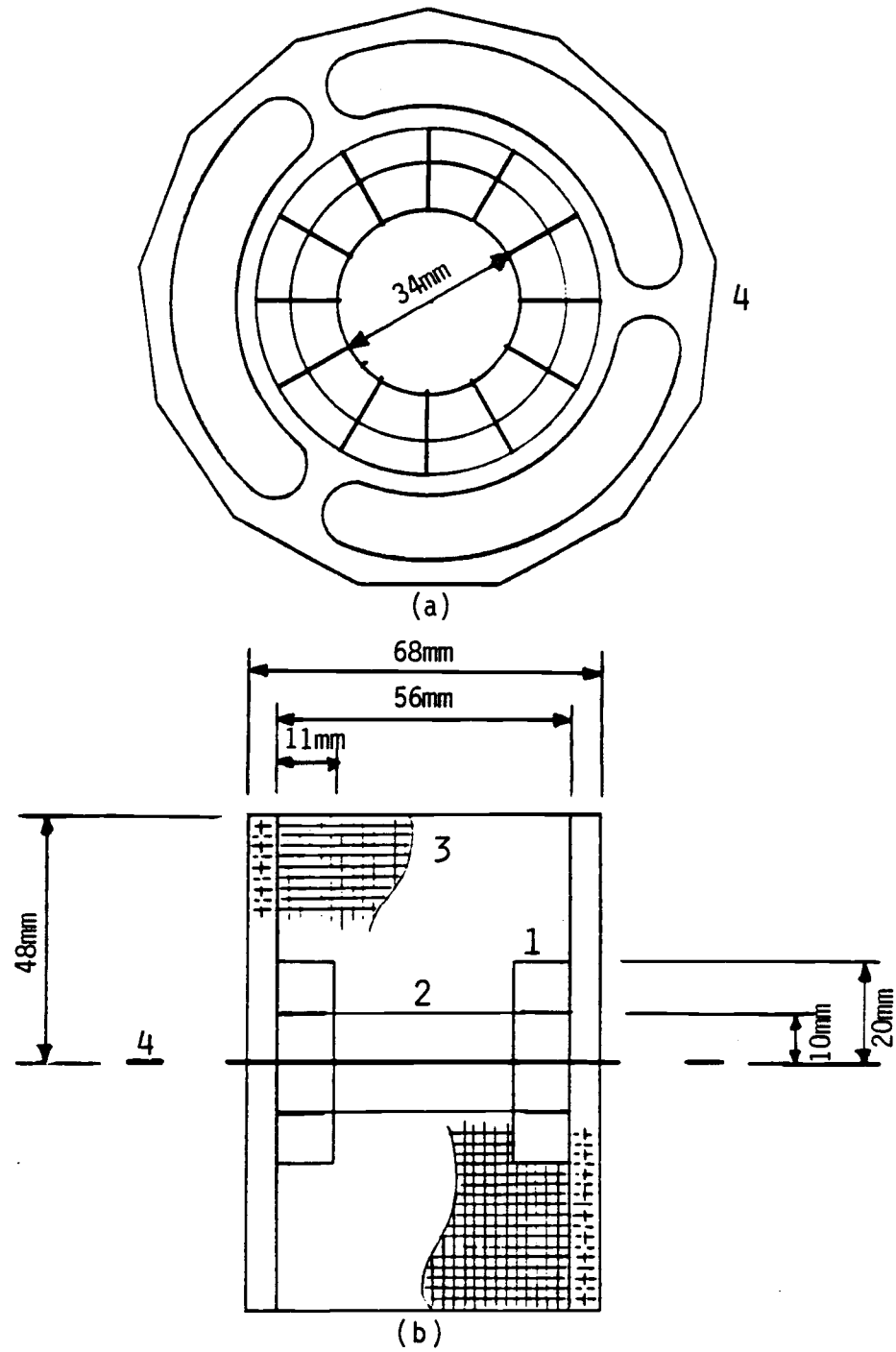

Figure (4.12). Twelve baffles with ring and two wiremesh cylinders combination. a. Top view, b. Side view. 1. Baffles 2. Ring, 3. Wiremesh of 2mm square openings, 4. Interface plate. Scale 1/1.4

Figure (4.13) illustrates a side view section in the assembled experimental cell.

4.1.2 Continuous Process Systems

A continuous process system was designed and constructed for both liquid phases so that the systems could be run in continuous operation, as shown in Figure (4.14). It consisted generally of make-up tanks, pumps, flowmeters, receiver tanks and the cell itself.

The aqueous phase system included a 120 liter plastic make-up tank. It was connected by 19.05 mm (3/4 inch) plastic tube to a 1/10 hp Little Glant Centrifugal pump. The tank could be drained through a 19.05 mm (3/4 inch) valve, connected to the tank outlet through a tee-connection. The pump outlet tube of 19.05 mm (3/4 in.) divided into two tubes. A 19.05 mm (3/4 inch) tube returned to the same tank as a recycle stream, and the other 19.05 mm (3/4 inch) tube was reduced to 9.53 mm (3/8 inch) plastic tube by a brass connector. The recycle line helped to adjust the flow to the cell. The 9.53 mm (3/8 inch) tube was connected to a FP-1/4 Fisher-Porter flowmeter. A needle valve was mounted on the tube before the flowmeter to adjust the flow rate. The flowmeter outlet was connected to the cell through a reducing fitting, which reduced from 9.53 mm (3/8 inch) to 6.35 mm (1/4 inch)to the inside of the cell. The outlet hole of the cell was 6.35 mm (1/4 inch) diameter, connected by a fitting to the 9.53 mm (3/8 inch) plastic tube of a U-shape arm before going to the receiver tank, as shown in Figure (4.15).

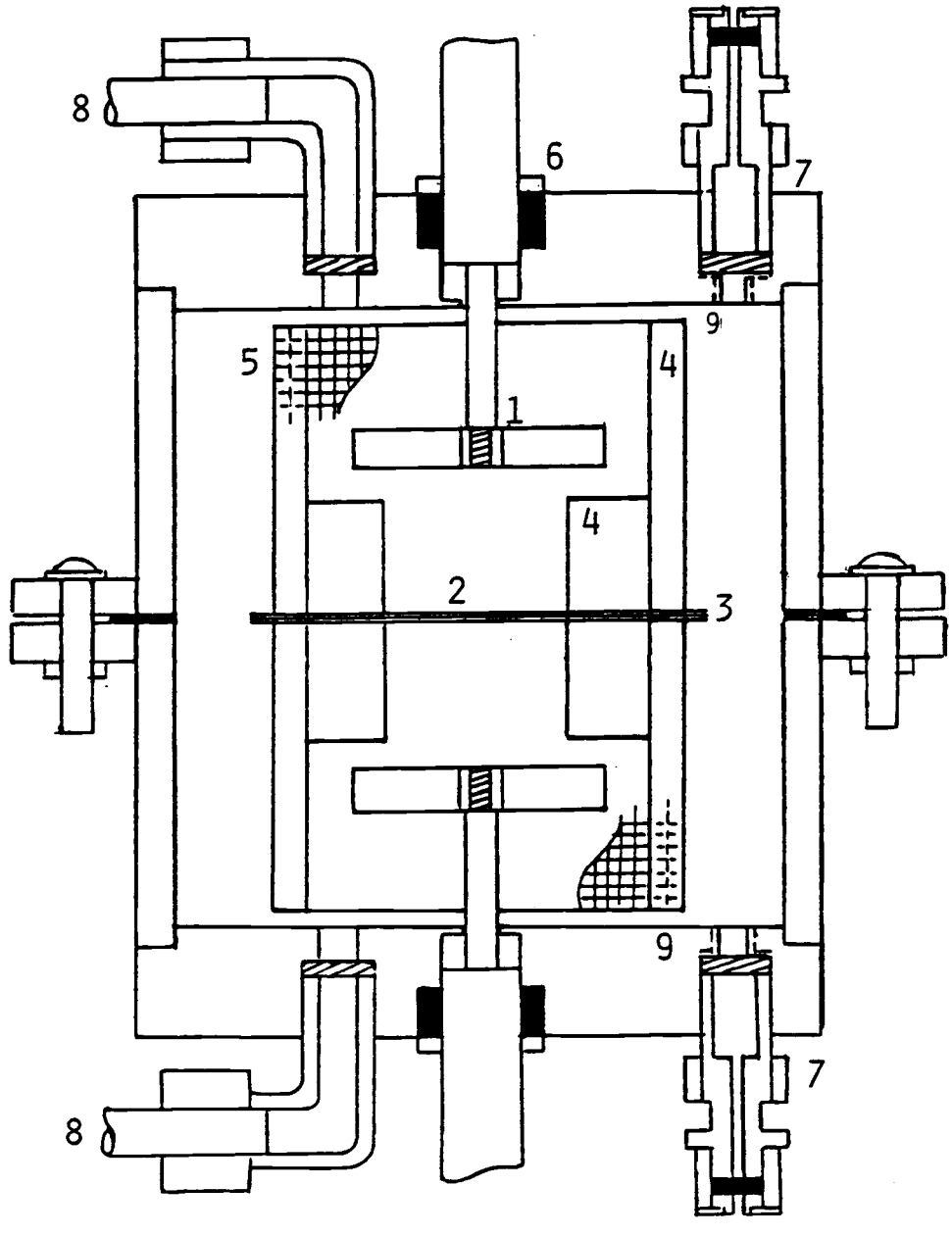

Figure (4.13). Side view section in the assembled experimental cell. 1. Impeller, 2. Interface plate, 3. Interface, 4. Baffles, 5. Wiremesh cylinders, 6. Impeller shaft sealing, 7. Sampling port, 8. Inlet stream, 9. Outlet stream.

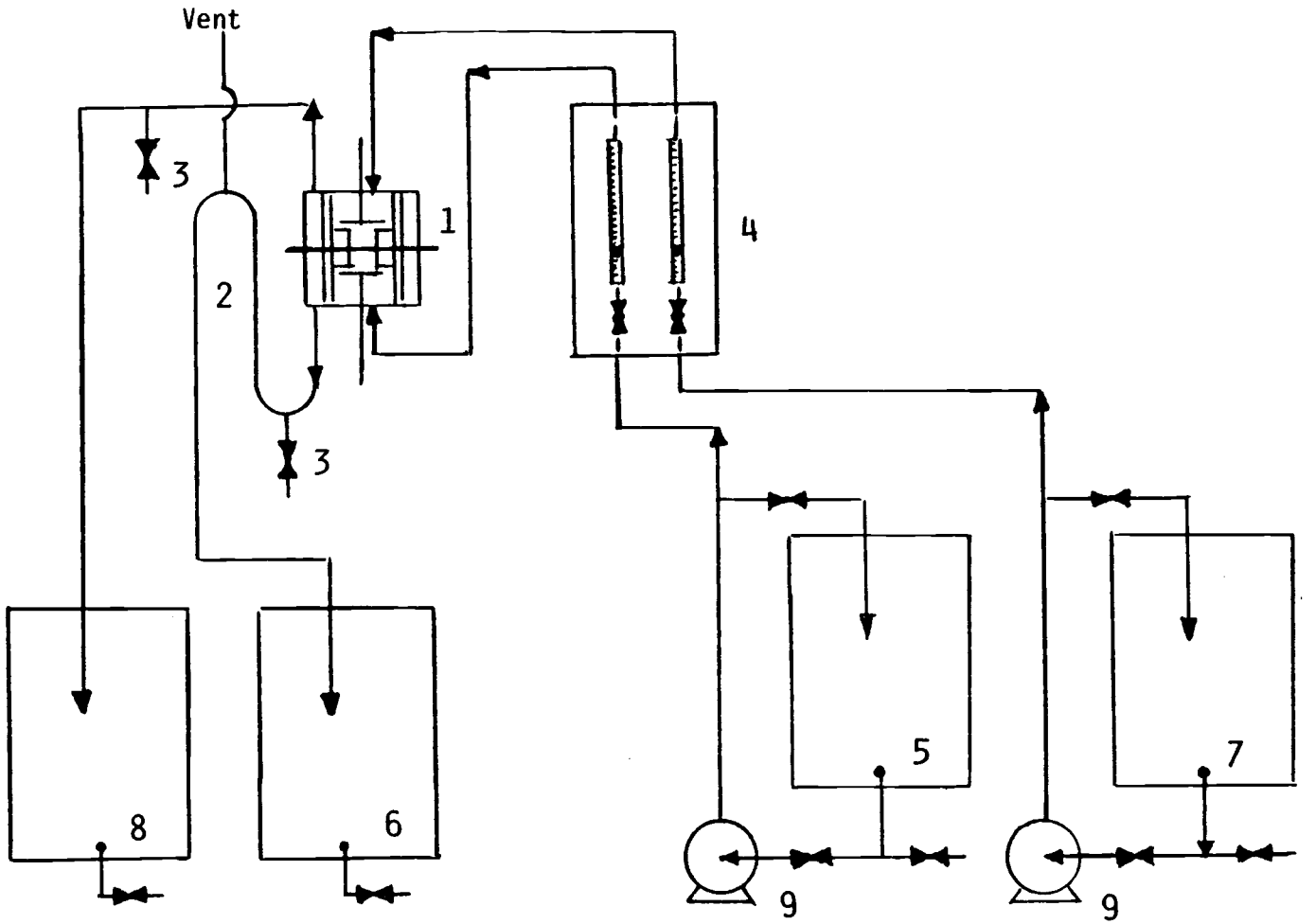

Figure (4.14). Continuous process systems. 1. Cell, 2. U-shape arm, 3. Sampling valve, 4. Flowmeter, 5. Aqueous phase make-up tank, 6. Aqueous phase receiver tank, 7. Organic phase make-up tank, 8. Organic phase receiver tank, 9. Centrifugal pumps.

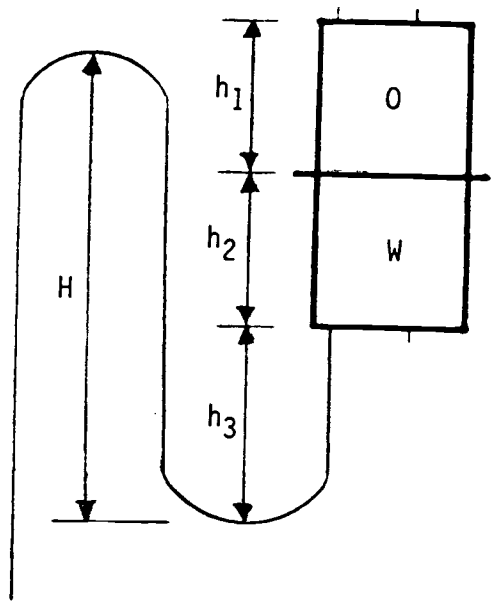

Figure (4.15). U-shape arm of the aqueous outlet stream to control the interface level.

The height of U-shape arm was changeable to control the level of the interface inside the cell. The desire height of the arm could be evaluated as follows:

$$H\rho_w = h_1\rho_o + (h_2 + h_3)\,\rho_w \qquad (4.1)$$

$$H = \frac{h_1\rho_o + (h_2 + h_3)\,\rho_w}{\rho_w} \qquad (4.2)$$

A 9.53 mm (3/8 inch) plastic tube vent was connected to the top of the U-shape arm. A needle valve was mounted on the outlet tube for sample drawing. The outlet tube was connected to the receiver tank.

The organic phase system was constructed in the same manner as the aqueous phase system, except there was no U-shape arm in the outlet tube.

4.1.3 Support Structure

The support structure was constructed in a movable wood frame (72 cm x 130 cm x 82 cm). Figure (4.16) shows its front view, while Figure (4.17) shows its side view. The motors and cell support were designed to hold them in the same central line. Their supports were designed so that they could be easily dismantled and assembled, with flexibility to move them easily up and down, forward and backward, and to the left and right for setting their proper position. The support consisted of two steel pipes of 2.54 cm diameter and 78 cm high. They were fixed vertically by screwing the flanges to the base and the top of the frame. The space between them was 189 mm. Each motor was supported on a steel plate, 175 cm wide by 139 mm high. Two angle iron pieces, 50.8 mm wide by 139 mm long, were welded on each side of the back face of the plate. They were drilled to form three holes of 7 mm diameter. Four slots of 7 mm wide by 25 mm long were milled on the plate to fit the motor's four mount holes. Six steel sleeves were made of 26.7 mm I.D. and 33.6 mm O.D. by 146 mm long. Four of them were welded on their interior, tangent to a steel plate, 86 mm wide by 139 mm high. Three slots, 7 mm wide and 50 mm long, were made on four welded sleeve plates to fit the holes of the motor plate angle iron. These sleeves were slipped onto the vertical support rods. A pair of the sleeves were used to hold each motor, as shown in Figure (4.18a). The last pair of sleeves were used for the cell support as shown in Figure (4.18b). They were connected to a piece of angle iron, 50.8 mm wide by 180 mm long, which was welded to each sleeve at its center. Three slots, 7 mm wide and 23 mm long,

were milled in the angle iron to hold the cell seat. The cell seat, as shown in Figure (4.18c), was designed to hold the cell from the bottom. It was constructed from a plastic plate, which was sawed and machined to fit the cell cap dimension. Three slots, 7 mm wide and 74 mm long, were milled to fit the angle iron slots of the cell support. A wood holder, as shown in Figure (4.18d), was made to hold the upper cell cap to eliminate the vibration of the cell while the motors operated. The flowmeter support plate and the motor's control units were mounted on the front wall of the movable wood frame as shown in Figures (4.16) and (4.17). The tanks and the pumps lay on the ground beside the support structure.

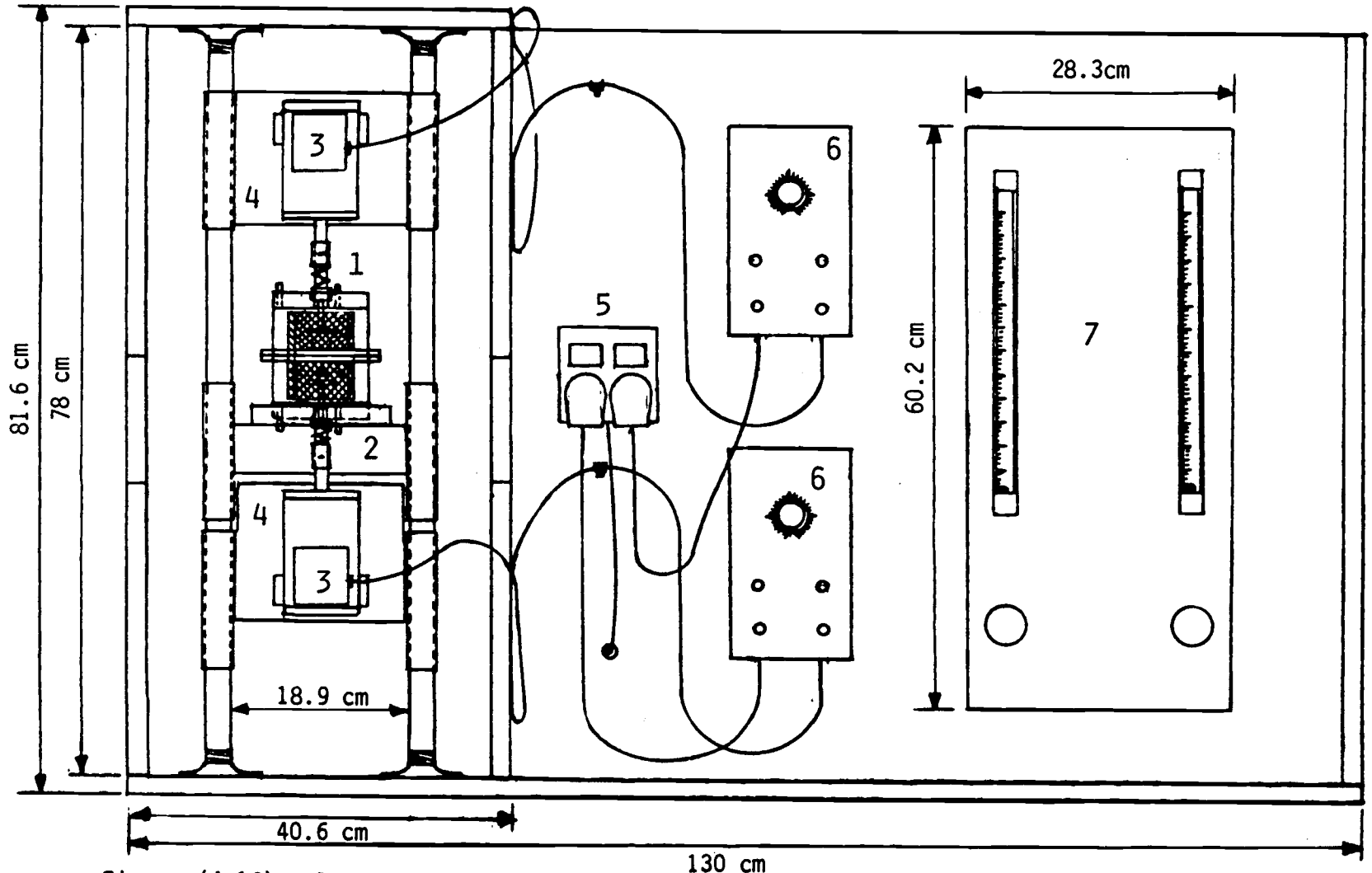

Figure (4.16). Support structure front view. 1. The cell, 2. Cell seat and support, 3. Motors, 4. Motors' support, 5. Electricity connection, 6. Motor controlles, 7. Flow meter. Scale 1/6.6

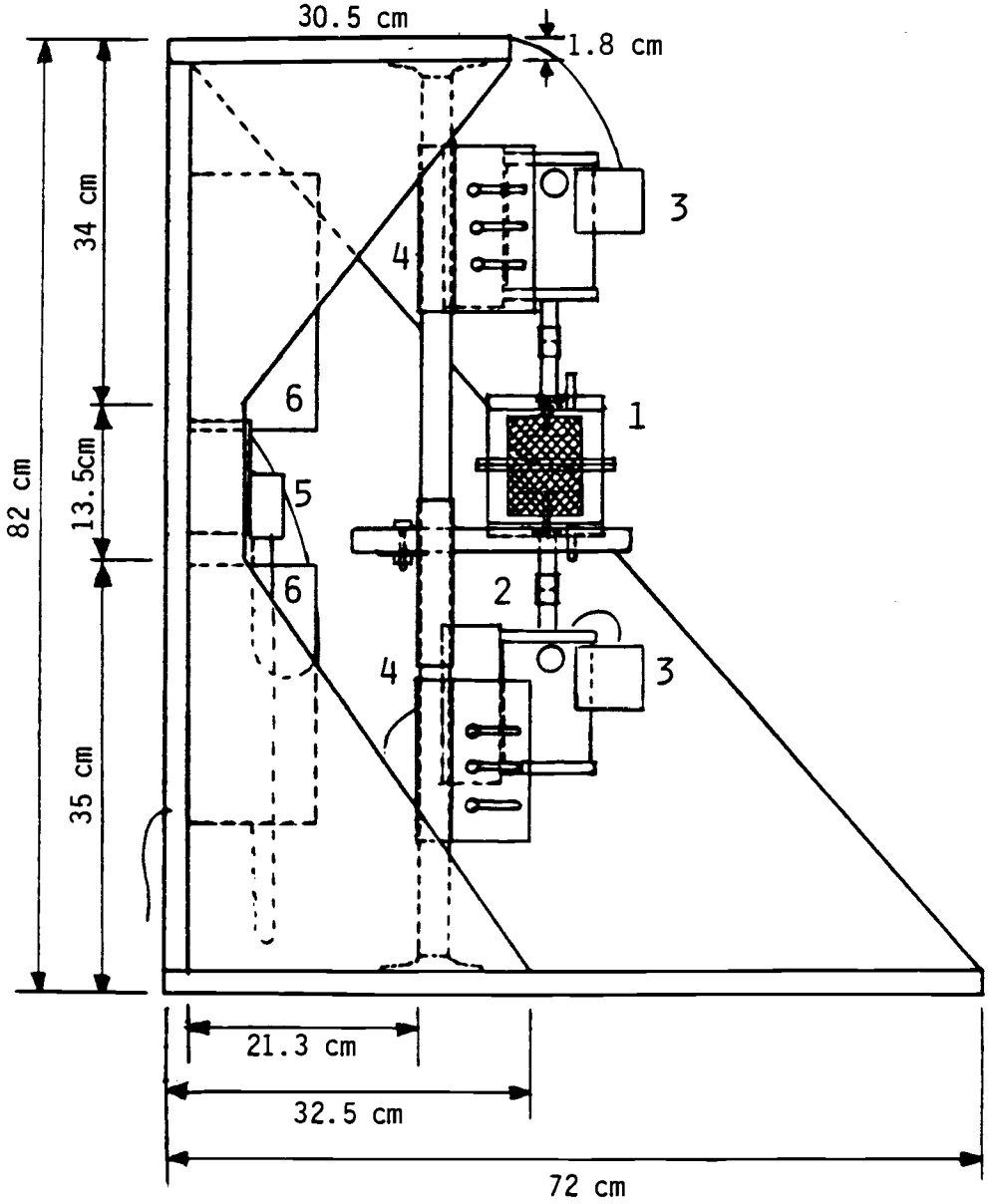

Figure (4.17). Support structure side view. 1. The cell, 2. Cell seat and support, 3. Motors, 4. Motors' support, 5. Electricity connection, 6. Motor controllers. Scale 1/6.6

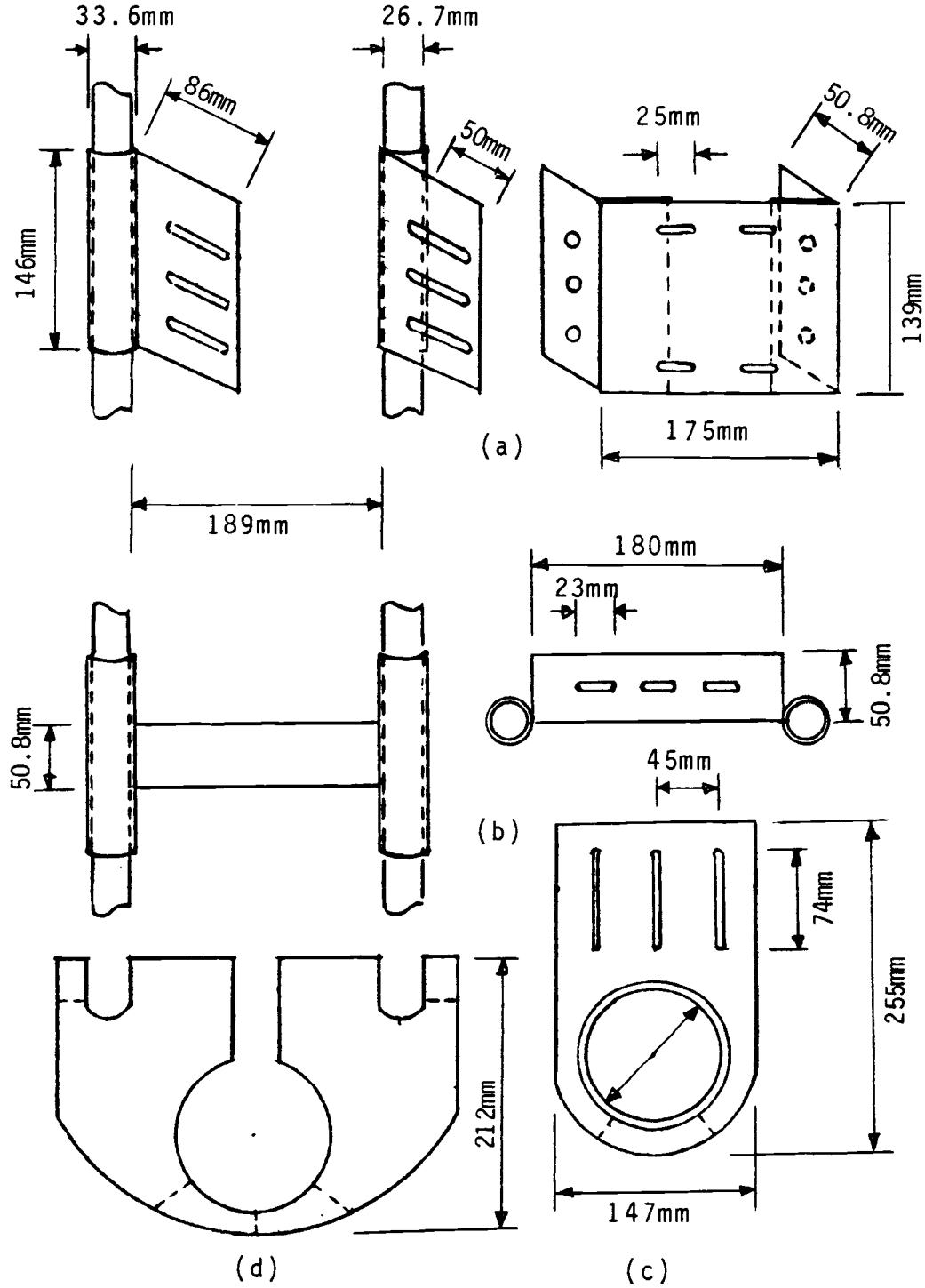

Figure (4.18). Equipment support. a. Motor's support, b. Cell support, c. Cell seat, d. Wood holder.

4.2 The Cell Testing

The following tests on the experimental cell were made:

4.2.1 Leakage Test

The first test on the cell was made to verify that there was no leakage from the cell flanges, caps, impeller shaft sealing, sampling ports, etc. This was done by filling the cell with water and letting it be stored for one day. No leakage was observed. The cell was filled with n-butanol and allowed to stand for two days. It was found that there was no leakage observed. It was also observed that there was no effect on the gasket or the sealing material.

4.2.2 Interface Stability Test

This was achieved by using a pitched blade turbine of the dimensions shown in Table (4.2b). It was observed that the original design did affect the interface stability when operated at the desired rpm range. Accordingly, its dimensions were altered to these shown in Table (4.2a).

The cell was tested with different configurations of baffles and wiremesh cylinders combination to determine if sufficient stability of the interface could be obtained. The various configurations were discussed in 4.1.1 (5. Baffles and Wiremesh Cylinders). Figures (4.8-4.12) show these configurations. It was found that the dimension of the pitched blade shown in Table (4.2a) with the configuration of baffles and wiremesh cylinders shown in

Figure (4.8) were sufficient but not necessarily the most optimum to achieve a sufficient stability of the interface with the desired range of mixing rate (rpm).

4.2.3 Mixing Performance Test

Mixing performance tests were performed in two steps as follows:

1 - Dye Injection Test

Drops of red dye were injected into the water phase and the n-butanol phase separately. The color quickly spread homogeneously throughout the particular liquid phase. When it was used for the water phase test,the organic phase was also colored due to the dye transferring across the interface and vice versa.

2 - Tracer Injection Test

The batch mixing performance was studied to verify that the designed cell provided the required mixing uniformity. This was performed by using a tracer system, as shown in Figure (4.19) below.

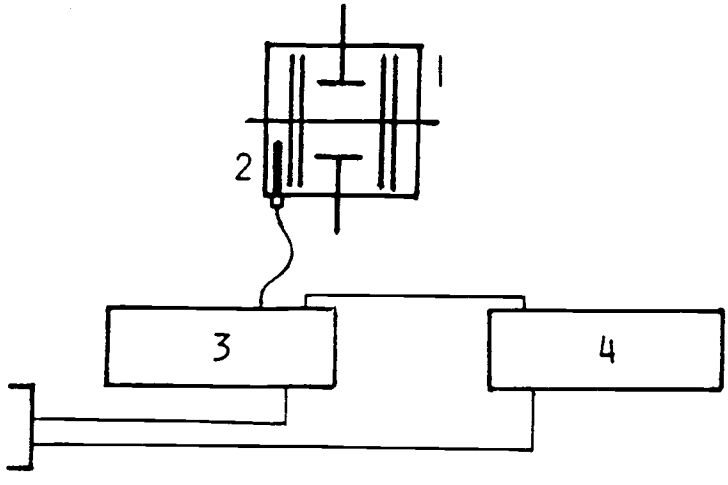

Figure (4.19). Tracer system, 1. The cell, 2. Probe, 3. Conductivity detector, 4. Recorder.

It consists of a conductivity probe, conductivity detector and a Omniscribe Houston instrument recorder. Since the two cell sections were geometrically identical, the mixing studies were performed on the water phase section of the cell. A potassium chloride tracer was used for this test. The conductivity probe was mounted in the lower cell section through its sampling port. The tracer was injected to the cell via lower section inlet stream hole. The other probe end was connected to the conductivity detector which was in turn connected to the recorder. The recorder was fixed on a speed of 20 cm/min. A potassium chloride tracer of 0.33 gm/cm^3 was prepared. The lower cell section was filled with distilled water to the edge of the interface plate, which was equivalent to 380 cm^3. The impeller's (rpm) was adjusted to the desired rate. A 300 μl of the tracer was injected by a syringe. The recorder started to record the concentration at the probe tip point in the cell at a time representing the mixing time in the cell.

The test was performed for the following cases:

a. The agitation rate was set at approximately 180 rpm which represent appropximately the lower agitation rate used in this mass transfer investigation. The probe tip was fixed at approximately 20 mm below the interface; this point represented the point where samples were to be drawn during the cell batch operation. Figure (4.20) shows the mixing time curve of this case.

b. The agitation rate was set at approximately 180 rpm, while the probe tip was fixed at the point 5 mm below the interface. Figure (4.21)shows the mixing time curve for this case.

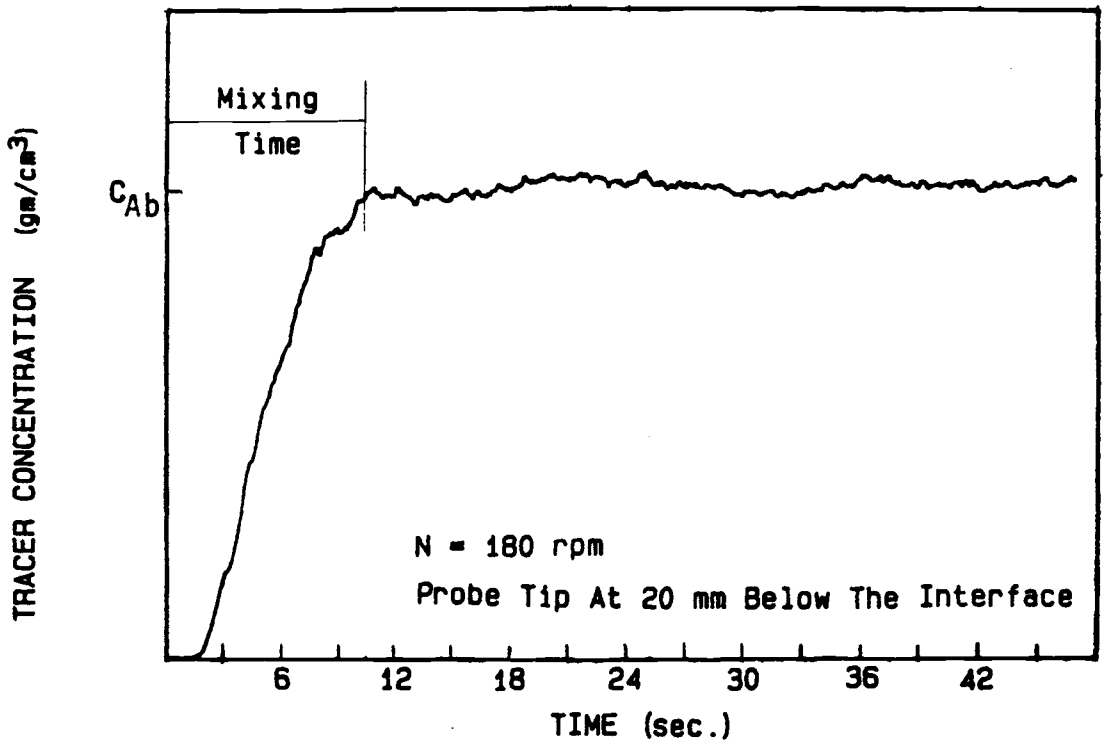

Figure (4.20). Mixing time curve for case a.

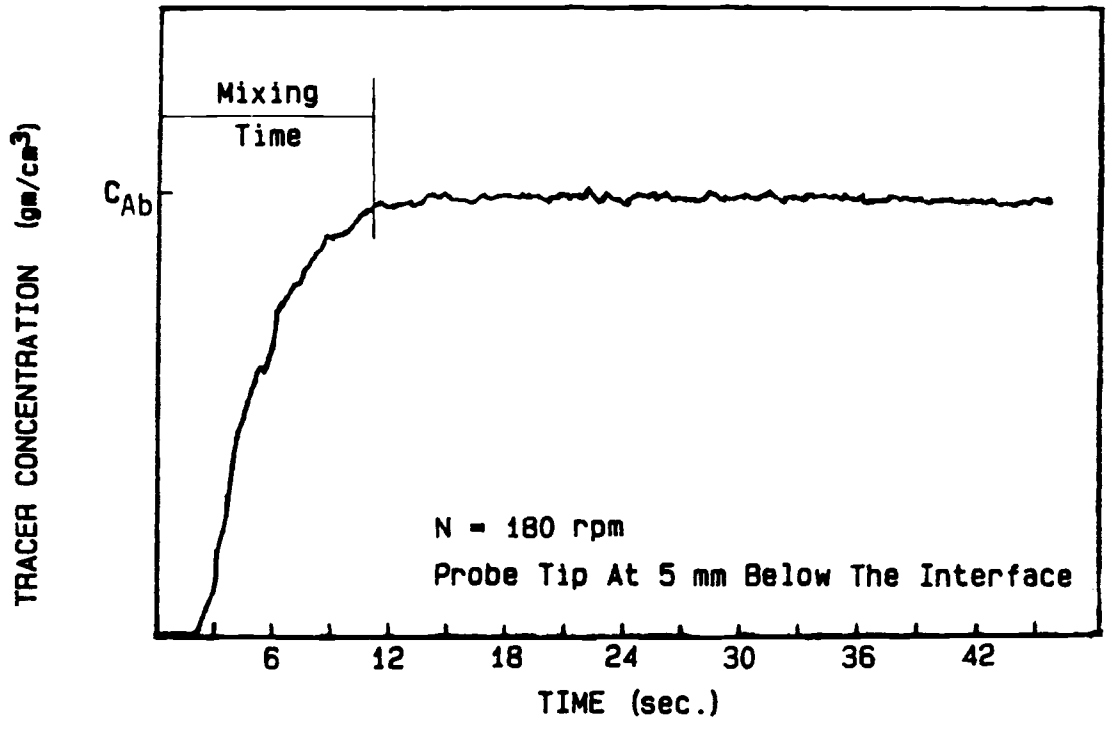

Figure (4.21). Mixing time curve for case b.

c. The agitation rate was set at approximately 300 rpm, while the probe tip was fixed at the point 20 mm below the interface. Figure (4.22) shows the mixing tine curve of this case.

These mixing time curves represent well-mixing performance in the cell section. The uniformity of the concentration was due to the wiremesh cylinders, which partitioned large eddies into smaller ones to achieve a uniform mixing. The mixing time, including the time probe delay, was about 10, 11 seconds for the case a and b, respectively, while about 7.5 seconds for the case c. These times were within the range of the sampling drawing period in the batch operation process. In actual cell operation the mixing time should be less than those represented for cases a, b and c since the species would be transferred across the entire cell interface. In case a, b and c, the tracer was injected at only one point located a distance away from the probe; this effect was clear when the probe time delay of the cases a and b were compared. It was observed that in case a the probe time delay was 1.5 seconds, while in case b, was 2.1 seconds where the probe was further from the injection point than that in case b.

The mixing in the cell was determined to be adequate; meeting the desired design criteria.

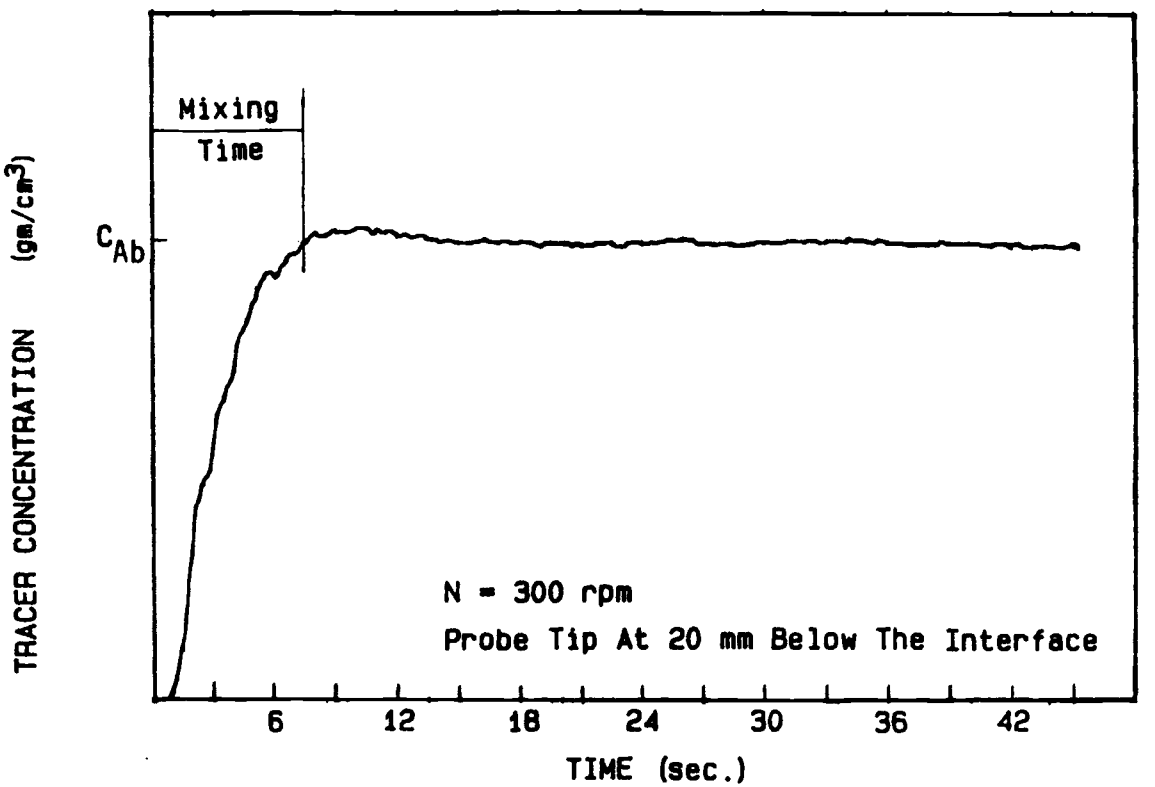

Figure (4.22). Mixing time curve for case c.

Chapter Five

Operational Procedure

5.1 System Used

The binary system of partially miscible water-n-butanol was used in a batch operation process. This system was chosen since it has been shown by previous investigation to be a system in which the transfer between the two phases occurs in between the boundary layer model and surface renewal model [45, 46]. Binary systems of limited mutual solubility are particularly well suited for mass transfer coefficient studies since they allow simultaneous evaluation of both mass transfer coefficients under otherwise identical conditions [4]. The solubility of water in n-butanol is approximately 19.9%, while it is approximately 7.7% for n-butanol in water. The physical properties of water-n-butanol are shown in Table (5.1).

Table 5.1. Physical Properties of Water-n-Butanol [4]

Phase	Temperature °C	$\mu \times 10^{3}$ kg $m^{-1}s^{-1}$	$\rho \times 10^{-3}$ kg m^{-3}	$D \times 10^{9}$ $m^{2}s^{-1}$	Equil. Mass Fraction	$\sigma \times 10^{3}$ (N/m)
Water (H_2O)	20	1.00	1.00	0.78	0.077	1.6
n-butanol (C_4H_9OH)	20	2.95	0.81	0.26	0.199	

5.2 Experimental Procedure

5.2.1 Batch Operation

Before assembling the cell for an experiment, each part of it was carefully cleaned. All cell parts were washed with distilled water and dried before using them. In order to make all the experiments identical in their hydrodynamic conditions, the cell was assembled using the following steps:

1 - The impellers were mounted at 25 mm away from the interface plate in each section of the cell.

2 - The sampling hole of each section was located at the center of the same annular interfacial area.

3 - The cylindrical wiremesh was kept in identical position for each experiment.

4 - All samples were drawn from approximately the same point in the cell, approximately 20 mm away from the interface.

After the cell was assembled, the number of the impeller revolution per minute (rpm) was adjusted for each section. A digital phototach (Cole Parmer) was used to determine the impeller rpm. The allowable agitation rate was determined qualitatively by observing the interface surface stability. The filling of the cell with a given solvent was done with great care to avoid contaminating a given section of the cell with the second solvent. A funnel with a long tube was used to fill a section of the cell with either the aqueous or the organic solvent. First 400 cm^3 of distilled water was prepared. The funnel tube was inserted to the lower section through the upper sampling hole. Water was poured in until the top surface

was tangent to the interface plate. The volume of the distilled water added to the cell was carefully measured. The same volume of organic solvent was prepared. For the organic filling, the funnel was washed several times by the same organic phase to remove any water contamination. The same organic solvent volume was poured into the upper cell compartment. In order to avoid rippling of the interface while the organic phase was pouring, the funnel tube was inserted from the inlet stream hole, which is faced to the central solid part of the interface plate. Due to the variable tightening of the interface flanges, the variation in the volume of the organic solvent was within $\pm$ 4 ml. The upper sampling diaphragm fitting and the plug to the upper inlet stream hole were screwed in as quick as possible. At the same time, both the stop-watch and the motors were started.

Once the run started, the following measurements were carefully determined:

1 - Both phases were sampled subsequently at intervals of (5-20) minutes. Samples were withdrawn by inserting a long fine needle of Hamilton 500 μl syringe to the mentioned point in each section. A 10-20 microliters volumetric sample was removed. This was found convenient for the gas chromotography apparatus. The error of volume reduction introduced by drawing samples was negligible. All samples were kept in each sample bottles. Each one was covered with a piece of parafilm before putting on its cover; this was done to eliminate any sample evaporation, which could affect the concentration within the sample.

2 - The motor speeds were measured during the operation and adjusted, if necessary, to maintain a constant speed.

3 - The interface level and its stability was observed frequently during the operation. It is desirable to keep the interfacial surface as smooth as possible. Slight movement of the interface was acceptable. Occurrences such as pulsing, rippling or general surface breakup of the interfacial surfaces were not acceptable.

4 - The room temperature was measured during the operation by a mercury thermometer.

Most runs lasted for a period less than 120 minutes, even if the phases did not approach their equilibrium concentration. Longer runs were avoided to maintain the phases volume relatively constant.

After the operation was over, the cell was discharged through the lower section sampling hole. All the cell parts were dismantled to prepare them for the next operation.

5.2.2 Continuous Operation

Although all the experiments were done as a batch operation, the continuous operation could be done easily by following the same batch operations procedure, except the following:

1 - The organic phase and the aqueous phase would be in continuous fed to the cell. Accordingly, the flow rates of phase would need to be adjusted and controlled during the operation.

2 - The interface level would be adjusted by the U-shape arm of the aqueous phase outlet stream, depending on the equation (4.2).

3 - The samples would be drawn frequently from the sampling values on the outlet streams.

5.3 Method of Sampling Analysis

An HP-5804A gas chromatography (GC) was used to analyze the samples of both phases. Two 1/8 inch, 6 feet long stainless steel columns filled with 80/100 mesh hysep Q were used for water and n-butanol analysis. One of the columns was used for the analysis, while the other was used as a reference for the apparatus detector. Gas chromatography calibration for each phase was done by preparing five standard solutions for each phase. Each time that the GC was used for analysis, the standard solutions for each phase were injected to calibrate it for that set of samples. Microliter Hamilton syringe of 5 μl was used to inject the samples to the apparatus. It was found that 3 μl was convenient to inject to the apparatus. Figures (A.1) and (A.2) illustrate the GC output for the aqueous and organic phases, respectively. Calibration curves were treated by simple regression method, using the Statgraf software package.

Chapter 6

Experimental Data and Results

The mass transfer coefficient and the effect of the agitation rate on the coefficient were evaluated for the binary system water-n-butanol at room temperature (17°C-20°C). This was done by running the experiment at three different sets of operating conditions which were:

1. The experimental cell was operated for several runs using the same agitation rate (rpm) for each phase. The agitation rate was varied from 241 rpm to 422 rpm. The concentration of the transferred component in each phase was measured during the experimental time using the GC and their calibration curve. The time dependence curves of the transferred water in the n-butanol phase are shown in Figure (6.1). The concentration of the transferred n-butanol in the water phase with time is shown in Figure (6.3). By applying equation (2.17a) and (2.18a), the mass transfer coefficient was evaluated for each agitation rate in both phases. The variables Cw_i and Co_i in the equations (2.17a) and (2.18a) were zero. A plot of $\ln (C_w^*/C_w^* - C_{wt})$ for n-butanol phase and $\ln (C_o^*/C_o^* - C_{ot}$ for the water phase versus time revealed a straight line. Each curve was treated by a simple regression method using Statgraf software package. The slope of the fitted line is:

$$\text{slope} = \frac{kA}{V}$$

Since the interfacial area, A, and the volume, V, are known, the mass transfer coefficient can be evaluated for each phase per a

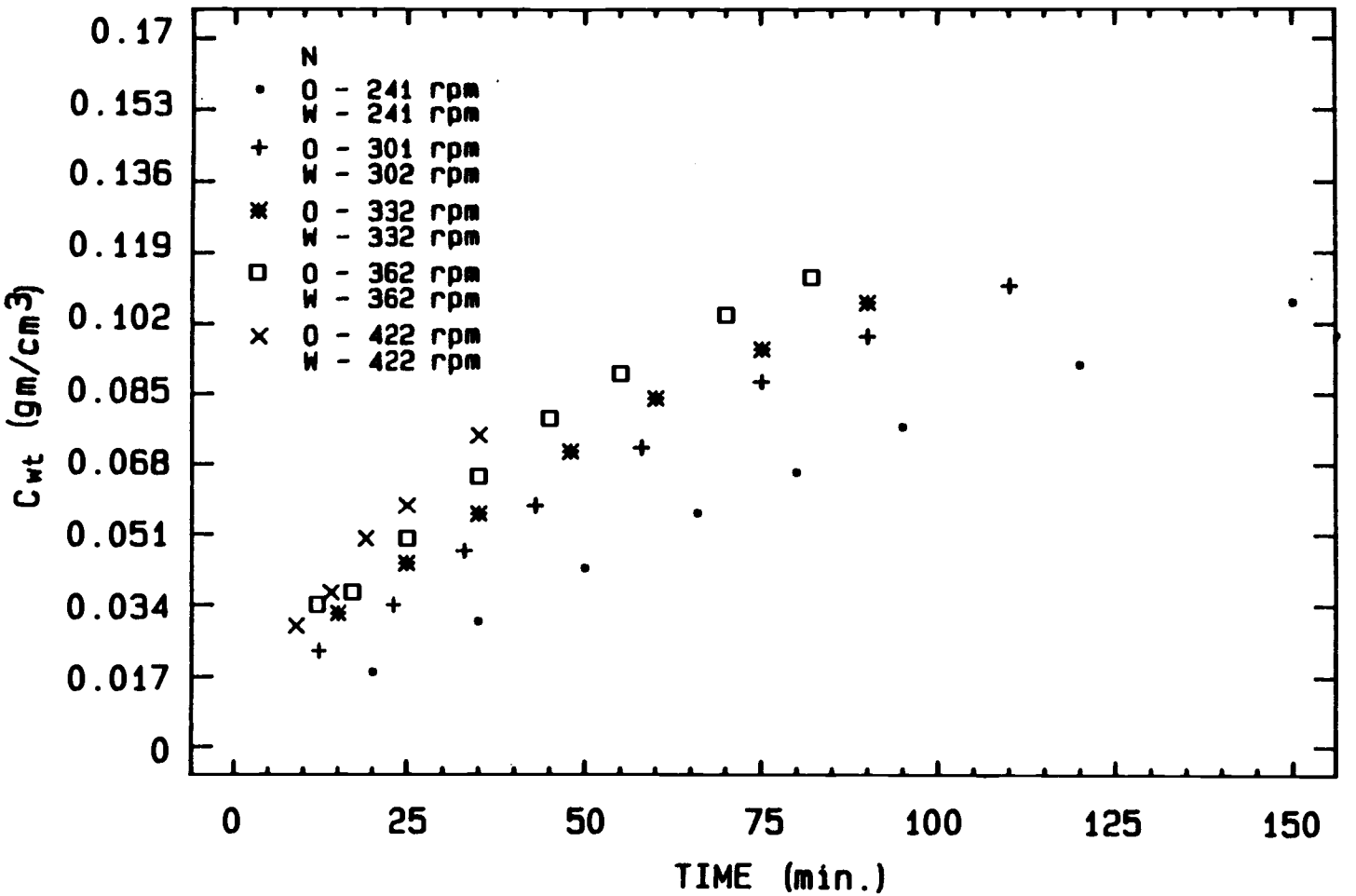

Figure (6.1). Time dependence of transferred water concentration in the n-butanol phase when both phases were at the same agitation rate (rpm).

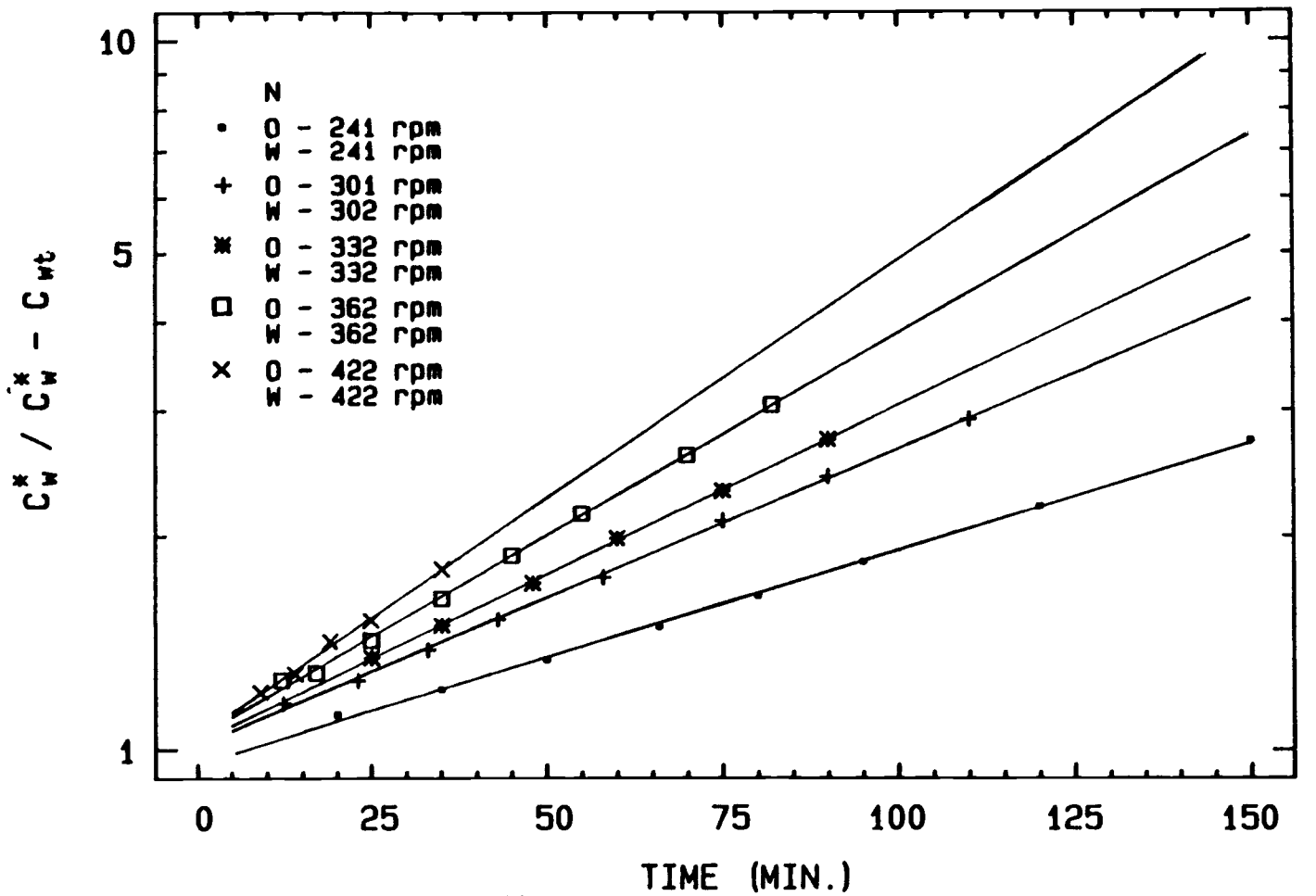

Figure (6.2). Fitted lines of $\ln \frac{C_w^*}{C_w^* - C_{wt}}$ vs. time in the n-butanol phase when both phases were at the same speed.

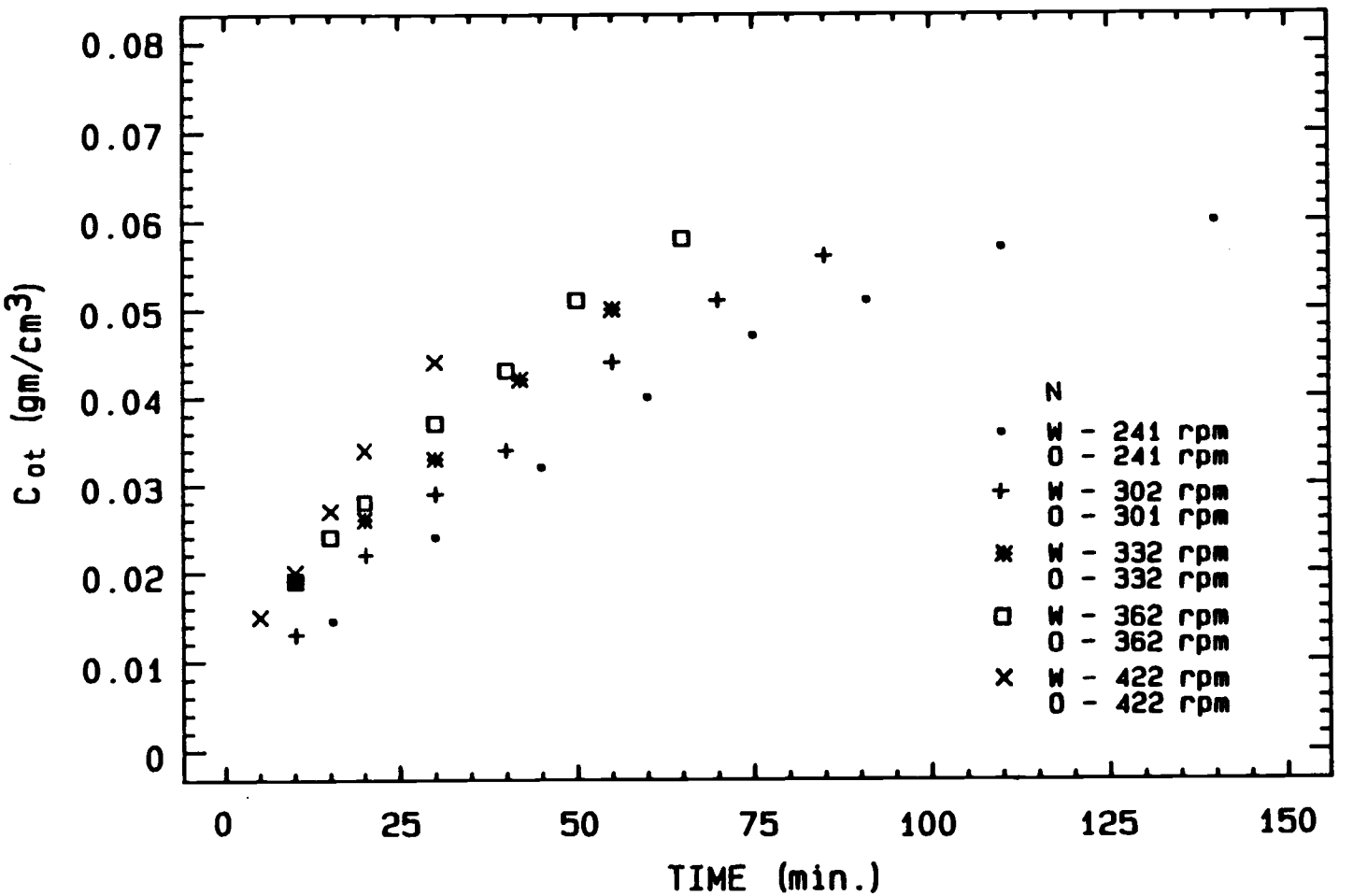

Figure (6.3). Time dependence of transferred n-butanol concentration in the water phase when both phases were at the same agitation rate (rpm).

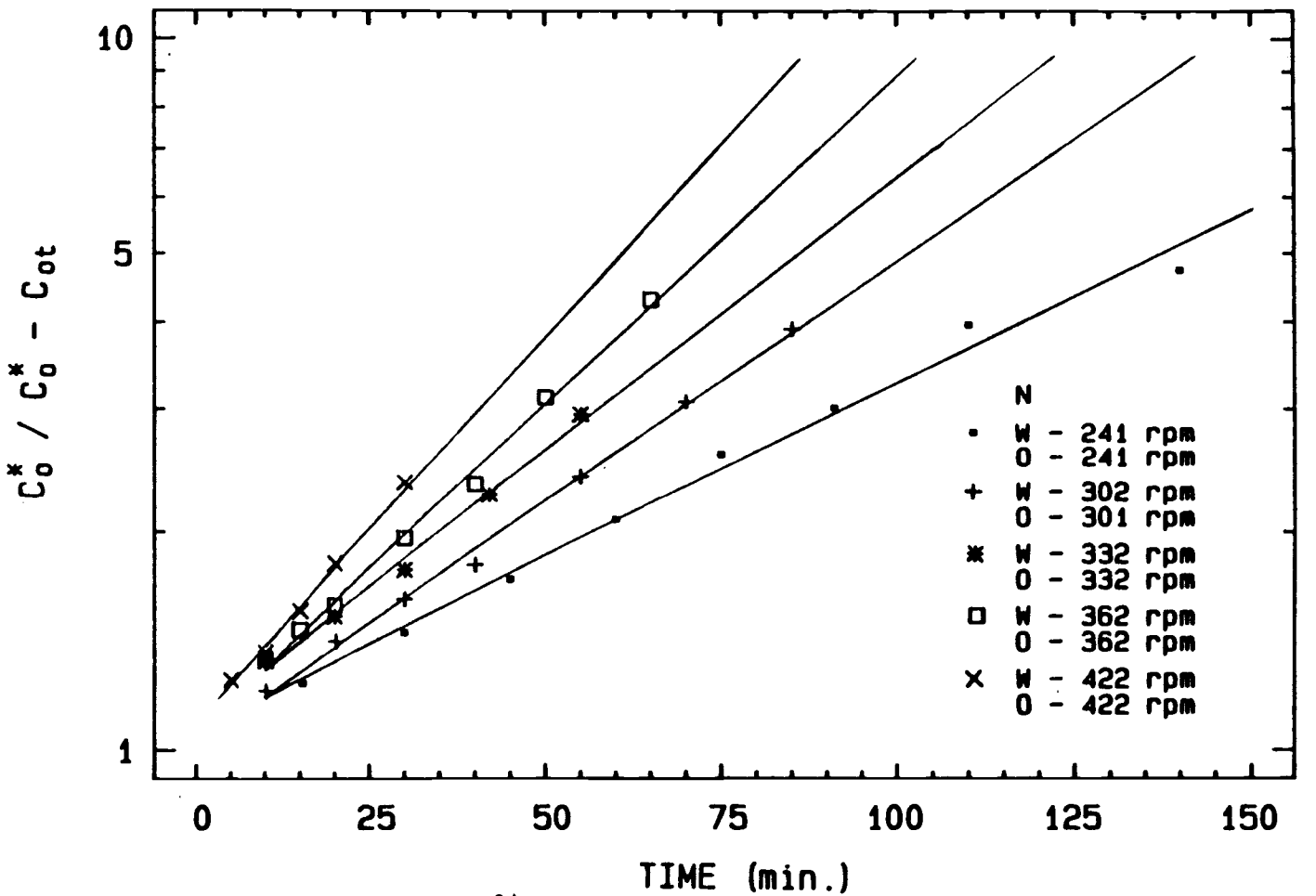

Figure (6.4). Fitted lines of $\ln \frac{C_o^*}{C_o^* - C_{ot}}$ vs. time in the water phase when both phases were the same agitation rate.

given run. Figures (6.2) and (6.4) show the fitted lines for the transferred water in the n-butanol phase and the transferred n-butanol in the water phase, respectively. In Table (6.1), the evaluated mass transfer coefficients for both phases and their fitted line statistical analysis parameters are presented.

2. The experimental cell was operated for several runs to study only the effect of the organic phase agitation rate (rpm or R_e) on the mass transfer coefficient in the aqueous phase. By applying the same procedure of calculation and statistical treatment that were previously mentioned, the mass transfer coefficients in both phases were evaluated. The set of runs are:

a. Three runs were investigated in which the n-butanol phase was kept unagitated while the water phase was agitated. The agitated rates of the water phase were 181, 241, 360 rpm, respectively. Figure (6.5) illustrates the concentration of n-butanol within the water phase changed with time. Figure (6.6) shows the fitted lines of $\ln (C_o^*/C_o^* - C_{ot})$ versus time.

b. Four runs were investigated in which the n-butanol phase agitation rate was kept constant about (301-303) rpm, while the agitation rate of the water phase was varied. The agitation rates of the water phase were 182, 242, 302 and 362 rpm, respectively. Figure (6.7) and Figure (6.9) illustrate the time dependence of transferred n-butanol concentration in the water phase and transferred water concentration in the n-butanol phase, respectively. Figure (6.8) and Figure (6.10) show the fitted lines of their $\ln (C_o^*/C_o^* - C_{ot})$ and $\ln (C_w^*/C_w^* - C_{wt})$ versus time, respectively.

Table(6.1). Evaluated k and Parameters for Equation $\ln(C^*/C^* - C_t) = (kA/V)t$, where kA/V = slope, when both Phases were Agitated at the Same Speed.

Phase	Figure number	Run number	N rpm	N rps	Fitted line slope	Standard error (±)	Probability level	R-squared %	Phase volume V (cm^3)	Interfacial area A (cm^2)	$k(\frac{cm}{min})$	$k(\frac{cm}{sec})$	Temp. C^o	$Re\ (\frac{NL^2\rho}{\mu})$	k_w/k_o
n-butanol	6.2	1	O-241 W-241	O-4.02 W-4.02	6.926E-3	9.699E-5	0.0	99.88	380	31.6	0.0833	0.00139	19	1912	1.633
		2	O-301 W-302	O-5.02 W-5.03	9.624E-3	1.224E-4	0.0	99.90	381	31.6	0.116	0.00193	19.2	2388	1.642
		3	O-332 W-332	O-5.53 W-5.53	1.092E-2	8.766E-5	0.0	99.97	380	31.6	0.1313	0.00219	18	2630	1.630
		4	O-362 W-362	O-6.03 W-6.03	1.306E-2	2.134E-4	0.0	99.54	382	31.6	0.1579	0.00263	20.2	2868	1.642
		5	O-422 W-422	O-7.03 W-7.03	1.543E-2	6.378E-5	0.00015	99.49	384.5	31.6	0.1877	0.00313	19.5	3344	1.630
Water	6.4	1	W-241 O-241	W-4.02 O-4.02	1.132E-2	4.798E-4	0.0	98.93	380	31.6	0.1361	0.00227	19	6964	1.633
		2	W-302 O-301	W-5.03 O-5.02	1.575E-2	4.107E-4	0.0	99.66	381	31.6	0.1899	0.00317	19.2	8713	1.642
		3	W-332 O-332	W-5.53 O-5.53	1.784E-2	9.074E-4	0.00029	99.23	380	31.6	0.2145	0.00357	18	9579	1.630
		4	W-362 O-362	W-6.03 O-6.03	2.142E-2	6.530E-4	0.0	99.54	382	31.6	0.2590	0.00432	20.2	10445	1.642
		5	W-422 O-422	W-7.03 O-7.03	2.515E-2	9.987E-4	0.00014	99.53	384.5	31.6	0.306	0.0051	19.5	12178	1.630

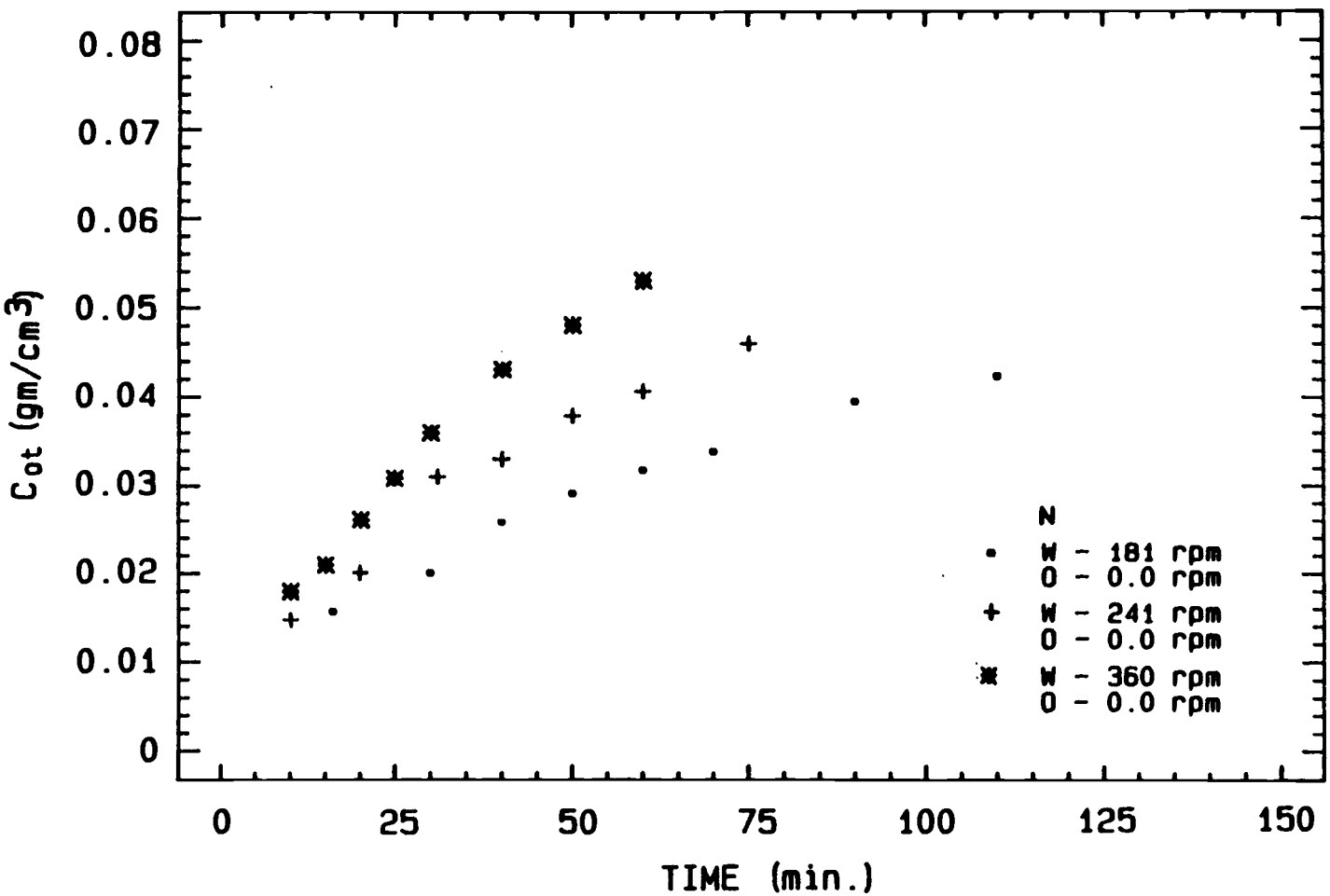

Figure (6.5). Time dependence of transferred n-butanol concentration in the water phase when the n-butanol phase was kept unagitated while the water phase agitation rate was varied.

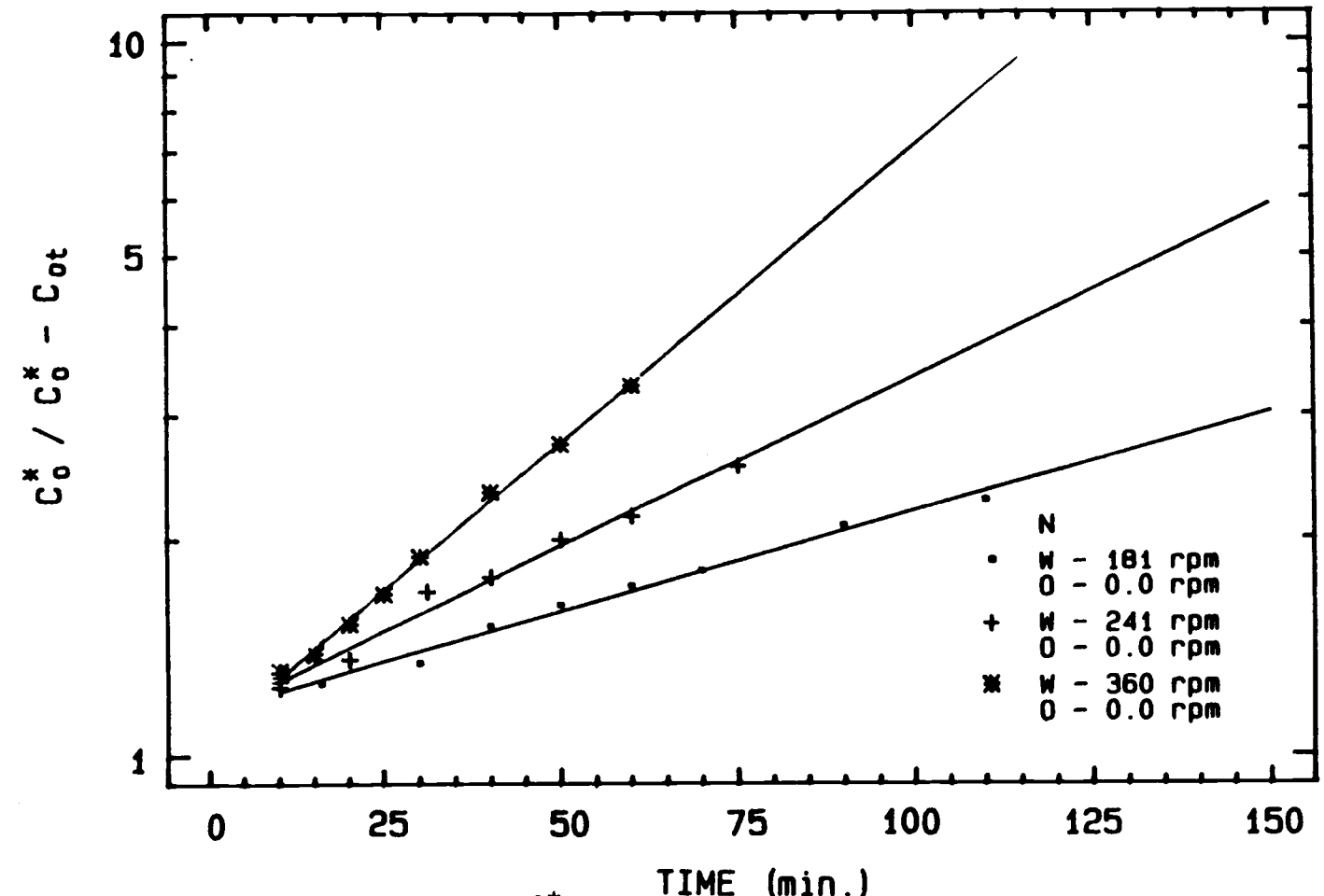

Figure (6.6). Fitted lines of $\ln \frac{C_o^*}{C_o^* - C_{ot}}$ vs. time in the water phase when the n-butanol phase was kept unagitated while the water phase agitation rate (rpm) was varied.

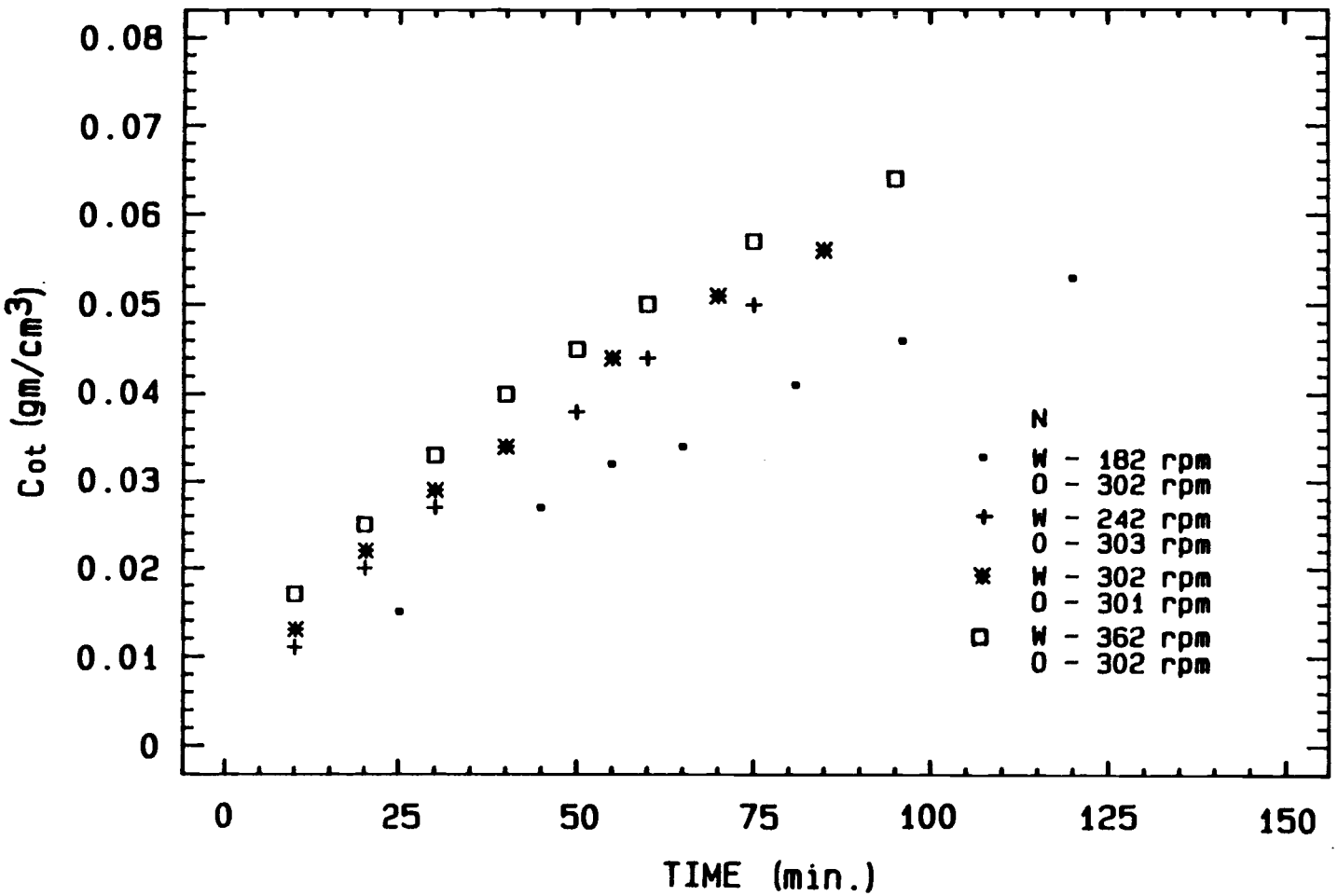

Figure (6.7). Time dependence of transferred n-butanol concentration in the water phase when the n-butanol phase agitation rate (rpm) was kept about (301-303) rpm while the water phase agitation rate was varied.

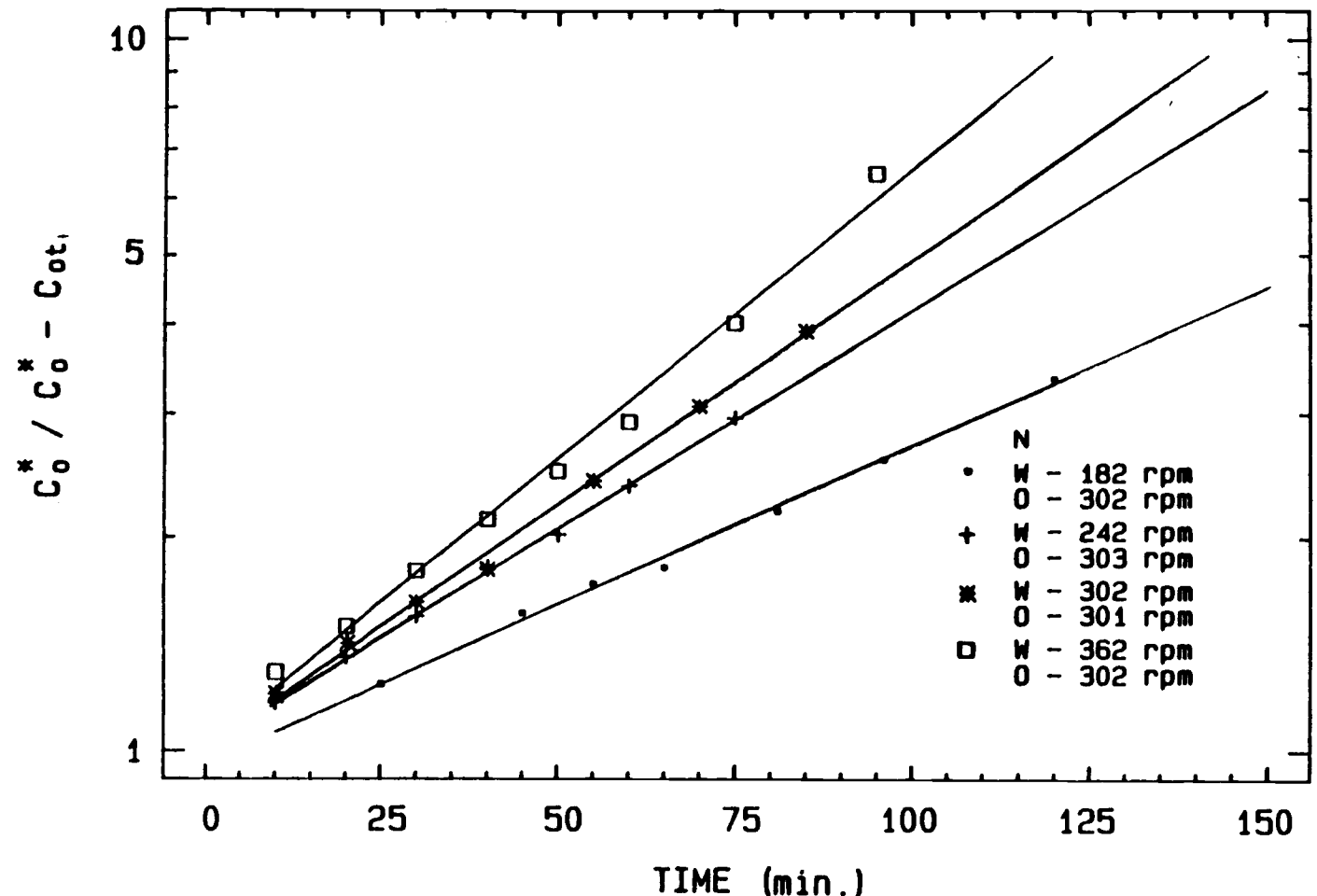

Figure (6.8). Fitted lines of $\ln \frac{C_o^*}{C_o^* - C_{ot}}$ vs. time in the water phase when the n-butanol phase agitation rate was kept about (301-303) rpm while the water phase agitation rate was varied.

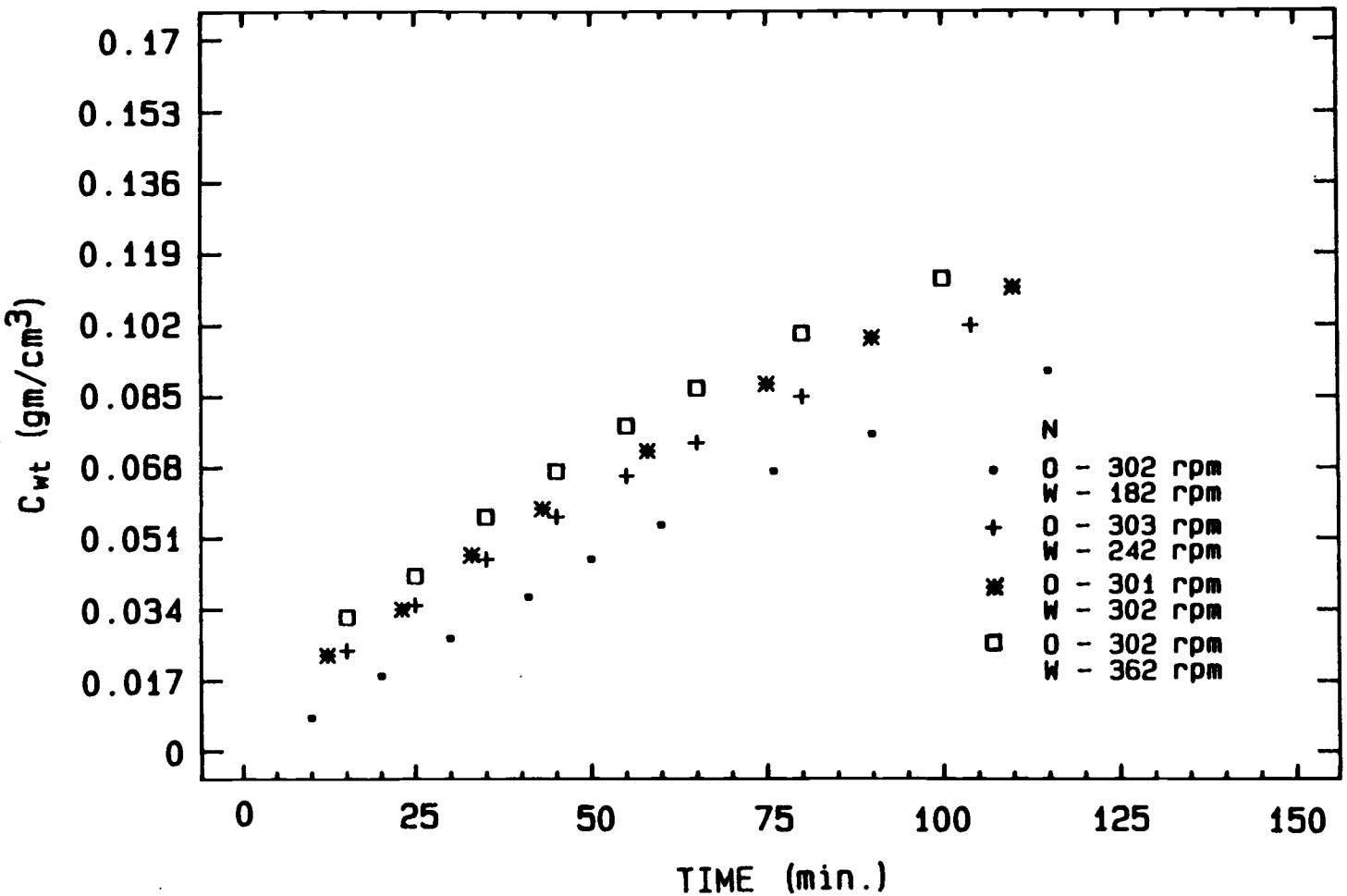

Figure (6.9). Time dependence of transferred water concentration in the n-butanol phase when the n-butanol phase agitation rate was kept about (301-303) rpm while the water phase agitation rate was varied.

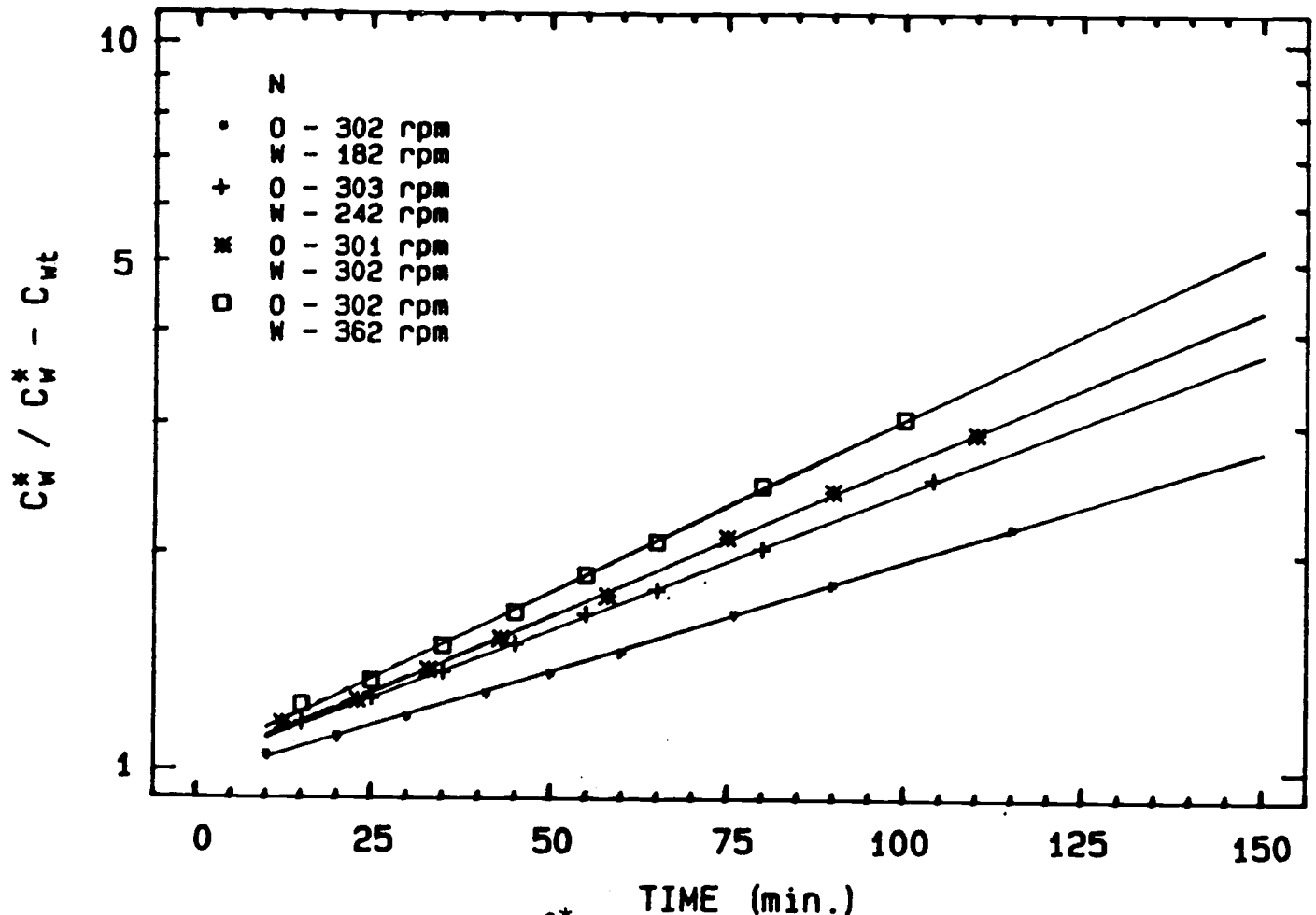

Figure (6.10). Fitted lines of $\ln \frac{C^*_w}{C^*_w - C_{wt}}$ vs. line in the n-butanol phase when the n-butanol phase agitation was kept about 301-302 rpm while the water phase agitation was varied.

c. Three runs were investigated in which the n-butanol phase agitation rate was kept constant at about (362-365) rpm, while the water phase agitation rate was varied. The agitation rates were 185, 302, and 362, respectively. Figure (6.11) and Figure (6.13) show the time dependence of the transferred n-butanol concentration in the water phase and the transferred water concentration in the n-butanol phase, respectively. Figure (6.12) and Figure (6.14) show the fitted line of their ln $(C_o^*/C_o^* - C_{ot})$ versus time, respectively.

The evaluated mass transfer coefficients in each phase and their statistical analysis parameters for this set of runs are presented in Table (6.2).

3. The experimental cell was operated for several runs to study the effect of the aqueous phase agitation rate on the mass transfer coefficient in the organic phase. Similar operating procedures and calculations, as in set of runs (2), were done for this set of runs as follows:

a. Three runs were investigated in which the water phase was kept unagitated while the n-butanol phase was agitated. The agitated rates of the n-butanol phase were 242, 302, and 423 rpm, respectively. Figure (6.15) shows the concentration changing of transferred water in the n-butanol phase, while Figure (6.16) shows the fitted lines of their ln $(C_w^*/C_w^* - C_{wt})$ versus times.

b. Three runs were investigated in which the water phase was kept constant about 302 rpm, while the n-butanol phase agitation rate was varied. It was 212, 301 and 363, respectively.

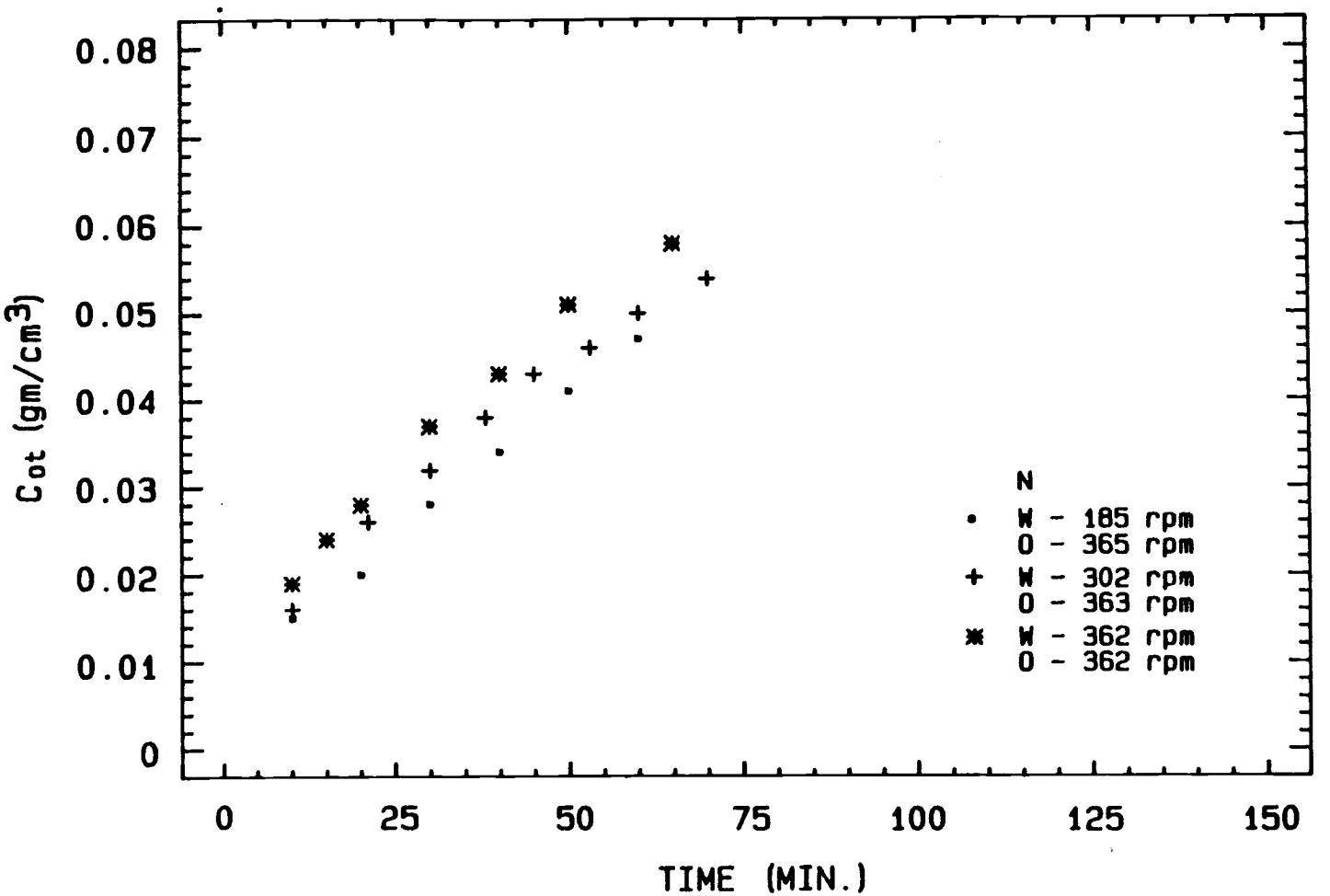

Figure (6.11). Time dependence of transferred n-butanol concentration in the water phase when the n-butanol phase agitation rate was kept about (362-365) rpm, while the water phase agitation rate was varied.

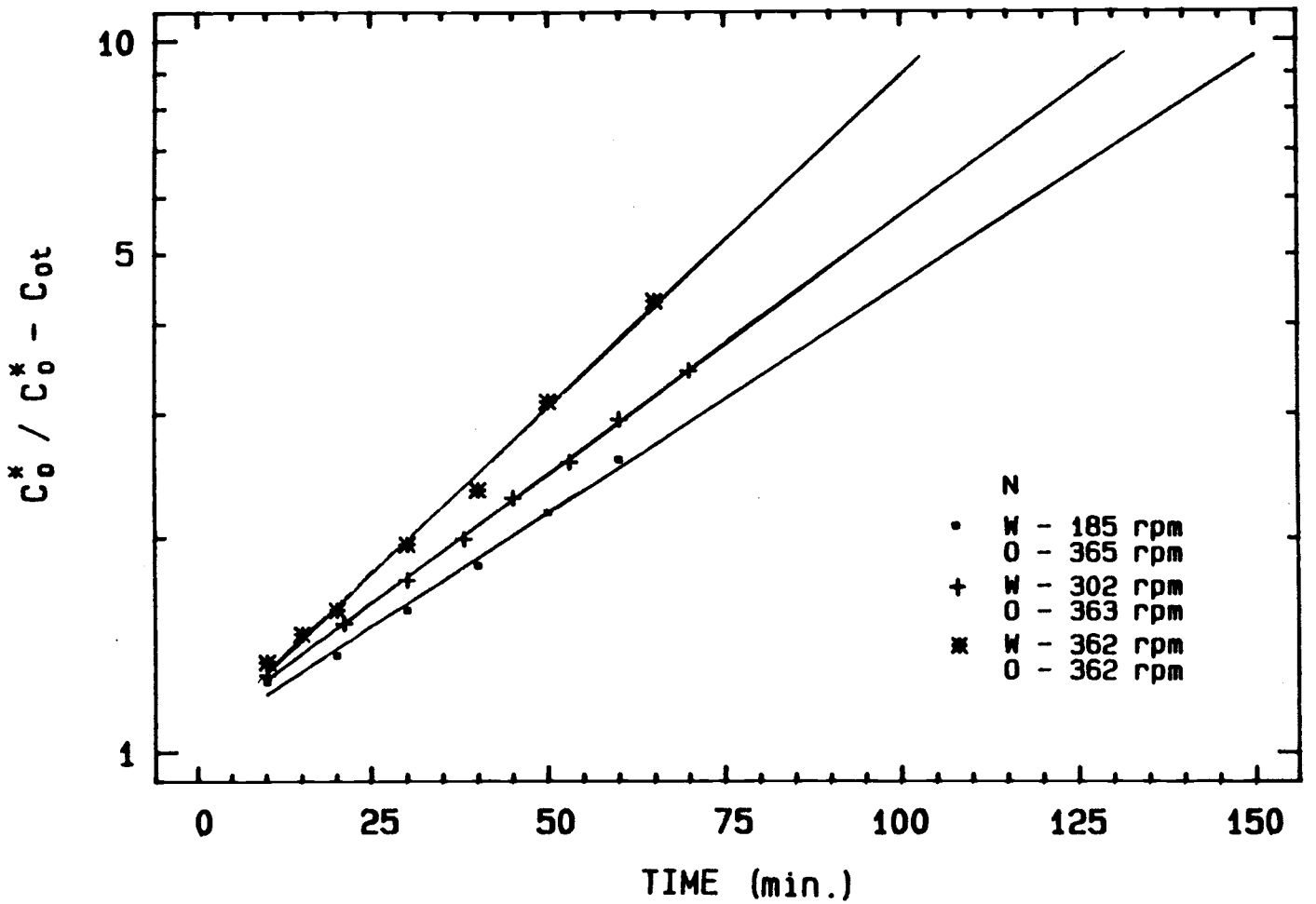

Figure (6.12). Fitted lines of $\ln \frac{C_o^*}{C_o^* - C_{ot}}$ vs. time in the water phase when the n-butanol phase agitation was kept about 362-365 rpm while the water phase agitation rate was varied.

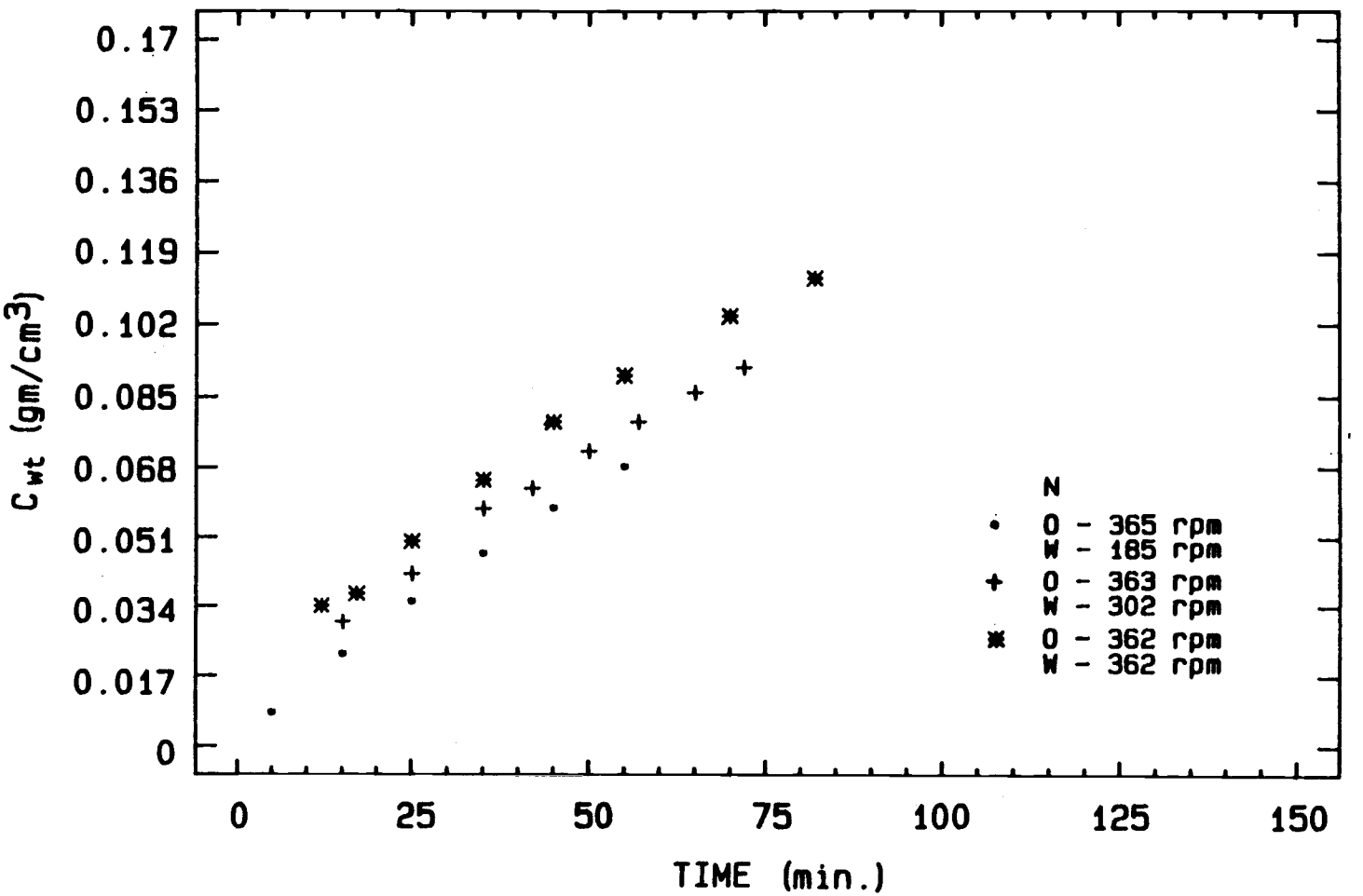

Figure (6.13). Time dependence of transferred water concentration in the n-butanol phase when the n-butanol phase agitation rate was kept about (362-365) rpm, while the water phase agitation rate was varied.

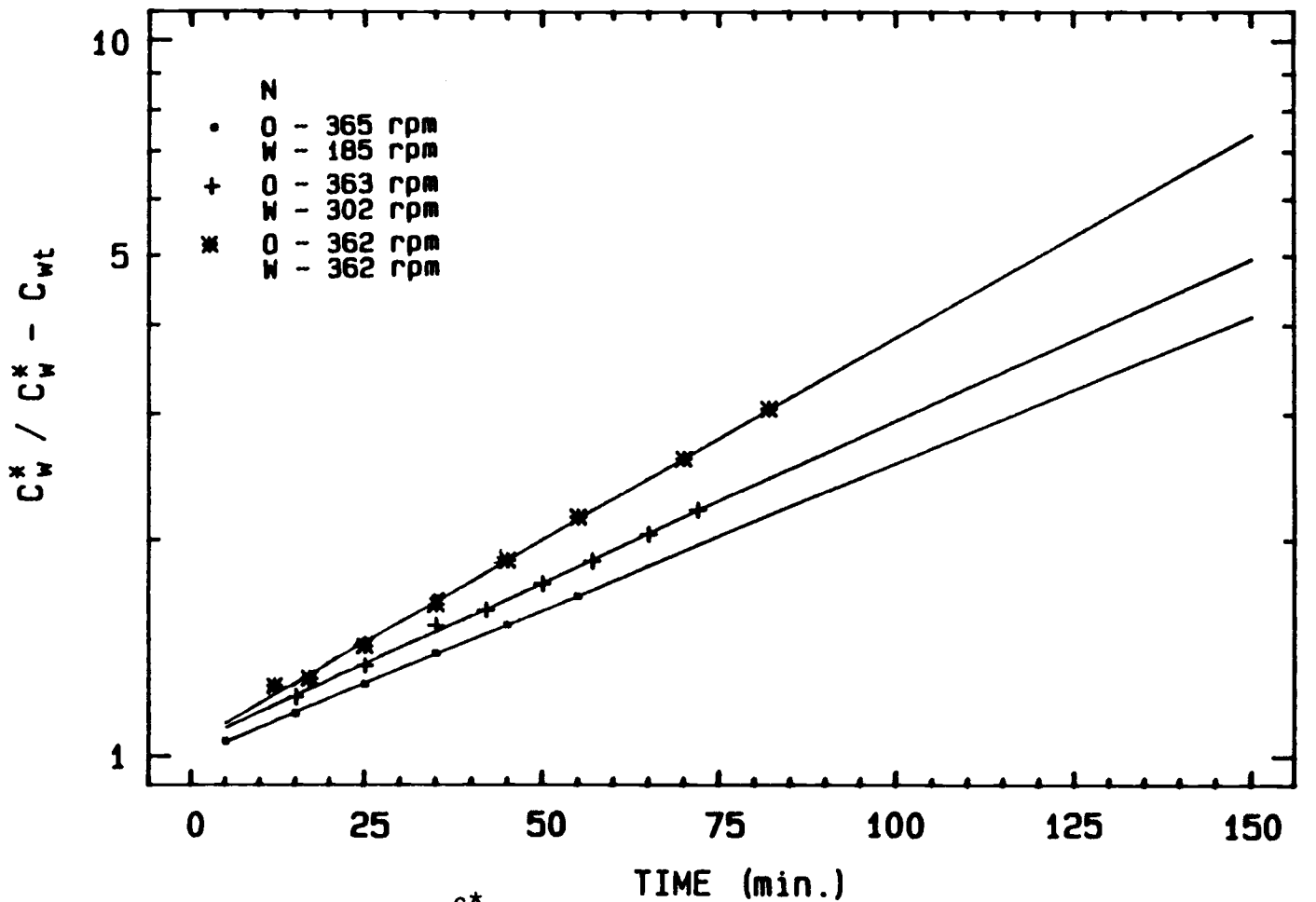

Figure (6.14). Fitted lines of $\ln \frac{C_w^*}{C_w^* - C_{wt}}$ vs. time in the n-butanol phase when the n-butanol phase agitation rate was kept about (362-365) rpm, while the water phase agitation rate was varied.

Table(6.2). Evaluated k and Parameters for Equation $\ln (C^*/C^*-C_t) = (kA/V)t$, where kA/V = slope, when the n-butanol Phase was Agitated at Constant Rate while the Water Phase Agitation Rate was Varied.

Phase	Figure number	Run number	N rpm	N rps	Fitted line slope	Standard error (±)	Probability level	R-squared %	Phase volume V (cm^3)	Interfacial area A (cm^2)	k($\frac{cm}{min}$)	k($\frac{cm}{sec}$)	Temp. C^o	Re ($\frac{NL^2\rho}{\mu}$)
Water	6.6	6	W-181 O-0.0	W-3.02 O-0.0	6.450E-3	3.119E-4	0.0	98.62	376	31.6	0.0767	0.00128	19	5231
		7	W-241 O-0.0	W-4.02 0.0.0	1.098E-2	6.466E-4	0.00001	98.3	376.5	31.6	0.1308	0.00218	18.2	6964
		8	W-360 O-0.0	W-6.0 O-0.0	1.906E-2	4.092E-4	0.0	99.72	376.5	31.6	0.2271	0.00379	18	10393
Water	6.8	9	W-182 O-302	W-3.03 O-5.03	1.030E-2	2.728E-4	0.0	99.65	380	31.6	0.1238	0.00206	19.8	5249
		10	W-242 O-303	W-4.03 O-5.05	1.415E-2	2.220E-4	0.0	99.88	380	31.6	0.1701	0.00284	18.5	698[illegible]
		2	W-302 O-301	W-5.03 O-5.02	1.575E-2	4.107E-4	0.0	99.66	381	31.6	0.1899	0.00317	19.2	8713
		11	W-362 O-302	W-6.03 O-5.03	1.865E-2	6.868E-4	0.0	99.18	380	31.6	0.2243	0.00374	18	10445
n-butanol	6.1	9	O-302 W-182	O-5.03 W-3.03	6.970E-3	6.023E-5	0.0	99.95	380	31.6	0.0838	0.0014	19.8	2392
		10	O-303 W-242	O-5.05 W-4.03	8.699E-3	8.505E-5	0.0	99.97	380	31.6	0.1046	0.00174	18.5	2402
		2	O-301 W-302	O-5.02 W-5.03	9.624E-3	1.224E-4	0.0	99.9	381	31.6	0.116	0.00193	19.2	2388
		11	O-302 W-362	O-5.03 W-6.03	1.086E-2	1.468E-4	0.0	99.89	380	31.6	0.1306	0.00218	18	2392

Table (6.2). continued

Phase	Figure number	Run number	N rpm	N rps	Fitted line slope	Standard error (±)	Probability level	R-squared %	Phase volume V (cm^3)	Interfacial area A (cm^2)	$k(\frac{cm}{min})$	$k(\frac{cm}{sec})$	Temp. C^o	$(\frac{NL^2\rho}{\mu})$
Water	6.12	12	W-185 O-365	W-3.08 O-6.08	1.476E-2	7.664E-4	0.00004	98.93	383	31.6	0.1789	0.00298	17.7	5335
		13	W-302 O-363	W-5.03 O-6.05	1.670E-2	1.988E-4	0.0	99.81	383	31.6	0.2024	0.00337	17	8713
		4	W-362 O-362	W-6.03 O-6.03	2.142E-2	6.530E-4	0.0	99.54	382	31.6	0.2590	0.00432	20.2	10445
n-butanol	6.14	12	O-365 W-185	O-6.08 W-3.08	9.434E-3	7.157E-5	0.0	99.98	383	31.6	0.1143	0.00191	17.7	2892
		13	O-363 W-302	O-6.05 W-5.03	1.042E-2	1.845E-4	0.0	99.81	383	31.6	0.1262	0.0021	17	2878
		4	O-362 W-362	O-6.03 W-6.03	1.306E-2	2.134E-4	0.0	99.54	382	31.6	0.1579	0.00263	20.2	2868

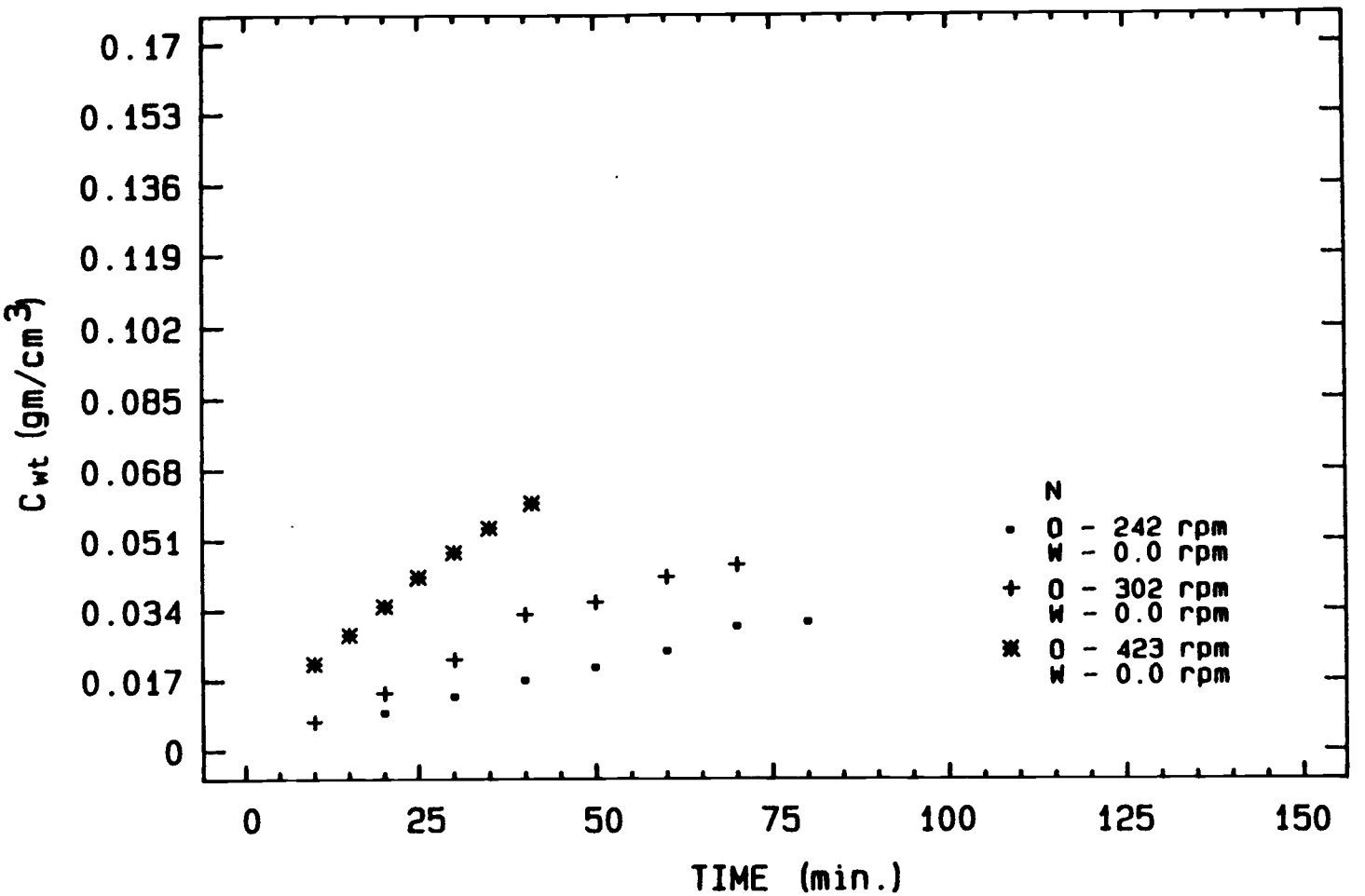

Figure (6.15). Time dependence of transferred water concentration in the n-butanol phase when the water phase was kept unagitated, while the n-butanol phase agitation rate was varied.

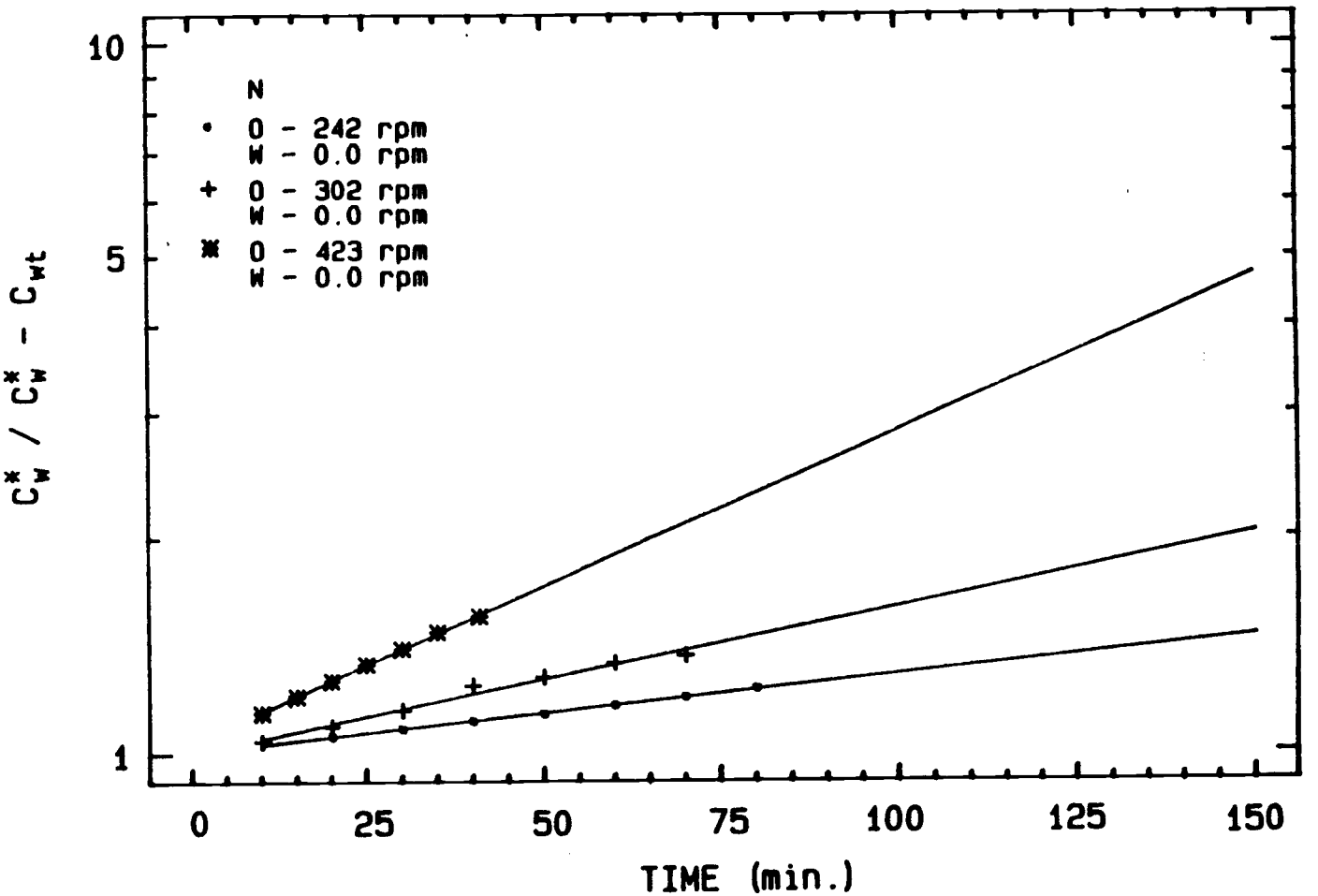

Figure (6.16). Fitted lines of $\ln \frac{C_w^*}{C_w^* - C_{wt}}$ vs. time in the n-butanol phase when the water phase was kept unagitated, while the n-butanol phase agitation rate was varied.

Figure (6.17) and Figure (6.19) show the time dependence of transferred water concentration in the n-butanol phase and transferred n-butanol concentration in the water phase, respectively. Figure (6.18) and Figure (6.20) show the fitted lines of their ln $(C_w^*/C_w^* - C_{wt})$ and ln $(C_o^*/C_o^* - C_{ot})$ versus time, respectively.

c. Three runs were investigated in which the water phase agitation rate was kept constant about (362-365) rpm, while the n-butanol phase agitation rate was varied. It was 212, 302 and 362 rpm , respectively. Figure (6.21) and Figure (6.23) show the time dependence of transferred water concentration in the n-butanol phase and transferred n-butanol concentration in the water phase, respectively. Figure (6.22) and Figure (6.24) show the fitted lines of their ln $(C_w^*/C_w^* - C_{wt})$ and ln $(C_o^*/C_o^* - C_{ot})$ us time, respectively.

The evaluated mass transfer coefficient in both phases and their statistical analysis parameter for this set of runs are presented in Table (6.3).

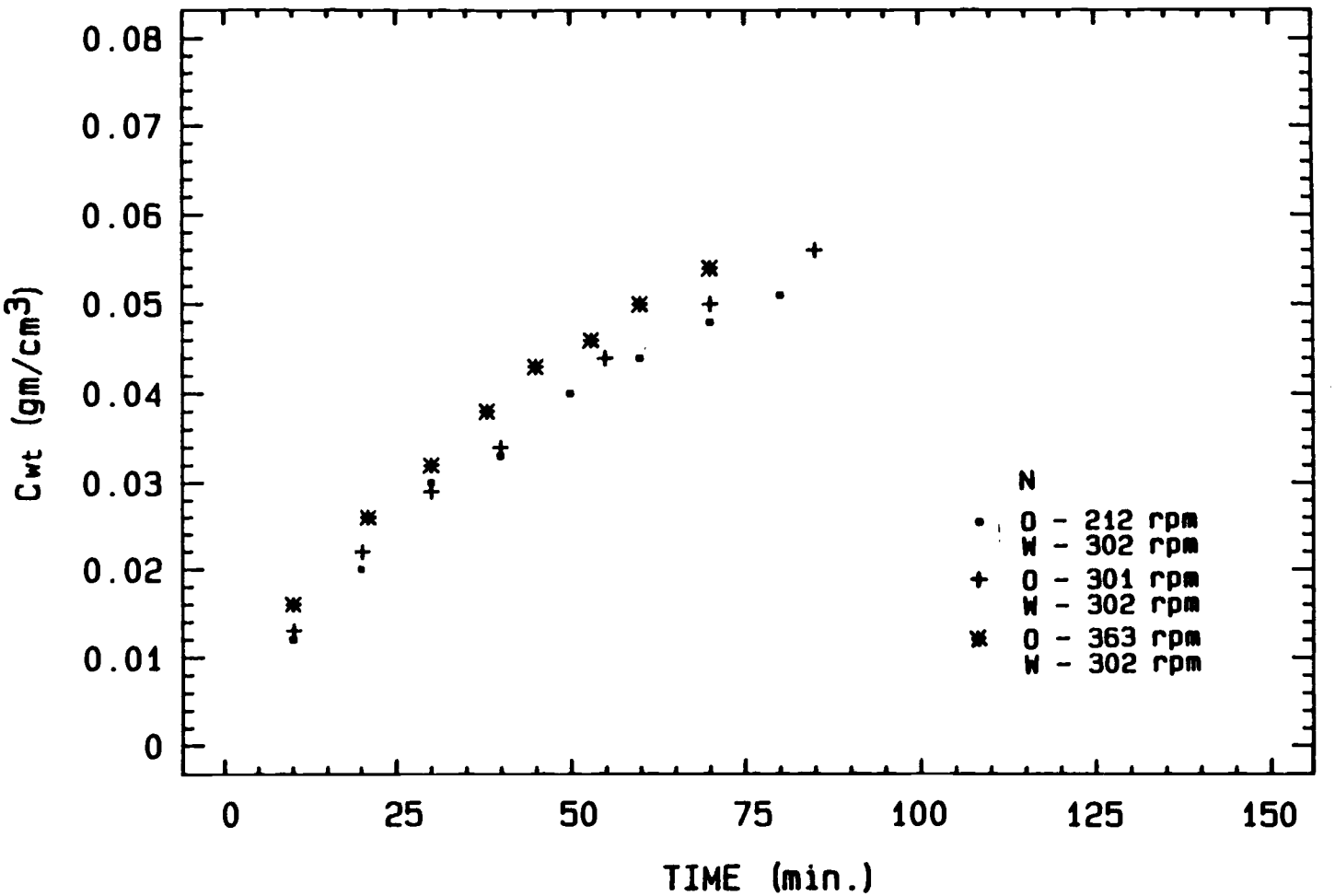

Figure (6.17). Time dependence of transferred water concentration in the n-butanol phase when the water phase agitation rate was kept about 302 rpm, while the n-butanol phase was varied.

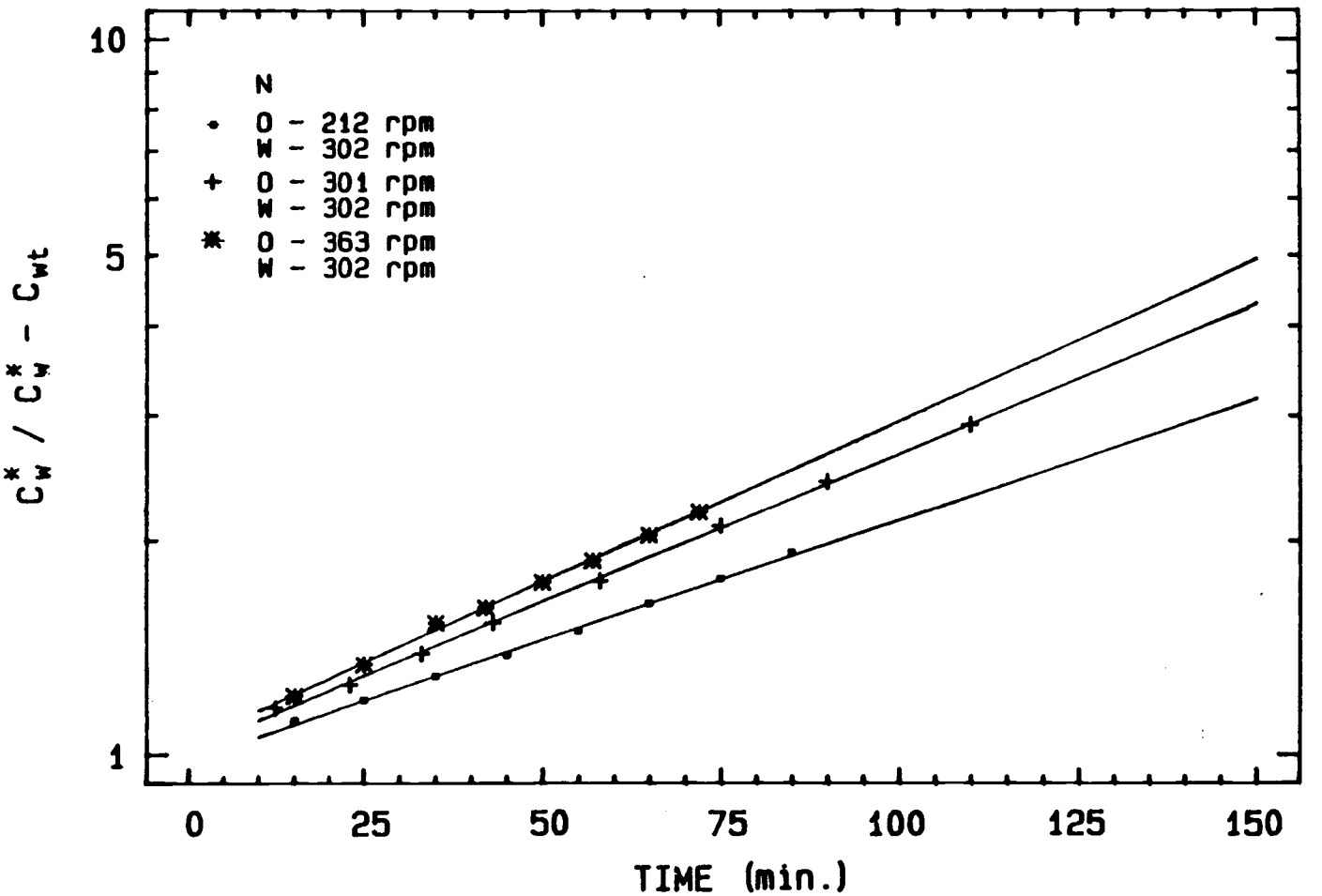

Figure (6.18). Fitted lines of $\ln \frac{C_w^*}{C_w^* - C_{wt}}$ vs. time in the n-butanol phase when the water phase agitation rate was kept about 302 rpm, while the n-butanol phase agitation rate was varied.

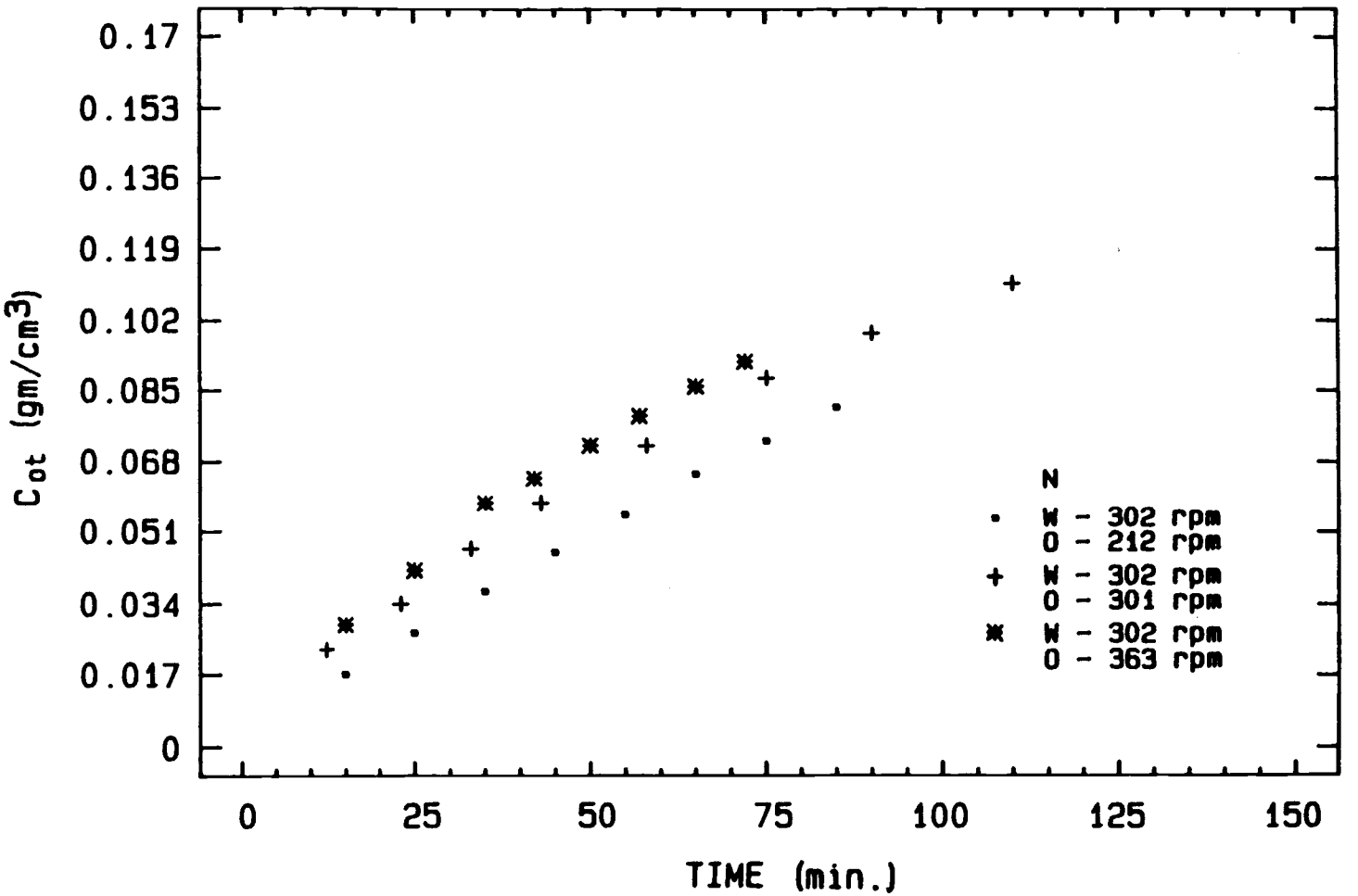

Figure (6.19). Time dependence of transferred n-butanol concentration in the water phase when the water phase agitation was kept about 302, while the organic phase agitation rate was varied.

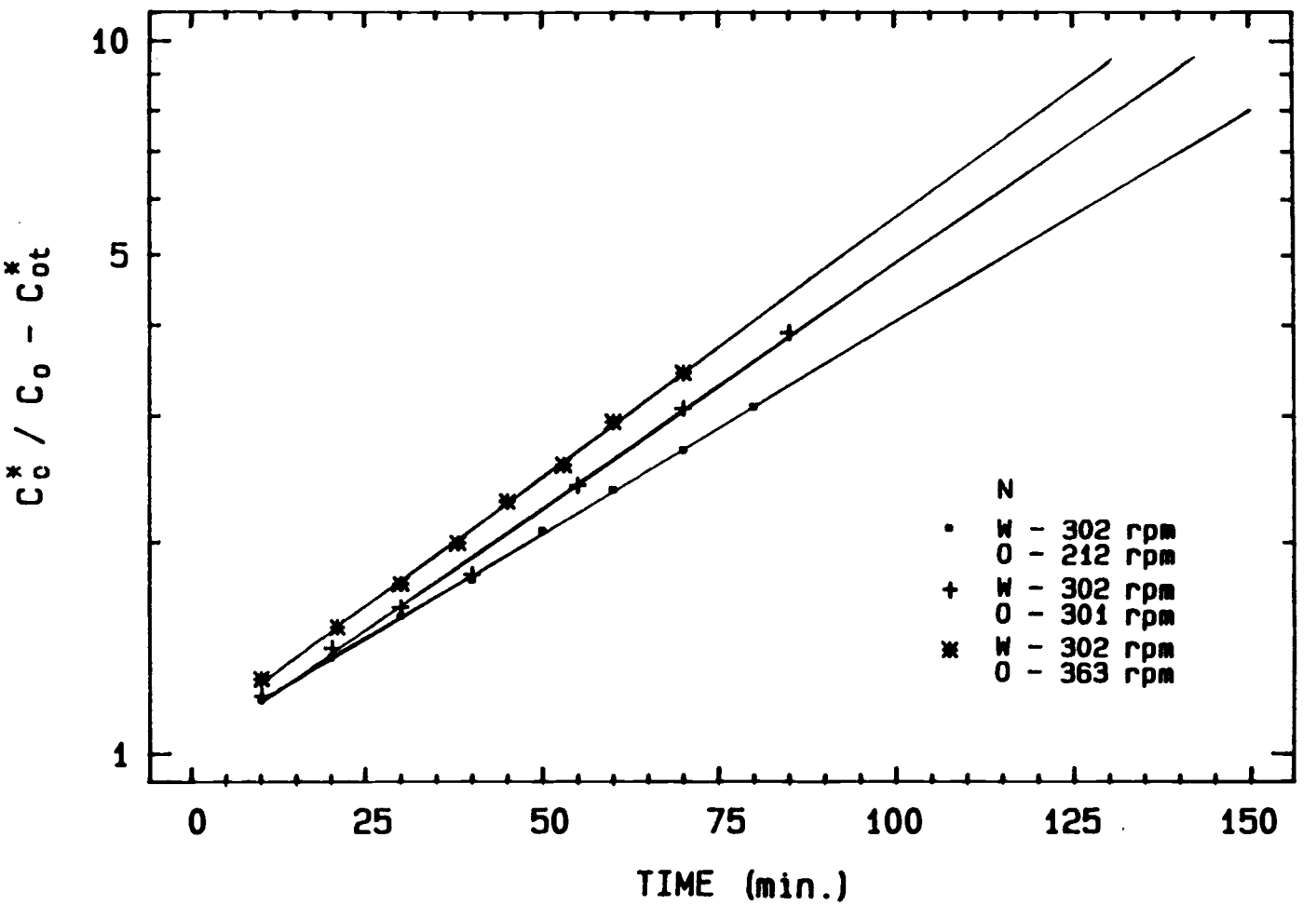

Figure (6.20). Fitted lines of $\ln \frac{C_o^*}{C_o^* - C_{ot}}$ vs. time in the water phase when the water phase agitation rate was kept about 302 while the n-butanol phase was varied.

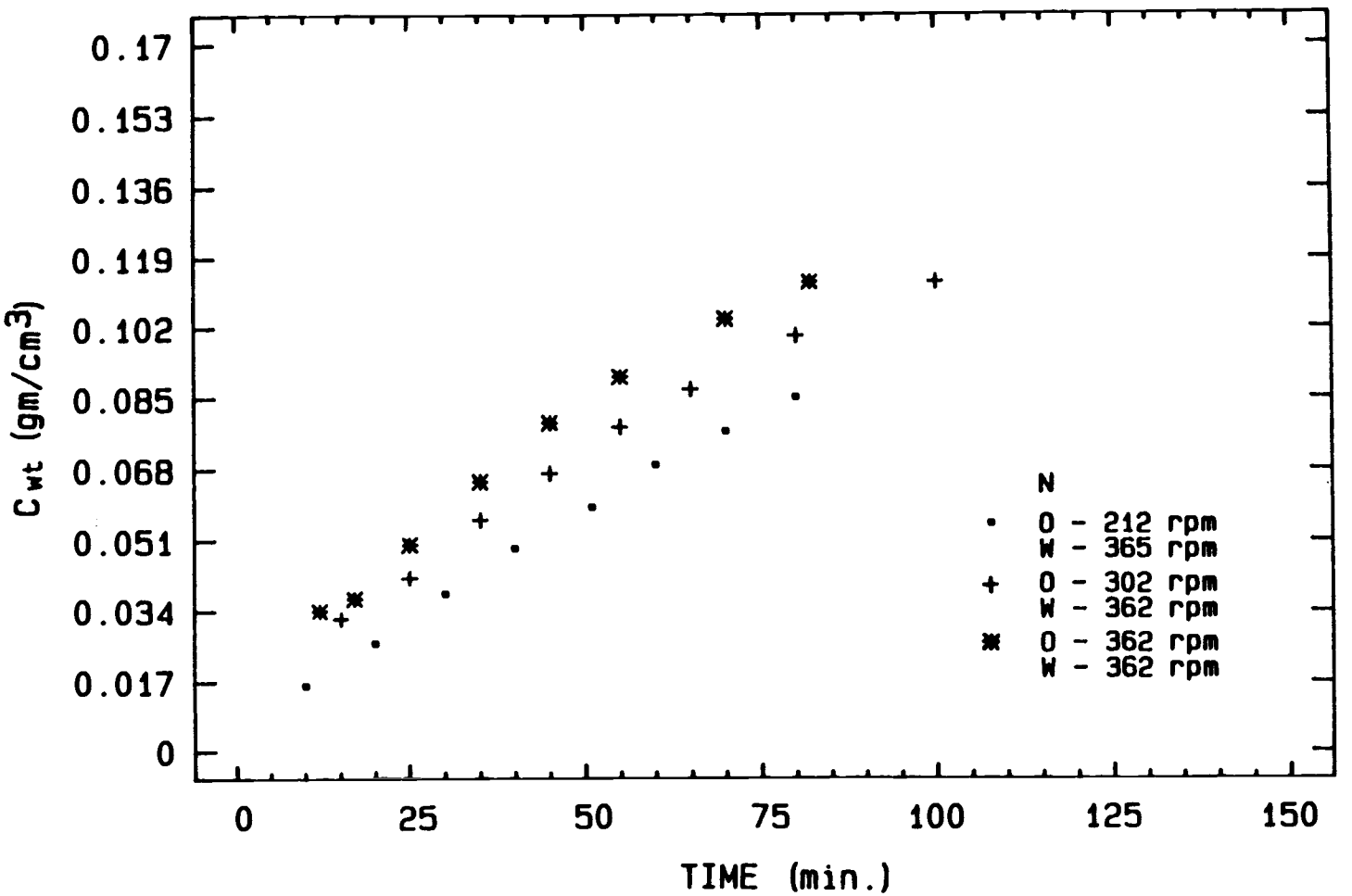

Figure (6.21). Time dependence of transferred water concentration in the n-butanol phase when the water phase agitation rate was kept about (362-365) rpm, while the n-butanol phase was varied.

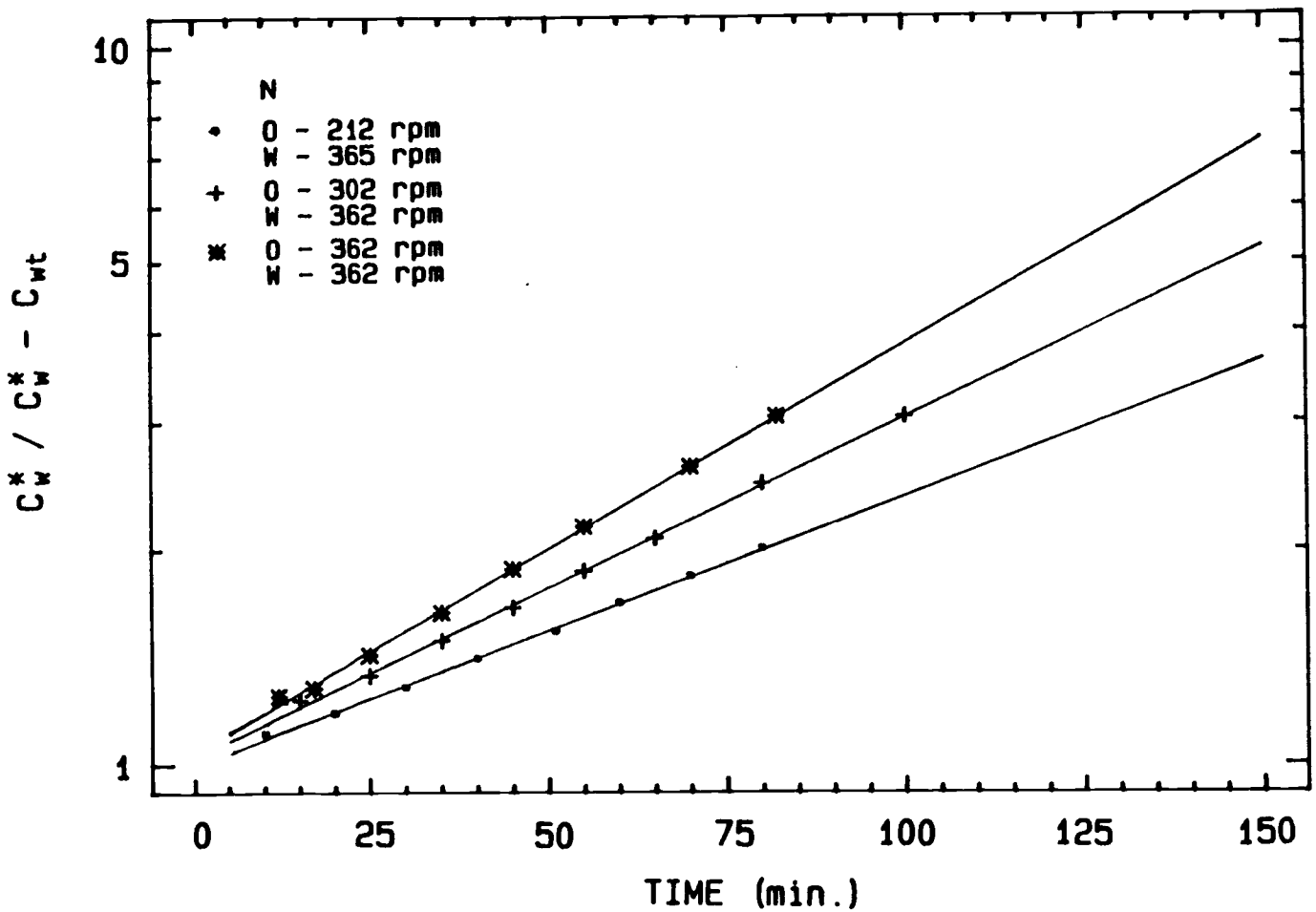

Figure (6.22). Fitted lines of $\ln \frac{C_w^*}{C_w^*-C_{wt}}$ vs. time in the n-butanol phase when the water phase agitation rate was kept about 362-365, while the n-butanol phase agitation rate was varied.

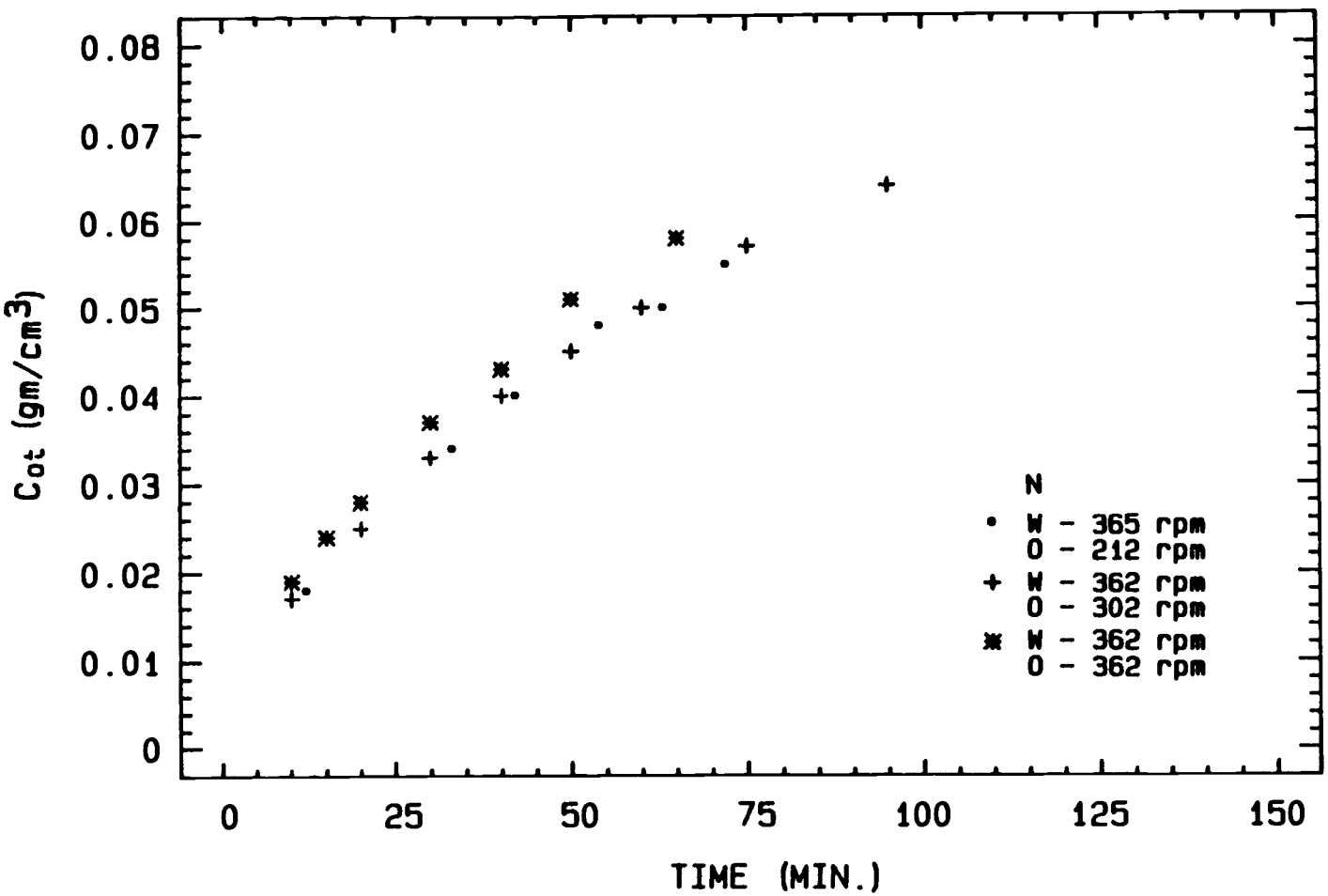

Figure (6.23). Time dependence of transferred n-butanol concentration in the water phase when the water phase agitation rate was kept about (362-365) rpm, while the n-butanol phase agitation rate was varied.

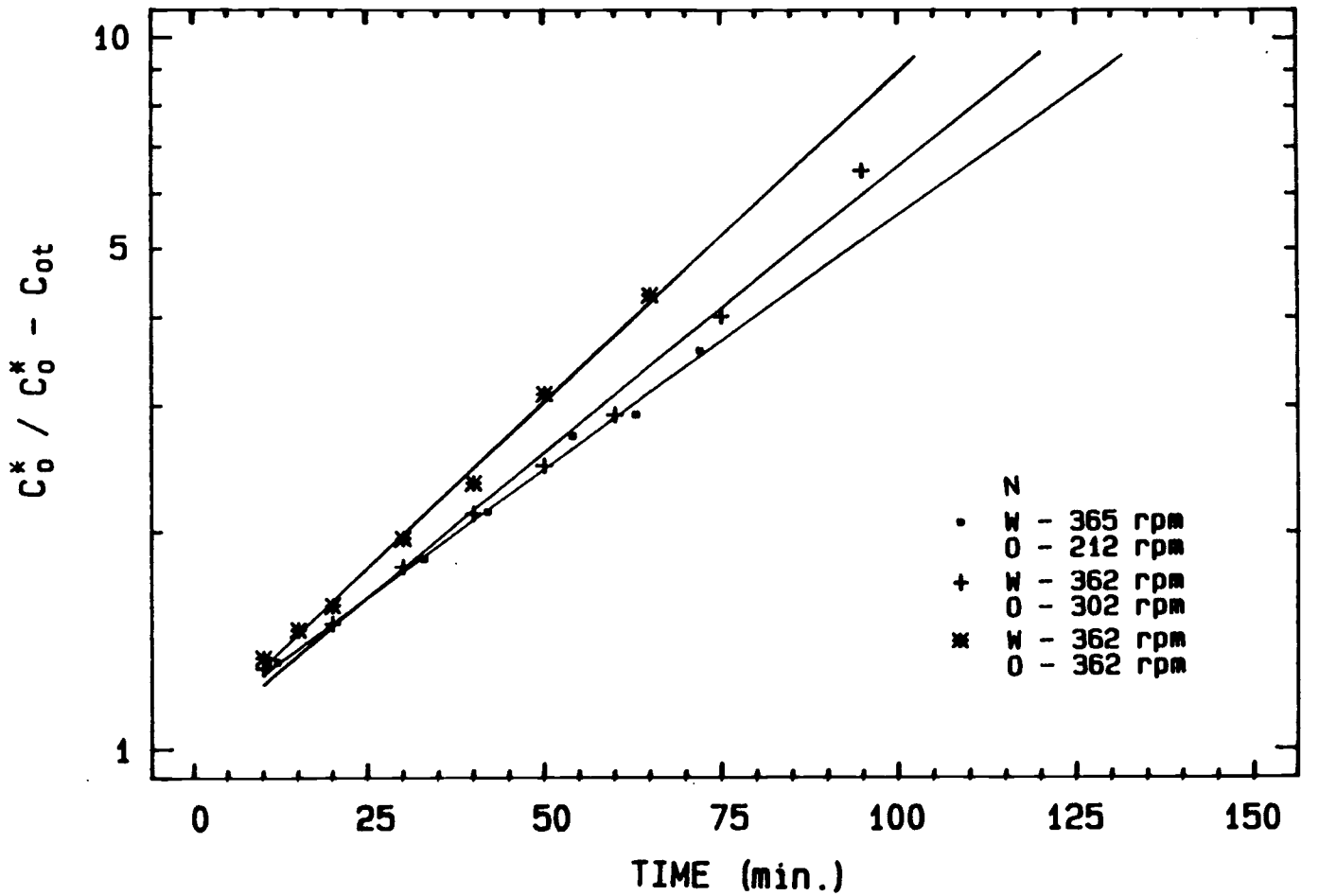

Figure (6.24). Fitted lines of $\ln \frac{C_o^*}{C_o^* - C_{ot}}$ vs. time in the water phase when the water phase agitation rate was kept about (362-365) rpm while the n-butanol phase agitation rate was varied.

Table(6.3). Evaluated k and Parameters for Equation $\ln (C^*/C^*-C_t) = (kA/V)t$, where kA/V = Slope, when the Water Phase was Agitated at Constant Rate while the n-butanol Phase Agitation Rate was Varied.

Phase	Figure number	Run number	N rpm	N rps	Fitted line slope	Standard error (±)	Probability level	R-squared %	Phase volume V (cm^3)	Interfacial area A (cm^2)	k($\frac{cm}{min}$)	k($\frac{cm}{sec}$)	Temp. C^o	Re ($\frac{NL^2\rho}{\mu}$)
n-butanol	6.16	14	O-242 W-0.0	O-4.03 W-0.0	2.483E-3	3.984E-5	0.0	99.87	387.5	31.6	0.0304	0.0005	19	1917
		15	O-302 W-0.0	O-5.03 W-0.0	4.721E-3	3.011E-4	0.00002	98.01	386	31.6	0.0577	0.00096	18.5	2392
		16	O-423 W-0.0	O-7.05 W-0.0	1.013E-2	1.158E-4	0.0	99.93	386	31.6	0.1237	0.00206	18	3353
n-butanol	6.18	17	O-212 W-302	O-3.53 W-5.03	7.822E-3	1.396E-4	0.0	99.81	385	31.6	0.0953	0.00159	18.4	1679
		2	O-301 W-302	O-5.02 W-5.03	9.624E-3	1.224E-4	0.0	99.90	381	31.6	0.1160	0.00193	19.2	2388
		13	O-363 W-302	O-6.05 W-5.03	1.042E-2	1.845E-4	0.0	99.81	383	31.6	0.1261	0.0021	17	2878
Water	6.20	17	W-302 O-212	W-5.03 O-3.53	1.360E-2	1.236E-4	0.0	99.95	385	31.6	0.1657	0.00276	18.4	8713
		2	W-302 O-301	W-5.03 O-5.02	1.575E-2	4.107E-4	0.0	99.66	381	31.6	0.1899	0.00317	19.2	8713
		13	W-302 O-363	W-5.03 O-6.05	1.670E-2	1.988E-4	0.0	99.81	383	31.6	0.2024	0.00337	17	8713

Table(6.3). continued

Phase	Figure number	Run number	N rpm	N rps	Fitted line slope	Standard error (±)	Probability level	R-squared %	Phase volume V (cm^3)	Interfacial area A (cm^2)	$k(\frac{cm}{min})$	$k(\frac{cm}{sec})$	Temp. C^o	$(\frac{Ni^2\rho}{\mu})^{Re}$
n-butanol	6.22	18	O-212 W-365	O-3.53 W-6.08	8.606E-3	1.355E-4	0.0	99.85	382	31.6	0.1040	0.00173	17	1679
		11	O-302 W-362	O-5.03 W-6.03	1.086E-2	1.468E-4	0.0	99.89	380	31.6	0.1306	0.00218	18	2392
		4	O-362 W-362	O-6.03 W-6.03	1.306E-2	2.134E-4	0.0	99.54	382	31.6	0.1579	0.00263	20.2	2868
Water	6.24	18	W-365 O-212	W-6.08 O-3.53	1.653E-2	6.211E-4	0.00001	98.44	382	31.6	0.1998	0.00333	17	10532
		11	W-362 O-302	W-6.03 O-5.03	1.865E-2	6.868E-4	0.0	99.18	380	31.6	0.2243	0.00374	18	10445
		4	W-362 O-362	W-6.03 O-6.03	2.142E-2	6.530E-4	0.0	99.54	382	31.6	0.2590	0.00432	20.2	10445

Chapter 7

Analysis and Discussion of Results

For the stirred mixing cell, the mixing Reynolds number (Re), Schmidt number (Sc) and Sherwood number (Sh) are defined as follows:

$$Re = \frac{NL^2\rho}{\mu} \tag{7.1}$$

$$Sc = \frac{\mu}{\rho D} \tag{7.2}$$

$$Sh = \frac{kL}{D} \tag{7.3}$$

where N is the number of revolutions per time, L is the impeller diameter, D is the diffusivity, k is the mass transfer coefficient, ρ is the fluid density and is the fluid viscosity. By using the physical properties of water and n-butanol as listed in Table (5.1), the dimensionless numbers for both phase are:

a. Water phase

$$Re_w = 1732.3\ N\ (rps) \tag{7.4}$$

$$Sc_w = 1282.1 \tag{7.5}$$

$$Sh_w = 533590\ k_w\ (\frac{cm}{sec.}) \tag{7.6}$$

b. n-butanol phase

$$Re_o = 475.6\ N\ (rps) \tag{7.7}$$

$$Sc_o = 14007.6 \tag{7.8}$$

$$Sh_o = 1600769\ k_o\ (\frac{cm}{sec.}) \tag{7.9}$$

7.1 The Effect of Agitation Rate on the Mass Transfer Coefficient

The agitation rate (rps) in each phase of the mixing cell represents the degree of the turbulency in that phase in terms of its Reynolds number (Re). The effect of the phase agitation rate in one phase on the mass transfer coefficient in the other phase were evaluated by the following analysis:

7.1.1 The Effect of the Agitation Rate when the Agitation Rate (rps) is Identical in Both Phases

The data listed in Table (6.1) represents the experimental investigated with the same impeller speeds (rps) in both phases. A log-log plot of the mass transfer coefficient for each phase, k_w, k_o, versus agitation rate (rps) is presented in Figure (7.1). This plot reveals that the values of the mass transfer coefficients in both phases increase as the agitation rate increases. This increase is due to the high degree of turbulence and the increased convection flow at the higher agitation rates. The circulated turbulent eddies that carry the transferred component will be increased causing high rate of mass transfer coefficient across the interface. This figure also shows that the increase in the k_w values with the mixing rate, N, is approximately parallel to the increase in the k_o values with the mixing rate, N. This infers that both k_w and k_o are proportional to the same power of N (rps) when both phases are mixed at the same agitation speed. In addition, k_w is not apparently affected by the N (rps) of the organic phase and vice versa. The mass transfer coefficient in the water phase, k_w, is higher than that in the

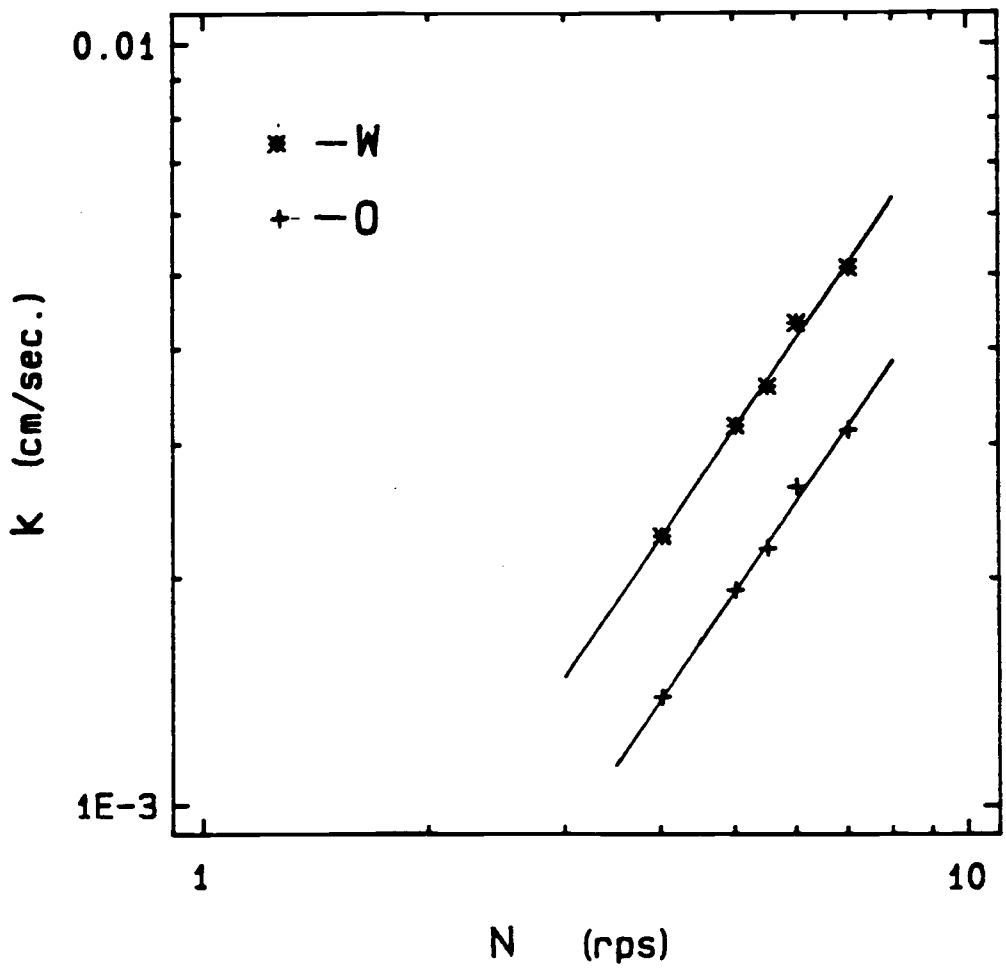

Figure (7.1). k_w and k_o changing with respect to the agitation rate, N (rps), when both phases were agitated at the same speed.

n-butanol phase, k_o. This is partly due to the fact that the diffusivity of n-butanol in water is higher than the diffusivity of water in n-butanol, as mentioned in Table (5.1). In addition, the viscosity of water phase is less than that of the n-butanol phase which gives higher turbulence in terms of Reynolds number (Re) in the water phase than in n-butanol phase. Figure (7.2) shows a plot of k_w/k_o versus N (rps). It indicates that the ratio of k_w/k_o remains constant at an average value of 1.635 as the agitation rate of both phases increases. This confirms Figure (7.1) which infers the two coefficients, k_w and k_o, are not affected by the agitation rate of the organic phase and water phase, respective if both phases are mixed at the same agitation rate. Bulicka and Prochazka [4, 54] and McManamey et al [46] have shown the same behavior when k_w/k_o was plotted versus N (rps) at similar high speed of agitation in the two phases. Their results showed some deviation from the constant ratio of k_w/k_o with N (rps) the ratio increasing at low agitation rate (rps). The same behavior would be expected at very high agitation rates due to an increase in the interfacial area from the interface rippling.

7.1.2 The Effect of the Organic Phase Agitation on the Aqueous Phase Mass Transfer Coefficient

The data for these experiments are listed in Table (6.2); in these runs, the n-butanol phase was kept at a constant agitation rate

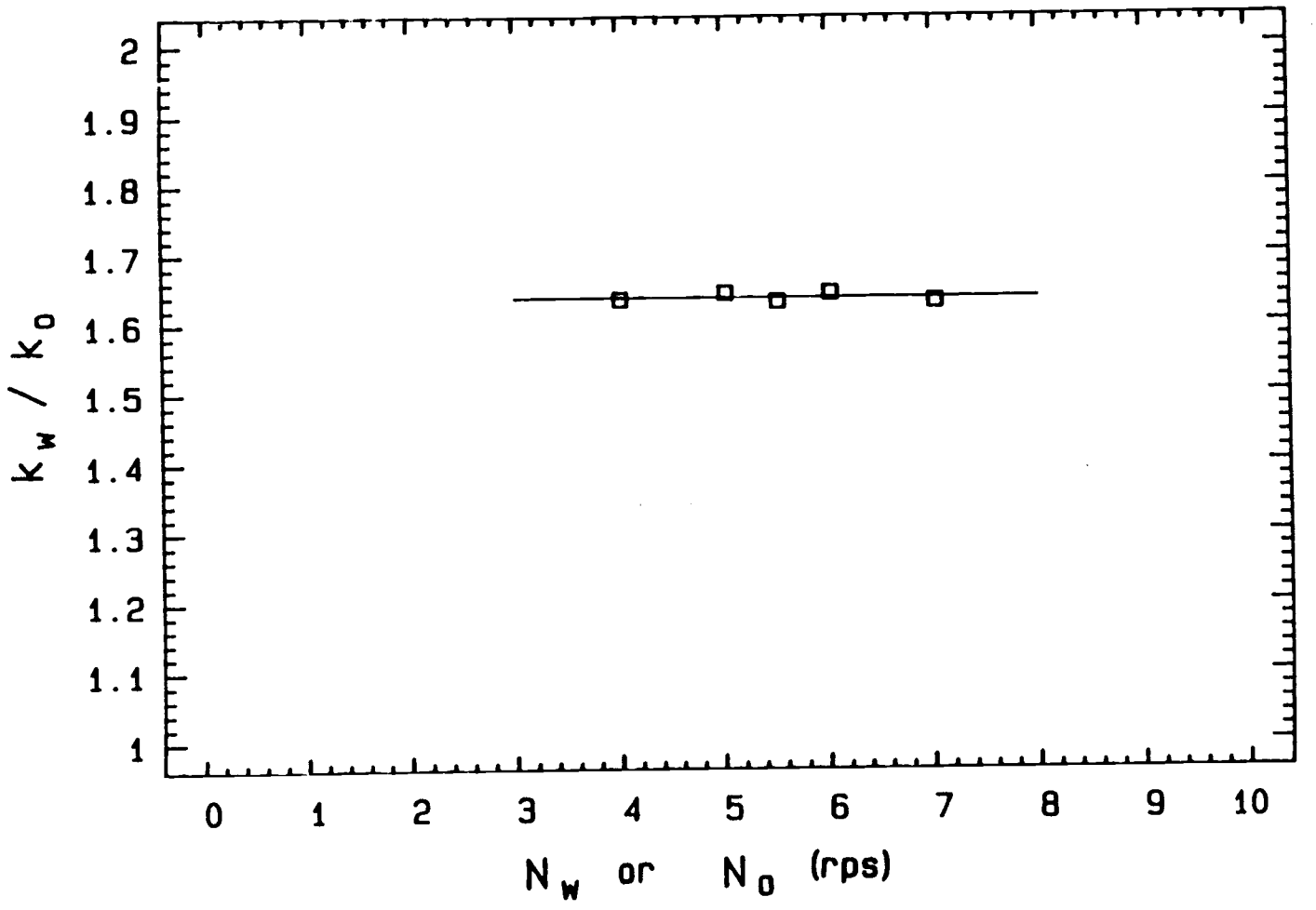

Figure (7.2). A plot of k_w/k_o versus N_w or N_o (rps) when both phases were agitated at the same speed.

while the water phase agitation rate was varied. To illustrate the effect, the mass transfer coefficient in the water phase, k_w, was plotted on a log-log scale versus the Reynolds number of its phase, Re_w, for different Reynolds numbers of the n-butanol phase; this is shown in Figure (7.3). This figure shows that the fitted line (the solid line) of k_w versus the same agitation rates in both phases, as shown in Figure (7.1), becomes the asymtotic line when it is plotted in Figure (7.3). The investigated case, in which the n-butanol phase was unagitated (Re_o = 0.0) reveals in Figure (7.3) that the mass transfer coefficient in the water phase, k_w, at low Re_w is lower than the asymototic line. As the Re_w increases and n-butanol phase remains unagitated, k_w approaches the asymototic line. If the n-butanol phase agitation rate is kept constant at Re_o = 2394 and the water agitation rate is varied below Re_w = 8000, the k_w values are higher than the asymototic line as shown in the figure. As Re_w increases, k_w increases and approaches the asymtotic line near Re_w = 8000 where the effect of Re_o diminishes. By increasing the constant agitation rate of the n-butanol phase to be Re_o = 2879 and keeping Re_w varied below 8000, the figure reveals that k_w is higher even than the value when Re_o = 2394. It also reveals that as Re_w increases, k_w also increases and approaches the asymototic line near Re_w = 8000 where the effect of Re_o diminishes. Asai et al in 1983 [2] studied this effect by plotting k_w versus Re_w at different values of Re_o for the different systems investigated. They also obtained similar behavior as observed in this investigation; however, Asai et al assumed the asymtotic line is the value of k_w versus Re_w which would be obtained with an unagitated organic phase. They ended up with

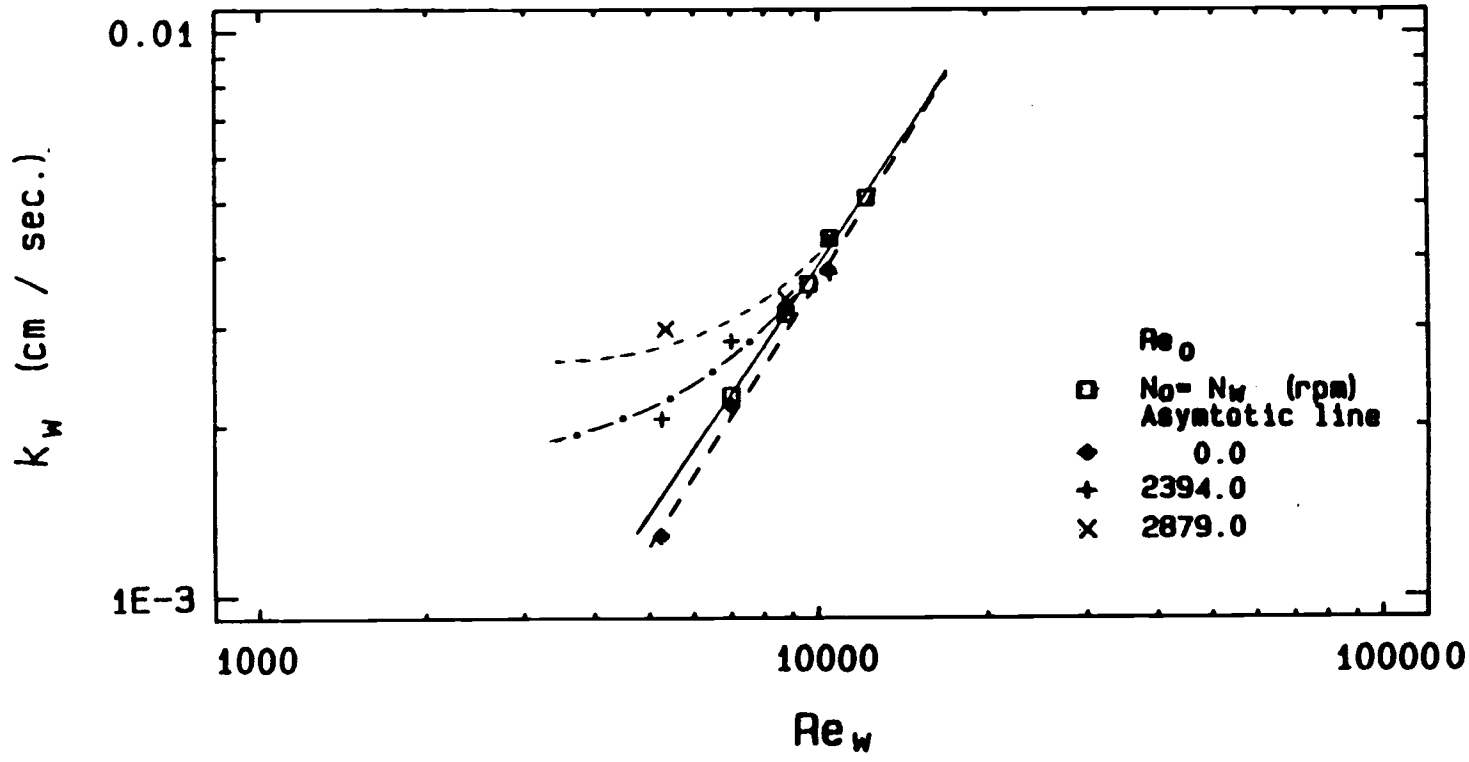

Figure (7.3). The effect of the organic phase Reynolds number on the mass transfer coefficient in the aqueous phase.

this conclusion since they did not include in their analysis the effect of the same agitation rates in both phases on the mass transfer coefficient. Accordingly they did not plot k_w versus Re_w at different Re_o when both phases had the same agitation speed, N (rps), in order to determine the correct asymtotic line. In general Figure (7.3) indicates that when Re_w is lower than approximately 8000 for water-n-butanol system and Re_o increases (higher than approximately 2000 for water-n-butanol (system) the mass transfer coefficient in the water phase increases. This could be explained by the fact that the viscosity of the n-butanol is higher than that of water. Accordingly, when the organic phase's agitation rate is higher than that of the water phase, the momentum of the eddies in the organic phase are transmitted across the interface into the adjacent region of the water, producing an increase in the water coefficient, k_w [12]. Asymtotic line of Figure (7.3) reveals a new concept that at a certain region of Re_w, the effect of Re_o and the organic phase physical properties diminish. Accordingly there is no momentum of the organic phase transmitted to the water phase which effects its mass transfer coefficient. The region in Figure (7.3) is when Re_w is approximately higher than 7000. This concept would lead to a new approach for mass transfer coefficient correlation development.

7.1.3 The Effect of the Aqueous Phase Agitation on the Organic Phase Mass Transfer Coefficient

The data of these experiments are listed in Table (6.3); in these runs, the water phase was kept at a constant agitation rate while the n-butanol phase agitation rate was varied. In Figure

(7.4), k_o is plotted versus Re_o on a log-log scale for different Re_w. This figure illustrates the effect of the water phase agitation rate, Re_w, on the organic mass transfer coefficient, k_o. It presents a similar behavior to that observed in Figure (7.3). Also, it shows that the fitted line (the solid line) of k_o versus the same agitation rates (rps) in both phases, as shown in Figure (7.1), is the asymtotic line. The experiments involving an unagitated water phase indicates the n-butanol phase coefficient, k_o, is lower than that of the asymptotic value at the lower Re_o values. The difference between them is higher than the difference between k_w and its asymtotic line in Figure (7.3). This would be because at the same agitated rate of N (rps), Re_w is higher than Re_o. For instance, where N = 3.016 rps, Re_w is 5226 while Re_o is 1435; Re_w is 3.64 times Re_o. Hence, the effect of the water agitation rate, Re_w, on the n-butanol phase coefficient, k_o, is higher than that of the n-butanol agitation rate, Re_o, on the water phase coefficient, k_w, particularly for the comparison of the mass transfer coefficient difference between the values of asymtotic line and the values when one of the phases is unagitated as shown in Figures (7.3) and (7.4). Also in this case, as Re_o increases while the water phase remains unagitated, k_o increases and approaches the asymtotic line. If the water phase agitation rate is kept constant at approximately Re_w - 8713 while the n-butanol agitation phase is varied below Re_o = 2000, the k_o values are higher than the asymtotic line. As Re_o increases, k_o increases and approaches the asymtotic line near Re_o = 2000 where the effect of Re_w diminishes. When the water phase agitation rate was increased to

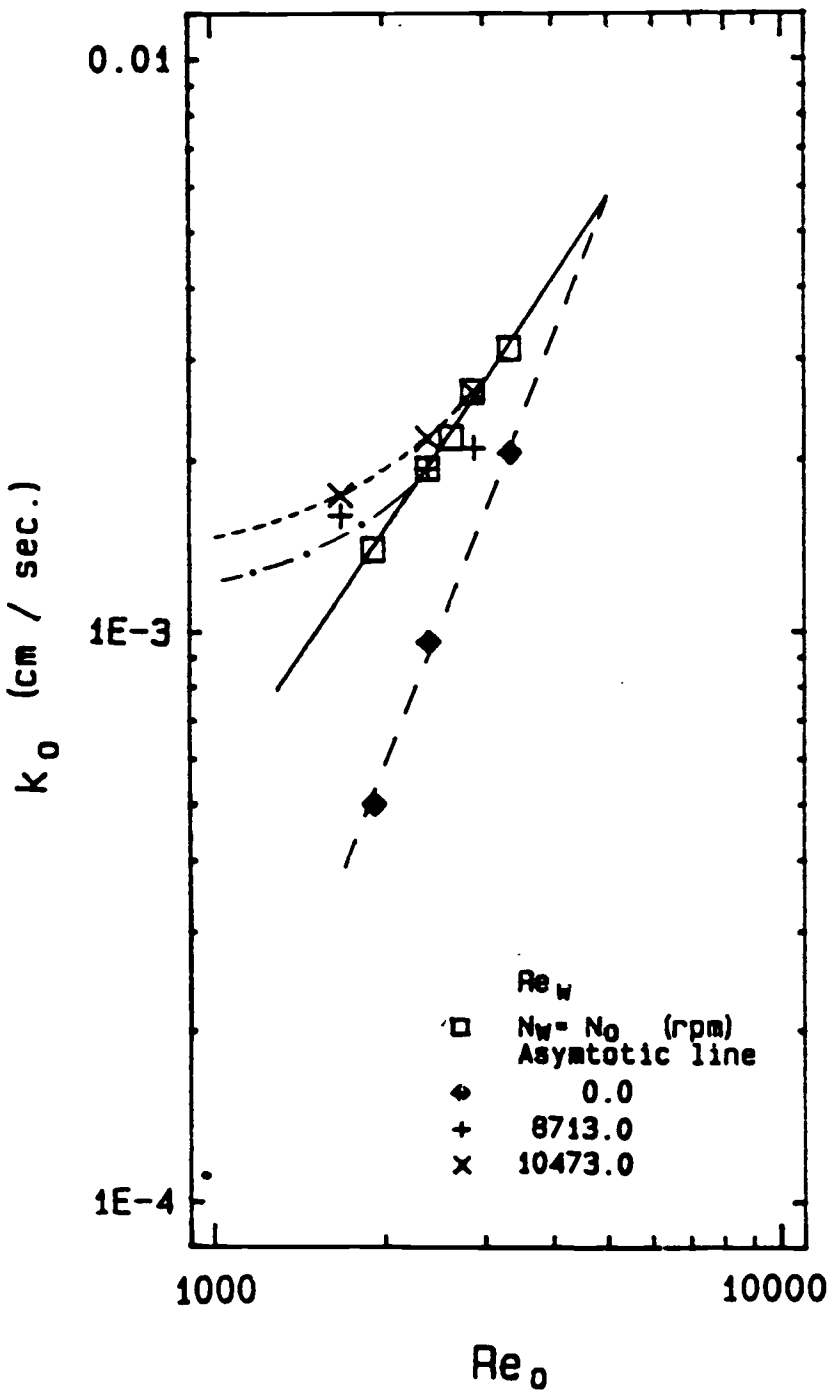

Figure (7.4). The effect of the water phase Reynolds number on the mass transfer coefficient in the organic phase.

Re_w = 10473, the organic phase coefficient, k_o, increased and approached the asymtotic value also near Re_o = 2000 where the effect of Re_w also diminishes. In this case the increasing in k_o is less than the increasing in k_w presented in Figure (7.3) at the same N (rps). The viscosity of the n-butanol apparently plays an important role in the effect of k_w by Re_o through the momentum transmitted across the interface, as previously mentioned in 7.1.2. As long as the viscosity of water is less than that of n-butanol, the momentum of the eddies in the water phase transmitted across the interface to the n-butanol phase is less than that transmitted by the n-butanol phase to the water phase at the same increasing value of the agitation rate (rps). Therefore, the effect of k_o by Re_w increasing is less than on k_w by Re_o increasing in the region away from the asymtotic line. Also the asymtotic line of Figure (7.4) reveals that there is no momentum transfer from the water phase to the n-butanol phase when Re_o is approximately higher than 1900 where the effect of Re_w and water phase physical properties diminish.

7.2 Mass Transfer Coefficient Correlation Development

From the previous studies and the literature review it appears that mass transfer coefficient in the liquid phase for liquid-liquid systems and gas-liquid systems is proportional to $D^{0.5}$ - $D^{0.67}$ [45, 68]. This means that the change in dependence of the mass transfer coefficient on the diffusivity is between the penetration model or surface renewal model and laminar boundary layer model [33, 45, 68]. Previous investigations involving the water-n-butanol system verified that this system involves a transition regime between surface renewal

and laminar boundary layer [45]. Accordingly, data involving the water-n-butanol system could be used to develop a simple correlation in which the mass transfer coefficient is proportional to $D^{0.5}$-$D^{0.67}$. For this reason, the water-n-butanol system was chosen for this study.

As previously mentioned Versteeg et al [68] proved that King's model was capable of explaining the observed transition in the dependency of the mass transfer coefficient (or Sh number) on diffusivity. This model can also account qualitatively for the apparent discrepancies in the literature data. With King's model, Versteeg et al [68] interpreted qualitatively their liquid phase mass transfer coefficient data for gas-liquid systems. This was shown previously in Figure (2.7). This figure showed that k is proportional to $D^{0.5}$ for small D and k is proportional to $D^{0.67}$ for large D. Versteeg et al [68] studied liquid mass transfer coefficients in gas-liquid systems using an agitated cell with a horizontal interface; the interface between the two fluid phases of gas-liquid and liquid-liquid was relatively free to move and was deformable. Since there is apparently no great difference in the basic mechanism of mass transfer at the gas-liquid and liquid-liquid interface [12, 46], Versteeg et al's interpretation and comparison of the King's model could be relied on to develop mass transfer coefficients for the liquid phases in the liquid-liquid systems involving a wide range of diffusivity. Since water-n-butanol represents the transition region between surface renewal ($k \propto D^{0.5}$) and laminar boundary layer ($k \propto D^{0.67}$), it was used to develop the general mass transfer coefficient

correlations in the liquid-liquid system for both the organic and aqueous phases.

According to Versteeg et al (68) analysis, the mass transfer coefficient, k, in the liquid phase, having relatively small diffusivity, D, of the transfer component, is proportional to $D^{0.5}$. The mass transfer coefficient in the liquid phase having relatively large diffusivity, D, of the transferred component is proportional to $D^{0.67}$. Therefore, the general form of the mass transfer coefficient correlation in both phases is proposed to be as follows:

a. Aqueous phase

1. For small D or large Sc number

$$Sh_w = P_{w1} \; Re^{ew1} \; Sc^{1/2} \tag{7.10}$$

2. For large D or small Sc number

$$Sh_w = P_{w2} \; Re^{ew2} \; Sc^{1/3} \tag{7.11}$$

b. Organic phase

1. For small D or large Sc number

$$Sh_o = P_{o1} \; Re^{eo1} \; Sc^{1/2} \tag{7.12}$$

2. For large D or small Sc number

$$Sh_o = P_{o2} \; Re^{eo2} \; Sc^{1/3} \tag{7.13}$$

7.2.1 Correlations Constants and Re Exponents Evaluation

Since the change in the mass transfer coefficient value with agitation rate (rps) when both phases are agitated at the same speed is represented by the asymptotic line in the Figures (7.3) and (7.4),

the values of this line were used to evaluate the correlation constant and Re exponents for both phases as follows:

1. Reynold's Exponents Evaluation:

By taking the logarithm for each side of the equations (7.10-7.13) in terms of k and N yields a straight line equation which is

$$\ln k = \ln (\text{constant}) + e \ln N \qquad (7.14)$$

Hence plotting k versus N on a log-log scale should produce a straight line with a slope equal to the exponent of N or its equivalent Re. Accordingly from Figure (7.1) in which k_w and k_o are plotted versus N, the Re exponent can be evaluated. By treating the data of k_w and k_o versus N statistically by a simple regression analysis using Statgraf software package, the slope of the fitted lines represents the N exponent, which is equal to the Re exponent. Table (7.1) represents the slope of fitted lines and their statistical parameter.

Table (7.1). Slope of the Fitted Lines, k versus N, and their Statistical Parameter

Phase	Figure Number	Fitted Line Slope	Standard Error ±	Probability Level	Re-squared %
n-butanol	7.1	1.48	0.061	0.00015	99.49
water	7.1	1.48	0.0699	0.00023	99.33

The slope of the two lines is equal to 1.48. Therefore

$$k_w \propto N_w^{1.48} \propto Re_w^{1.48} \tag{7.15}$$

and

$$k_o \propto N_o^{1.48} \propto Re_o^{1.48} \tag{7.16}$$

Figures (7.5) and (7.6) illustrate the effect of $k_w/N_w^{1.48}$ by N_o and $k_o/N_o^{1.48}$ by the N_w. The ratio, $k/N^{1.48}$ is approximately constant, except for those points which are above the asymtotic value shown in Figure (7.3) at Re_w below approximately 7000 and Figure (7.4) at Re_o below approximately 1900. Accordingly equation (7.15) is valid for Re_w above 7000, while equation (7.16) is valid for Re_o above 1900, for water-n-butanol system.

2. Correlations Constant Evaluation

According to equations (7.10-7.13), plotting $Sh/Sc^{1/2}$ or $Sh/Sc^{1/3}$ for both phases versus its corresponding $Re^{1.48}$ should give a straight line. The slope of this line is equal to the correlation constant P_w or P_o. The data were treated statistically by simple regression analysis using Statgraf software package. Figures (7.7), (7.8), (7.9), (7.10) show the plotting $Sh/Sc^{1/2}$ or $Sh/Sc^{1/3}$ versus $Re^{1.48}$ and their fitted lines in both phases. Tables (7.2) and (7.3) presented the calculated values of the fitted lines and their statistical parameters.

A summary of the general mass transfer coefficient correlations for both phases is presented in the following Table (7.4).

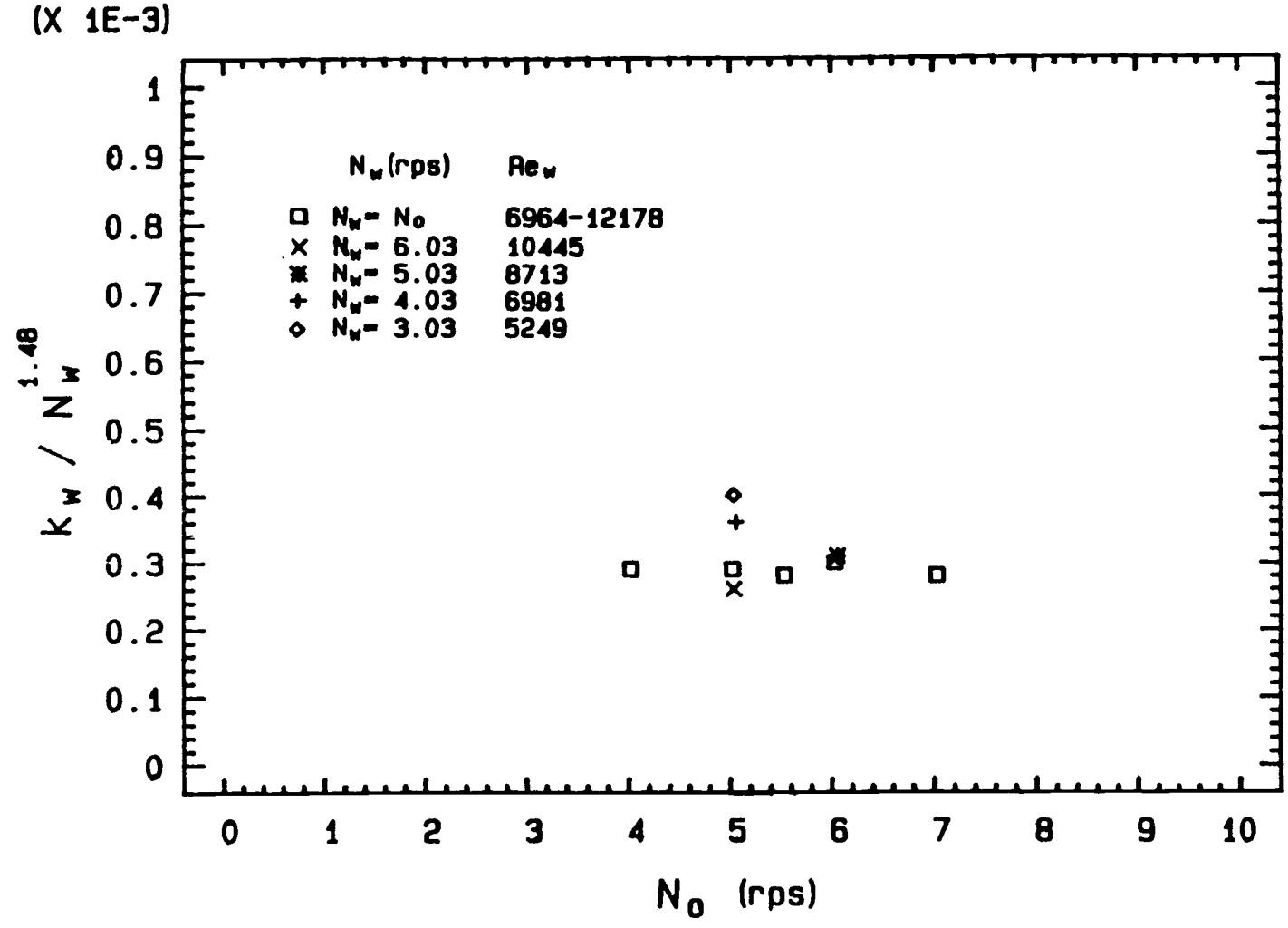

Figure (7.5). A plot of $k_w/N_w^{1.48}$ versus N_o (rps).

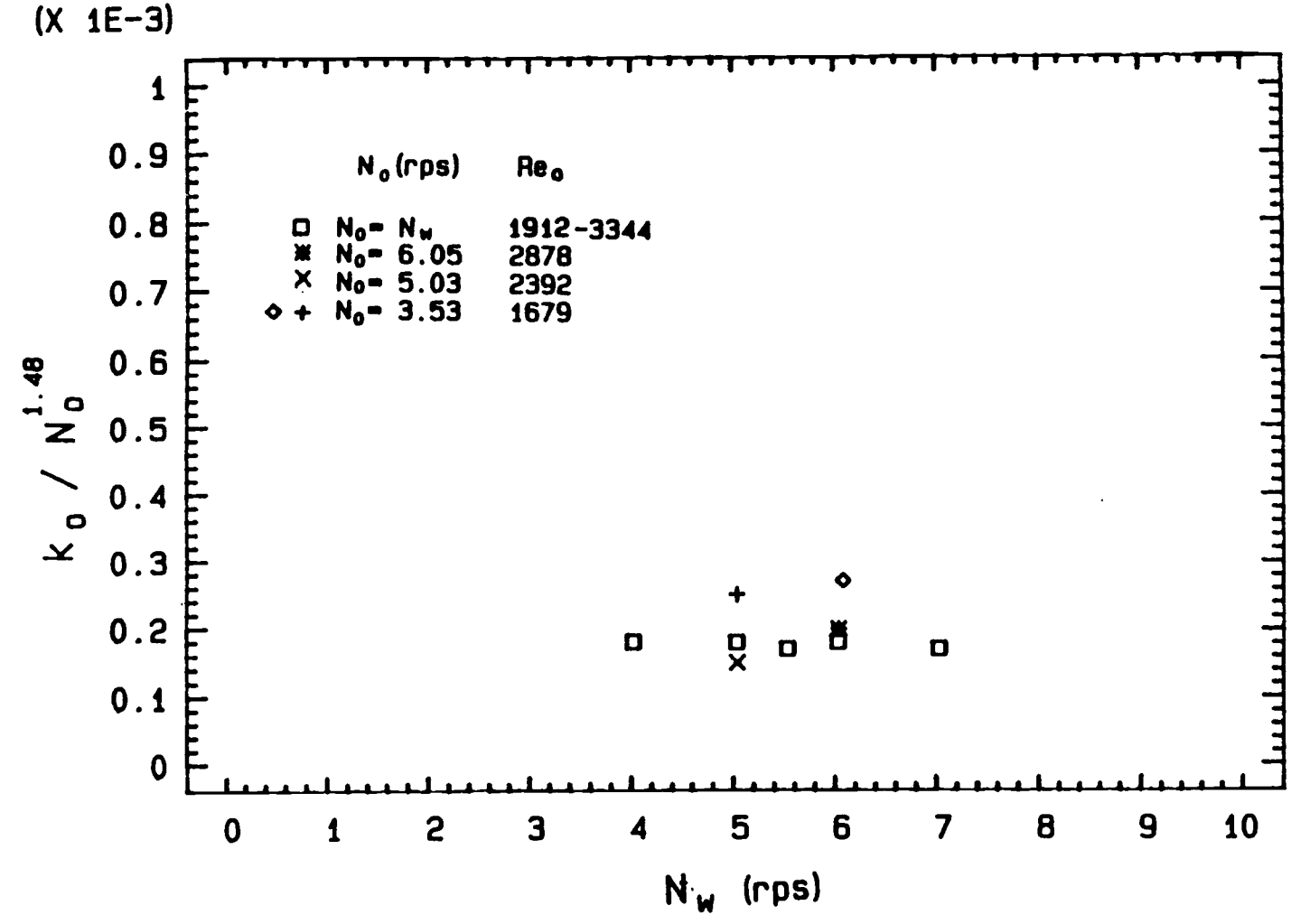

Figure (7.6). A plot of $k_o/N_o^{1.48}$ versus N_w (rps).

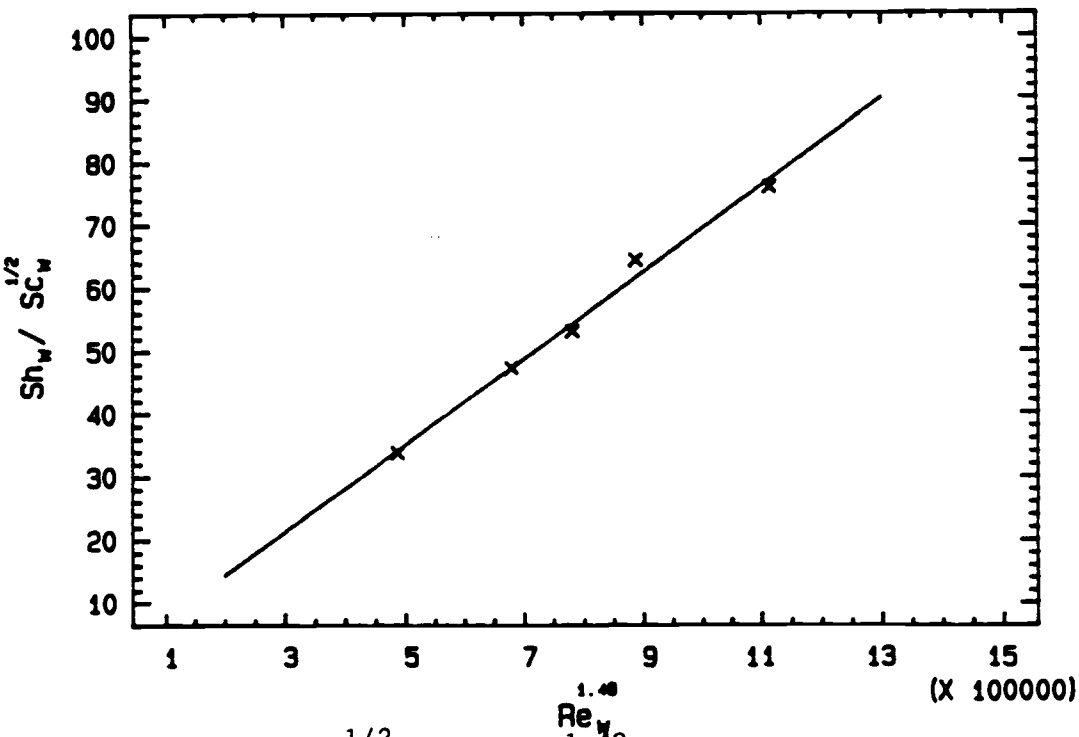

Figure (7.7). $Sh_w/Sc_w^{1/2}$ versus $Re_w^{1.48}$ for the evaluation of the evaluation of the equation (7.10) constant.

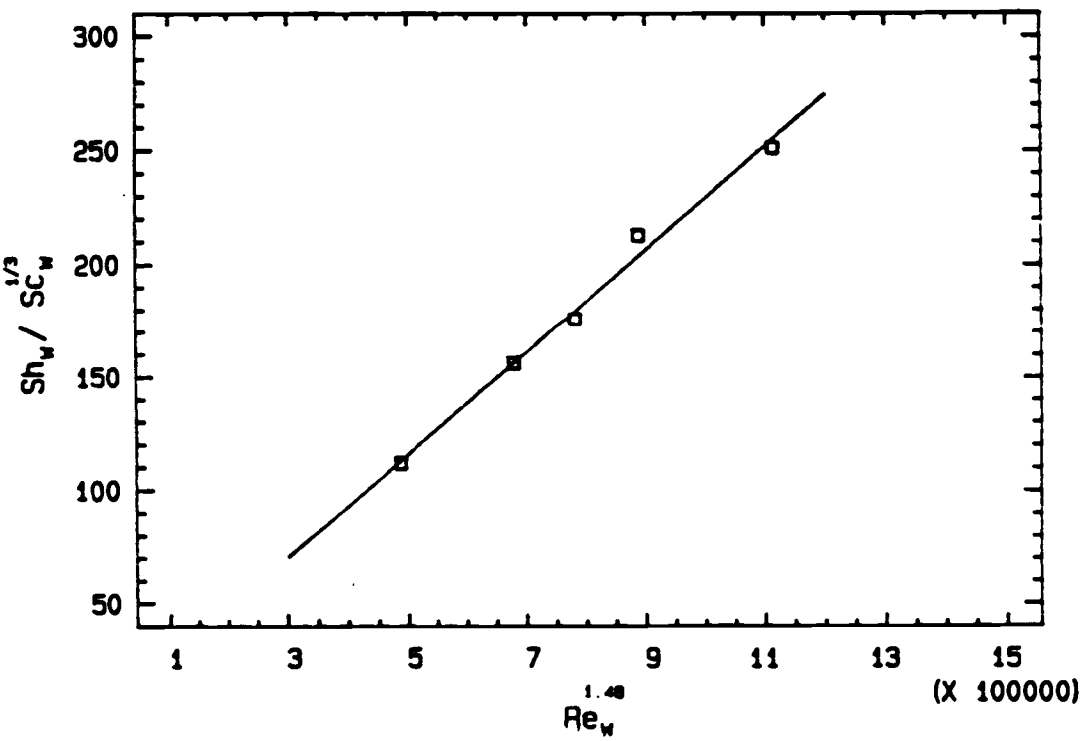

Figure (7.8). $Sh_w/Sc_w^{1/3}$ versus $Re_w^{1.48}$ for the evaluation of the equation (7.11) constant.

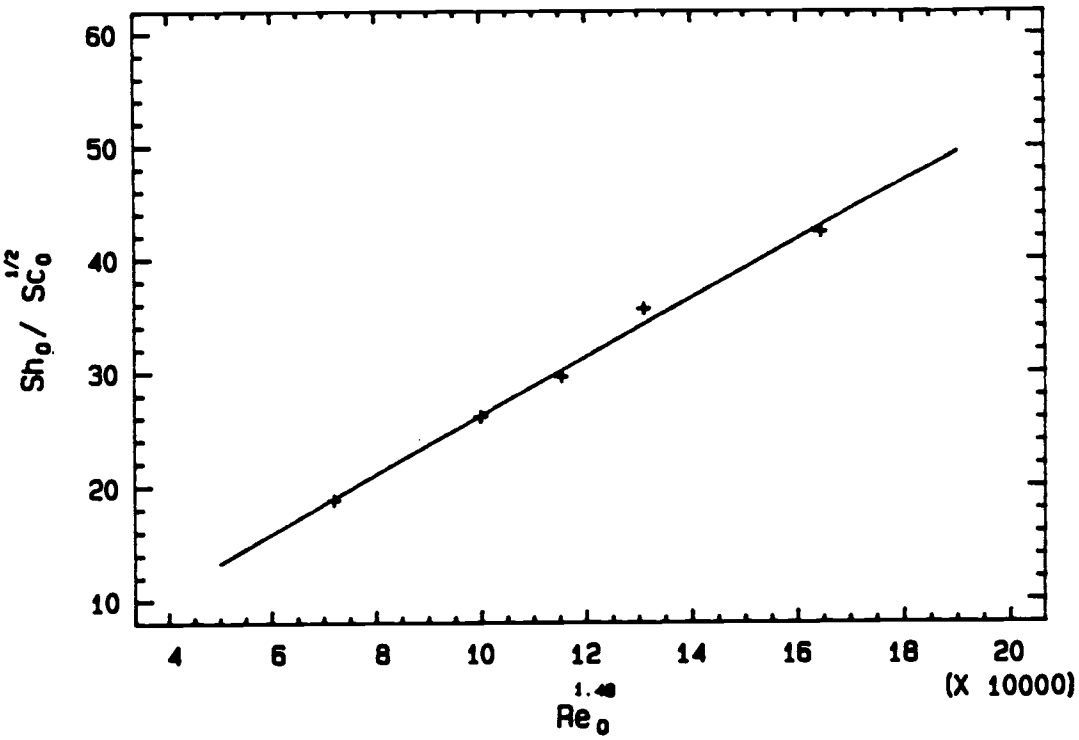

Figure (7.9). $Sh_w/Sc_o^{1/2}$ versus $Re_o^{1.48}$ for the evaluation of the equation (7.12) constant.

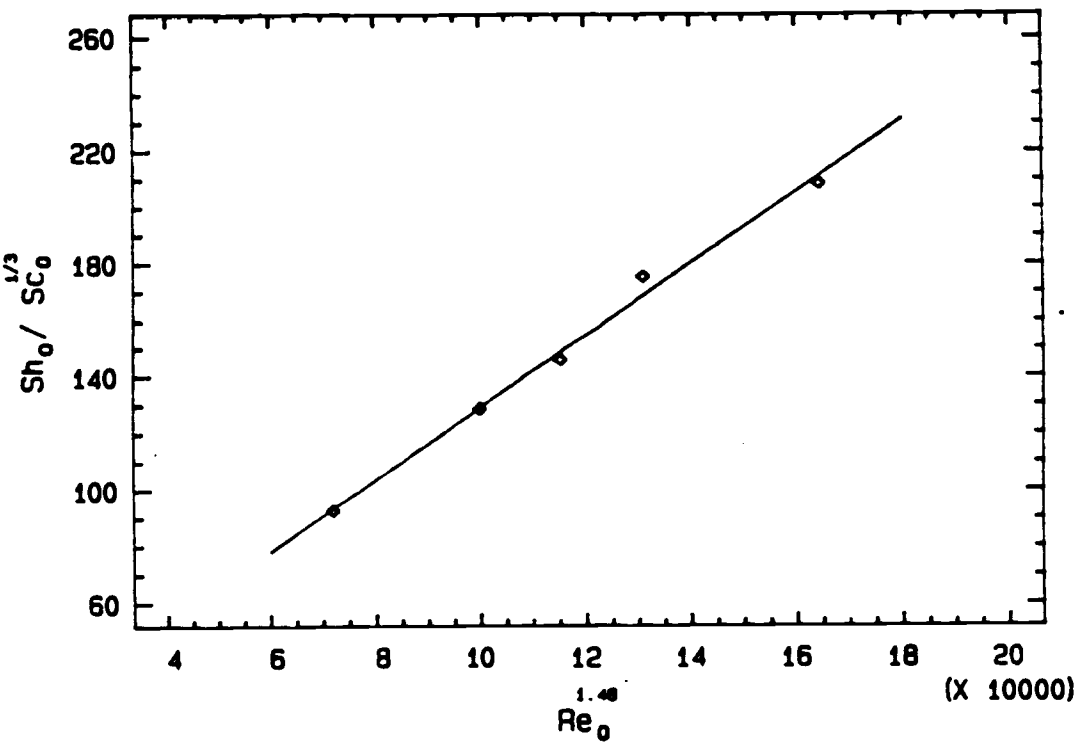

Figure (7.10). $Sh_o/Sc_o^{1/3}$ versus $Re_o^{1.48}$ for the evaluation of the equation (7.13) constant.

Table (7.2). Slopes and their statistical parameters of the water phase fitted lines which represent the correlations constant.

Line	Figure number	Slope	Standard error (±)	Probability level	R-squared %
$Sh_w/Sc_w^{1/2}$ vs. $Re_w^{1.48}$	7.7	6.87 E-5	3.955 E-6	0.00042	99.01
$Sh_w/S_c^{1/3}$ vs. $Re_w^{1.48}$	7.8	2.270 E-4	1.306 E-5	0.00042	99.02

Table (7.3). Slopes and their statistical parmeters for the n-butanol phase fitted lines which represent the correlations constant.

Line	Figure number	Slope	Standard error (±)	Probability level	R-squared %
$Sh_o/Sc_o^{1/2}$ vs. $Re_o^{1.48}$	7.9	2.59 E-4	1.295 E-5	0.00027	99.26
$Sh_o/Sc_o^{1/3}$ vs. $Re_o^{1.48}$	7.10	1.276 E-3	6.373 E-5	0.00027	99.26

Table (7.4). Correlations Constants and Re Exponents with their Validity Limitation for the Asymtotic Line Region.

Correlations	D	Sc	Pw, Po	ew,eo	Limitation
a. water phase					
1. $Sh_w = Pw1\ Re_w^{ew1}\ Sc_w^{1/2}$	Small	Large	6.87E-5	1.48	>7000
2. $Sh_w = Pw2\ Re_w^{ew2}\ Sc_w^{1/3}$	Large	Small	2.27E-4	1.48	>7000
b. Organic phase					
1. $Sh_o = Po1\ Re_o^{eo1}\ Sc_o^{1/2}$	Small	Large	2.59E-4	1.48	>1900
2. $Sh_o = Po2\ Re_o^{eo2}\ Sc_o^{1/3}$	Large	Small	1.276E-3	1.48	>1900

7.3 Comparison Between the Experimental Sherwood Number and the Theoretical Sherwood Number

To compare the mass transfer coefficient predicted by the developed correlations with the earlier correlations, the experimental Sherwood number, Sh, was plotted versus the theoretical Sherwood number, as shown in Figure (7.11) and (7.12) for the water phase and n-butanol phase, respectively. Figures (7.13) and (7.14) were plotted to reveal mass transfer coefficient prediction in the water phase and n-butanol phase, respectively by the earlier correlation at the range of a given phase Re where the other phase Re affects its mass transfer coefficient. Tables (7.5) and (7.6) presents the predicted values of the coefficient by the developed and earlier correlations with their percentage deviation from the experimental values. It was found for water-n-butanol system that the earlier correlations produced a considerable error in the prediction of water phase mass transfer coefficient in the range of Re_w which represents the asymtotic line, while the developed correlation gave good agreement with the experimental data, which was developed for this range of Re_w. Figure (7.13) shows that the simple correlation of McManamey et al gave less error in the predicted water phase coefficient than the other earlier correlations which considered in their derivation the effect of the other phase Re, i.e. Re_o. In fact, McManamey et al [45] was developed for the helium and butanol transfer across water-butanol interface. But in the range of the asymtotic line, its error was higher than the developed correlations. This is because it was developed in the range of Re_w less than 7000 [45], in which there was

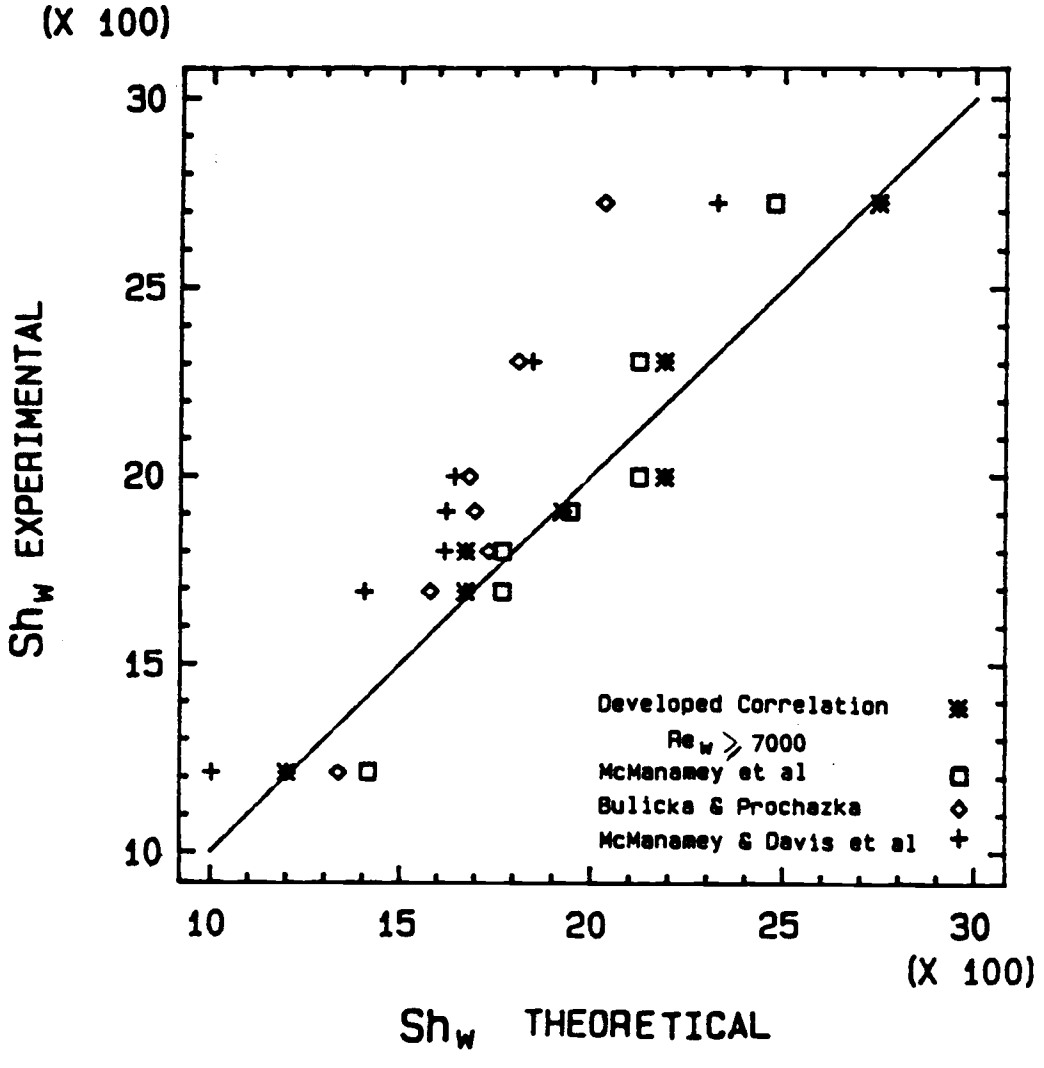

Figure (7.11). Comparison of the water phase experimental Sh_w with the theoretical Sh_w obtained by the developed correlation in the asymtotic line region and the earlier correlations.

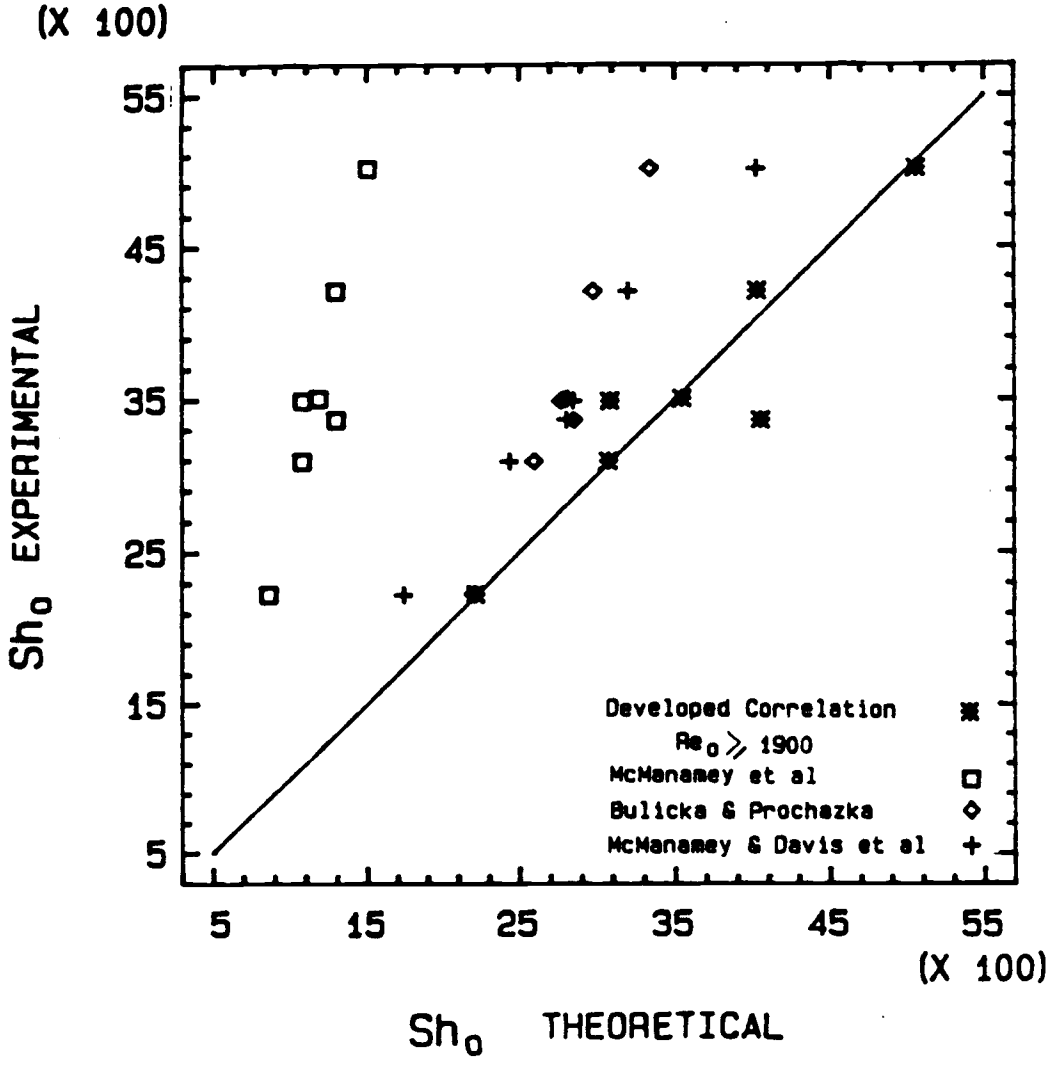

Figure (7.12). Comparison of the n-butanol phase experimental Sh_o with the theoretical Sh_o obtained by the developed correlation in the asymtotic line region and the earlier correlations.

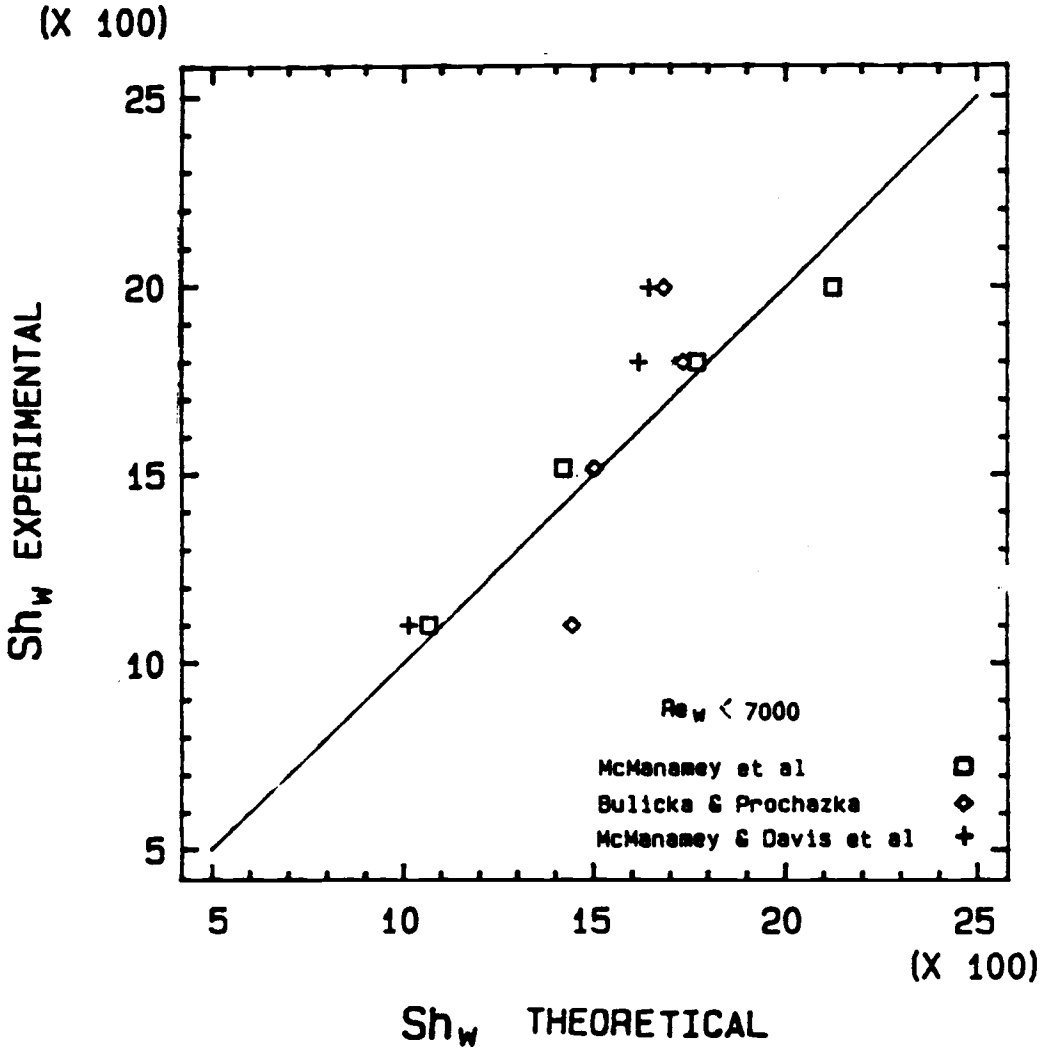

Figure (7.13). Comparison of the water phase experimental Sh_w with the theoretical Sh_w obtained by the earlier correlations in the low Re_w region (Re_w < 7000)

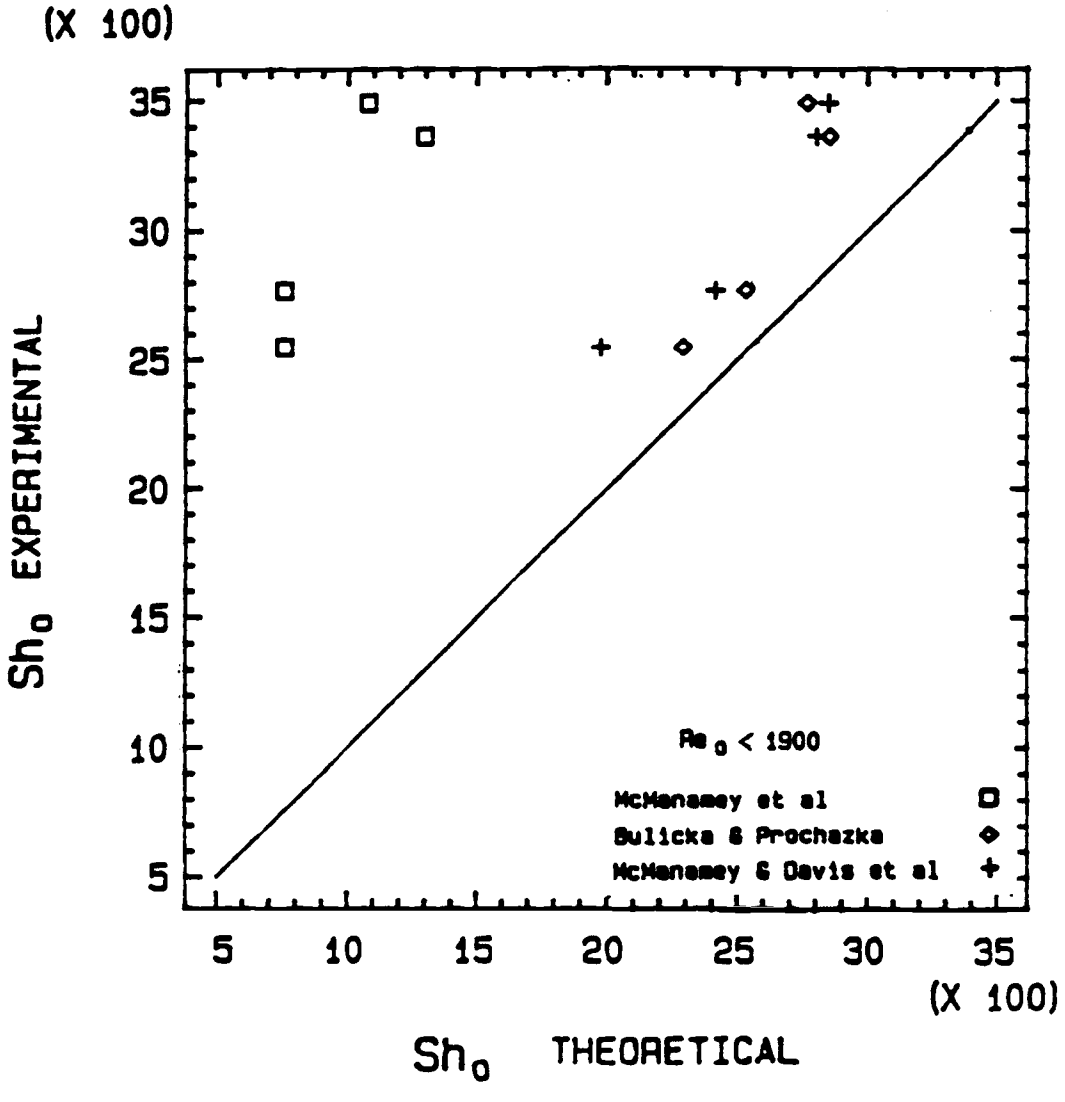

Figure (7.14). Comparison of the n-butanol phase experimental Sh_0 with the theoretical Sh_0 obtained by the earlier correlations in the low Re_0 region (Re_0 < 1900)

Table(7.5) Comparison of the Experimental Water Phase Sherwood Number with the Theoretical one Obtained by the Developed and Earlier Correlations.

a - Asymtotic line region

k_w ($\frac{cm}{sec}$)	Sh_w Experimental	Sh_w equation (7.13) Table (7.6)	Error %	Sh_w McManamery et al. equation (2.52)	Error %	Sh_w Bulicka - Prochazka equation (2.60)	Error %	Sh_w McManamey - Davis et al. equation (2.50)	Error %
0.00227	1211.3	1200.6	-0.9	1414.7	+16.8	1335.74	+10.3	1004.5	-17.0
0.00317	1691.5	1672.8	-1.1	1770.0	+4.6	1580.2	-6.6	1404.2	-17.0
0.00357	1905.0	1924.7	+1.0	1946.0	+2.2	1696.6	-10.9	1620.7	-15.0
0.00432	2305.1	2187.7	-5.1	2121.9	-8.0	1810.8	-21.5	1845.5	-20
0.0051	2721.3	2745.7	+0.9	2474.0	-9.1	2031.2	-25.4	2323.2	-14.6
0.00374	1995.6	2187.7	+9.6	2121.9	+6.3	1682.0	-15.7	1642.5	-7.7
0.00337	1798.2	1672.8	-7.0	1770.0	-1.6	1733.8	-3.6	1616.5	-10.1

b - low Re_w region

0.00374	1995.6	--	--	2121.9	+6.33	1682.0	-15.7	1642.5	-7.7
0.00337	1798.2	--	--	1770.0	-1.57	1733.8	-3.58	1616.5	-10.1
0.00284	1515.4	--	--	1418.2	-6.41	1502.1	0.88	1199.0	-21
0.00206	1099.2	--	--	1066.3	-3.0	1441.9	+31.2	1012.9	-7.9

Table (7.6). Comparison of the Experimental n-butanol Phase Sherwood Number with the Theoretical one Obtained by the Developed and Earlier Correlations.

a - Asymtotic line region

k_o $(\frac{cm}{sec})$	Sh_o Experimental	Sh_o equation (7.13) Table (7.6)	Error %	Sh_o McManamery et al. equation (2.52)	Error %	Sh_o Bulicka - Prochazka equation (2.60)	Error %	Sh_o McManamey - Davis et al. equation (2.50)	Error %
0.00139	2225.1	2211.0	-0.63	861.9	-61.3	2195.7	-1.32	1740.2	-21.8
0.00193	3089.5	3072.3	-0.56	1076.5	-65.2	2594.1	-16.0	2432.0	-21.3
0.00219	3505.7	3544.1	+1.1	1185.5	-66.2	2788.8	-20.5	2807.6	-19.9
0.00263	4210.0	4029	-4.3	1292.8	-69.3	2976.0	-29.3	3196.7	-24.1
0.00313	5010.4	5057.0	+9.3	1507.4	-70	3339.3	-33.4	4024.2	-19.7
0.0021	3361.6	4049.7	+20.5	1297.3	-61.4	2850.5	-15.2	2799.7	-16.7
0.00218	3489.7	3080.0	-11.7	1078.3	-69.1	2764.8	-20.8	2845.6	-18.5

b - low Re_o region

0.0021	3361.6	--	--	1297.3	-61.4	2850.5	-15.2	2799.7	-16.7
0.00218	3489.7	--	--	1078.3	-69.1	2764.8	-20.8	2845.6	-18.5
0.00159	2545.2	--	--	756.8	-70.3	2289.0	-10.1	1975.1	-22.4
0.00173	2769.3	--	--	756.8	-72.7	2532.7	-8.54	2413.2	-18.9

the effect of the other phase Re, i.e. Re_o. The good agreement of the predicted k_w by McManamey et al [45] correlation with our experiment data in the region of Re_w below 7000 than that in the region of Re_w above 7000 is confirmed in our experimental data behavior. Asai et al's [68] correlation did not meet the experimental data condition for Re_w and Ca_w. It gave high error in the prediction experimental mass transfer coefficient. Therefore it was not compared in Tables (7.5) and (7.6) and Figures (7.13) and (7.14). For the organic phase, Figures (7.12) and (7.14) show that the earlier correlations would not be applied to predict organic phase mass transfer coefficient.

7.4 Correlations Discussion

7.4.1 Discussion of the Earlier Correlations

The stirred cells which were used to obtain the data used to develop the earlier correlations, as summarized in Table (7.7) for water phase, was so different in configuration and dimensions that it would be impractical to attempt a quantitative comparison of the mass transfer coefficient measured by the various investigators. The behavior of mass transfer coefficient with respect to the relevant variable is briefly discussed relative to the above nine correlations.

The qualitative behavior of k_w due to Re_w and Re_o were the same for correlations (1), (2), (3), (5), (6) and (7) in Table (7.7). This means that there is an effect of the organic phase Reynolds number, Re_o. The term Re_o indicates that its quantitative effect on

Table (7.7). A summary of the earlier correlations.

Correlation No.	Investigator	Reference No.	Correlation	k
1	Lewis	38	$\frac{60\ k_w}{\nu_w} = 6.76 \times 10^{-6} \left(Re_w + Re_o \frac{\mu_o}{\mu_w}\right)^{1.65} + 1$	$k \alpha D^0$
2	McManamey	44	$\frac{60\ k_w}{\nu_w} = \beta_1\ Sc_w^{-0.37}\ Re^{0.9} \left(1 + \frac{\mu_o}{\mu_w} \frac{Re_o}{Re_w}\right)$ $\beta = 0.102$ for brass stirrer $= 0.0861$ for glass stirrer	$k \alpha D^{0.37}$
3	Mayers	42	$\frac{k_w L}{D_w} = 0.00316\ (Re_w\ Re_o)^{1/2} \left(\frac{\mu_o}{\mu_w}\right)^{1.9} \left(0.6 + \frac{\mu_o}{\mu_w}\right)^{-2.4} Sc_w^{5/6}$	$k \alpha D^{1/6}$
4	Orland and Benedict	49	$\frac{k_w}{\nu_w} = 0.046 \left(\frac{N_w}{\nu_w}\right)^{0.67} Sc_w^{-0.44}$	$k \alpha D^{0.44}$
5	McManamey Davis et al.	46	$Sh_w = 0.023\ Sc_w^{0.5}\ (We_w')\left[Re_w + \frac{\nu_o}{\nu_w} Re_o\right]^{0.5} \times \ldots$ $\times \left[1 + \left(\frac{\rho_o\ \nu_o^2}{\rho_w\ \nu_w^2}\right)\left(\frac{Re_o}{Re_w}\right)^2\right]^{0.5}$	$k \alpha D^{0.5}$
6	McManamey et al.	45	$Sh_w = 0.0187\ Re_w\ Sc_w^{1/3}$	$k \alpha D^{0.67}$

Table (7.7). continued

Correlation No.	Investigator	Reference No.	Correlation	k
7	Bulicka and Prochazka	4	$Sh_w = 0.06\ Sc_w^{0.5}\ Re_w^{3/4} \left[\frac{1 + \left(\frac{N_o}{N_w}\right)^3 \left(\frac{\nu_o}{\nu_w}\right)^{1/2} \frac{\rho_o}{\rho_w}}{1 + \left(\frac{\nu_o}{\nu_w}\right)^{3/2} \left(\frac{\rho_o}{\rho_w}\right)} \right]^{1/4}$	$k \alpha D^{0.5}$
8	Asai et al.	2	$Sh_w = 0.0119\ Sc_w^{1/3}\ Ca_w^{6/13}\ [\Phi^4\ Re_w^3 + Re_o^{8/3}]^{1/4}$	$k \alpha D^{0.67}$
9	Versteeg et al.	68	$Sh = 0.064\ Re_w^{0.72}\ Sc_w^{1/2}$ for large Sc or small D	$k \alpha D^{0.5}$
			$Sh = 0.181\ Re^{0.72}\ Sc^{1/3}$ for small Sc or large D	$k \alpha D^{0.67}$

the k_w was different among these correlations. As discussed, at a certain range of Re_w the effect diminishes, which was found for water-n-butanol system to be at Re_w above 7000. The correlations showed that Re_o effect did not diminish at a certain range of Re_w. For instance, Bulicka and Prochazka's correlation number (7) in Table (7.7) showed that the correlation has a $(N_o/N_w)^3$ parameter. This parameter produced a considerable deviation in k_w from the experimental values when N_w is higher than N_o where it should be no effect, as discussed previously. Correlation (8) shows that k_w at $Re_w = 0$ is independent of the second viscosity μ_o in the region of low viscosity ($\Phi = 1.0$). This agrees well with correlation (7), (1) and (2). There was no effect of μ_o in the case of $Re_w << Re_o$, as observed by correlation (5), (1) and (8).

There has been a lack of agreement about the influence of molecular diffusion on the mass transfer process. The dependence of k_w on the diffusivity is shown in Table (7.7) for each correlation.

The effect of the interfacial tension σ was taken into account only by correlation (5) and (8). Correlation (5) yielded the relations of $k_w \propto \bar{\sigma}^{0.5}$ for $Ca_w | \Delta\rho | / \rho_w << 178$ and of $k_w \propto \sigma^0$ for $Ca_w | \Delta\rho | / \rho_w >> 178$. Correlation (8) yielded the relation of $k_w \propto \bar{\sigma}^{6/13}$. It was difficult to find systems that could verify experimentally the dependence of k_w on

The ratio ρ_o / ρ_w appears in the correlation (1), (2), (3), (5), (7), and (8) for given values of Re_o. Correlation (8) revealed no appreciable effect on Sh_w at ρ_o / ρ_w over 5.5.

The disagreement regarding the influence of various variables on

the mass transfer coefficients among the correlations may be partly attributed to the fact that the properties used for some previous correlations varied over a fairly narrow range and it might be due to the differences in their data analysis approach.

7.4.2 Developed Correlations Discussion

The summary of the developed correlation is represented in Table (7.4). It has the following features:

1. The new correlations are simple compared with many previous correlations.

2. The new correlations were developed for only one system of water-n-butanol. The water-n-butanol system was found to represent the transition region between the surface renewal model and laminar boundary layer mode in the mass transfer coefficient dependence on the diffusivity. Accordingly, the correlations probably are not as good for other systems other than the water-n-butanol system. More investigation on different systems are recommended to adjust the correlations constants and Reynolds number exponents for a general form. These forms of correlations should be capable of covering a wide range of diffusivity.

3. The new correlations have been developed depending on the asymtotic values of k, as shown in Figures (7.3) and (7.4), in which both phases were mixed at the same agitation speed. As discussed before, in this case there is no effect of a given phase Reynolds number on the other phase mass transfer coefficient. Accordingly, the correlations are valid for the condition of the asymtotic line for the water-n-butanol system, when both phases of the Reynolds

number corresponding to the same agitation speed or when Re_w is above 7000 for water phase and Re_o is above 1900 for n-butanol phase.

4. For the low Reynolds number conditions where there is an effect of a phase Reynolds number on the mass transfer coefficient of the other phase, McManamey et al's correlation [45] was found to agree well with our experimental data as shown in Figure (7.11) and Table (7.5). Accordingly, developing general correlations similar to that of the asymtotic line condition might be helpful to predict mass transfer coefficient with accepted error in this range of condition instead of complicating it by including the other phase Re effect. This definitely needs enough data for different investigated systems in this range of Re to verify this concept.

5. It does not have a dimensionless group which represents the effect of the surface tension. The correlation was developed depending on the ability of the King model to explain the change in the dependency of the mass transfer coefficient on the diffusivity. In this model, the surface tension effect was introduced in the damping of the eddy diffusivity near an interface. Thereby, the constant b in the equation (2.9) was omitted. Further investigations involving more than one system with varying surface tensions may reveal that constant b can not be omitted.

Chapter 8

Conclusions and Suggestions for Future Work

8.1 Conclusions

Following are some of the conclusions deduced from this study:

1. This study developed an excellent contactor for the experimental studies of mass transfer in liquid-liquid systems and developed simple correlations for liquid convective coefficient that covered a wide range of diffusivity. It also presented important new concepts about the transport phenomena in turbulent mass transfer across a liquid-liquid interface.

2. The contactor that was designed and constructed is flexible enough to overcome the shortcomings of other experimental equipments (discussed in Chapter 3). It worked very well. It was found easy to operate. It could be used for experimental studies for gas-liquid systems as well as for the liquid-liquid systems. It has the ability to study a wide range of the variables affecting the mass transfer coefficient.

3. The contactor has been designed and constructed to operate as a batch or continuous process. In this study, only the batch process has been operated. It was found that it is sufficient to study mass transfer coefficients in liquid-liquid systems. For gas-liquid mass transfer studies, continuous process operation is much more suitable than batch process, as discussed in Section 2.5.

4. All the operations were done at room temperature, which varied between 17°C-20°C. Therefore, the effect of temperature on

the mass transfer coefficients need to be investigated.

5. The mass transfer coefficient for a given phase evaluated when both phases were agitated at the same speed, was found to be independent of the agitation rate or Reynolds number of the second phase, as shown in Figures (7.1) and (7.2). These values were asymtotic to the mass transfer coefficient values for both phases when the two phases were agitated at different speeds; this was presented in Figures (7.3) and (7.4).

6. When the water phase was agitated at a slower rpm than the organic phase, its mass transfer coefficient was found to be higher than the value obtained when the agitation speed in both phases were the same, i.e. the asymtotic values. As the agitation of the water phase increased while the organic phase agitation remained constant, the water mass transfer coefficient increased and approached its asymtotic values. When the agitation rate became higher than the organic phase, its mass transfer coefficient increased through the asymtotic line. This was shown in Figure (7.3). The same behavior was found for the mass transfer coefficient in the organic phase, as shown in Figure (7.4).

7. For the water-n-butanol system, it was found that when the water phase Reynolds number, Re_w, is less than approximately 7000, k_w was higher than its asymptotic value, while for n-butanol phase when Re_o is less than approximately 1900, k_o was higher than its asymtotic value as shown in Figures (7.3) and (7.4); this was due to the effect of Re in the other phase.

8. If the agitation speed of the water phase is higher than

that of the organic phase, k_w will be the same as the asymtotic value of k_w when both phases are agitated at the same speed. The same behavior was found for the mass transfer coefficient in the organic phase, as illustrated in Tables (6.1), (6.2) and (6.3), and Figures (7.3) and (7.4). In general this means that a lower agitation rate in the other phase than in a given phase does not affect the mass transfer coefficient of the given phase. Lewis [38], McManamey [44], Mayers [42], McManamey and Davis et al [46], Bulick and Prochazka [4] and Asai et al [2] correlations, as shown in Table (7.7), did not predict the mass transfer coefficient in this condition.

9. The earlier correlations did not represent the prediction of the organic phase mass transfer coefficient, since they were developed depending only on the experimental data of water phase and mass transfer coefficients.

10. Based on the water-n-butanol system data, correlations were developed for the mass convective coefficient for a liquid phase with either high or small diffusivity. The correlations, constants and Reynolds number exponents show good agreement for the water-n-butanol system. These constants will probably need to be adjusted for other systems having different diffusivity values and for Reynolds number outside of the range investigated.

11. The correlations of mass transfer coefficient were developed using the mass transfer coefficient values of both phases when the two phases were agitated at the same speed as in Figure (7.1); by doing this, the correlations were based on the asymtotic lines of Figures (7.3) and (7.4). Therefore, it is valid for the water phase

Reynolds number, Re_w, above 7000 and for the n-butanol phase Reynolds number, Re_o, above 1900 for water-n-butanol system. In general, it seems that the range represented by the asymtotic line conditions occur in the desired range of Reynolds number for many industrial process operations, particularly for the organic phase. Accordingly, there is no need to include the deviation of mass transfer coefficient below this range of Reynolds number in developing the correlation.

12. For low Reynolds number conditions where there is an effect of one phase Reynolds number on the other phase mass transfer coefficients, similar correlations of the asymtotic line conditions could be developed. More investigation on many different systems are needed to verify this approach.

13. The correlations were simpler than the previous correlations and covered a wide range of diffusivity.

14. The correlations did not include the surface tension affect. As discussed in section 7.4, this was done based on King's model, which eliminated the surface tension variable. Investigations are recommended on systems having different interface surface tensions to determine whether King's model assumption is correct; if not the investigation could determine dependency on the surface tension.

15. The physical properties of one phase did not play a role in the mass transfer coefficient correlations of the second phase. This may have been due to the system investigated or the mixing range involved.

16. The percentage error in the predicted Sherwood number of the water-n-butanol system was small compared to the range of errors in earlier correlations as shown in Tables (7.5) and (7.6) and Figures (7.11-7.14).

17. Although the predicted Sherwood numbers by the developed correlations were well in agreement with the water-n-butanol experimental data, the correlations still are not necessarily as good as for other systems. Therefore investigations involving different systems may adjust the overall percentage error of the developed correlations through adjusting their constants and Reynolds number exponents.

8.2 Suggestions for Future Work

For future work there are many research areas which could be investigated. The following are some suggestions for future work:

1. The contactor was designed to operate as either a batch or a continuous process. This investigation verified its batch process capabilities. The same water-n-butanol system should be investigated using the continuous process and the results compared with the batch process.

2. The effect of the hydrodynamics conditions on the mass transfer coefficient should be investigated. The contractor was designed with enough flexibility to permit easy modification for the investigation of the most important hydrodynamic conditions, such as impeller position and dimensions, impeller type, baffle configuration, wiremesh cylinders, flow rate in the continuous process, etc.

3. Investigate a ternary system in which a solute is transferred between two immiscible fluids.

4. Different systems with a wide range of physical properties, such as diffusivities and surface tension should be investigated.

5. Investigate the effect of the physical properties on the qualitative behavior of the mass transfer coefficient in one phase with the agitation speed of the other phase.

6. Continued investigation on the diffusivity dependency should be made. This could be achieved by studying systems of large diffusivity and systems of small diffusivity.

7. Investigations are needed to verify the degree of the surface tension effect on the mass transfer coefficient; this would verify whether the b term in equation (2.9) is important.

8. Investigate the effect of the temperature on the mass transfer coefficient, while varying the agitation speeds of both phases. This would require jacketing the contactor to control its temperature.

9. Investigate the effect of surface-active agents or impurities on the rate of mass transfer. This is of practical importance since small amounts of impurities might conceivably concentrate on the interface and reduce the capacity of mass transfer equipments [17, 38].

10. Verify the effect of the agitation speed on the mass transfer coefficient dependency on the diffusivity. McManamey et al [45] has pointed out that a transition to laminer boundary layer ($k \propto D^{0.67}$) at the interface occurs at reduced intensity of agitation. Kozinski and King [34] have pointed out that ($k \propto D^{0.5}$) obtained at

low stirring speeds. The increase in the exponent as the stirring speed increases is in accord with the continuous transition toward a mass transfer regime controlled by steady state transport into the damped eddy diffusivity profile.

BIBLIOGRAPHY

[1] AIChE, 1987, "Equipment testing procedure - mixing equipment - impeller type".

[2] Asai S., Hatanka J., Uekawa, Y., 1983, "Liquid-liquid mass transfer in an agitated vessel with a flat interface", Journal of Chemical Engineering of Japan, vol. 16, no. 6, pp. 463-469.

[3] Beyer W. H. (ed.), 1987, "CRC Standard Mathematical Tables", 28th ed., CRC Press Inc.

[4] Bulicka J., Prochazlca J., 1976, "Mass transfer between two turbulent liquid phases", Chem. Engng. Sci., vol. 31, pp. 137-146.

[5] Churchill S.W., Usag R., 1972, "A general expression for the correlation of rates of transfer and other phenomena", AIChE Journal, vol. 18, no. 6, pp. 1121-1128.

[6] Colburn A.P., 1939, "The simplified calculation of diffusional process general consideration of two film resistances", Trans. Am. Inst. Chem. Engrs., vol. 35, pp. 211-236.

[7] Colburn A.P., Welsh D.G., 1942, "Experimental study of individual transfer resistances in countercurrent liquid-liquid extraction", Trans. Am. Inst. Chem. Engrs., vol. 38, pp. 179-202.

[8] Cornelisse R., Beenackers, A.A.C.M., Van Beckum F.P.H. and Van Swaaij W.P.M., 1980, "Numerical calculation of simultaneous mass transfer of two gases accompanied by complex reversible reaction", Chem. Engng. Sci., vol. 35, pp. 1245-1260.

[9] Danckwerts P.V., 1970, "Gas-Liquid Reactions", New York, McGraw Hill, 276 p.

[10] Danckwerts P.V., Gillham A.J., 1966, "The design of gas absorber. 1. Method for prediction rates of absorption with chemical reaction in packed columns and tests with 1½ in. rashing rings", Trans. Inst. Chem. Engrs., vol. 44, pp. T42-T54.

[11] Danckwerts P.V., Kennedy A.M., 1954, "Kinetics of liquid film process in gas absorption." Part II; Measurements of transient absorption rates", Transactions, Institute of Chemical Engineers, vol. 32, pp. S53-S60.

[12] Davies J.T., 1972, "Turbulence Phenomena", Academic Press.

[13] Davies J.T., Khan W., 1963, "Surface cleaning by eddies", Chemical Engineering Science, vol. 20, pp. 713-715.

[14] Davies J.T., Mayers G.R.A., 1961, "The effect of interfacial films on mass transfer rates in liquid-liquid extraction", Chemical Engineering Science, vol. 16, pp. 55-68.

[15] Godfrey J.H., 1973, "A new apparatus for studying mass transfer and reaction between two fluid phases", Ph.D. Thesis, Oregon State University.

[16] Godfrey J.C., Slater M.J., 1983, "Principle of Mixer-Settler Design", Handbook of Solvent Extraction, Tech. C. Lo, Halcolm H.J. Band Caril Hanson, A Wiley Interscience Publication, 275 p.

[17] Gordon K.F., Sherwood T.K., 1954, "Mass transfer between two liquid phases", Symposium Series, vol. 50, no. 10, pp. 15-23.

[18] Govindan T.S., Quiun J.A., 1964, "Transient absorption at a small contact times - moving band absorber", AIChE Journal, vol. 10, pp. 35-38.

[19] Hancil V., Rod U., Renakova M., 1978, "Mass transfer cell with vibration mixing", The Chemical Engineering Journal, vol. 16, pp. 51-56.

[20] Hanson C., Ingham J., Stewardson T.N., 1971, "Direct contact heat transfer between immiscible liquids in a mixer-settler apparatus. Proceeding International Solvent Extraction Conference, vol. 1, pp. 270-280.

[21] Hanson C., Kaye D.A., 1963, "General design of high capacity mixer-settlers. Part 1. Chemical and Process Engineering", vol. 44, pp. 27-30.

[22] Hanson C., Kaye D.A., 1963, "General design of high capacity mixer-settler. Part 2. Chemical and Process Engineering", vol. 44, pp. 651-654.

[23] Harnby N., Edwards M.F., Nienow A.W., 1985, "Mixing in the process industries. Chapter 7 - A Review of Liquid Mixing Equipment", Butterworths.

[24] Harriott P., 1962, "A random eddy modification of the penetration theory", Chemical Engineering Science, vol. 17, pp. 149-154.

[25] Hikita H., Asai S., Ishikawa H., Saito Y., 1975, "Kinetics of absorption of chlorine in aqueous acidic solution of ferrous chloride", Chemical Engineering Science, vol. 30, pp. 607-616.

[26] Holland F.A., Chapman F.S., 1966, "Liquid mixing and processing in stirred tanks", Reinhold Publishing Corporation.

[27] Hutchinson M.H., Sherwood T.K., 1937, "Liquid film in gas absorption", Industrial and Engineering Chemistry, vol. 29, p. 836.

[28] Ingham J., Marshland J.G., Pratt M.W.T., Slater M.J., 1970, "Solvent extraction technology - Report on the progress of applied chemistry", vol. 55, pp. 343-358.

[29] Jenkins I.L., 1970, "Solvent extraction in the atomic energy industry - Report on the Progress of Applied Chemistry", vol. 55, pp. 375-383.

[30] Kafarov V.V., 1960, "International Symposium on Distillation", Institution of Chemical Engineers (London), p. 153.

[31] Kafarov V.V., 1957, Trofimov V.I., vol. 30, p. 217.

[32] King C.J., 1964, "The additivity of individual phase resistances in mass transfer operations", AIChE Journal, vol. 10, no. 5, pp. 671-677.

[33] King C.J., 1966, "Turbulent liquid phase mass transfer at a free gas-liquid interface", I & EC Fundamental, vol. 5, no. 1, pp. 1-8.

[34] Kozinski A.A., King C.J., 1966, "The influence of diffusivity on liquid phase mass transfer to the free interface in a stirred vessel", AIChE Journal, vol. 12, no. 1, pp. 109-116.

[35] Laity D.S., Treyba R.E., 1957, "Dynamics of liquid agitation in the absence of an air-liquid interface", AlchE Journal, vol. 3, no. 2, pp. 176-179.

[36] Landau J., Chin M., 1977, "A contractor for studying mass transfer with reaction in liquid-liquid systems", The Canadian Journal of Chemical Engineering, vol. 55, pp. 161-167.

[37] Levich V.G., 1962, "Physiochemical Hydrodynamics," Chap. XII, pp. 135, 136, Prentice-Hall, Englewood Cliffs, N.J.

[38] Lewis J.B., 1954, "The mechanism of mass transfer of solutes across liquid-liquid interfaces, Part I: The determination of individual transfer coefficients for binary systems", Chemical

[39] Lewis W.K., Whitman W.G., 1924, Ind. Eng. Chem., vol. 16, p. 1215.

[40] Lynn S., Straatemeier J.H., Kramers H., 1953, "Absorption studies in the light of the penetration theory, Part III: Absorption by wetted spheres, singly and in column", Chemical Engineering Science, vol. 4, pp. 63-67.

[41] Maroudas N.G., Sawistowski H., 1964, "Simultaneous transfer of two solutes across liquid-liquid interface", Chemical Engineering Science, vol. 19, pp. 919-931.

[42] Mayers G.R.A., 1961, "The correlation of individual film coefficients of mass transfer in a stirred cell", Chemical Engineering Science, vol. 16, pp. 69-75.

[43] McCabe W.L., Smith J.C., Harriott P., 1985, "Unit Operations of Chemical Engineering", New York, McGraw Hill.

[44] McManamey W.J., 1961, "Molecular diffusion and liquid-liquid mass transfer in stirred transfer cell", Chemical Engineering Science, vol. 15, pp. 251-254.

[45] McManamey W.J., Multani S.K.S., Davis J.J., 1975, "Molecular diffusion and liquid-liquid mass transfer in stirred transfer cell", Chemical Engineering Science, vol. 30, pp. 1536-1538.

[46] McManamey W.J., Davies J.T., Woolen J.M., Coe J.R., 1973, "The influence of molecular diffusion on mass transfer between turbulent liquids", Chemical Engineering Science, vol. 28, pp. 1061-1069.

[47] Munford C.J., 1971, "Liquid Extraction in a Continuous Agitated Horizontal Contactors", Proceeding International Solvent Extraction Conference, The Hague, 19-23 April, pp. 260-269.

[48] Murdoch R., Pratt H.R.C., 1953, "Liquid-liquid extraction, Part VIII: The extraction of uranyl nitrate in a wetted wall column", Trans. Inst. Chem. Engrs., vol. 31, pp. 307-326.

[49] Olander D.R., Benedict H., 1962, "The mechanism of extraction by tributyl phosphate-n-Hexane solvents, Part I: Water extraction", Nuclear Science and Engineering, vol. 14, pp. 287-294.

[50] Olander D.R., Reddy L.B., 1964, "The effect of concentration driving force on liquid-liquid mass transfer", Chemical Engineering Science, vol. 19, pp. 67-73.

[51] Oldshue, T.Y., 1983, "Fluid Mixing Technology", New York, McGraw Hill.

[52] Perlmutter D.D., 1961, "Surface renewal models in mass transfer", Chemical Engineering Science, vol. 16, pp. 287-296.

[53] Perry T.H., (ed.), 1984, "Chemical Engineering Handbook", 6th edition, New York, McGraw Hill.

[54] Prochazka J., Bulicka J., 1971, "Mass transfer between two turbulent liquids", Proceedings International Solvent Extraction Conference, vol. 2, pp. 823-830.

[55] Ramshaw C., Mallinson R.H., April 11, 1981, "Mass transfer process", United States Patent, No. 4283255.

[56] Robert C.W., (ed.), 1986-1987, "CRC Handbook of Chemistry and Physics", 27th edition, CRC Press Inc.

[57] Sherwood T.K., Pigford R.L., 1952, "Absorption and extraction", New York, McGraw Hill.

[58] Shifftner K.C., Feb. 21, 1984, "Mass transfer contact apparatus", United States Patent, no. 4432914.

[59] Sincich T., 1985, "Statistic by Examples", Dellen Publishing Company.

[60] Stephens E.J., Morris G.A., 1951, "Determination of liquid film absorption coefficients. A new type of column and its application to problems of absorption in presence of chemical reaction", Chemical Engineering Progress, Vol. 47, No. 5, pp. 232-242.

[61] Strake F., Karcz F., 1985, "Optimization of geometrical parameter of the turbine with the pitched blades agitated vessel for heat transfer", 5th European Conference on Mixing, Wuzburg-Germany, June 10-12, p. 515.

[62] Szues L., Tasnada C., April 28, 1976, "Gas-liquid contact apparatus for effecting heat and mass transfer between fluids", U.K. Patent, no. 1433451.

[63] Szues L., Tasnada C., Lindner I., April 28, 1976, "Gas-liquid contact apparatus for effecting heat and mass transfer between fluids", U.K. Patent, no. 1433465.

[64] Toor H.L., Marchello J.M., 1958, "Film penetration model for mass and heat transfer", AIChE Journal, vol. 4, no. 1, pp. 97-101.

[65] Treybal R.E., 1980, "Mass Transfer Operation", 3rd edition, Chemical Engineering Series, New York, McGraw Hill.

[66] Uhl V.W., Gray J.B., 1966, "Mixing Theory and Practice", Part I, II, Academic Press.

[67] Vermijs H.J.A., Kramers H., 1954, "Liquid-liquid extraction in a rotating disc contactor", Chemical Engineering Science, vol. 3, pp. 55-64.

[68] Versteeg G.F., Blauwhoff P.M.M., Van Swaau W.P.M., 1987, "The effect of diffusivity on gas-liquid mass transfer in stirred vessels experiments at atmospheric and elevated pressure", Chemical Engineering Science, vol. 42, no. 5, pp. 1103-1119.

[69] Vivian J.E., King C.J., 1964, "Diffusivities of slightly soluble gases in water", AIChE Journal, vol. 10, no. 2, pp. 220-227.

[70] Welty J.R., Wicks C.E., Wilson R. E., 1984, "Fundamentals of Momentum, Heat and Mass Transfer", John Wiley and Sons.

[71] Wicks C.E., 1987, "Diffusional Operations", class lecture notes, Oregon State University, winter term.

[72] Wylie C.R., Barrett L.C., 1985, "Advanced Engineering Mathematics", 5th edition, New York, McGraw Hill.

APPENDICES

Appendix A

Gas Chromatography Measurements

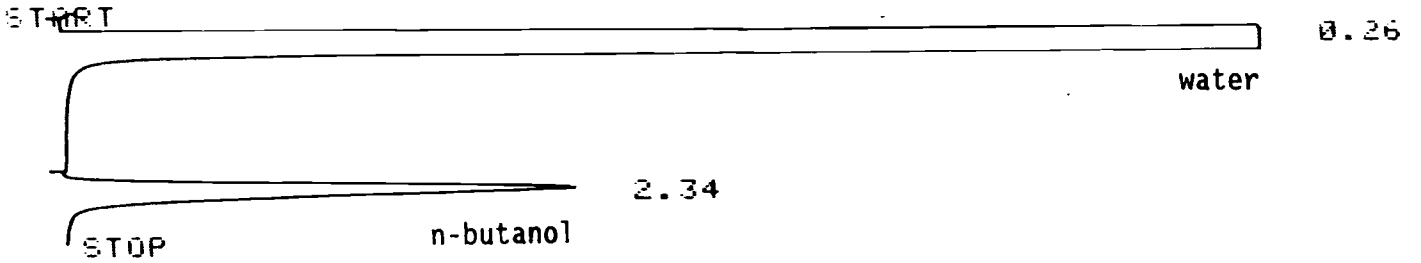

S HP RUN # 0
AREA %

RT	AREA	AREA %
0.26	11290000	97.098
2.34	337400	2.902

DIL FACTOR: 1.0000 E+ 0

Figure (A.1). Gas chromatography measurement to a standard sample of 0.04 gm/cm^3 n-butanol in water

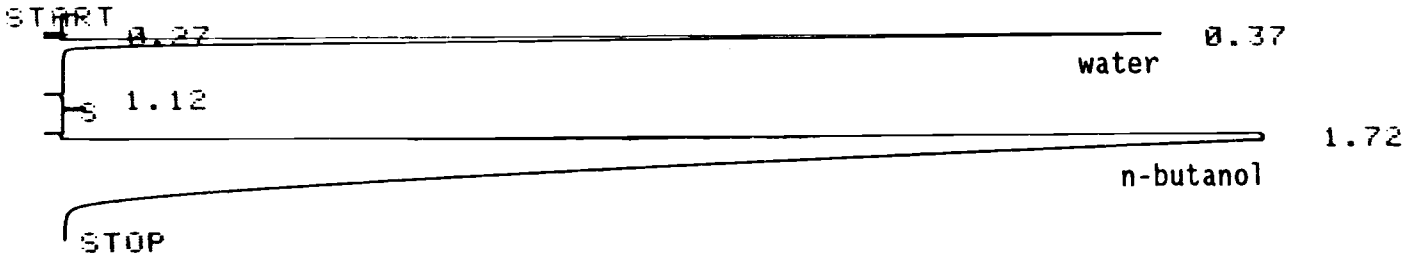

S HP RUN # 5
AREA %

RT	AREA	AREA %
0.27	1418	0.018
0.37	808600	10.345
1.72	7006000	89.636

DIL FACTOR: 1.0000 E+ 0

Figure (A.2). Gas chromatography measurement to a standard sample of 0.058 gm/cm^3 water in n-butanol

Appendix B

Experimental Data

Table (B.1). Experimental data for both phases when they were agitated at the same speed.

Run #1 - n-butanol phase
rpm = O-241, Vol. = 380 cm^3, Temp. = 19°C, Fig. (6.1)
W-241

Time min.	20	35	50	66	80	95	120	150
C_w gm/cm^3	0.018	0.03	0.043	0.056	0.066	0.077	0.092	0.107

water phase
rpm = W-241, Vol. = 380 cm^3, Temp. = 19°C, Fig. (6.3)
O-241

Time min.	15.3	30	45	60	75	91	110	140
C_o gm/cm^3	0.015	0.024	0.032	0.04	0.047	0.051	0.057	0.06

Run #2 - n-butanol phase
rpm = O-301, Vol. = 381 cm^3, Temp. = 19°C, Fig. (6.1)
W-302

Time min.	12.3	23	33	43	58	75	90	110
C_w gm/cm^3	0.023	0.034	0.047	0.06	0.073	0.089	0.099	0.111

water phase
rpm = W-302, Vol. = 381 cm^3, Temp. = 19.2°C, Fig. (6.3)
O-301

Time min.	10.1	20.2	30	40	55	70	85
C_o gm/cm^3	0.013	0.022	0.029	0.034	0.044	0.051	0.056

Run #3 - n-butanol phase
rpm = O-332, Vol. = 380cm^3, Temp. = 18°C, Fig. (6.1)
W-332

Time min.	25	35	48	60	75	90
C_w gm/cm^3	0.044	0.056	0.071	0.084	0.096	0.107

water phase
rpm = W-332, Vol. = 380cm^3, Temp. = 18°C, Fig. (6.3)
O-332

Time min.	10	20	30	42	55
C_o gm/cm^3	0.019	0.026	0.033	0.042	0.05

Run #4 - n-buterol phase
rpm = O-362, Vol. = 382 cm³, Temp. = 20.2°C, Fig. (6.1)
W-362

Time min.	12	17	25	35	45	55	70	82
C_w gm/cm³	0.034	0.037	0.05	0.065	0.079	0.09	0.104	0.113

water phase
rpm = W-362, Vol. = 382 cm³, Temp. = 20.2°C, Fig. (6.3)
O-362

Time min.	10	15	20	30	40	50	65
C_o gm/cm³	0.019	0.024	0.028	0.037	0.043	0.052	0.058

Run #5 - n-buterol phase
rpm = O-422, Vol. = 384.5 cm³, Temp. = 19.5°C, Fig. (6.1)
W-422

Time min.	9	14	19	25	35
C_w gm/cm³	0.029	0.037	0.05	0.058	0.075

water phase
rpm = W-422, Vol. = 384.5 cm³, Temp. = 19.5°C, Fig. (6.3)
O-422

Time min.	5	10	15	20	30
C_o gm/cm³	0.015	0.02	0.027	0.034	0.044

Table (B.2). Experimental data for water phase when the n-butanol phase was unagitated.

Run #6 - water phase
rpm = W-181, Vol. = 376 cm³, Temp. = 19°C, Fig. (6.5)
O-0.0

Time min.	16	30	40	50	60	70	90	110
C_o gm/cm³	0.016	0.02	0.026	0.03	0.032	0.034	0.04	0.042

Run #7 - water phase
rpm = W-241, Vol. = 376.5 cm^3, Temp. = 18.2°C, Fig. (6.5)
O-0.0

Time min.	10	20	31	40	50	60	75
C_o gm/cm^3	0.015	0.02	0.031	0.033	0.038	0.041	0.046

Run #8 - water phase
rpm = W-360, Vol. = 376.5 cm^3, Temp. = 18°C, Fig. (6.5)
O-0.0

Time min.	10	15	20	25	30	40	50	60
C_o gm/cm^3	0.018	0.021	0.026	0.031	0.036	0.043	0.048	0.053

Table (B.3). Experimental data for both phases when the the n-butanol phase was agitated at 301-303 rpm while the water phase agitation rate was varied.

Run #9 - water phase
rpm = W-182, Vol. = 380 cm^3, Temp. = 19.8°C, Fig. (6.7)
O-302

Time min.	25	45	55	65	81	96	120
C_o gm/cm^3	0.015	0.027	0.032	0.034	0.041	0.046	0.053

n-butanol phase
rpm = O-302, Vol. = 380 cm^3, Temp. = 19.8°C, Fig. (6.9)
W-182

Time min.	10	20	30	41	50	60	76	90	115
C_w gm/cm^3	0.0083	0.018	0.027	0.037	0.046	0.054	0.067	0.076	0.091

Run #10 - water phase
rpm = W-242, Vol. = 380 cm^3, Temp. = 18.5°C, Fig. (6.7)
O-303

Time min.	10	20	30	40	50	60	75
C_o gm/cm^3	0.011	0.02	0.027	0.034	0.038	0.044	0.05

n-butanol phase
rpm = O-303, Vol. = 380 cm³, Temp. = 18.5°C, Fig. (6.9)
W-242

Time min.	15	25	35	45	55	65	80	104
C_w gm/cm³	0.024	0.035	0.046	0.056	0.066	0.074	0.085	0.102

Run #2 - water phase
rpm = W-302, Vol. = 381 cm³, Temp. = 19.2°C, Fig. (6.7)
O-301

Time min.	10.1	20.2	30	40	55	70	85
C_o gm/cm³	0.013	0.022	0.029	0.034	0.044	0.051	0.056

n-butanol
rpm = O-301, Vol. = 381 cm³, Temp. = 19.2°C, Fig. (6.9)
W-302

Time min.	12.3	23	33	43	58	75	90	110
C_w gm/cm³	0.023	0.034	0.047	0.06	0.073	0.08	0.099	0.11

Run #11 - water phase
rpm = W-362, Vol. = 380 cm³, Temp. = 18°C, Fig. (6.7)
O-302

Time min.	10	20	30	40	50	60	75	95
C_o gm/cm³	0.017	0.025	0.033	0.04	0.045	0.05	0.057	0.064

n-butanol phase
rpm = O-302, Vol. = 380 cm³, Temp. = 18°C, Fig. (6.9)
W-362

Time min.	15	25	35	45	55	65	80	100
C_o gm/cm³	0.032	0.042	0.056	0.067	0.078	0.087	0.1	0.113

Table (B.4). Experimental data for both phases when the n-butanol phase was agitated at 362-365 rpm while the water phase agitation rate was varied.

Run #12 - water phase
rpm = W-185, Vol. = 383 cm^3, Temp. = 17.7°C, Fig. (6.11)
O-365

Time min.	10	20	30	40	50	60
C_o gm/cm^3	0.015	0.02	0.028	0.034	0.041	0.047

n-butanol phase
rpm = O-365, Vol. = 383 cm^3, Temp. = 17.7°C, Fig. (6.13)
W-185

Time min.	5	15	25	35	45	55
C_w gm/cm^3	0.008	0.022	0.035	0.047	0.058	0.068

Run #13 water phase
rpm = W-302, Vol. = 383 cm^3, Temp. = 17°C, Fig. (6.11)
O-363

Time min.	10	21	30	38	45	53	60	70
C_o gm/cm^3	0.016	0.026	0.032	0.038	0.043	0.046	0.05	0.054

n-butanol
rpm = O-363, Vol. = 383 cm^3, Temp. = 17°C, Fig. (6.13)
W-302

Time min.	15	25	35	42	50	57	65	72
C_w gm/cm^3	0.029	0.042	0.058	0.064	0.072	0.079	0.086	0.092

Run #4 - water phase
rpm = W-362, vol. = 382 cm^3, Temp. = 20.2°C, Fig. (6.11)
O-362

Time min.	10	15	20	30	40	50	65
C_o gm/cm^3	0.019	0.024	0.028	0.037	0.043	0.052	0.058

n-butanol phase
rpm = O-362, Vol. = 382 cm^3, Temp. = 20.2°C, Fig. (6.13)
W-362

Time min.	12	17	25	35	45	55	70	82
C_w gm/cm^3	0.034	0.037	0.05	0.065	0.079	0.09	0.104	0.113

Table (B.5). Experimental data for n-butanol phase when the water phase was unagitated.

Run #14 - n-butanol phase
rpm = 0-242, Vol. = 387.5 cm³, Temp. = 19°C, Fig. (6.15)
W-0.0

Time min.	20	30	40	50	60	70	80
C_w gm/cm³	0.0091	0.013	0.017	0.02	0.024	0.028	0.031

Run #15 - n-butanol phase
rpm = 0-302, Vol. = 386 cm³, Temp. = 18.5°C, Fig. (6.15)
W-0.0

Time min.	10	20	30	40	50	60	70
C_w gm/cm³	0.0066	0.014	0.022	0.033	0.036	0.042	0.045

Run #16 - n-butanol phase
rpm = 0-423, Vol. = 386 cm³, Temp. = 18°C, Fig. (6.15)
W-0.0

Time min.	10	15	20	25	30	35	41
C_w gm/cm³	0.021	0.028	0.035	0.042	0.048	0.054	0.06

Table (B.6). Experimental data for both phases when the water phase was agitated at 302 rpm while the n-butanol phase agitation rate was varied.

Run #17 - n-butanol phase
rpm = 0-212, Vol. = 385 cm³, Temp. = 18.4°C, Fig. (6.17)
W-302

Time min.	15	25	35	45	55	65	75	85
C_w gm/cm³	0.017	0.027	0.037	0.046	0.055	0.065	0.073	0.081

water phase
rpm = W-302, Vol. = 385 cm^3, Temp. = 18.4°C, Fig. (6.19)
O-212

Time min.	10	20	30	40	50	60	70	80
C_o gm/cm^3	0.012	0.02	0.028	0.033	0.039	0.044	0.048	0.052

Run #2 - n-butanol phase
rpm - O-301, Vol. = 381 cm^3, Temp. = 19.2°C, Fig. (6.17)
W-302

Time min.	12.3	23	33	43	58	75	90	110
C_w gm/cm^3	0.023	0.034	0.047	0.06	0.073	0.089	0.099	0.111

water phase
rpm = W-241, Vol. = 380 cm^3, Temp. = 19°C, Fig. (6.19)
O-241

Time min.	10.1	20.2	30	40	55	70	85
C_o gm/cm^3	0.013	0.002	0.029	0.034	0.044	0.051	0.056

Run #13 - n-butanol phase
rpm - O-363, Vol. = 383 cm^3, Temp. = 17°C, Fig. (6.17)
W-302

Time min.	15	25	35	42	50	57	65	72
C_w gm/cm^3	0.029	0.042	0.058	0.064	0.072	0.079	0.086	0.092

water phase
rpm = W-302, Vol. 383 cm^3, Temp. = 17°C, Fig. (6.19)
O-363

Time min.	10	21	30	38	45	53	60	70
C_o gm/cm^3	0.016	0.026	0.032	0.038	0.043	0.046	0.05	0.054

Table (B.7). Experimental data for both phases when the water phase was agitated at 362-365 rpm while the n-butanol phase agitation rate was varied.

Run #18 - n-butanol phase
rpm = O-212, Vol. = 382 cm³, Temp. = 17°C, Fig. (6.21)
W-365

Time min.	10	20	30	40	51	60	70	80
C_w gm/cm³	0.016	0.026	0.038	0.049	0.059	0.069	0.077	0.085

water phase
rpm = W-365, Vol. = 382 cm³, Temp. = 17°C, Fig. (6.23)
O-212

Time min.	12	33	42	54	63	72
C_o gm/cm³	0.018	0.034	0.04	0.048	0.05	0.055

Run #11 - n-butanol phase
rpm = O-302, Vol. = 380 cm³, Temp. = 18°C, Fig. (6.21)
W-362

Time min.	15	25	35	45	55	65	80	100
C_w gm/cm³	0.032	0.042	0.056	0.067	0.078	0.087	0.1	0.113

water phase
rpm = W-362, Vol. = 380 cm³, Temp. = 18°C, Fig. (6.23)
O-302

Time min.	10	20	30	40	50	60	75	95
C_o gm/cm³	0.017	0.025	0.033	0.04	0.045	0.05	0.057	0.064

Run #4 - n-butanol
rpm = O-362, Vol. 382 cm³, Temp. = 20.2°C, Fig. (6.21)
W-362

Time min.	12	17	25	35	45	55	70	82
C_w gm/cm³	0.034	0.037	0.05	0.065	0.079	0.09	0.104	0.113

water phase
rpm = W-362, Vol. = 382 cm³, Temp. = 20.2°C, Fig. (6.23)
O-362

Time min.	10	15	20	30	40	50	65
C_o gm/cm³	0.19	0.024	0.028	0.037	0.043	0.052	0.058